Mineral storage of carbon in basaltic rocks

Sandra Ósk Snæbjörnsdóttir

Faculty of Earth Sciences
University of Iceland
2017

Mineral storage of carbon in basaltic rocks

Sandra Ósk Snæbjörnsdóttir

Dissertation submitted in partial fulfilment of a
Philosophiae Doctor degree in geology

Advisors

Dr. Sigurður R. Gíslason
Institute of Earth Sciences, University of Iceland

Prof. Eric H. Oelkers
University College London
CNRS, Université Paul Sabatier, France

PhD Committee

Dr. Sigurður R. Gíslason
Institute of Earth Sciences, University of Iceland

Prof. Eric H. Oelkers
University College London, UK
CNRS, Université Paul Sabatier, France

Dr. Hjalti Franzson
ISOR, Iceland GeoSurvey

Prof. Martin Stute
Columbia University, New York, USA
Barnard College, New York, USA

Opponents

Dr. Jordi Cama
Institute of Environmental Assessment and Water Research, Spain

Prof. R. Stuart Haszeldine
University of Edinburgh, UK

Faculty of Earth Sciences
School of Engineering and Natural Sciences
University of Iceland
Reykjavik, 19th of April 2017

Mineral storage of carbon in basaltic rocks

Dissertation submitted in partial fulfilment of a *Philosophiae Doctor* degree in Geology

Faculty of Earth Sciences
School of Engineering and Natural Sciences
University of Iceland
Askja – Sturlugata 7
101 Reykjavik
Iceland

Telephone: 525 4000

Bibliographic information:
Sandra Ósk Snæbjörnsdóttir, 2017, *Mineral storage of carbon in basaltic rocks*, PhD dissertation, Faculty of Earth Sciences, University of Iceland, 156 pp.

Printing: Háskólaprent
Reykjavik, Iceland, April 2017

Abstract

*In-situ c*arbonation of basaltic rocks could provide a carbon storage solution for the long term. Permanence is essential for the success and public acceptance of carbon storage. The aim of this study was twofold, to evaluate and make a first estimate of the theoretical mineral storage potential of CO_2 in basaltic rocks, and to characterise the mineralisation process using geochemical data from the CarbFix test site in Hellisheidi, SW-Iceland, which comprises both injection and monitoring wells.

Studies on mineral storage of CO_2 in basaltic rocks are still at an early stage. Therefore, natural analogues are important for gaining a better understanding of the carbon mineralisation process in basaltic rocks at elevated pCO_2. The amount and spatial distribution of CO_2 stored as calcite in the bedrock of geothermal systems in Iceland indicate a large storage potential for CO_2 in basaltic rocks. These natural analogues were used as a guideline for evaluating the theoretical potential of CO_2 storage in basaltic formations. The largest storage potential lies offshore, where CO_2 may be stored in minerals for the long term in mid-ocean ridges. The theoretical mineral CO_2 storage capacity of the mid-ocean ridges exceeds, by orders of magnitude, the amount of CO_2 that would be released by the burning of all fossil fuel on Earth. Iceland is the largest landmass found above sea level on the mid-ocean ridges, about 103,000 km^2. It is mostly made of basaltic rocks (~90%), which makes it ideal for demonstration of the viability of this carbon storage method.

Two injection experiments were carried out in 2012 at the CarbFix site where 175 tonnes of pure CO_2 and 73 tonnes of a CO_2-H_2S-gas mixture were injected into basaltic rocks at 500-800 m depth with temperatures ranging from 20-50°C. All gases were dissolved in water during their injection. Extensive geochemical monitoring was carried out prior to, during, and after these injections. Sampled fluids from the first monitoring well, HN-04, showed a rapid increase in Ca, Mg, and Fe concentrations during the injections. Pyrite was identified in water samples from the injection well, which indicates that the H_2S was mineralised before it reached the first monitoring well. In July 2013, the fluid sampling pump in the well broke down due to calcite precipitation, confirming the mineralisation of the

injected CO_2. Calculations indicate that the sampled fluids were saturated with respect to siderite about four weeks after the injections began, and with respect to calcite about three months after each injection. Pyrite was supersaturated prior to and during the mixed gas injection and in the following months. Mass balance calculations, based on the recovery of non-reactive tracers co-injected into the subsurface together with the acid gases, confirm that more than 95% of the CO_2 injected into the subsurface was mineralised within two years. Essentially all of the injected H_2S was mineralised within four months of its injection.

Data collected prior to, during, and after the CO_2 injection was used in an attempt to model the CO_2-water-rock interaction during and after the injection. The results suggest that the mineralisation of the second and main breakthrough of the injected carbon is mainly driven by basaltic glass dissolution. The results also point towards dissolution of crystalline basalts during the first breakthrough of the injected solution. This breakthrough path is dominated by fracture flow, indicating that the fracture transects the more crystalline interiors of the lavas. No carbonates are saturated in the injection fluid, but iron rich carbonates, such as siderite, are predicted to form if the pH exceeds ~4.6. With progressive dissolution of basaltic rock, and a subsequent rise of pH along with a decrease in the dissolved CO_2 concentration, more Ca-rich carbonates, such as calcite, are calculated to become saturated. At this stage, carbonates become more abundant, forming along with chalcedony, and later, both zeolites and smectites appear. The efficiency of the carbon injection is limited by the porosity and the availability of cations, both of which are restricted by the formation of zeolites and smectites at pH above ~6.

Ágrip

Steinrenning koltvíoxíðs (CO_2) í basalti er aðferð sem nýst gæti til að binda kolefni til frambúðar. Mikilvægt er að bindingin verði varanleg, svo sátt verði um hana í samfélaginu og tilætlaður árangur náist. Markmið þessarar rannsóknar var tvíþætt, annars vegar að meta getu basalts til kolefnisbindingar, og hins vegar að varpa ljósi á steinrenningarferlið með jarðefnafræðilegum gögnum af CarbFix-svæðinu á Hellisheiði, en þar eru borholur bæði til niðurdælingar og vöktunar.

Rannsóknir á aðferðinni eru enn á frumstigi. Til að öðlast skilning á ferlinu er mikilvægt að skoða náttúrulegar hliðstæður á svæðum þar sem kolefni binst í basalti við háan hlutþrýsting koltvíoxíðs. Magn og dreifing karbónatsteinda í bergi íslenskra háhitasvæða nýtast til þess að leggja mat á það hversu mikið kolefni má binda í basalti, en vísbendingar eru um mikla bindigetu basalts. Möguleikarnir eru mestir á hafsvæðum, þar sem binda má kolefni í úthafshryggjum á öruggan hátt til langs tíma. Fræðilega séð væri unnt að binda þar margfalt magn þess koltvíoxíðs sem ætla mætti að losna myndi ef öllu jarðefnaeldsneyti á jörðinni yrði brennt. Ísland er stærsta landmassi ofansjávar á úthafshrygg, um 103.000 km2 að flatarmáli. Það er að mestu úr basalti og því kjörinn vettvangur til að þróa þessa aðferð til kolefnisbindingar.

Tvær niðurdælingartilraunir voru gerðar á CarbFix-svæðinu árið 2012; 175 tonnum af hreinu koltvíoxíði, og 73 tonnum af blöndu koltvíoxíðs og brennisteinsvetnis, var dælt niður í basaltlög á 500-800 m dýpi við 30-50°C hita. Gasið var leyst í vatni við niðurdælingu. Efnasamsetning vökvans var vöktuð fyrir, eftir og á meðan á niðurdælingu stóð. Í báðum tilraunum mátti greina hraða aukningu í styrk kalsíums, magnesíums og járns í vatnssýnum, sem safnað var úr vöktunarholu næst niðurdælingarholunni á meðan á niðurdælingu stóð. Pýrít greindist í vatnssýnum úr niðurdælingarholunni, og sýnir það að brennisteinsvetnið steinrann áður en það náði vöktunarholunni. Í júlí 2013 bilaði dæla í holunni af völdum kalsítútfellinga, og staðfesti þar með steinrenningu koltvíoxíðsins sem dælt var niður. Efnavarmafræðilegir útreikningar benda til síderít-mettunar um fjórum vikum, og til kalsít-mettunar um þremur mánuðum eftir upphaf hvorrar niðurdælingar. Pýrít reiknast yfirmettað í sýnum teknum bæði fyrir og eftir niðurdælingu blöndunnar, og meðan á henni stóð. Massajafnvægisútreikningar, byggðir á óhvarfgjörnum ferilefnum sem dælt var niður með gasinu, staðfesta að meira

en 95% koltvíoxíðsins hafði bundist í steindir innan tveggja ára, og megnið af brennisteinsvetninu innan fjögurra mánaða.

Efnagreiningar og önnur gögn úr koltvíoxíðniðurdælingunni voru notuð til að herma samspil koltvíoxíðs, vatns og bergs á meðan á niðurdælingu stóð og eftir hana. Niðurstöður benda til þess að steinrenning þorra koltvíoxíðsins sé drifin af leysingu basaltglers. Þær benda þó einnig til leysingar á kristölluðu basalti þegar fyrstu merki um niðurdælingarvökvann koma fram í vöktunarholunni. Sú rennslisleið tengist sprungulekt, sem bendir til þess að sprungan skeri kristallaðri hluta hraunlagasyrpunnar. Engin karbónatsteind nær mettun í niðurdælingarvökvanum, en járnrík karbónöt á borð við síderít reiknast mettuð ef pH er hærra en ~4.6. Með aukinni leysingu bergs, og hækkandi pH-gildi, koma fram kalsíumríkari karbónöt á borð við kalsít. Á þessu stigi myndast meira af karbónatsteindum, auk kalsedóns, og síðar birtast zeólítar og smektít. Árangur niðurdælingarinnar ræðst af poruhluta og framboði á katjónum, en hvort tveggja takmarkast af myndun zeólíta og smektíts við pH hærra en ~6.

Dedicated to my children, Agla and Styrmir

The future is yours - with all its challenges.

Table of Contents

Acknowledgements

This study was funded by the European Commission through the CarbFix project (EC coordinated action 283148) and the Nordic fund NORDICCS (11029-NORDICCS). I also received a travel grant from GEORG - Geothermal Research Group. I am grateful for these grants that made this study possible.

It is a big task to acknowledge all of the people: colleagues, friends, and family that have inspired, supported, celebrated, and accompanied me during this time. I am truly blessed.

First of all I want to thank my supervisors, Sigurður Reynir Gíslason and Eric H. Oelkers

Dear Siggi, thank you for this adventure. Thank you for the encouragement, the scientific brainstorming, and for always believing in me. Thank you for teaching me the value of having a feeling for things, and the importance of a good glass of wine at the end of the day.

Dear Eric, thank you for helping me to put things in perspective, and for showing me the big picture. Thank you for pushing me forward, pushing my limits, and pulling me down to Earth when all the brainstorming was getting out of hand.

I would also like to thank my PhD committee; Hjalti Franzson, who raised me in the field and taught me all about the beauty of mineralogy, and Martin Stute who provided me with the unforgettable opportunity to stay at the Lamont Doherty Earth Observatory of Columbia University in New York.

I want to thank my colleagues in the CarbFix project; I particularly want to thank Edda Sif Aradóttir, Ingvi Gunnarsson, Juerg Matter, Knud Dideriksen, Trausti Kristinsson, Einar Örn Þrastarson, and Halldór Bergmann, - all whom I worked closely with during the time of this PhD project. I also want to thank my colleagues from WP6 of the NORDICCS project; Per Aagaard, Karen L. Anthonsen, Per Bergmö, Gry M. Morthensen, and Ane Lothe.

I want to thank my colleagues at Askja and ÍSOR throughout this time, and my fellow members of the Bambi Research group. This includes a list of people that is too long to be included here, but I especially want to mention Eydís S. Eiríksdóttir, Iwona M. Galeczka, Deirdre Clark, Sveinborg H. Gunnarsdóttir, Helga M. Helgadóttir, Gunnlaugur M. Einarsson, Björn S. Harðarson, Hrönn Egilsdóttir, Chiara Marieni, Snorri Guðbrandsson, Helgi Arnar Alfredsson, Jonas Olsson, Chris Grimm, Flora Brocza, Jan Přikryl, Matylda Heřmanská, Nicole Keller, Hanna Kaasalainen, Jón Örn Bjarnason, Þorsteinn Jónsson, and Sveinbjörn Steinþórsson.

During my stay in New York I met a lot of people that made me feel welcome and at home, both at Lamont and on 116th street. Special thanks to Dan Rasmussen, Frankie Pavia, Angela Slagle, Natalia Zakharova, Dave Goldberg, Dóra Jóhannsdóttir, Jörundur Ragnarsson, Dima Trakovsky, and Ragnar Eldur Jörundsson.

Thank you for the music: Beyoncé, Bach, Björk, Hjaltalín, Händel, Víkingur Heiðar, and all the other artists that made the soundtrack to this adventure.

Last but not least, I want to thank my friends and my family for all their support and encouragement.

I especially want to mention Sigríður Ingibjörg Ingadóttir and Birgir Hermannsson, who made sure I would apply for this PhD position, my close friends Steinunn G. Guðjónsdóttir and Ragnar Heiðar Þrastarson, who became my family during the time in NYC, and Becca Neely, who started off as my office mate – but became my sister-in-science.

But mostly, my mother, Guðrún Ósk Ólafsdóttir, for being there for me – always, my daughter Agla Steinþórsdóttir and my son Styrmir Steinþórsson, that have yet to get to know their mother outside of this PhD project, and my friend and my husband Steinþór Níelsson, that celebrated every victory with me, supported me through the tougher times – and always told me to keep going.

1 Introduction

The Earth's climate is warming.

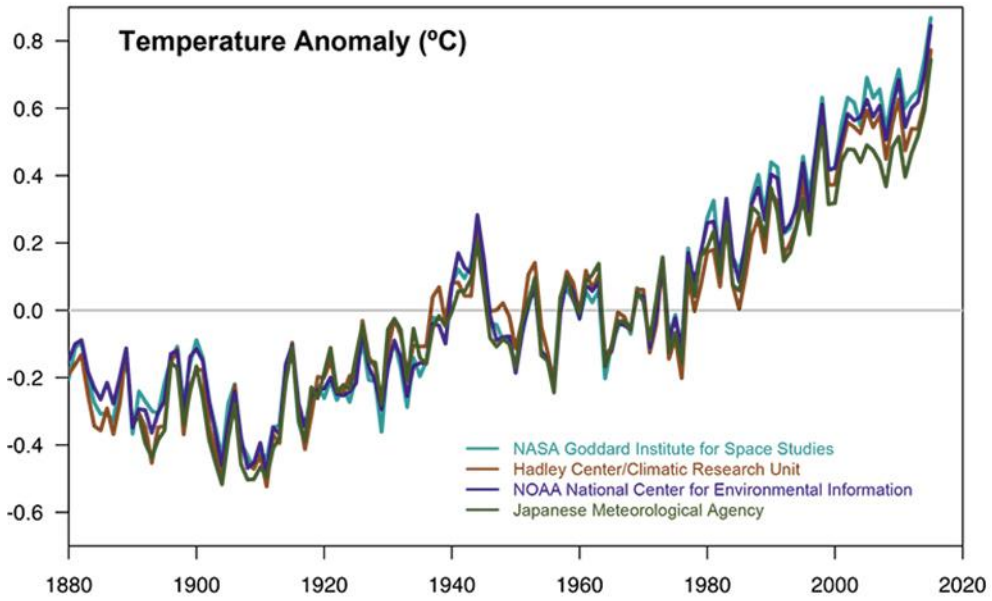

Figure 1. *Data from NASA's Goddard Institute for Space Studies, NOAA National Climatic Data Center, Met Office Hadley Centre/Climatic Research Unit and the Japanese Meteorological Agency, showing the globally-averaged surface temperature anomaly from 1880-2015. The average temperatures at 1950 are shown as a reference value. A positive anomaly indicates that the observed temperature was warmer than the reference value, while a negative anomaly indicates that the observed temperature was cooler than the reference value. Modified from NASA (2017a).*

Earth's 2016 surface temperatures were the warmest since modern recordkeeping began in 1880, with globally-averaged temperatures some 1°C warmer than the 1950's average (Figure 1). This makes 2016 the third year in a row to set a new record for global average surface temperatures (NASA, 2017a; NASA, 2017b).

Human influence on the climate system is clear (e.g. Cook et al., 2016). The leading cause of this rapid change in climate over the past half century is the increase in the amount of atmospheric greenhouse gases (GHG), mainly emitted by human activities. These include methane (CH_4), nitrous oxide (NO_2), and the major contributor: carbon dioxide (CO_2). Since the industrialisation, CO_2 concentrations have risen from about 270 parts per million (ppm) to over 400 ppm, and are currently rising at over 2 ppm annually (NOAA, 2017a).

The consequences of this rapid warming are already apparent with signs including diminished ice sheets (e.g. Watkins et al., 2015), glacial retreats (e.g. Marzeion et al., 2014), sea level rise (e.g. Church and White, 2006), ocean acidification (e.g. Caldeira and Wickett, 2003), and an increased number of extreme weather events (e.g. NOAA, 2017b). The continued emission of greenhouse gases will cause further warming of the atmosphere and oceans. This, in turn, will cause long-lasting changes in all components of the climate system with increased likelihood of severe, inescapable and irreversible impacts for people and ecosystems. Not only are the direct consequences of climate change a risk to societies; climate change will amplify existing risks and create new risks for natural and human systems. A rise exceeding 2˚C above pre-industrial level will cause serious environmental consequences, including increased droughts, floods, and storms. Millions will lose their livelihoods and have to migrate, causing increased tensions and the risk of war (IPCC, 2014b).

In spite of this knowledge, the annual global CO_2 emissions rose more rapidly from 2000-2010 than in the previous three decades, and exceeded earlier predictions of their rate of change by a factor of two. In the past three years (2014-2016), the growth in annual CO_2 emissions has stalled (IEA, 2016b). In 2016, these global annual emissions from the burning of fossil fuels, and from industrial processes totalled some 36 gigatonnes (Gt)CO_2 (Global Carbon Project, 2017).

To prevent a rise in temperature beyond 2˚C with 50% probability requires that the atmospheric CO_2 concentrations are stabilised at a maximum of 450 ppm (IPCC, 2014b). This requires a substantial and sustained reduction in the net flow of new CO_2 into the atmosphere from now onwards. The Paris Agreement (UN, 2015), the first universal and legally binding climate deal, aims to keep the global temperature rise "well below 2°C" from the pre-industrial levels, and to pursue efforts to limit the temperature increase to 1.5 °C, "recognizing that this would significantly reduce the risks and impacts of climate change".

Achieving the goals of the Paris Agreement, and balancing emissions during the second half of this century, requires rapid and extensive employment of low-emission technologies and adaption and mitigation options. Many options can help in addressing climate change - but no single option is sufficient by itself. Here we focus on the role of carbon capture and storage, now and into the future.

1.1 The role of carbon capture and storage

Carbon Capture and Storage (CCS) includes a range of different technologies, involving various processes for CO_2 capture, separation, transport, storage, and monitoring. These technologies are expected to play a significant role in the global climate response following the ratification of the Paris Agreement for the following reasons:

1) CCS is the only available technology that can significantly reduce emissions from fossil fuel-based power generation that will remain a feature of power production for the foreseeable future.

2) CCS is the only option available to significantly reduce direct emissions from many industrial processes at the large scales needed in the longer term, such as production of steel and cement.

3) Since some “non-zero” sources are unavoidable, CCS will also be needed to deliver "negative emissions" in the second half of the century if these ambitious goals are to be achieved.

In the World Energy Outlook 450 Scenario, which is consistent with a 50% chance of limiting global increase in average temperature to 2 °C in the long term (Figure 2), CCS is increasingly adopted from 2020 and onwards, with deployment accelerating around 2030, and capturing around 5.1 $GtCO_2$ annually by 2040, accounting for one-third of the CO_2 reductions needed (IEA, 2016b). Furthermore, most of the IPCC model assessments that have a better than 50% chance of limiting global increase in average temperature to less than 2°C assume large scale deployment of negative emission technologies in order to stay within the proposed limits (IPCC, 2014).

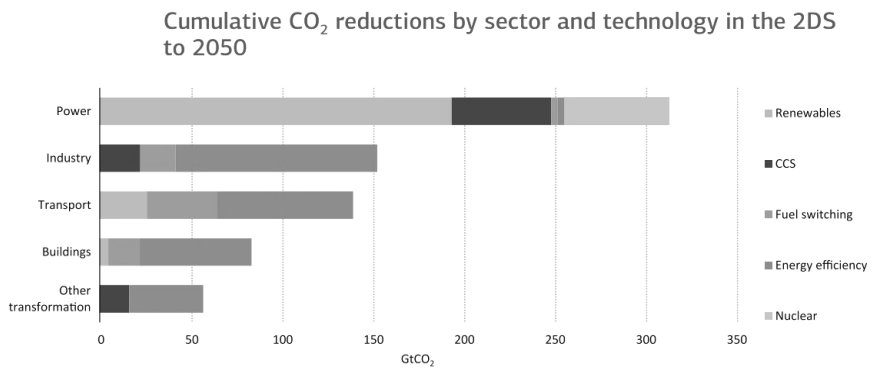

Figure 2. *Cumulative CO_2 reductions by sector and technology in IEA's "450 scenario", which aims on limiting the global increase in average temperature to 2 °C in the long term. This includes further employment of renewables, fuel switching, nuclear power - and extensive deployment of carbon capture and storage. Modified from IEA, (2015).*

The emission goals in Europe aim at reducing GHG emissions by 20% by 2020, and 40% by 2040, compared to the 1990 emissions. The Commission's proposal for a 2030 climate and energy policy framework acknowledges the role of CCS in reaching Europe's emission goals, and states that "CCS may be the only option available" for direct emission reduction from industrial processes on the scale needed in the longer term (European Commission, 2017). The bottom line is that the implementation of CCS will not be optional if the Paris Agreement is to be fulfilled.

Yet, the pace of CCS deployment is a long way from meeting expectations despite the growing recognition by climate experts of its importance as a climate mitigation option (IEA, 2016a; IPCC, 2014b). In 2005, IPCC released an ambitious special report on CCS, where the deployment of CCS is considered of significant importance to reach climate goals (IPCC, 2005). Since then the development of CCS has been slow (Figure 3). For every large-scale CCS project that has been operating since 2010, at least two projects have been cancelled (IEA, 2016a). In 2016 there were 15 large-scale CCS projects in operation around the world with a capture capacity of about 30 $MtCO_2$ per year, which is less than 0.001% of the global CO_2 emissions in that same year (Global Carbon Project, 2017). This year, three large-scale projects in the US are planned to start operation, bringing the capture capacity up to about 40 $MtCO_2$ per year (Global CCS Institute, 2016). This

capture capacity is though trivial compared to the 5.1 $GtCO_2$ that are required to be stored via CCS by 2030 within IEA's "450 scenario" (IEA, 2016a)

After many years of research, development, and rather limited practical experience, it is crucial to shift to a higher gear if CCS is supposed to meet expectations as a true mitigation option. Increased research, development efforts, and commercial demonstrations are essential over the next decade, along with continued deployment of large scale CCS projects already underway. This is extremely important given that CCS is currently the only mitigation option to reduce emissions from point sources.

The priorities for supporting CCS are well-recognised; it requires both identification and characterisation of CO_2 storage resources and the introduction of financial incentives. This includes both investment and targeted financial support for research, development and demonstration of CCS, mapping of storage sites, and other enabling factors, which all needs to begin now (e.g. IEA, 2013). This support is vital for CCS development, aiming at cost reduction for scaled up projects, that is of high importance for its implementation in both industry and power production. The lack of scaled-up of pilot projects also points towards the fact that the incentives already in place are not sufficiently large and long term enough for the projects to be successfully followed through.

Even though cost reductions are important for driving the industry and energy sectors towards implementation of CCS technologies, lower costs alone are not enough. Inadequate legal framework for CO_2 transport and storage, both on- and offshore, is a great inhibitor in the deployment of CCS, which needs to be tackled at governmental level. More importantly, there is no legal framework in place, such as a carbon tax, that penalises large CO_2-emitting sources. The EU emission trading system, which was set up in 2005 as a tool for reducing GHG emissions, has failed dramatically. With the price of carbon set far too low, it has been almost impossible for CCS to compete within a business-as-usual atmosphere.

For the successful deployment of CCS in the coming years there are many challenges that need to be addressed. These require scientific effort and economic support. Lastly, but maybe most importantly, significant steps need to be taken at the governmental level.

1.2 Solving the climate change issue

The world's societies will need to both mitigate and adapt to climate change if they are to effectively avoid or diminish the harmful climate impacts (IPCC, 2014a). The failure of climate change mitigation and adaption is, for the sixth year in a row, considered in the top five impactful risks for the years to come (WEF, 2017). Since before the first IPCC report in 1990 an effort has been made to raise awareness about the urgency of climate change but, without success. In fact, in a survey from 2015 only some 42% of Europeans and Americans considered climate change to be a major threat (PewResearchCenter, 2015).

The scientific community has, up until now, failed in its role of communicating to the public. The message has not been clear – quite the contrary: with technical climate reports filling thousands of pages and where potential climate scenarios are presented as "2DS", "450", and"RCP6.0", the climate problem becomes the problem of scientists. The fact is though, that climate change is neither a problem of scientists, nor the general public. The climate issue will not be solved solely by individuals, and no country will be able to solve it on their own. Voluntary initiatives will not only be insufficient, but insignificant relative to the magnitude of the problem.

It is the role of the scientific community to work on the possible adaption and mitigation options, but solving the climate change issue requires huge effort on the governmental level, otherwise the difficulty and cost of stabilising climate will steadily worsen (IPCC, 2014a). When communities are faced by a threat due to a war, or a natural disaster, it is the role of the governments to take action. The same applies for climate change, one of the greatest environmental challenges facing human kind. Strong government actions are required at international, regional, national, and sub-national scales. International co-operation is critical.

1.3 Mineral storage of carbon in basaltic rocks

The study presented here has been carried out at the Faculty of Earth Science, University of Iceland, and at Lamont Doherty Earth Observatory of Columbia University in New York. It is a part of two larger projects:

1. The CarbFix project - which has the overall objective to develop an industrial solution for mineral storage of CO_2 in basaltic rocks, and in the process to train young scientists to bring this novel knowledge rapidly to future generations.

2. The NORDICCS project – with the overall aim at increasing the deployment of CCS in the Nordic countries, by creating a network integrating research and development capacities, and the relevant industries.

Most of the ongoing CCS-projects are injecting CO_2 into large sedimentary basins where the CO_2 is injected as a separate buoyant phase which is trapped below an impermeable cap rock (e.g. IPCC, 2005). In Iceland an alternative method is being developed as a part of the CarbFix project, where the CO_2 is dissolved in water during, or before injection into porous and fractured basaltic rocks. Because the CO_2 is dissolved it is not buoyant, solubility trapping happens immediately and no cap rock is required. Basalts are very reactive and contain about 25 weight percent of calcium, magnesium, and iron oxides. The CO_2 charged water accelerates metal release and formation of solid carbonates such as calcite, magnesite, and siderite and solid solutions thereof form resulting in long term storage of CO_2 (e.g. Gislason and Oelkers, 2014; Matter et al., 2016; Sigfusson et al., 2015).

The CarbFix project is a collaborative research project founded by Reykjavik Energy, the University of Iceland, Columbia University, and CNRS, in 2007. In 2012, two pilot-scale injections were carried out in Iceland, where 175 tonnes of CO_2 and 73 tonnes of CO_2-H_2S gas mixture were injected, respectively. Extensive geochemical monitoring was carried out prior to, during, and after both injections. After the success of the two pilot scale injections, the project was scaled up in 2014. The scaled-up injection began during June 2014, and is on-going. By the 1st of January 2016, about 6,000 tons of CO_2 had been injected (Gunnarsson et al., *in prep*).

As previously mentioned, one of the priorities for further deployment of CCS is mapping and characterisation of storage resources. One of the objectives of NORDICCS was to create a Nordic CO_2 storage atlas comprising potential storage sites in all the Nordic countries, including the theoretical storage potential of basaltic rocks (NORDICCS, 2015).

The scope of this PhD study is twofold:

1) To evaluate and make a first estimate of the theoretical mineral storage potential of basaltic rocks, both on- and offshore Iceland, and at the ocean ridges.

2) To use geochemical data from the CarbFix injection site in Hellisheiði, SW-Iceland to characterize the mineralisation process.

The results are presented in following research articles:

I. **Snæbjörnsdóttir, S.Ó.**, Wiese F., Fridriksson Th., Ármansson H., Einarsson G.M., Gislason S.R., 2014. CO_2 storage potential of basaltic rocks in Iceland and the oceanic ridges. Energy Procedia Volume 63, 2014, pages 4585-4600.

II. **Snæbjörnsdóttir**, **S. Ó**., Gislason, S. R. CO_2 storage potential of basaltic rocks offshore Iceland. Energy Procedia, Volume 86, 2016, pages 371-380.

III. Matter J.M, Stute M., **Snæbjörnsdóttir S.Ó**., Oelkers E.H., Gislason S.R., Aradottir E.A., Sigfusson B., Gunnarsson I., Sigurdardottir H., Gunnlaugsson E., Axelsson G., Alfredsson H.A., Wolff-Boenisch D., Mesfin K., Fernandez de la Reguera Taya D., Hall J., Dideriksen K., Broecker W.S. (2016). Rapid carbon mineralization for permanent disposal of anthropogenic carbon dioxide emissions. Science 352, 1312-1314.

IV. **Snæbjörnsdóttir, S.Ó.**, Oelkers, E.H., Mesfin, K., Aradóttir, E.S., Dideriksen, K., Gunnarsson, I., Gunnlaugsson, E., Matter, J.M., Stute, M., Gislason, S.R. (2017). The chemistry and saturation states of subsurface fluids during the in situ mineralisation of CO_2 and H_2S at the CarbFix site in SW-Iceland. International Journal of Greenhouse Gas Control 58, 87–102.

V. **Snæbjörnsdóttir S. Ó.**, Gislason S.R., Galeczka M.I., Oelkers E.H. (2017). Reaction path modelling of *in situ* mineralisation of CO_2 at the CarbFix site in SW-Iceland. *Manuscript prepared for submission to Geochimica et Cosmochimica Acta.*

References

Church, J.A. and White, N.J. (2006) A 20th century acceleration in global sea level rise. Geophysical Research Letters 33.

Cook, J., Oreskes , N., Doran, P.T., Anderegg, W.R.L., Verheggen, B., Maibach, E., W., Carlton, J.S., Lewandowsky, S., Skuce, A.G., Green, S.A., Nuccitelli, D., Jacobs, P., Richardson, M., Winkler, B., Painting, R. and Rice, K. (2016) Consensus on consensus: a synthesis of consensus estimates on human-caused global warming. Enviornmental Research Letters 11.

European Commission (2017). Carbon Capture and Gelogical storage. https://ec.europa.eu/clima/policies/lowcarbon/ccs_en. Webpage accesseed on the 6th of March 2017.

Gislason, S.R. and Oelkers, E.H. (2014) Carbon Storage in Basalt. Science 344, 373-374.

Global Carbon Project (2017). Global carbon budget. http://www.globalcarbonproject.org/carbonbudget/16/highlights.htm. Webpage accessed on the 2nd of March 2017.

Global CCS Institute (2016). The global Status of CCS 2016. Summary Report. Melbourne, Australia.

Gunnarsson, I., Aradóttir, E.S., Oelkers, E.H., Clark, D.E., Arnarsson, M.T., Sigfusson, B., Snæbjörnsdóttir, S.Ó., Matter, J.M., Stute, M., Júlíusson, B.M. and Gislason, S.R. Rapid and cost-effective capture and subsurface mineral storage of carbon and sulphur. *In preperation.*

Caldeira, K. and Wickett, M.E. (2003) Oceanography: Anthropogenic carbon and ocean pH. Nature 425.

IEA (2013) International Energy Agency. Technology roadmap: Carbon capture and storage. IEA, Paris, France.

IEA (2015) Energy Technology Perspectives 2015 - Mobilising Innovation To Accelerate Climate Action. International Energy Agency, Paris, France.

IEA (2016a) 20 years of carbon capture and storage - Accelerating future deployment. International Energy Agency, Paris, France.

IEA (2016b) World Energy Outlook 2016 - Executive summary. International Energy Agency, Paris, France.

IPCC (2005) Carbon Dioxide Capture and Storage (SRCCS). Bert Metz, Ogunlade Davidson, Heleen de Coninck, Manuela Loos, Meyer, L. (Eds.), Cambridge, United Kingdom, and New York, USA.

IPCC (2014a) Climate Change 2014: Mitigation of Climate Change. Contribution of Working Group III to the Fifth Assessment. Edenhofer, O., R. , Pichs-Madruga, r., Sokona, Y., Farahani, E., Kadner, S., Seyboth, K., Adler, A., Baum, I., Brunner, S., Eickemeier, P., Kriemann, B., Savolainen, J., Schlömer, S., von Stechow, C., Zwickel T., Minx, J.C. (Eds.). International Panel on Climate Change, Cambridge, United Kingdom, and New York, USA.

IPCC (2014b) Contribution of Working Groups I, II and III to the Fifth Assessment Report of the Intergovernmental Panel on Climate Change, in: Pachauri, R.K., Meyer, L.A. (Eds.), Synthesis Report. , Geneva, Switzerland.

Marzeion, B., Cogley, J.G., Richter, K. and Parkes, D. (2014) Attribution of global glacier mass loss to anthropogenic and natural causes. Science 345, 919-921.

Matter, J.M., Stute, M., Snæbjörnsdóttir, S.Ó., Oelkers, E.H., Gislason, S.R., Aradottir, E.S., Sigfusson, B., Gunnarsson, I., Sigurdardottir, H., Gunnlaugsson, E., Axelsson, G., Alfredsson, H.A., Wolff-Boenisch, D., Mesfin, K., Fernandez de la Reguera Taya, D., Hall, J., Dideriksen, K. and Broecker, W.S. (2016) Rapid carbon mineralization for permanent and safe disposal of anthropogenic carbon dioxide emissions. Science 352, 1312-1314.

NASA (2017a) Scientific consensus: Earth's climate is warming. https://climate.nasa.gov/scientific-consensus . Webpage accessed on the 24th of February 2017.

NASA, N. (2017b) NASA, NOAA Data Show 2016 Warmest Year on Record Globally, https://www.nasa.gov/press-release/nasa-noaa-data-show-2016-warmest-year-on-record-globally. Webpage accessed on the 24 th of February 2017.

NOAA (2017a) Trends in atmospheric Carbon Dioxide. http://www.esrl.noaa.gov/gmd/ccgg/trends/full.html. Webpage accessed on the 24 th of February 2017.

NOAA (2017b) U.S. Climate Extrenes Index (CEI): https://www.ncdc.noaa.gov/extremes/cei/regional-overview. Webpage accessed on the 24 th of February 2017.

NORDICCS (2015) The Nordic CO_2 storage atlas: https://data.geus.dk/nordiccs/map.xhtml. Webpage accessed on the 12th of March 2017.

The NordicPewResearchCenter (2015) Climate Change Seen as Top Global Threat: www.pewglobal.org/2015/07/14/climate-change-seen-as-top-global-threat/. Webpage accessed on the 6th of March 2017.

Sigfusson, B., Gislason, S.R., Matter, J.M., Stute, M., Gunnlaugsson, E., Gunnarsson, I., Aradottir, E.S., Sigurdardottir, H., Mesfin, K.G., Alfredsson, H.A., Wolff-Boenisch, D., Arnarson, M.T. and Oelkers, E.H. (2015) Solving the carbon-dioxide buoyancy challenge: The design and field testing of a dissolved CO_2 injection system. Int. J. Greenhouse Gas Control 37, 213-219.

United Nations/ Framework Convention on Climate Change, (2015). Adoption of the Paris Agreement, 21st Conference of the Parties, Paris: United Nations

Watkins, M., Wiese, D.N., Yuan, D.-N., Boening, C. and Landerer, F.W. (2015) Improved methods for observing Earth's time variable mass distribution with GRACE using spherical cap mascons. J. Geophys. Res. Solid Earth 120, 2648-2671.

WEF (2017) The Inclusive Growth and Development Report 2017. World Economic Forum, Geneva, Switzerland.

Paper I

CO_2 storage potential of basaltic rocks in Iceland and the oceanic ridges

Snæbjörnsdóttir, S.Ó., Wiese, F., Fridriksson, Th., Ármannsson, H., Einarsson, G.M., Gislason, S.R., 2014. Energy Procedia, volume 63, pages 4585-4600. *DOI:10.1016/j.egypro.2014.11.491*

Available online at www.sciencedirect.com

ScienceDirect

Energy Procedia 63 (2014) 4585 – 4600

Energy Procedia

GHGT-12

CO_2 storage potential of basaltic rocks in Iceland and the oceanic ridges

Sandra Ó. Snæbjörnsdóttir[a]*, Frauke Wiese[b], Thrainn Fridriksson[b], Halldór Ármansson[b], Gunnlaugur M. Einarsson[b], Sigurdur R. Gislason[a]

[a]*Institute of Earth Sciences, University of Iceland, Askja, Sturlugata 7, Reykjavik 101, Iceland*
[b]*ISOR, Iceland GeoSurvey, Grensásvegur 9, Reykjavik 108, Iceland*

Abstract

Iceland is the largest landmass found above sea level at the mid-ocean ridges, about 103,000 km^2 mostly made of basaltic rocks (~90%). Theoretically much of Iceland could be used for injection of CO_2, fully dissolved in water. Most of the pore space in the older rocks is filled with secondary minerals, thus the young and porous basaltic formations, found within the active rift zone and covering about one third of Iceland, are the most feasible for carbon storage onshore.

Studies on mineral storage of CO_2 in basaltic rocks are still at an early stage. Therefore, natural analogues are important for gaining a better understanding of CO_2 fixation in basaltic rocks. Volcanic geothermal systems serve as an applicable analogue since the systems receive considerable amounts of CO_2 from magma in the roots of the systems. Wiese et al. [1] quantified the amount and spatial distribution of CO_2 stored as calcite within the bedrock of three active geothermal systems in Iceland. The results from this study reveal a large storage potential of basaltic rocks and can be used as a guideline for the theoretical potential of CO_2 storage in basaltic formations. The largest storage potential lies offshore, with long-term advantages for safe and secure CO_2 storage in the mid-ocean ridges. The theoretical mineral CO_2 storage capacity of the ocean ridges, using the Icelandic analogue, is orders of magnitude larger than the anticipated release of CO_2 caused by burning of all fossil fuel on Earth.

Peer-review under responsibility of the Organizing Committee of GHGT-12

Keywords: Carbon storage, basalt, mineral storage, CarbFix, oceanic ridges

* Corresponding author. Tel.: +354-525-4495; fax: +354-525-4499
E-mail address: sos22@hi.is

Peer-review under responsibility of the Organizing Committee of GHGT-12
doi:10.1016/j.egypro.2014.11.491

1. Introduction

The reduction of CO_2 emissions to the atmosphere is one of the greatest challenges of this century. One solution to this is carbon capture and storage. Therefore, identifying locations for secure CO_2 storage is one of the most pressing scientific problems of our time. Injection of CO_2 into basaltic formations provides significant advantages including permanent storage by mineralisation and a great potential storage volume [2-4].

To date, most subsurface carbon storage projects have injected CO_2 as a separate, buoyant phase into large sedimentary basins; a method that requires high integrity cap-rock for long term storage [4, 5]. Some of the risks associated with CO_2 buoyancy can be mitigated by its dissolution into water during injection [6, 7]. Once dissolved, CO_2 is no longer buoyant, making it possible to inject into fractured rocks, such as the basalts along the ocean ridges.

Basaltic rocks are rich in divalent cations (e.g. Ca^{2+}, Mg^{2+} and Fe^{2+}). The CO_2-charged water accelerates metal release and the formation of solid carbonate minerals such as Calcite ($CaCO_3$), Magnesite ($MgCO_3$) and Siderite ($FeCO_3$) for long term storage of CO_2 [4, 6, 8, 9].

Iceland is the largest (103,000 km^2) landmass found above sea level at the mid-ocean ridges, made mostly (~90%) of basaltic rocks. Carbon capture and storage experiments conducted in Iceland can be used as analogues, along with natural analogues, for carbon storage along the ocean ridges. Theoretically much of Iceland could be used for injection of CO_2, fully dissolved in water. Most of the pore space in the older rocks is filled with secondary minerals, diminishing the transmissivity of the potential injection wells. Thus the young and porous basaltic formations, found within the active rift zone and covering about one third of Iceland, are the most feasible for carbon storage onshore.

2. Mineral storage potential of CO_2 in basaltic rocks

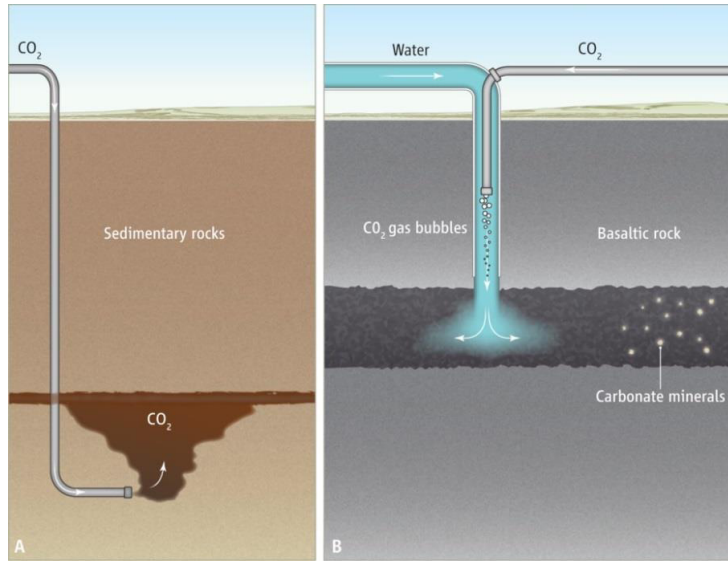

Fig. 1. Carbon storage in sedimentary basins and basaltic rocks. (A) Carbon storage in sedimentary basins; CO_2 is injected as a separate buoyant phase and is trapped below an impermeable cap rock. (B) In the CarbFix method, CO_2 is dissolved into water during its injection into porous basaltic rocks. No cap rock is required because the dissolved CO_2 is not buoyant and does not migrate back to the surface. Figure from Gislason and Oelkers, [4].

There are two ways of injecting CO_2 into rocks for geological storage. In the most common method (Fig. 1A) pure compressed CO_2 is injected as a separate buoyant phase into porous rock layers, such as sandstone or basalt, at more than 800 m depth; it is anticipated that the presence of an impermeable layer will keep the CO_2 from escaping back to the surface (structural trapping) (Fig. 2). Eventually some of this CO_2 becomes trapped in small pores, limiting its mobility (residual trapping). Over time, the CO_2 dissolves in the formation water (solubility trapping). Some of this dissolved CO_2 reacts to form stable carbonate minerals (mineral trapping). As the progress goes from structural to mineral trapping, the CO_2 becomes more immobile and thus the storage more secure. However, this process can take thousands of years or more [10, 11].

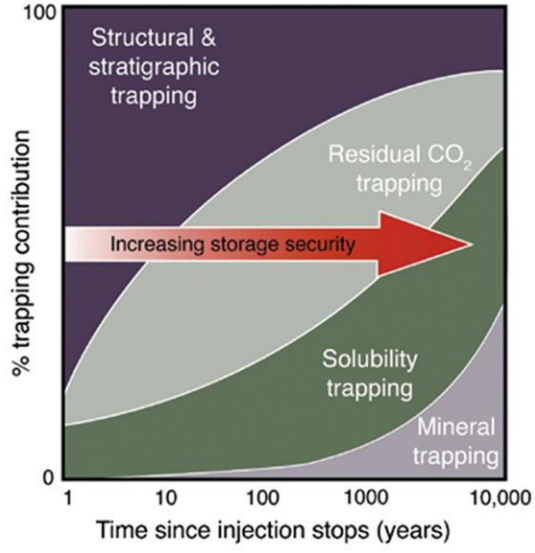

Fig. 2. A general representation by S. Bensson of the evolution of trapping mechanism of CO_2 over time when injected as a separate buoyant phase [10]. When CO_2 is dissolved in the water prior or during injection solubility trapping occurs immediately and the bulk of the carbon is mineralized within few years [4, 7, 12, 13].

In Iceland an alternative method is being tested, in a project called CarbFix (www.carbfix.com), where the CO_2 is dissolved during injection into porous basaltic rock (Fig. 1B). CO_2 is aspirated into down-flowing water within the injection well at 350 m depth. The CO_2 bubbles dissolve in the water before it enters the rock. Once dissolved in water, CO_2 is no longer buoyant and does not migrate back to the surface. The CO_2-charged water accelerates both the metal release from the basalt and subsequent formation of solid carbonate minerals. Solubility trapping occurs immediately, and the bulk of the carbon is trapped in minerals within few years [4, 7, 12, 13]. Once stored as a mineral, the CO_2 is immobilised for geological time scales [4, 6, 9].

In addition to CarbFix, one other field injection project is ongoing, assessing the feasibility of carbon storage in basalts; the Big Sky Carbon Sequestration Partnership (BSCP) in north-western USA, near Wallula, Washington [14, 15]. In the BSCP project, pure CO_2 is injected as a separate buoyant phase into a porous basaltic layer, anticipating that the presence of an impermeable layer will keep the CO_2 from escaping back to the surface.

3. Geological settings of Iceland

Iceland is one of the most active and productive sub-areal volcanic regions on Earth with magma output rates of more than five km^3 per century [16]. The most voluminous volcanism on the Earth occurs at the mid-ocean ridges where total magma production is about 400 times greater than in Iceland. Seafloor spreading generates about 20 km^3 per year of mid ocean ridge basalt (MORB) which is one of the dominant volcanic rock types on Earth [e.g. 17].

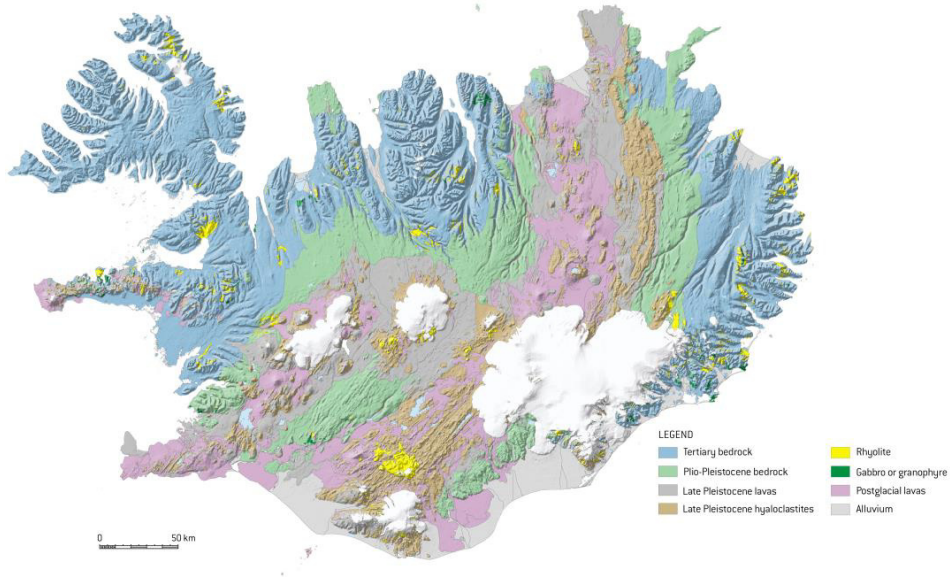

Fig. 3. Map based on Geological map of Iceland [18]. Iceland, 1:1.000.000. Icelandic Institute of Natural History.

The Iceland basalt plateau rises more than 3000 m above the surrounding sea floor and covers about 350,000 km^2 [16]. Iceland itself is 103,000 km^2, mostly made of young 0-20 M yr. igneous rocks and sediments thereof. Approximately 90% of the bedrock in Iceland is basalt (Fig. 3) indicating that theoretically much of Iceland could be used for injecting CO_2, fully dissolved in water, into basaltic rocks.

Studies on the permeability and porosity of Icelandic bedrock show that porosity and permeability generally decrease with progressive alteration, gradual burial and increasing rock age since most of the pore space in the older rocks is filled with secondary minerals [19, 20]. Thus, the youngest basaltic formations, found in the active rift zone, are the most feasible for carbon storage onshore in Iceland. These basalt formations consist of lavas, hyaloclastic (glassy) formations and associated sediments younger than 0.8 M yr covering about one third of Iceland.

4. Key parameters for mineral storage of CO_2

Mineral carbonation requires combining CO_2 with divalent metal cations to form carbonate minerals, such as calcite ($CaCO_3$), dolomite ($CaMg(CO_3)_2$), magnesite ($MgCO_3$), siderite ($FeCO_3$), and Ca-Mg and Mg-Fe carbonate solid solutions [4, 8].

With few exceptions, the required metals are divalent cations, including Ca^{2+}, Mg^{2+} and Fe^{2+}. The availability of divalent metal cations for carbonate precipitation is enhanced by rapid dissolution rates of Ca,Mg,Fe-rich silicate rocks such as basaltic and ultramafic rocks. These dissolution rates can be enhanced in several ways including increasing the mineral-fluid interfacial surface area, injecting into glassy rather than crystalline rocks, and choice of temperature/injection fluid composition. These enhancement methods are described in detail in Gislason et al. [6, 9].

The most abundant cation sources for mineral storage of CO_2 are silicate minerals and glasses [6, 21]. Basalt contains about 25% by weight of calcium, magnesium, and iron oxides [22, 23]. Basaltic rocks are reactive in water, thus the metals contained in basalts are readily available to combine with the injected CO_2 to form carbonate minerals [6, 22, 24, 25, 26, 27, 28].

Basaltic rocks are abundant at Earth's surface; a little less than 10% of the continents and much of the ocean floor is composed of basalt [6, 29, 30].

Whilst the availability of divalent metal cations remains the limiting factor for mineral storage of CO_2 it is not the only concern. For successful injection and mineral carbonation, other key parameters must also be considered.

4.1. Availability of water for injection

Mineral storage of CO_2 via the CarbFix method requires a substantial amount of water. The water demand to fully dissolve one ton of CO_2 at 25 bar pressure and 25°C is 27 tons of pure water. About 4% of the injected mass is CO_2. The CO_2 solubility increases, and thus the amount of water required for its dissolution decreases, by elevating the CO_2 partial pressure and lowering the temperature [6].

On the continents, the water present in the target storage formation can be pumped up and used to dissolve the CO_2 during the injection. Although the pumping of water from the subsurface may increase costs, water pumping is also necessary during the later stages of pure CO_2 injection into sedimentary basins, when a large portion of the pore space has been filled with CO_2.

The amount of water required could pose a problem in some areas, for example in places with insufficient ground water sources, low recharge rates or inefficient water management. In some cases seawater might be the only viable option. Porous basalts near the continental margins have enormous storage capacities adjacent to nearly unlimited supplies of seawater [31]. The CO_2 solubility decreases by about 10% at elevated partial pressure of CO_2 and therefore the amount of water required for its dissolution increases by 10% at seawater salinity.

The basaltic ocean ridges are porous and vast amounts of seawater are circulated annually through them by natural processes. Every year, about 100 Gton of water is circulated through the oceanic ridges; this is about three time's greater than the present mass of anthropogenic release of CO_2 to the atmosphere [32, 33].

Dissolution of basalt, basaltic glass and peridotite in seawater has been studied to some extent [25, 34]. The results show that dissolution of CO_2 into seawater prior to or during injection appears to be a promising approach but further modelling and experimental work is required to refine the concept.

4.2. Temperature

The release of the divalent cations needed from glassy basaltic rocks for carbonate formation can be enhanced by raising the temperature. Increasing the temperature from 0 to 100°C, at pH 3.5 and fixed total concentration of dissolved aluminum (10^{-6} mol/kg), increases dissolution rates by a factor of 60. The same temperature increase, at pH 9, results in a 4.5 order of magnitude increase in rates [35]. The dissolution rates of the secondary minerals present in altered basaltic rocks, such as zeolites and clays, are also raised at elevated temperature. They become unstable in the CO_2-charged injection waters resulting in their dissolution and thereby creating additional porosity in the near vicinity of injection wells [23]. The temperature can be raised by increasing the depth of injection wells and/or drilling into areas of high geothermal gradients.

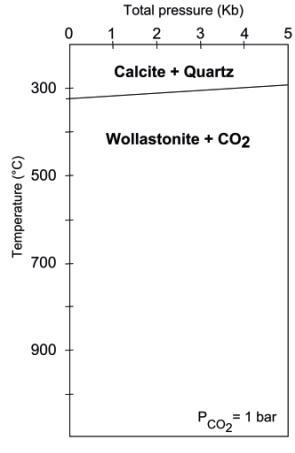

Fig. 4. Simple, thermodynamic system of calcite (Cc), quartz (Q) and wollastonite (Wo); total pressure (Kb) vs. temperature at fixed CO_2 pressure of 1 bar. Modified figure from Skippen et al. [36].

The lower boundary for mineral storage of carbon in basalt is dictated by the thermal gradient and the thermodynamic stability of carbonates such as calcite rather than the availability of divalent cations from the dissolution of basaltic rocks. At high temperatures the primary porosity of reactive rocks and therefore reactive surface area tend to decrease and the solubility of carbon dioxide in water decreases with increasing temperature.

The thermodynamic stability of carbonates is limited at temperature in excess of 300°C. Observations of hydrothermally altered basaltic rocks from Iceland show that calcite does not form at temperatures above 290°C [e.g. 37]. This finding is in a good agreement with thermodynamic data [36] as shown in Fig. 4 for the simplified calcite, quartz and wollastonite system.

Geothermal systems in Iceland typically have a thermal gradient above 200°C/km and a very similar overall pattern of calcite distribution has been reported by Wiese et al. [1] and Tómasson and Kristmannsdóttir [38] showing that, with some exceptions, generally below about 1000-1500 m depth very little calcite is present.

In terms of temperature, mineral storage of CO_2 could theoretically be executed at depths greater than 1500 m in basaltic rocks outside of the geothermal systems where carbonates remain stable at greater depths due to a lower temperature gradient, but other factors like decreased porosity and permeability with increased depth would have to be considered for it to be beneficial.

4.3. The partial pressure of CO_2

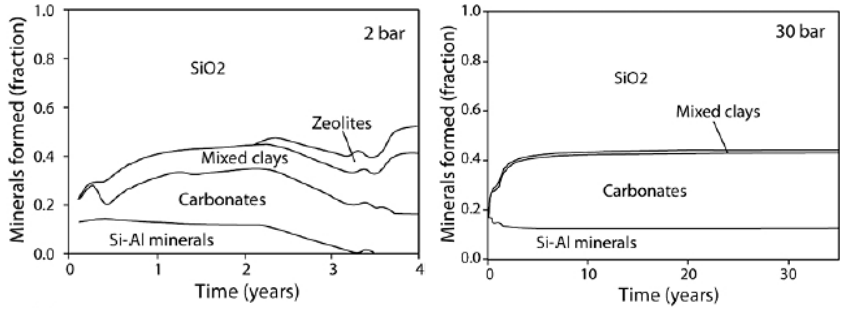

Fig. 5. The results of reaction progress modelling of basaltic glass-CO_2-water interactions. Mole fractions of secondary minerals formed as a function of reaction progress for groundwater in contact with basaltic glass saturated at 25 °C with 2 and 30 bars CO_2 pressure. Carbonate fraction increases relative to clays and zeolites with increasing pCO_2. Figure from Gysi and Stefansson, [39].

Thermodynamic model calculations suggest that elevated partial pressure of CO_2 will enhance the efficiency of carbon mineralisation as shown in Fig. 5 [39, 40].The higher the partial pressure of CO_2 the higher the fraction of released divalent cations that precipitate as carbonates rather than zeolites and clays.

Natural analogues for CO_2 injection into basaltic rocks at moderate temperature in West-Greenland suggest that at relatively high partial pressure of CO_2, Fe and Mg rich carbonates are stable; at intermediate CO_2 pressure Mg-Ca carbonates dominate and at the lowest partial pressure Ca-carbonates are most common [41].

4.4. Porosity, Permeability

Studies on permeability and porosity show that generally porosity and permeability decrease along with progressive alteration, gradual burial and increasing age. The oldest bedrock in Iceland, in NW- and E-Iceland, is so dense it is almost impermeable (Fig. 6). The permeability increases towards the active rift zone where the rocks are younger. The youngest formations in the active rift are made of highly porous and permeable basaltic lavas and hyaloclastic (glassy) formations with abundant groundwater flow [43].

Hydrothermal alteration and formation of secondary minerals takes place when the rocks are buried under younger formations and are then exposed to more heat and pressure. Most of the pore space in the older rocks is filled since the molar volume of secondary minerals is larger than the molar volume of primary minerals and some

secondary minerals contain water and CO_2. Gradual burial of the strata also causes compression on the underlying layers making them even less permeable [e.g. 19, 20].

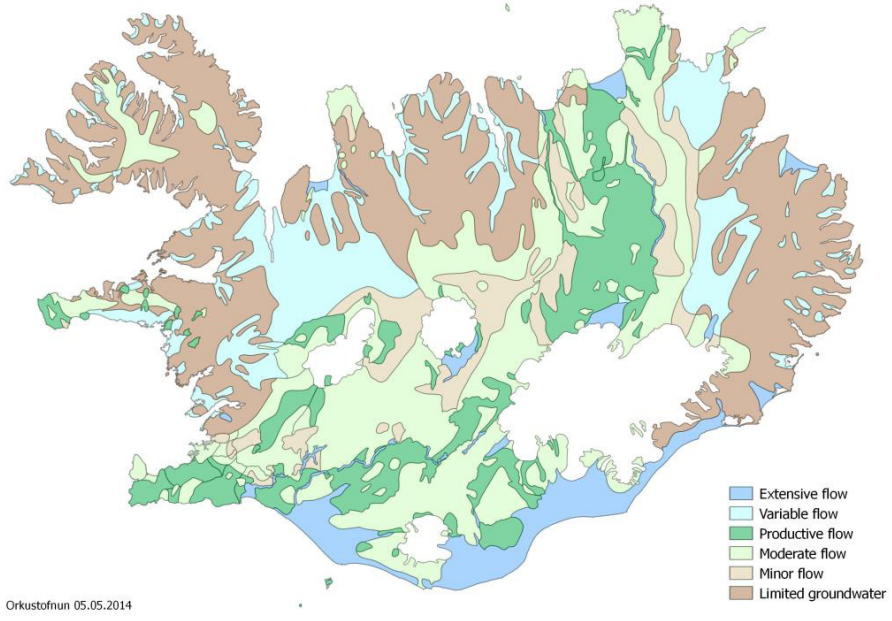

Fig. 6. Map based on hydrogeological map of Iceland from Hjartarson [42]. The most permeable rocks are situated within the active rift zone (blue and green colors). The permeability decreases towards the older formations, the oldest formations situated in the NW and E parts of Iceland (brown colors) are nearly impermeable. Prepared by the National Energy Authority.

Since 1992 the National Energy Authority of Iceland and later the Iceland GeoSurvey have carried out systematic sampling of fresh to highly altered igneous rocks of variable composition in order to define the petro-physical properties of Icelandic bedrock [e.g. 20, 44, 45]. The average permeability of the basaltic lava samples was measured to be 367 mD. The average porosity of the lavas was measured to be 8.09 %, however, the porosity of the unaltered lavas was measured to be 27.8% but as soon as secondary minerals started to appear the porosity dropped below 7% and was measured to be 6.13% in samples of highly altered basaltic lavas (Table 1).

Hyaloclastites are clastic, glassy rocks formed dominantly in sub-glacial phreatic eruptions. Hyaloclastic formations are extremely heterogeneous and show very broad variation both in porosity and permeability (Table 2). Frolova et al. (2004) analysed 80 samples of basaltic hyaloclastic tuffs of variable burial depth (0-1000 m) and age (>2.5 M yr). The porosity of the samples analysed varied between 14 and 57% and permeability between $1*10^{-3}$ mD to $6.4*10^{3}$ mD. The wide dispersion is mainly the result of different degree of alteration, with a general decrease both in porosity and permeability with increasing depth, although some exceptions are present.

These results establish the large effect alteration and formation of secondary minerals have both on porosity and permeability of both crystalline basalt and glassy formations. The most feasible formations for carbon storage onshore in Iceland are situated within the active rift zone where the basaltic rocks are young and still porous and normal faults are common. These formations are younger than 0.8 M yr. and cover about 34,000 km^2, which is about one third of Iceland.

It should be noted that the initial porosity and permeability of the bedrock prior to injection of dissolved CO_2 will be affected. As stated before, secondary minerals, such as zeolites and clays, present in altered basaltic rock become

unstable in the CO_2-charged injection waters resulting in their dissolution and thereby creating additional porosity in the near vicinity of injection wells [23].

Table 1. The effect of alteration on the porosity of basaltic lavas from Stefánsson et al. [45]

	Average porosity (%)	# of samples
All samples	8.09	108
Unaltered lavas	27.8	9
Smectite-zeolte alteration (alteration temperatures below 200°C)	6.69	31
Chlorite-epidote-actinolite alteration (alteration temperatures above 200°C)	6.13	56

Table 2. The average porosity and permeability of the main rock types in Iceland and the range in porosity and permeability measured in 80 samples of hyolaclastic tuffs.

	# of samples	Average porosity (%)	Standard Deviation	Average permeability, Klinkenberg (mD)	Standard deviation
Basltic lavas[1]	52	8.09	9.14	3.75	14.67
Basalt intrusions[1]	19	3.68	3.71	0.157	0.263
Acid rocks[1]	20	12.09	6.39	0.028	0.044
Hyaloclastic formations[2]	80	14-57		$1*10^{-3}$-$6.4*10^{3}$	

Data from Stefánsson et al.[1] [45] and Frolova[2] [20].

4.5. Depth

The minimum depth for injection of CO_2 using the CarbFix method is dictated by dissolution of CO_2 and water demand for injection. The CO_2 has to be dissolved at minimum pressure of 25 bars, which is 250 m below the water table, and some distance is needed for the descending CO_2-gas-bubbles to dissolve [6, 7]. The ideal depth for injection of CO_2 is therefore below 350 m.

Geothermal systems typically have a thermal gradient above 200°C/km compared to 50 to 150°C/km in dense and permeable rocks outside of them [43]. Defining the lower boundary for mineral storage of carbon at 1500 m depth allows inclusion of the areas with the highest thermal gradient, considering that stability of carbonates is limited at temperature in excess of 300°C, and therefor gives a rather conservative estimate of the storage potential. The benefit of injecting deeper than at 1500-2000 m is uncertain due to the rapid decrease of permeability with depth and temperatures over 300°C in areas with high temperature gradient. The targeted depth range for injection of fully dissolved CO_2 into basaltic rocks is therefore 500-1500m.

When injecting into high-temperature geothermal systems with steep thermal gradients it is important to stay below the liquid-vapour curve for water to prevent boiling.

4.6. Risk of contamination of groundwater

The reaction between the CO_2-charged water and the basaltic rocks not only releases divalent cations that end up in carbonates, but also other metals that can be harmful for the biota. The metals of main concern are Al and Cr, but some other elements, such as Fe and Mn, can be both essential for life and toxic depending on their concentration. The toxic metal release is the most dangerous at the early stage of CO_2 injection into basalt [46-48]. Natural analogues have shown the secondary minerals, such as carbonates, effectively scavenge the potential toxic metals that are released at early stages [46, 48].

A novel high pressure column reactor [49] was used to study the mobility of metals at the early stage (hours) of CO_2 injection into basalt. Dissolved Al, Fe, Cr and Mn exceeded the allowable drinking water limits according to the European Directive relating to the quality of the water intended for human consumption [47, 50].

Samples analysed from monitoring wells after injection of 175 tons of CO_2 at the CarbFix site in Hellisheiði, SW-Iceland showed that no dissolved metals exceeded the allowed drinking water limits during the field experiment.

5. Natural analogues for mineral storage of CO_2

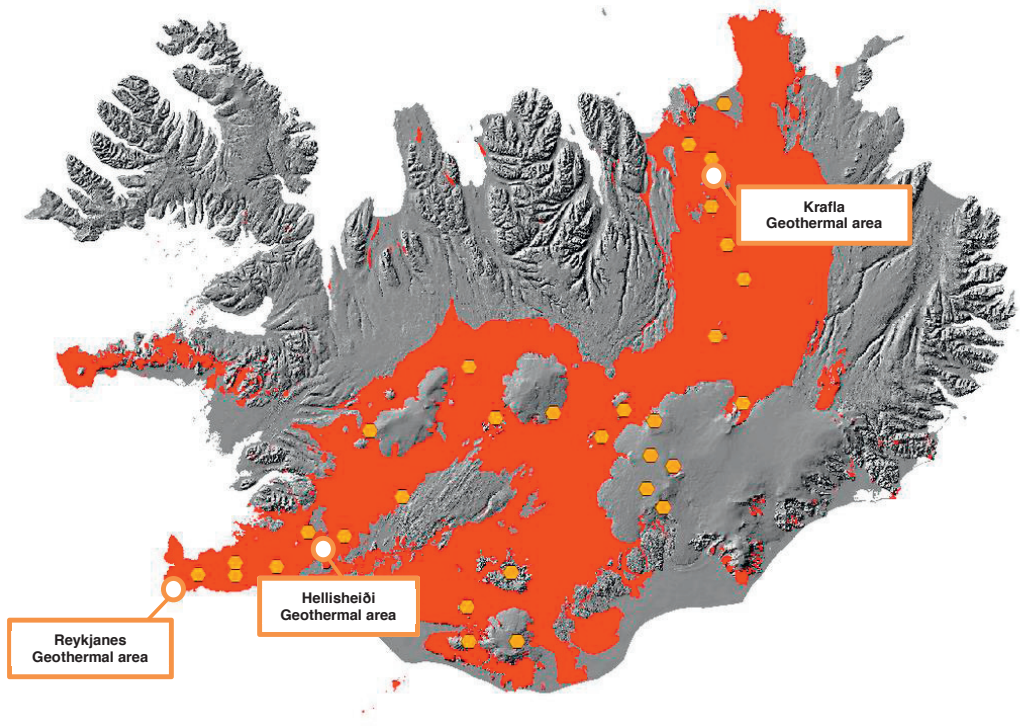

Fig. 7. Theoretical area feasible for CO_2 mineral storage in Iceland: Basaltic formations younger than 0.8 M yr within the active rift zone. Volcanic geothermal systems are marked with white dots but they serve as an applicable analogue as they receive considerable amounts of CO_2 from magma chambers or intrusion in their roots. High-temperature geothermal systems studied by Wiese et al. [1] are marked with white dots.

Studies on mineral storage of CO_2 in basalts are still at an early stage [e.g. 4, 23, 51]. Therefore, natural analogues are important for gaining a better understanding of CO_2 fixation in basaltic rocks. Volcanic geothermal systems serve as an applicable analogue; the systems receive considerable amounts of CO_2 from magma chambers or intrusions at the roots of the systems and can therefore be considered as a natural experiment to determine the CO_2 storage capacity of the bedrock [1, 52].

The large amounts of CO_2 that are already naturally fixed within the geothermal systems underscore the storage potential of basaltic rocks. Wiese et al. [1] estimate that the total CO_2 fixed within the active geothermal high-temperature systems in Iceland shown by orange dots in Fig. 7 amounts to 30-40 $GtCO_2$.

Wiese et al. [1] quantified the amount and spatial distribution of CO_2 stored in calcite within the bedrock of three active geothermal systems in Iceland: Krafla in the north-east of Iceland and Hellisheiði and Reykjanes in the south-west (Fig 7.). The CO_2 content was measured in 642 drill cutting samples from a total of 40 wells, located in the three geothermal systems.

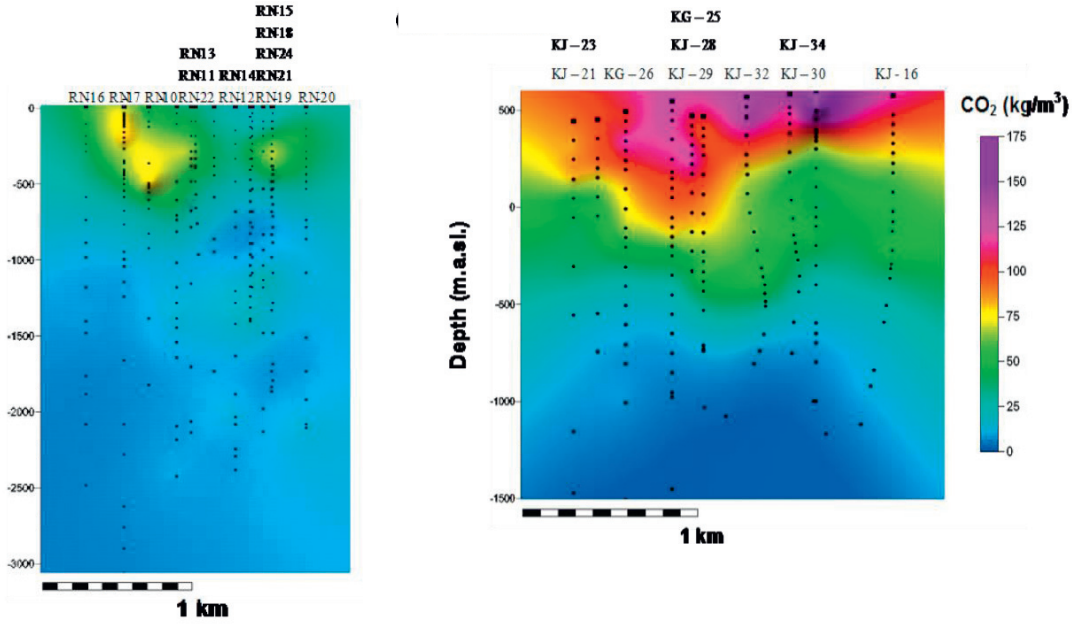

Fig. 8.Cross-sections extending from west to east (looking north) showing the distribution of CO_2 fixed in the bedrock at Reykjanes (left) and Krafla (right) geothermal systems. Concentration of fixed CO_2 is indicated by different colors, see bar for scale (From Wiese et al. [1]).

The values measured in the Reykjanes geothermal system, which is considered to be the youngest of the three geothermal systems (active for 10,000-100,000 years), were significantly lower than elsewhere in this study, on average 28.2 tons of CO_2 per m^2 of surface area fixed in the uppermost 1500 m of the wells. The average CO_2 load in the uppermost 1500 m in Hellisheiði geothermal system was measured 65.7 tons per m^2 of surface area. The highest values are measured in the Krafla geothermal system, which is considered to have been active for the longest, between 110,000 and 290,000 years, on average 73.1 tons of CO_2 per m^2 of surface area in the uppermost 1500 m [1] (Table 3, Fig. 8).

The amount of CO_2 fixed in the bedrock of the three geothermal systems obtained from this study can be used as a guideline for the theoretical CO_2 storage potential in onshore basaltic formations in Iceland.

Table 3.Average CO_2 load (tons/m^2 of surface area and kg/m^{-3}) and suggested age (years of activity) of the three geothermal systems of interest (from Wiese et al. [1])

	CO_2 fixed in uppermost 1500 m per unit surface area (tons/m^2)	CO_2 fixed in uppermost 1500 m (kg/m^{-3})	Activity of Geothermal system (years)
Reykjanes	28.2	18.8	10.000-100.000
Hellisheiði	65.7	43.8	>70.000*
Krafla	73.1	48.7	110.000-290.000

*Franzson, et al. [53]

5.1. Storage potential of the Icelandic rift zone

The active rift zone covers about 34,000 km^2, or about one third of Iceland (Fig. 9). By using the average CO_2 load in the uppermost 1500 m of the Reykjanes system as a minimum and the average CO_2 load in the uppermost 1500 m of the Krafla system as a maximum (Table 3) and applying these to a 1000 m thick segment at 500-1500 m

depth, of the relatively fresh basaltic formations within the rift zone yields a very large value; 2,470 Gt of CO_2 as a maximum (Krafla analogue) and 953 Gt as a minimum (Reykjanes analogue). This scenario is highly theoretical but underscores the large mineral storage potential within the rift zone of Iceland where the rocks are young and still porous and normal faults are common.

Other attempts have been made to estimate the capacity for mineral storage of CO_2 in basalt. McGrail et al. [2] estimated that the Colombia River basalts alone have the capacity to store over 100 Gt of CO_2, assuming an interflow thickness of 10 m, average porosity of 15% and 10 available interflow zones at an average hydrostatic pressure of 100 atm. Anthonsen et al. [54] applied McGrail's assumptions to all the bedrock of Iceland, giving an estimated capacity of about 60 Gt CO_2. Using the same assumption to calculate the potential capacity of mineral storage of CO_2 within the active rift zone in Iceland the number goes down to about 21 Gt CO_2.

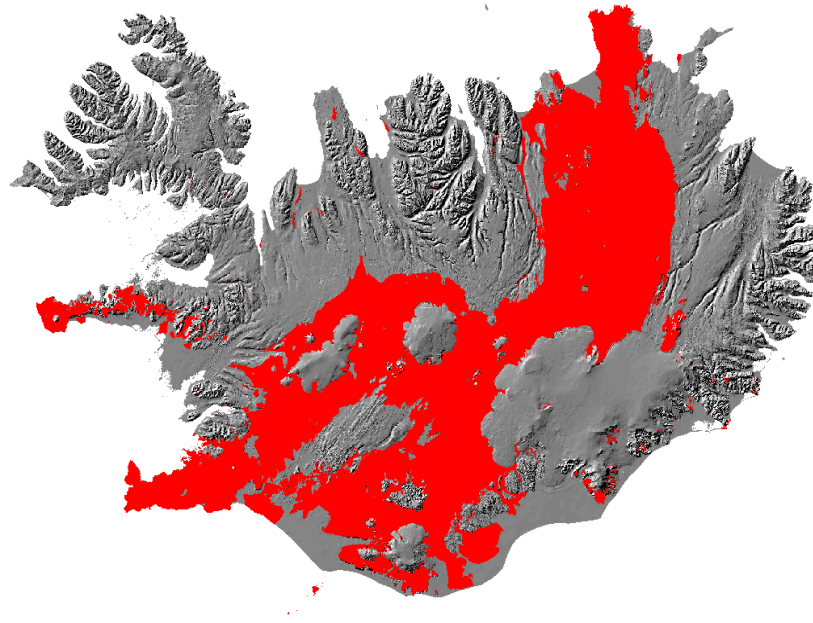

Fig. 9. Theoretical area feasible for CO_2 mineral storage in Iceland: Young and porous basaltic rocks (>0.8 M yr) within the active rift zone covering about one third of Iceland.

Furthermore, Goldberg et al. [3, 31] revealed the large storage capacity of sub-oceanic basalt formations at the Juan De Fuca plate west of Oregon, USA. The geologically feasible area at suitable depth for mineral storage of CO_2 there is calculated to be about 78,000 km^2. Assuming a channel system dominating permeability over one-sixth of the uppermost 600 m of the area, it is estimated to contain 7800 km^3 of highly permeable basalt. Given an average channel porosity of 10%, 780 km^3 of potential pore volume will be available for CO_2 storage. Anthonsen et al. [54] also applied Goldberg et al. [31] calculations to all of Iceland, resulting in an enormous number of about 1,200 $GtCO_2$. If these calculations are limited to the bedrock of the active rift zone in Iceland, over 400 Gt CO_2 could still be stored.

5.2. Storage potential for CO_2 transportation via pipeline

To get a more realistic value of the capacity for mineral storage in Icelandic basalt formations, transportation of CO_2 via pipeline was taken into consideration. The 30 km long, hot water pipeline from Nesjavellir to Reykjavík was used as an approximation and the area within 30 km radius of eight of the largest harbours proximal to the rift zone was selected (Fig. 10). The formations included were, as in the previous scenario, basaltic lavas, hyaloclastic

formations and associated sediments, younger than 0.8 M yr. Three harbours in the north-east were included (Húsavík, Kópasker, Raufarhöfn), one in the south-east (Höfn í Hornafirði) and four in the south-west (Reykjavík, Reykjaneshafnir, Grindavík, and Þorlákshöfn). In addition, an industrial harbour which is under construction in Helguvík, in SW-Iceland, was included. Population centres, water protection areas, national parks, natural monuments, nature reserves and country parks were excluded from the area. The area that fits the criteria is about 2390 km^2, close to 2% of Iceland.

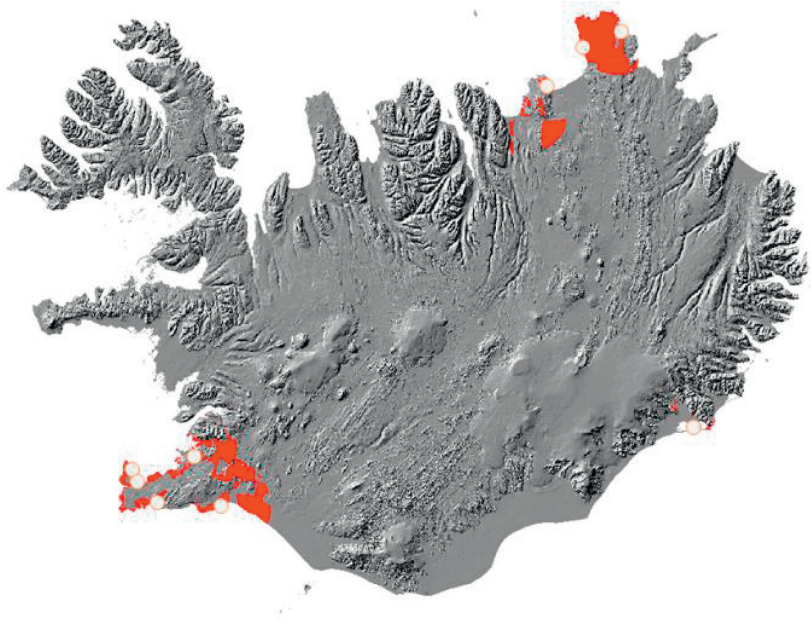

Fig. 10. Theoretical area feasible for CO_2 mineral storage in Iceland; Basaltic formations from Holocene and upper Pleistocene in the vicinity (radius of 30 km) of a large-scale harbour (white dots). Population centers, water protection areas, national parks, natural monuments, nature reserves and country parks were excluded from the area.

Using the results from Wiese et al. [1], as done in the previous example, and applying the average CO_2 load in the uppermost 1500 m of the Reykjanes system as a minimum and of the Krafla system as a maximum to a 1000 m thick segment of the defined area generates a maximum capacity of 175 Gt CO_2 and minimum of 67 Gt CO_2 . For comparison, in 2012 the global CO2 emissions to the atmosphere were 35.6 Gt from fossil fuel burning, cement production and land-use change [33].

Applying the study of McGrail et al. [2] and assuming an interflow thickness of 10 m, average porosity of 15% and 10 available interflow zones at an average hydrostatic pressure of 100 bar, the estimated capacity of the defined area goes down to about 1.4 $GtCO_2$.

Using the study of Goldberg et al. [31] and assuming a channel system dominating permeability over one-sixth of the uppermost 600 m of the area and average channel porosity of 10%, we get a number of 28.5 $GtCO_2$.

5.3. *The Icelandic analogue and the oceanic ridges*

The length of the rift zone in Iceland, the largest landmass found above sea level at mid–ocean ridges, is about 600 km. The oceanic ridges rise on average 1000–3000 m above the adjacent ocean floor (Fig. 11). The ridges extend through all of the major ocean basins, with a total length in excess of 60,000 km [29]. The theoretical mineral CO_2 storage capacity of the ocean ridges, using the Icelandic analogue, is of the order of 100,000–250,000 Gt CO_2. This theoretical storage capacity is significantly larger than the estimated 18,500 Gt CO_2 stemming from burning of all fossil fuel carbon on Earth [55].

Using the assumptions of McGrail et al. [2] and applying them to the ocean ridges gives an estimate of about 2,000 $GtCO_2$ and applying Goldberg's et al. [31] study gives an estimate about 40,000 $GtCO_2$.

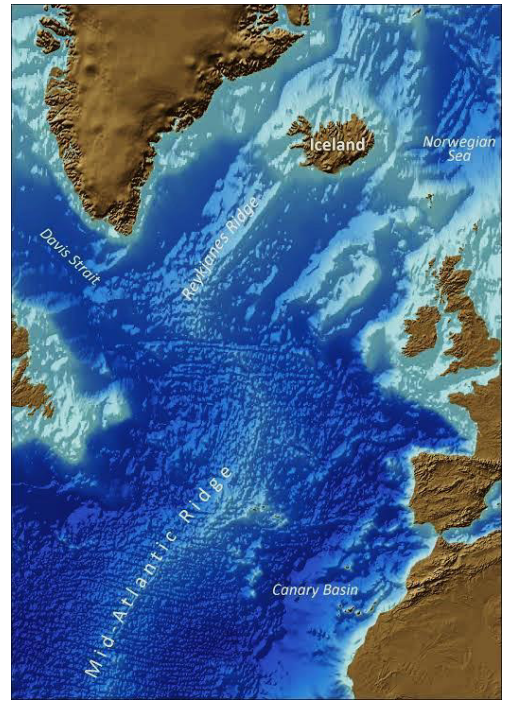

Fig. 11. Iceland and the Mid-Atlantic ridge. (Based on map from Amante and Eakins [56]).

As stated before, seafloor spreading generates about 20 km^3 per year of mid ocean ridge basalt (MORB). A minimum of about 9 tons of basaltic glass is required for mineralising one ton of carbon, assuming all calcium, magnesium and iron are converted into calcite, magnesite and siderite [8]. If the annual production of MORB by seafloor spreading would be used for mineral storage of CO_2, about 25 GtCO2 could be stored per year, which is about 70% of the annual global anthropogenic CO_2 emission to the atmosphere in 2012.

6. Conclusions

There is a high potential for mineral storage of CO_2 in Icelandic basalts and 30-40 $GtCO_2$ are estimated to be already naturally fixed within the active geothermal systems [1]. This amounts to the anthropogenic global annual emission of CO_2 to the atmosphere in 2012 [33].

Onshore projects on mineral storage of CO_2 in basalt, such as the CarbFix project in SW-Iceland and the Big Sky Carbon Sequestration Partnership in the northwest United States near Wallula, Washington are yet the only projects where CO_2 is stored in basalt.

Results from CarbFix injection experiments on rapid mineralisation of injected CO_2 when dissolved prior or during injection [4, 7, 12, 13] show a very promising outcome for mineral storage of CO_2 in basaltic rocks.

The largest storage potential lies offshore, where theoretically all CO_2 from burning of fossil fuel carbon could be stored with long-term advantages for safe and secure CO_2 storage in the mid-ocean ridges. The question remains; how much of this storage potential is practical to use?

Acknowledgement

This publication has been produced with support from the NORDICCS Centre, performed under the Top-level Research Initiative CO_2 Capture and Storage program and Nordic Innovation (Project number 11029) and by the 7th Framework Programme of the EC through the CarbFix project (project no. 283148).

Special thanks to Per Aagaard, Karen L. Anthonsen, Per Bergmö, Gry M. Morthensen and Ane Lothe from WP6 for of the NORDICCS project of their comments and informative discussions and partners of the CarbFix project, Ragnar H. Þrastarson at Lehman College in NY and Becca Neely at the University of Iceland for their help and support.

References

[1] Wiese F, Fridriksson Th, Armannsson H. CO_2 Fixation by Calcite in High-temperature Geothermal Systems in Iceland. Tech. Rep., ISOR−2008/003, Iceland Geosurvey, www.os.is/gogn/Skyrslur/ISOR-2008/ISOR-2008-003.pdf (2008).

[2] McGrail BP, Schaef HT, Ho AM, Chien Y-J, Dooley JJ, Davidson CL. Potential for carbon dioxide sequestration in flood basalts. J. Geophys. Res. 2006; 111: B12201

[3] Goldberg DS, Kent DV, Olsen PE. Potential on-shore and off-shore reservoirs for CO_2 sequestration in Central Atlantic magmatic province basalts. Proceedings of the National Academy of Sciences of the United States of America Sciences 2010; 107: 1327–1332

[4] Gislason SR, Oelkers EH. Carbon Storage in Basalt. Science 2014; 344: 373−374.

[5] Rutqvist J, Birkholzer J, Cappa F, Tsang C-F. Estimating maximum sustainable injection pressure during geological sequestration of CO_2 using coupled fluid flow and geomechanical fault-slip analysis. Energy Conversion and Management; 2007: 48, 1798–1807

[6] Gislason SR, Wolff-Boenisch D, Stefansson A, Oelkers EH, Gunnlaugsson E, Sigurdardottir H, Sigfusson B, Broecker WS, Matter JM, Stute M, Axelsson G, Fridriksson T. Mineral sequestration of carbon dioxide in basalt: A preinjection overview of the CarbFix project. Int. J. Greenhouse Gas Control 2010; 4: 537−545

[7] Sigfusson B, Gislason SR, Matter JM, Stute M, Gunnlaugsson E, Gunnarsson I, Aradottir ES, Sigurdardottir H, Mesfin KG, Alfredsson HA, Wolff-Boenisch D, Arnarson MT, Oelkers EH. Solving the carbon-dioxide buoyancy challenge: The design and field testing of a dissolved CO_2 injection system. Int. J. Greenhouse Gas Control 2014 (in press).

[8] Oelkers EH, Gislason SR, Matter J. Mineral carbonation of CO_2. Elements 2008; 4: 331–335

[9] Gislason SR, Broecker WS, Gunnlaugsson E, Snæbjörnsdóttir SÓ, Mesfin KG, Alfredsson HA, Aradottir ES, Sigfusson B, Gunnarsson I, Stute M, Matter JM, Arnarson MTh, Galeczka IM, Guðbrandsson S, Stockman G, Wolff-Boenisch D, Stefansson A, Ragnheidardottir W, T. Faathen, Gysi AP, Olssen J, Didriksen K, Stippe S, Menez B and Oelkers EH. Rapid solubility and mineral storage of CO_2 in basalt. Energy Procedia; 2014: This issue

[10] Benson S, Cook P, Anderson J, Bachu S, Nimir H, Basu B, Bradshaw J, Deguchi G, Gale J, von Goerne G, Heidug W, Holloway S, Kamal R, Keith D, Loyd P, Rocha P, Senior B, Thomson J, Torp T, Wildenborg T, Wilson M, Zarlenga F, D. Zhou D, Celia M, Gunter B, King JE, Lindeberg E, Lombardi S, Oldenburg C, Pruess K, Rigg A, Stevens S, Wilson ES Whittaker S. In: Metz B, Davidson O, Coninck H, Loos M, Meyer L. editors. IPCC Special Report on Carbon Dioxide Capture and Storage, New York :Cambridge Univ. Press; 2005), p. 195−276

[11] Gilfillan SMV, Sherwood Lollar B, Holland G, Blagburn D, Stevens S, Schoell M, Cassidy M, Ding Z, Zhou Z, Lacrampe-Couloume, Ballentine CJ. Solubility trapping in formation water as dominant CO_2 sink in natural gas fields. Nature 2009; 458: 614–618

[12] Matter JM, Stute M, Hall J, Mesfin K, Snæbjörnsdóttir, Gislason SR, Oelkers EH, Sigfusson B, Gunnarsson I, Aradottir ES, Alfredsson HA, E. Gunnlaugsson E.H.and Broecker WS. Monitoring permanent CO_2 storage by in situ mineral carbonation using a reactive tracer technique. Energy Procedia 2014; (this issue).

[13] Snæbjörnsdóttir SÓ, Mesfin KG, Gunnarsson I, Aradottir ES, Sigfusson B, Gunnlaugsson, Oelkers EH, Stute M, Matter J, Gislason SR. CarbFix: Injection of CO_2 and CO_2-H2S gas mixture at Hellisheidi SW-Iceland. First results on chemical monitoring. International Carbon Conference, Reykjavik, Iceland. http://www.or.is/en/projects/international-carbon-conference-2014 (2014)

[14] McGrail BP, Spane FA, Sullivan EC, Bacon DH, Hund G. The Wallula basalt sequestration pilot project. Energy Procedia 2011; 4: 5653−5660

[15] McGrail BP, Freeman CJ, Brown CF, Sullivan EC, White SK, Reddy S, Garber RD, Tobin D, Gilmartin JJ, Steffensen EJ. Overcoming business model uncertainty in a carbon dioxide capture and sequestration project: Case study at the Boise White Paper Mill. Int. J. Greenhouse Gas Control 2012; 9: 91−102

[16] Thordarson Th, Höskuldsson Á. Postglacial volcanism in Iceland. Jökull; 2008: 58, 197-228.

[17] Searle R. Mid-Ocean Ridges. Cambridge: Cambridge University Press; 2013

[18] Jóhannesson H and Sæmundsson K. Geological map of Iceland, 1:500.000; 1998. Icelandic Institute for Natural History.

[19] Neuhoff PS, Fridriksson Th, Arnorsson S, Bird DK. Porosity evolution and mineral paragenesis during low-grade metamorphism of basaltic lavas at Teigarhorn, Eastern Iceland. Am. J. Sci.; 1999: 299, 467–501.

[20] Frolova J, Franzson H, Ladygin V, Sigurdsson O, Stefánsson V, Shustrov V. Porosity and permeability of hyaloclastites tuffs, Iceland. Proceedings of International Geothermal Workshop IGW2004 “Heat and light from the heart of the earth”; 2004 August 9-16; Petropavlovsk-Kamchatsky, Russia. 2004. 10 p.

[21] Matter JM, Kelemen PB. Permanent storage of carbon dioxide in geological reservoirs by mineral carbonation. Nature Geoscience 2009: 837–841
[22] Schaef HT, McGrail BP, Owen AT. Carbonate mineralization of volcanic province basalts. Int. J. Greenhouse Gas Control 2010; 4: 249−261.
[23] Alfredsson HA, Oelkers EH, Hardarsson BS, Franzson H, Gunnlaugsson E, Gislason SR. The geology and water chemistry of the Hellisheidi, SW-Iceland carbon storage site. Int. J. Greenhouse Gas Control 2013; 12: 399–418
[24] Wolff-Boenisch D, Gislason SR and Oelkers EH. The effect of crystallinity on dissolution rates and CO_2 consumption capacity of silicates. Geochimica et Cosmochimica Acta; 2006: 70, 858-870.
[25] Wolff-Boenisch D, Wenau S, Gislason SR, Oelkers EH. Dissolution of basalts and peridotite in seawater, in the presence of ligands, and CO_2: Implications for mineral sequestration of carbon dioxide. Geochim. Cosmochim. Acta. 2011; 75: 5510−5525
[26] Rosenbauer RJ, Thomas B, Bischoff JL, Palandri J. Carbon sequestration via reaction with basaltic rocks: Geochemical modeling and experimental results. Geochim. Cosmochim. Acta 2012; 89: 116−133
[27] Gysi AP, Stefansson A. CO_2–water–basalt interaction. Low temperature experiments and implications for CO_2 sequestration into basalts. Geochim. Cosmochim. Acta 2012; 81: 129–152
[28] Galeczka I, Wolff-Boenisch D, Oelkers EH, Gislason SR. An experimental study of basaltic glass–H_2O–CO_2 interaction at 22 and 50 °C: implications for subsurface storage of CO_2. Geochim. Cosmochim. Acta 2014; 126: 123–145.
[29] Wilson, M. Igneous Petrognesis. A global Tectonic Approach. Springer, 1989.
[30] Dessert C, Dupre B, Gaillardet J, Francois LM, Allegre CJ. Basalt weathering laws and the impact of basalt weathering on the global carbon cycle. Chem. Geol. 2003; 202: 257−273
[31] Goldberg DS, Takahashi T, Slagle AL. Carbon dioxide sequestration in deep−sea basalt. Proc. Nat. Acad. Sci. 2008; 105(29): 9920−9925.
[32] Wolery TJ and Sleep NH. Hydrothermal circulation and geochemical flux at mid-ocean ridges. J. Geol. 1976; 84: 249-275
[33] The Global Carbon Project. [internet] [cited 2nd of May 2014] Available from: http://www.globalcarbonproject.org/carbonbudget/13/hl-compact.htm
[34] Mesfin KG, Wolff-Boenisch D, Gislason SR. Effect of ionic strength on the dissolution rates of basaltic glass and bytwonite at pH 3.6 and 25°C. Poster presentation. 30th Nordic Geological Winter Meeting; 2012 9th-12th of January; Reykjavík. (2012).
[35] Gislason SR and Oelkers E. Mechanisms, rates and consequences of basaltic glass dissolution: II. An experimental study of the dissolution rates of basaltic glass as a function of temperature. Geochim. Cosmochim. Acta; 2003: 67, 3817-3832.
[36] Skippen GB. Dehydration and decarbonation equilibria. In Greenwood H. J. ed. Application of thermodynamics to petrology and ore deposits, Mineralogical Association of Canada Short Course. Toronto, Canada: Evergreen Press; 1980. p 66-83.
[37] Franzson, H. Reservoir Geology of the Nesjavellir High-Temperature Field in SW-Iceland. Proceedings 19th Annual PNOC-EDC Geothermal Conference; 1998 March 5-6th; Manila, Philippines; 1998. p. 13-20.
[38] Tómasson J and Kristmannsdóttir H. High temperature alteration minerals and thermal brines, Reykjanes, Iceland. Contributions to Mineralogy and Petrology 1972; 36: 132–134.
[39] Gysi AP, Stefansson A. Numerical modelling of CO_2–water–basalt interaction. Miner. Mag 2008; 72: 55–59
[40] Gysi AP, Stefansson A. CO_2–water–basalt interaction. Numerical simulation of low temperature CO_2 sequestration into basalts. Geochim. Cosmochim. Acta 2011; 75: 4728−4751
[41] Rogers KL, Neuhoff PS, Pedersen AK, Bird DK. CO_2 metasomatism in a basalt-hosted petroleum reservoir, Nuussuaq, West Greenland. Lithos 2006; 92: 55−82
[42] Hjartarson Á, Sigbjarnarson G, Karrenberg H. International Hydrogeological Map of Europe; 1980. Sheet B2. Island. Bundensanstalt fur Geowissenhaften und Rohstoffe. Hannover and UNESCO. Paris.
[43] Flóvenz ÓG., Saemundsson K. Tectonophysics; 1993: 225, p. 123-138. http://dx.doi.org/10.1016/0040-1951(93)90253-G
[44] Franzson H, Guðfinnsson GH, Helgadóttir HM, Frolova J. Porosity, density and chemical composition relationships in altered Icelandic hyaloclastites. Water-Rock Interaction – Birkle & Torres-Alvarado; 2010: 199-202
[45] Stefánsson, V, Sigurðsson, Ó, Guðmundsson, Á, Franzson, H, Friðleifsson GÓ, Tulinius, H. Core measurements and geothermal modelling. Second Nordic Symposium on Petrophysics; 1997: Fractured reservoirs. Nordic Petroleum Technology Series One, 199-220.
[46] Flaathen TK, Gislason SR, Oelkers EH, Sveinbjörnsdóttir ÁE. Chemical evolution of the Mt. Hekla, Iceland, groundwaters: A natural analogue for CO_2 sequestration in basaltic rocks, App. Geochem. 2009; 24: 463−474.
[47] Galeczka I, Wolff-Boenisch D, Gislason SR. Experimental studies of basalt–H_2O–CO_2 interaction with a high pressure column flow reactor: the mobility of metals. Energy Procedia 2013; 37: 5823–5833
[48] Olsson J, Stipp SLS, Makovicky E, and Gislason SR. Metal scavenging by calcium carbonate at the Eyjafjallajökull volcano: A carbon capture and storage analogue. Chem. Geol. 2014; 384: 135–148.
[49] Galeczka I, Wolff-Boenisch D, Jonsson, Th, Sigfusson B, Stefansson A, Gislason SR. A novel high pressure column flow reactor for experimental studies of CO_2 mineral storage. Applied Geochemistry; 2013: 30; 91-104.
[50] European Community. Council directive 80/778/EC of 15 July 1980 relating to the quality of water intended for human consumption as amended by Council Directives 81/858/EEC and 91/692/EEC (further amended by Council Regulation 1882/2003/EC).
[51] Aradottir ES, Sonnenthal EL, Björnsson G, Jonsson H. Multidimensional reactive transport modeling of CO_2 mineral sequestration in basalts at the Hellisheidi geothermal field, Iceland. Int. J. Greenhouse Gas Control 2012; 9: 24−40
[52] Ármannsson H, Fridriksson Th, Wiese F, Hernández P, Pérez N.CO_2 budget of the Krafla geothermal system, NE Iceland. Water-Rock Interaction (Editors T.D. Bullen and Y. Wang); 2013. Taylor and Francis Group, London, 189-192

[53] Franzson H, Kristjánsson BR, Gunnarsson G, Björnsson G, Hjartarson A, Steingrímsson B, Gunnlaugsson E, Gíslason, G. The Hengill-Hellisheiði Geothermal Field. Development of a Geothermal conceptual model. Proceedings World Geothermal Congress; 2005 24-29. April; Antalya, Turkey: 7 p.

[54] Anthonsen KL, Aagaard P, Bergmo PES, Erlström M, Fareidei JI, Gislason SR, Mortensen GM, Snæbjörnsdóttir, SÓ. CO_2 storage potential in the Nordic region. Energy Procedia; 2013: 37, 5080-5092.

[55] Archer D. Fate of fossil fuel CO_2 in geologic time. J. Geophys. Res. 2005; 110(C9): C09S05

[56] Amante C and Eakins BW. ETOPO1 1 Arc-Minute Global Relief Model: Procedures, Data Sources and Analysis. NOAA Technical Memorandum NESDIS NGDC-24. National Geophysical Data Center, NOAA; 2009. doi:10.7289/V5C8276M [accessed 9.9.2014]

Paper II

CO_2 storage potential of basaltic rocks offshore Iceland

Snæbjörnsdóttir, S. Ó., Gislason, S. R., 2016. Energy Procedia, volume 86, pages 371-380. *DOI:10.1016/j.egypro.2016.01.038*

Available online at www.sciencedirect.com

ScienceDirect

Energy Procedia 86 (2016) 371 – 380

Energy Procedia

The 8th Trondheim Conference on CO_2 Capture, Transport and Storage

CO_2 storage potential of basaltic rocks offshore Iceland

Sandra Ó. Snæbjörnsdóttir*, Sigurdur R. Gislason

Institute of Earth Sciences, University of Iceland, Askja, Sturlugötu 7, 101 Reykjavik, Iceland

Abstract

Injection of CO_2 into basaltic formations provides significant benefits including permanent storage by mineralisation and large storage volume. The largest geological storage potential lies offshore and in the case of basalt, along the mid-oceanic ridges where CO_2 could be stored as carbonate minerals for thousands of years. Most of the bedrock, both on land and offshore Iceland consists of basalt that could theoretically be used for injection of CO_2, fully dissolved in water. The most feasible formations are the youngest formations located within the active rift zone. It is estimated that up to 7000 $GtCO_2$ could be stored offshore Iceland within the Exclusive Economic Zone. Site specific geological research and pilot studies are required for refining the concept and offshore pilot scale projects should be considered as the next steps in evolving the method.

Peer-review under responsibility of the Programme Chair of the 8th Trondheim Conference on CO_2 Capture, Transport and Storage

Keywords: carbon capture and storage; mineral storage; calcite

1. Introduction

The reduction of carbon dioxide ($CO_{2)}$ emissions to the atmosphere is one of the greatest challenges of this century and multiple approaches are needed for halting climate change by reversing the rise in emissions. One solution to this is carbon capture and storage (CCS). In fact, the International Energy Agency estimates that under the 2°C scenario, CCS will provide one sixth of required emission reduction in 2050 [1]. Injection of CO_2 into basaltic formations provides significant benefits including permanent storage by mineralisation and a great potential storage volume [2-5]. Mineral carbonation requires combining CO_2 with divalent metal cations to form carbonate minerals, such as Calcite ($CaCO_3$), Dolomite ($CaMg(CO_3)_2$), Magnesite ($MgCO_3$), siderite ($FeCO_3$), and solid

* Corresponding author. Tel.: +354-525-5248.
E-mail address: sos22@hi.is

Peer-review under responsibility of the Programme Chair of the 8th Trondheim Conference on CO_2 Capture, Transport and Storage
doi:10.1016/j.egypro.2016.01.038

solutions thereof [3, 6]. Basaltic rocks contain over 25 wt% Ca, Mg, and Fe-oxides and are reactive in water, thus the metals contained in basalts are readily available to combine with the injected CO_2 to form carbonate minerals [7-12]. Once dissolved in water, CO_2 is no longer buoyant and does not migrate back to the surface. The CO_2-charged water accelerates both the metal release from the basalt and subsequent formation of solid carbonate minerals for long term storage of CO_2 (fig 1.) [3].

The method of dissolving the CO_2 during injection into reactive basaltic rocks changes the time scale for mineral storage significantly with solubility trapping occurring immediately, and the bulk of the carbon trapped in minerals within only few years [3, 13, 14]. Once stored as a mineral, the CO_2 is immobilised for geological time scales [3, 6, 11, 15]. This method will be referred to as the CarbFix method, named after the project that pioneered it.

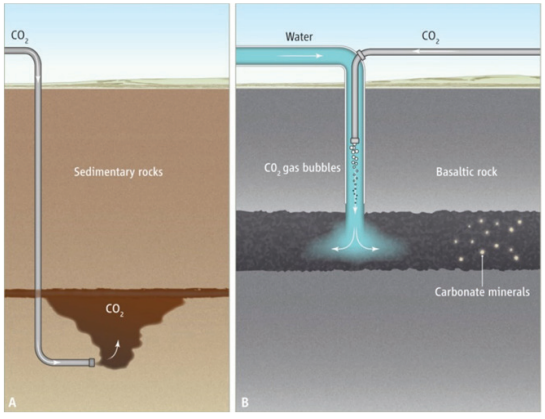

Fig. 1. Carbon storage in sedimentary basins and basaltic rocks. (A) Carbon storage in sedimentary basins; CO_2 is injected as a separate buoyant phase and is trapped below an impermeable cap rock. (B) In the CarbFix method, CO_2 is dissolved into water during its injection into porous basaltic rocks. No cap rock is required because the dissolved CO_2 is not buoyant and does not migrate back to the surface. Figure from Gislason and Oelkers [3].

Most of the oceanic floor and about 10% of the continents is composed of basalt which is the dominant rock type on Earth's surface [16, 17]. The most voluminous volcanism on the Earth occurs at the mid-ocean ridges where seafloor spreading generates about 20 km^3 per year of mid-ocean ridge basalt (MORB) [18]. The offshore formations offer a unique environment for CO_2 storage with a vast volume of pore space, and fresh and reactive rocks. The ridges extend through all of the major ocean basins, with a total length in excess of 60,000 km [29]. The theoretical integrated CO_2 storage capacity of the ridge system has been estimated to be of the order of 100,000-250,000 $GtCO_2$ [2] considerably larger than the estimated CO_2 emission from burning all fossil fuels on Earth [19].

The physical properties of the mid-oceanic ridges have been studied extensively, mainly through scientific drilling, and geophysical and bathymetric surveys [e.g. 20]. The flanks of the ridges are known to contain highly fractured and permeable basaltic layers [21] with pervasive circulation of seawater initiating at the spreading axis and continuing for millions of years as the oceanic crust moves away from the axis and cools and ages [22]. The advective heat flow for the entire oceanic ridge system is estimated to be about 10^{13} W, with about two thirds of the heat loss occurring in seafloor younger than 8 Ma. The mass flow of seawater necessary to produce this heat loss at the oceanic ridges is about 1,000 GtH_2O/yr [23].

A vast amount of water is required to dissolve the CO_2, depending mostly on pressure, temperature, and salinity [11]. At 25 bar CO_2 pressure and 4°C, about 20 tonnes of seawater of average salinity (35‰) are required for dissolving each tonne of CO_2 [24, 25]. The 2014 anthropogenic CO_2 emissions to the atmosphere were 36 $GtCO_2$/yr [26]. It would take about 720 GtH_2O to dissolve all of that CO_2 in seawater at 25 bar CO_2 pressure, about three-quarters of the amount that percolates into the ridge system every year.

Here, a first attempt is made to estimate the theoretical capacity for mineral storage of CO_2 in young basaltic

formations offshore Iceland, within the Icelandic Exclusive Economic Zone which extends 200 nautical miles from the coastal line, covering area of about 740,000 km^2. Observations made during screening of basaltic formations onshore are initially used to calculate a first order estimate of the offshore potential. However, further work and a more thorough study of the available data is required for selection of suitable formations for mineral storage of CO_2 and estimation of the CO_2 storage potential, including lab and field injection experiments using seawater and extensive monitoring and characterization of current onshore injection experiments.

2. Geological settings of Iceland and the North Atlantic Basin

Iceland sits astride the North Atlantic Ridge where the North American and the Eurasian plates are separated (fig. 2). Iceland is one of only two places on Earth where an oceanic spreading centre rises above sea level and is the largest area of sub-aerially exposed mid-ocean ridge on Earth [27].

Fig. 2. Iceland and the Mid-Atlantic ridge. Based on map from Amante and Eakins [28].

The plate boundary in, and close to Iceland is composed of several rift segments and transform zones, forming an overlapping spreading centre with propagating rifts both at the southern and northern parts of the island (fig. 2 and 3) [29, 30], with a spreading rate of about 18-20 mm/yr [31]. In SW-Iceland, at the tip of the Reykjanes peninsula, the offshore Reykjanes Ridge (RR) meets the on-land Reykjanes Oblique Rift which extends to form the West Volcanic Zone (WVZ) as shown in Fig. 3. In N-Iceland the Northern Volcanic Zone (NVZ) is linked to the offshore Kolbeinsey Ridge (KR) by the NW-trending Tjörnes Fracture Zone (TFZ) [e.g. 32, 33] (fig. 3).

The plate boundary is affected by the existence of a mantle plume located beneath Iceland [34]. The mantle plume has profoundly influenced the creation of the oceanic crust along the North Atlantic basin. The thickness of the crust along the Reykjanes Ridge is of 10-11 km [35] which is about 6–7 km higher than normal oceanic crust [36] but the influence of the mantle plume appears to extend less far north along the Kolbeinsey Ridge with 1-2 km thinner crust than along Reykjanes Ridge [37]. The effect of the mantle plume results in the anomalously shallow bathymetry of the Reykjanes Ridge and Kolbeinsey Ridges compared to mid-oceanic ridges in general; the depth of the Iceland sea north of Iceland is about 1000-2000 m and as shallow as 500 m at Reykjanes Ridge closest to land and up to 1500-2000 m at the southern end of the ridge [38]. These areas, north and south of Iceland, are shown by the shaded part of the ridges in Figure 3.

The excessive volcanism associated with the combination of a mantle plume and divergent rifting has led to the forming of the Iceland basalt plateau shown in Fig. 2 and Fig. 3. The plateau rises more than 3000 m above the surrounding sea floor and covers about 350,000 km^2 including the terrestrial 103,000 km^2 of Iceland [39]. Iceland is mostly made of young 0-20 M yr. igneous rocks and sediments thereof, but approximately 90% of the bedrock is basalt [40]. The relatively flat shelf around Iceland is generally at depths of between 100-200 m and its average width is 80 km [41]. Sediments, mostly originate onshore and are abundant at the edge of the shelf, close to and below the slope of it. The thickness of the sediments below the slope are estimated to be up to 1000-2000 m, except in one area north of Iceland within the TFZ, between Skjálfandi bay and Eyjafjörður fjord in Figure 3, where the sedimentary pile is estimated to be as thick as 4000 m [42].

The ridges consist, as stated before, of MORB but are somewhat covered with sediments; very thin layers, or none at all, above the axis of the ridges where new crust is being formed but thickening towards the seafloor as the rocks gets older, reaching 1000-1500 m at the end of the slope of the ridges [38].

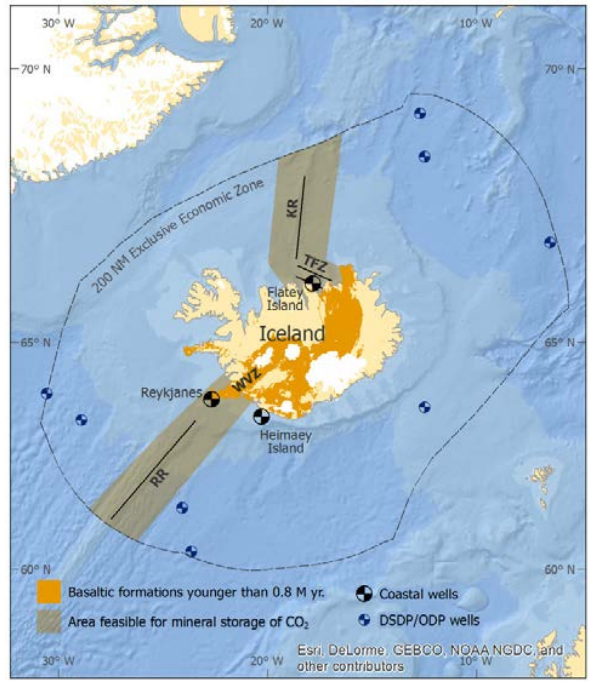

Fig. 3. General outlines of the plate boundary in Iceland. Reykjanes Ridge (RR) enters Iceland at the tip of the Reykjanes Peninsula which extends to form the Western Volcanic Zone (WVZ). The Northern Volcanic Zone (NVZ) extends north where it is linked to the offshore Kolbeinsey Ridge (KR) by the NW-trending Tjörnes Fracture Zone (TFZ). Large hourglass circles indicate wells drilled in the coastal areas and small hourglass circles indicate wells drilled offshore as a part of DSDP and ODP. The area that fits our criteria as feasible for CO_2 mineral storage offshore Iceland is shaded. It extends 30 km to each side of the axis of the Reykjanes Ridge SW of Iceland and the Kolbeinsey Ridge N of Iceland, from the costal line and to the boundary of the Iceland Economic Zone. Modified after Einarsson and Sæmundsson, [43], map based on data from Esri, GEBCO and NOAA [44].

3. Data available on offshore formations

The areas offshore of Iceland have been studied to some extent, especially the areas north and north-east of Iceland, in connection with oil and gas exploration. The research includes gas-analysis, multi-beam bathymetry, side scan sonar, seismic surveys, seafloor photography, and coring of sediments in selected areas [45]. The most concrete

information on offshore formations is from wells drilled at the coastal line of Iceland, on the shelf, and seafloor which could give valuable information on formations for mineral storage of CO_2 offshore of Iceland (fig. 3)

Wells drilled in Heimaey Island south of Iceland and Flatey Island in the Skjálfandi Bay north of Iceland can give information on the formations at the shelf south and north of Iceland. Wells drilled at the coast at the Reykjanes peninsula can somewhat represent the stratigraphy offshore SW-Iceland. Several wells have also been drilled offshore of Iceland as a part of the Deep See Drilling Project (DSDP) in 1970-1976 and Ocean Drilling Program (ODP) in 1993-1995, ranging from about 120 to about 620 m in depth from the seafloor These are mostly sedimentary cores, but in some cases cored down to the basalt basement at about 300-600 m depth [e.g. 20].

Two deep wells have been drilled in Heimaey Island, the largest island of the Vestmannaeyjar Islands south of Iceland; 1565 m and 2277 m deep (fig. 3). The stratigraphy of the wells consists mostly of alternating sedimentary formations and basaltic hyaloclastites; glassy formations formed under water resulting in fragmentation of the magma. The chemical composition of the sediments indicates that the formations are derived from weathering of volcanic rocks on land, located within the East Volcanic Zone north of Vestmannaeyjar Island [46].

A 554 m deep well was drilled in Flatey Island in the bay of Skjálfandi north of Iceland in 1982 (fig. 3). The stratigraphy of the well is mostly sedimentary rocks formed in shallow water or on land during glaciation and three 10-20 m thick basaltic lava sequences [e.g. 42, 47]. Seismic- and gravity-surveys conducted in the area indicate that the island is located on top of the sedimentary formation located between Skjálfandi bay and Eyjafjörður fjord which is estimated to be about 4 km thick [42].

Several wells have been drilled at the south-western tip of the Reykjanes peninsula (fig. 3), in connection with geothermal utilisation in the area, which show some trends in stratigraphy. Below about 100 m and down to about 900-1000 m depth the formation consists of glassy basaltic hyaloclastic formations and marine sediments indicating eruptions under water and formations of sediments in water depth less than 50 m. The dominant rock type below 900-1000 m depth is crystalline basalt, most likely pillow basalt formed offshore, but hyaloclastites and sedimentary tuff-units are also cut by the wells [e.g. 48].

4. Most feasible formations for CO_2 mineral storage offshore Iceland

Seismological studies on the internal structure of the oceanic crust reveal a remarkably homogeneous structure compared to the continental crust. Two igneous crustal layers are identified; layer 2 characterized by low velocities and steep velocity gradients and layer 3 by high velocities and low velocity gradient. These seismic velocities are related to bulk porosity and rock composition within the oceanic crust [22].

The feasible formations for mineral storage of CO_2 lie within the so called layer 2 which is associated with the upper crust. The top-part of layer 2 consists of a few hundred metres thick extrusive section that caps the crust along the ridges with the highest bulk porosities (20-40%) within the oceanic crust. Below this section lies a 1.5-2 km thick sheeted dike section with porosities of less than 10%. The permeability and porosity structure of the crust is the result of both tectonic and magmatic processes [22]. Little is published on the mean thickness of the porous top-part of layer 2 at the Mid Atlantic ridges but the thickness at the Reykjanes Ridge is measured to be 400 ± 100 m, decreasing with crustal ages over 5 Ma [49].

The velocity of the top-part of layer 2 increases as the crust ages away from the spreading axis, reaching typical levels of deeper crustal rocks by <10 Ma [22]. The young (<3.2 Ma) DSDP basalts are pervasively altered [50-52] indicating that the alteration must commence very soon after the crust is formed [53]. The first stages of alteration of the oceanic crust are formation of palagonites and later smectites but both processes are the results of seawater-basalt interaction. This involves large amounts of water and can produce major chemical fluxes between layer 2 and the oceanic reservoir, but these processes typically occur in Atlantic type crust younger than 3 Ma [52]. Radiometric dating of vein smectites from MORB also indicates that most of the alteration occurs within 3 Ma [54]. Porosity data from DSDP and ODP sites show a similar relationship for samples with crustal ages >5 Ma [55] but the crust retains roughly half of its porosity after 10-15 Ma with continuing alteration at decreasing rate [56].

Studies on Icelandic bedrock show that, as with oceanic crust porosity and permeability generally decrease with progressive alteration, gradual burial, and increasing rock age since most of the pore space is filled with secondary minerals in the older rocks [57, 58]. Average porosity of young and un-altered basaltic lavas has been measured to be about 27% compared to 6-7% in highly altered samples [59]. Thus, the youngest basaltic formations found within

the active rift zone (<0.8 Ma), have been evaluated as the most feasible for carbon storage onshore Iceland [2]. As for the porosity and permeability, the structure of the top-part of the Icelandic crust, as studied in wells drilled within the active rift zone, also reveals a similar structure as the oceanic crust with the top few hundred meters dominated by extrusive rocks; glassy formations and pillow basalts erupted during glacial times and lava flows during inter-glacials, sheeted dykes becoming more dominant with increasing depth and finally gabbro or granophyre-like intrusions in the deepest parts [e.g. 60].

The same criteria are therefore used here for the assessment of mineral carbon storage potential offshore as for the onshore formations in Iceland. The selected area for the storage estimate reaches from the axis of the Reykjanes Ridge SW of Iceland and the Kolbeinsey ridge NE of Iceland and extends 30 km to each side of the ridge axis which is the width of the active rift zone in Iceland (fig. 3). Using the spreading rate of about 18-20 mm/yr it can be estimated that the age of the formations is <3 Ma, eliminating the more altered and less porous formations. This includes area from the costal line and to the boundary of the Iceland Economic Zone which covers about 93,000 km^2.

The difference between injecting CO_2 dissolved in water and in a buoyant supercritical stage is underscored in Figure 1 and discussed in chapter 1 of this paper. Supercritical CO_2 is kept trapped below an impermeable cap rock, but since dissolved CO_2 is heavier than the formation fluids, the injection wells are not dependent on cap-rocks or seals. In fact, the dissolved CO_2 can be injected into fractured and even open aquifers, as long as the flow path is long enough for alkalinity generation and eventually mineralisation of the CO_2. As stated before, the time required for mineralisation is of the orders of months to years [3, 13, 14]. The total depth of injection, including the seawater column, should be at least 300 m yielding about 30 bar pressure, enough for considerable solubility of the CO_2 in the seawater, as also discussed in chapter 1. Site specific studies and further experience with the CarbFix method will inform how far the injection wells would have to reach into the basalt formation for successful injection. However, the experience from the on-shore injection experiments of the CarbFix project in Hellisheiði has shown that 200 m below the water table in the basalt formation is more than enough [13].

5. Storage potential estimates

Few attempts have been done to estimate the mineral storage potential of CO_2 in basaltic rocks. The first attempt was made by McGrail et al. [61] that estimated the storage potential of continental flood basalts for storage of buoyant, supercritical CO_2 assuming that the Columbia River basalts which cover more than 164,000 km^2 of Washington, Oregon, and Idaho, have the capacity to store over 100 $GtCO_2$. The targeted depth of the injection was 1000 m assuming interflow thickness of 10 m, average porosity of 15% and 10 available interflow zones at an average hydrostatic pressure of 100 atm.

Applying the same criteria to the selected area of 93,000 km^2 offshore Iceland gives storage potential estimate of about 60 $GtCO_2$ (fig. 4, Scenario 1). This is a rather conservative estimate considering that the total CO_2 measured to be fixed within the active high temperature geothermal systems in Iceland, an area which covers less than 1 km^2 of Iceland, amounts to 30-40 $GtCO_2$ [62]. McGrail's study [61] differs from this study in two fundamental ways. Firstly, the basaltic formations of the study are continental basalts with different structure and petro-physical properties than the young and glassy basaltic formations of the oceanic crust. Secondly and more importantly, they anticipate that the CO_2 is injected as a supercritical buoyant phase into the basaltic rocks which requires deeper wells and a cap rock to prevent the supercritical CO_2 from leaking out of the reservoir. Injecting supercritical CO_2 also results in orders of magnitude lower mineralisation rate than if the CO_2 is dissolved in water prior to or during the injection using the CarbFix method [3, 14].

Goldberg et al. [63] revealed the large storage capacity of sub-oceanic basalt formations at the Juan de Fuca plate east of Oregon, USA. Assuming a channel system dominating permeability over one-sixth of the uppermost 600 m of the area, it is estimated to contain 7800 km^3 of highly permeable basalt feasible for mineral storage. Given an average channel porosity of 10%, 780 km^3 of potential pore volume will be available for CO_2 storage. If liquefied CO_2 is injected to fill this volume and it remains in liquid form, about 750 $GtCO_2$ could be stored in this area. If the CO_2 reacts with the basalt and is mineralised about 900 $GtCO_2$ could be stored in the area.

The Goldberg et al. study is done on oceanic crust which makes it more applicable to the area offshore Iceland. However, with McGrail et. al, Goldberg et al. assume injection of buoyant supercritical CO_2 which puts more

constrains on the targeted area, requiring more than 200 m thick sediment cover as a seal and water depth greater than 2700 m. If the petro-physical criteria from Goldberg et al. [63] are applied to the 93,000 km^2 area offshore Iceland, estimating 9300 km^3 of permeable basaltic rocks along the ridge axis, with 10% average channel porosity., then 930 km^3 of potential pore volume would be available, yielding to a mineral storage potential of 1100 $GtCO_2$ (fig. 4, Scenario 2).

Snæbjörnsdóttir et al. [2] used a study done by Wiese et al. [62] on the amount and spatial distribution of CO_2 stored as calcite within the bedrock of three active high-temperature geothermal systems in Iceland, as a natural analog for mineral storage of CO_2 in young basaltic formations. A significant amount of CO_2 is naturally fixed within basaltic rocks in geothermal areas which receive CO_2 from their heat source; magmatic intrusions in their roots. The amount of CO_2 stored as calcite in the three geothermal systems; Krafla in the north–east of Iceland and Hellisheiði and Reykjanes in the south-west, was estimated by measuring the CO_2 content of about 700 samples of drill cuttings from 42 wells in these three areas. The results indicate that about 28.2 to 73.1 tonnes of CO_2 per m^2 of surface area are already naturally fixed in the uppermost 1500 m of the three areas. The lowest values are measured in the Reykjanes geothermal area, which is considered to be the youngest of the three geothermal areas (active for 10,000-100,000 years) and the highest values are measured in the Krafla geothermal area, considered to have been active for the longest (between 110,000 and 290,000 years). These time scales are orders of magnitude larger than the time scales CCS requires, but considering how fast these reactions occur when CO_2 is dissolved in water during injection [3, 15, 64] the results can be used as a guideline for the theoretical CO_2 storage potential.

The CO_2-load in the uppermost 1500 m of the Reykjanes system was used to as a minimum and the Krafla system as a maximum and the values applied to the uppermost 1500 m of the relatively fresh basaltic formations within the active rift zone of Iceland [2]. If the same method is used to estimate the storage potential offshore Iceland gives values of 2600 $GtCO_2$ (fig. 4, Scenario 3) and 6800 $GtCO_2$ (fig. 4, Scenario 4) respectively.

As stated before, the permeability, porosity and general structure of the Icelandic crust within the active rift zone is similar to the oceanic crust. The formations on-shore can therefore give valuable information on offshore storage of CO_2. The storage potential estimates using the Icelandic analogue give results of the same order of magnitude as Goldberg et al. [63]. The main difference lies within the different approaches: Goldberg et al. estimate the storage potential from petro-physical properties of the oceanic crust for injection of supercritical CO_2 whilst Snæbjörnsdóttir et al. [2] use natural analog for mineral storage of CO_2.

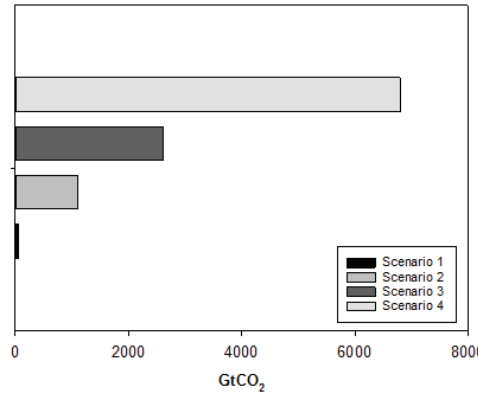

Fig. 4. Storage potential estimates of the selected area feasible for mineral storage of CO_2 offshore Iceland along the of the axis of the Reykjanes Ridge SW of Iceland and the Kolbeinsey Ridge N of Iceland within the Exclusive Economic Zone using criteria from McGrail et al. [61] as scenario 1, Goldberg et al. [63] as Scenario 2 and Snæbjörnsdóttir et al. [2] as Scenario 3 and 4.

6. Conclusions

The largest geological storage potential for CO_2 lies offshore, and in the case of basalt along the oceanic ridges where theoretically CO_2 from burning of all fossil fuel on Earth could be stored as carbonate minerals for thousands of years [2]. There is a large storage potential of CO_2 within basaltic rocks offshore Iceland, which is underscored by the theoretical storage potential estimates ranging from about 60 to about 7,000 $GtCO_2$. There are however large uncertainties due to lack of data and experience within the field which require site-specific geological research and pilot studies.

A significant challenge faced by the CarbFix method is the vast amount of water that is required to dissolve CO_2 during injection. The total mass initially injected will be about 15 to 25 times greater when compared to the conventional method. Both methods run into risks of overpressure in the aquifers when scaled up to millions of tonnes and the great mass injected using the CarbFix method increases this risk. At Hellisheiði geothermal field in SW-Iceland about 22 Mt of waste water from the Hellisheiði geothermal power plant have been re-injected into the fractured reservoir annually for the last four years using 12 injection wells. The injection initially led to some overpressure and induced seismicity which faded out with time during operation [65]. Today it is an ongoing operation that continues to show the feasibility of injecting large volumes of fluid into young and fractured basaltic rocks.

One of the advantages of going offshore is that the oceans provide an unlimited reservoir for the required water. In addition to that, the flanks of the ridges contain highly fractured and permeable basaltic layers with great circulation of seawater, or about 1,000 GtH_2O/yr [23], as mentioned in chapter 1 of this paper. Considering that the CO_2-charged water is heavier than seawater and does therefore not migrate back to the surface, and the fast reactions between the carbonated water and the basaltic rocks [3] it could be a feasible option to extract and re-inject the same water about five years after injection, thus accelerating flow through the formation.

On-shore pilot studies on CO_2 storage within basaltic rocks such as the two CarbFix field injection experiments [e.g. 11, 13, 66] and Big Sky Carbon Sequestration [67, 68] give valuable information on the feasibility of the concept together with modelling work and laboratory injection experiments, since offshore drilling and monitoring is both more expensive and harder to conduct. However, offshore pilot scale projects should be considered as the next steps in evolving the CarbFix method.

Acknowledgements

This publication has been produced with support from the NORDICCS Centre, performed under the Top-level Research Initiative CO_2 Capture and Storage program and Nordic Innovation (Project number 11029) and by the 7th Framework Programme of the EC through the CarbFix project (project no. 283148).

This paper was written while the first author stayed as a visiting scientist at Lamont Doherty Earth Observatory, at Columbia University in New York. Sandra Ó. Snæbjörnsdóttir wishes to thank Martin Stute, David Goldberg and Angela Slagle for their hospitality and fruitful discussions.

The authors would also like to thank Becca Neely at the University of Iceland for her endless help and advice, Ragnar H. Þrastarson at the Icelandic Met Office for the GIS work, Per Aagaard, Karen L. Anthonsen, Per Bergmö, Gry M. Morthensen and Ane Lothe from WP6 of the NORDICCS project for their comments and informative discussions and partners of the CarbFix project for their help and support.

References

[1] International Energy Agency. Technology roadmap: Carbon capture and storage. Paris, France: IEA, 2013.

[2] Snæbjörnsdóttir SÓ, Wiese F, Fridriksson T, Ármannsson H, Einarsson GM, Gislason SR. CO_2 storage potential of basaltic rocks in Iceland and the oceanic ridges. Energy Procedia. 2014; 63 : 4585-600.

[3] Gislason SR, Oelkers EH. Carbon Storage in Basalt. Science. 2014; 344 : 373-4.

[4] Goldberg DS, Kent DV, Olsen PE. Potential on-shore and off-shore reservoirs for CO_2 sequestration in Central Atlantic magmatic province basalts. Proceedings of the National Academy of Sciences of the United States of America Sciences. 2010; 107: 1327-32.

[5] Goldberg D, Slagle AL. A global assessment of deep-sea basalt sites for carbon sequestration. Energy Procedia. 2009; 1: 3675-82.

[6] Oelkers EH, Gislason SR, Matter J. Mineral carbonation of CO_2. Elements. 2008; 4: 331–5.

[7] Galeczka I, Wolff-Boenisch D, Jonsson T, Sigfusson B, Stefansson A, Gislason SR. A novel high pressure column flow reactor for experimental studies of CO_2 mineral storage. Applied Geochemistry. 2013; 30: 91-104.
[8] Alfredsson HA, Oelkers EH, Hardarsson BS, Franzson H, Gunnlaugsson E, Gislason SR. The geology and water chemistry of the Hellisheidi, SW-Iceland carbon storage site. International Journal of Greenhouse Gas Control. 2013; 12: 399-418.
[9] Gysi AP, Stefánsson A. CO_2-water–basalt interaction. Low temperature experiments and implications for CO_2 sequestration into basalts. Geochimica et Cosmochimica Acta. 2012; 81: 129-52.
[10] Wolff-Boenisch D, Wenau S, Gislason SR, Oelkers EH. Dissolution of basalts and peridotite in seawater, in the presence of ligands, and CO_2: Implications for mineral sequestration of carbon dioxide. Geochimica et Cosmochimica Acta. 2011; 75 (19): 5510-25.
[11] Gislason SR, Wolff-Boenisch D, Stefansson A, Oelkers EH, Gunnlaugsson E, Sigurdardottir H, et al. Mineral sequestration of carbon dioxide in basalt: a preinjection overview of the CarbFix project. International Journal of Greenhouse Gas Control. 2010; 4: 537-45.
[12] Rosenbauer RJ, Thomas B, Bischoff JL, Palandri J. Carbon sequestration via reaction with basaltic rocks: Geochemical modelling and experimental results. Geochimica et Cosmochimica Acta. 2012; 89: 116−33.
[13] Sigfusson B, Gislason SR, Matter JM, Stute M, Gunnlaugsson E, Gunnarsson I, et al. Solving the carbon-dioxide buoyancy challenge: The design and field testing of a dissolved CO_2 injection system. International Journal of Greenhouse Gas Control. 2015; 37: 213-9.
[14] Matter JM, Stute M, Hall J, Mesfin K, Snæbjörnsdóttir SÓ, Gislason SR, et al. Monitoring permanent CO_2 storage by in situ mineral carbonation using a reactive tracer technique. Energy Procedia. 2014; 63: 4180-5.
[15] Snæbjörnsdóttir SÓ, Mesfin K, Gunnarsson I, Aradottir ES, Stute M, Matter J, et al. Rapid mineralisation of CO_2 and CO_2-H_2S-H_2-gas mixture at the CarbFix site in SW-Iceland. Conference abstract. Goldschmidt 2015; 16-22th of August 2015; Prague, Czech Republic 2015.
[16] Wilson M. Igneous Petrogenesis. A Global Tectonic Approach: Springer; 1989.
[17] Dessert C, Dupre B, Gaillardet J, Francois LM, Allegre CJ. Basalt weathering laws and the impact of basalt weathering on the global carbon cycle. Chemical Geology. 2003; 202: 257−73
[18] Searle R. Mid-Ocean Ridges. Cambridge, UK: Cambridge University Press; 2013.
[19] Archer D. Fate of fossil fuel CO_2 in geologic time. Journal of Geophysical Research. 2005; 110: C09S5.
[20] Talwani M, Udintsev G. Initial Reports of the Deep Sea Drilling Project 38. Washington, U.S.: 1976.
[21] Fisher AT. Permeability within basaltic oceanic crust. Reviews of Geophysics. 1998; 36 (2): 143-82.
[22] Carboette SM, Scheirer DS. Variability of ocean crustal structure created along the global mid-ocean ridge. Davis EE, Elderfield H, editors. Cambridge: Cambridge University Press; 2004.
[23] Harris RN, Chapman DS. Deep-seated oceanic heat flux, heat deficits and hydrothermal circulation. Davis EE, Elderfield H, editors. Cambridge: Cambridge University Press; 2004.
[24] Duan ZH, Sun R. An improved model calculating CO_2 solubility in pure water and aqueous NaCl solutions from 273 to 533 K and from 0 to 2000 bar. Chemical Geology. 2003; 193 (3-4): 257-71.
[25] Duan ZH, Sun R, Zhu C, Chou IM. An improved model for the calculation of CO_2 solubility in aqueous solutions containing Na^+, K^+, Ca^{2+}, Mg^{2+}, Cl^-, and SO_4^{2-}. Marine Chemistry. 2006; 98 (2-4): 131-9.
[26] Global Carbon Project 2015; Global carbon budget. Available from: http://www.globalcarbonproject.org/carbonbudget/14/hl-full.htm. [cited 4.9.2015].
[27] Höskuldsson Á, Hey R, Kjartansson E, Guðmundsson GB. The Reykjanes Ridge between 63°10'N and Iceland. Journal of Geodynamics. 2007; 43: 73-86.
[28] ETOPO1 1 Arc-Minute Global Relief Model: Procedures, Data Sources and Analysis. National Geophysical Data Center, NOAA. 2009 [cited 9.9.2014].
[29] Einarsson P. Plate boundaries, rifts and transforms in Iceland. Jökull 2008; 58 : 35–58.
[30] Sigmundsson F. Iceland Geodynamics. Crustal Deformation and Divergent Plate Tectonics. Berlin, Germany: Springer-Verlag; 2006.
[31] Arnadottir T, Geirsson H, Jiang W. Crustal deformation in Iceland: Plate spreading and earthquake deformation. Jökull. 2008; 58: 59-74.
[32] Einarsson P. Earthquakes and present day tectonism in Iceland. Tectonophysics. 1991; 189: 261–79.
[33] Einarsson P. Relative location of earthquakes in the Tjörnes Fracture Zone. Geodynamica Acta Islandica. 1976; V : 45–60.
[34] Bjarnason I. An Iceland Hotspot Saga. Jökull. 2008; 58: 3-16.
[35] Smallwood JR, White RS, Minshull TA. Sea-floor spreading in the presence of the Iceland plume: the structure of the Reykjanes Ridge at 61 ° 40′ N. J Geol Soc London, . 1995; 152: 1023-29.
[36] White RS, Brown JW, Smallwood JR. The temperature of the Iceland plume and the origin of outward-propagating V-shaped ridges. J Geol Soc London,. 1995; 152 : 1039-45.
[37] Howell SM, Ito G, Breivik AJ, Rai A, Mjelde R, Hanan B, et al. The origin of the asymmetry in the Iceland hotspot along the Mid-Atlantic Ridge from continental breakup to present-day. Earth and Planetary Science Letters. 2014; 392: 143-53.
[38] Gunnarsson K. The oceanic floor around Iceland. Evolution and sedimentary formations. Overview report on the status of exploration (in Icelandic). Reykjavik, Iceland: National Energy Authotrity of Iceland, 1980 OS80025/JHD14.
[39] Thordarson T, Höskuldsson Á. Postglacial volcanism in Iceland. Jökull. 2008; 58: 197-228.
[40] Hjartarson Á, Sæmundsson K. Geological Map of Iceland. Bedrock. 1:600 000. Reykjavik: Iceland GeoSurvey; 2014.
[41] Kristjánsson L. The shelf around Iceland. Jökull. 1979; 29: 3-6.
[42] Gunnarsson K, Kjartansdóttir M. Core drilling in Flatey, Skjálfandi. First results. (In Icelandic). National Energy Authority of Iceland, 1982 OS82126/JHD38.
[43] Einarsson P, Sæmundsson K. Earthquake epicenters 1982–1985 and volcanic systems in Iceland. Menningarsjóður, Reykjavík.; 1987.
[44] Esri, GEBCO, NOAA, National Geographic and DeLorme. National Geographic World Map [accessed 28.8.2015].

[45] Richter B, Gunnarsson K. Overview of hydrocarbon related research in Tjörnes. Reykjavik, Iceland: Iceland GeoSurvey, 2010 ISOR-2010/007.
[46] Franzson H, Björnsson G, Ásmundsson R, Blischke A. Heimaey: Well HH-8 - drilling and research (in Icelandic). Reykjavik, Iceland: Iceland GeoSurvey, 2010 ISOR-2010/027.
[47] Eiríksson J, Guðmundsson AI, Kristjánsson L, Gunnarsson K. Palaeomagnetism of Pliocene-Pleistocene sediments and lava flows on Tjörnes and Flatey, North Iceland. Boreas. 1990; 19: 39-55.
[48] Marks N, Schiffman P, Zierenberg RA, Franzson H, Fridleifsson GÓ. Hydrothermal alteration in the Reykjanes geothermal system: Insights from Iceland deep drilling program well RN-17. Journal of Volcanology and Geothermal Research. 2010; 189 (1–2): 172-90.
[49] Smallwood JR, White RS. Crustal accreation at the Reykjanes Ridge, 61°-62°N. Journal of Geophysical Research. 1998; 103(B3): 5185-201.
[50] Muehlenbachs K, Hodges FN. Oxygen isotope geochemistry of rocks from DSDP leg 46. U.S. Governmental Print Office: 1978.
[51]Muehlenbachs, K. Low temperature alteration oxygen isotope exchange between the oceanic crust and seawater. Proceedings 2nd International Syrup Water-Rock Interaction. 1977; 317-26.
[52] Staudigel H, Hart SR, H. RS. Alteration of the oceanic crust: Processes and timing. Earth and Planetary Science Letters. 1981; 52 : 311-27.
[53] Brady PV, Gíslason SR. Seafloor weathering controls on atmospheric CO_2 and global climate. Geochimica et Cosmochimica Acta. 1997; 61 (5): 965-73.
[54] Richardson SH, Hart SR, Staudigel H. Vein minerals of old oceanic crust. J. Geophys. Res. 85, 7195-7200. Journal of Geophysical Research. 1980; 85 : 7195-000.
[55] Gillis KM, Robinson PT. Distribution of alteration zones in the upper oceanic crust. Geology. 1988; : 262-6.
[56] Jarrard RD, Abrams LJ, Pockalny R, Larson RL, Hirono T. Physical properties of upper oceanic crust: Oceanic Drilling Program Hole 801C and the waning of hydrothermal circulation. Journal of Geophysical Research. 2003; 108 (B4).
[57] Frolova J, Franzson H, Ladygin V, Sigurdsson O, Stefánsson V, Shustrov V, editors. Porosity and permeability of hyaloclastites tuffs, Iceland. International Geothermal Workshop IGW2004. August 9-16; Petropavlovsk-Kamchatsky.
[58] Neuhoff PS, Fridriksson T, Armannsson H. Porosity evolution and mineral paragenesis during low-grade metamorphism of basaltic lavas at Teigarhorn, Eastern Iceland. American Journal of Science. 2008; 299: 467-501.
[59] Stefánsson V, Sigurðsson Ó, Guðmundsson Á, Franzson H, Friðleifsson GÓ, Tulinius H. Core measurements and geothermal modelling. Second Nordic Symposium on Petrophysics 1997 p. 199-220.
[60] Franzson H. The Nesjavellir high-temperature field, SW-Iceland, reservoir geology. Proceedings 19th Annual PNOC-EDC Geothermal Conference, Manilla, Phillippines, March 5-6th 1998. 1998; 13-20.
[61] McGrail BP, Schaef HT, Ho AM, Chien Y-J, Dooley JJ, Davidson CL. Potential for carbon dioxide sequestration in flood basalts. Journal of Geophysical Research 2006; Solid Earth (111) (B12201).
[62] Wiese F, Fridriksson T, Armannsson H. CO2 Fixation by Calcite in High-temperature Geothermal Systems in Iceland. Iceland Geosurvey, 2008, ISOR−2008/003
[63] Goldberg DS, Takahashi T, Slagle AL. Carbon dioxdie sequestration in deep-sea basalt. PNAS. 2008; 105 (29): 9920-5.
[64] Aradóttir ESP, Sonnenthal EL, Björnsson G, Jónsson H. Multidimensional reactive transport modeling of CO_2 mineral sequestration in basalts at the Hellisheidi geothermal field, Iceland. International Journal of Greenhouse Gas Control. 2012; 9: 24-40.
[65] Gunnarsson, G. Temperature Dependent Injectivity and Induced Seismicity – Managing Reinjection in the Hellisheiði Field, SW-Iceland. GRC Transactions. 2013: 37: 1020-1025.
[66] Gislason SR, Broecker WS, Gunnlaugsson E, Snæbjörnsdóttir SÓ, Mesfin KG, Alfredsson HA, et al. Rapid solubility and mineral storage of CO_2 in basalt. Energy Procedia. 2014; 63: 4561-74.
[67] McGrail BP, Spane FA, Sullivan EC, Bacon DH, Hund G. The Wallula basalt sequestration pilot project. Energy Procedia. 2011;4: 5653-60.
[68] McGrail BP, Freeman CJ, Brown CF, Sullivan EC, White SK, Reddy S, et al. Overcoming business model uncertainty in a carbon dioxide capture and sequestration project: Case study at the Boise White Paper Mill. International Journal of Greenhouse Gas Control. 2012; 9: 91-102.

Paper III

Rapid carbon mineralization for permanent disposal of anthropogenic carbon dioxide emissions

Matter J.M, Stute M., **Snæbjörnsdóttir S.Ó**., Oelkers E.H., Gislason S.R., Aradottir E.S., Sigfusson B., Gunnarsson I., Sigurdardottir H., Gunnlaugsson E., Axelsson G., Alfredsson H.A., Wolff-Boenisch D., Mesfin K., Fernandez de la Reguera Taya D., Hall J., Dideriksen K., Broecker W.S., 2016. Science 352, 1312-1314. *DOI: 10.1126/science.aad8132*

Author's contribution:
Study conception and design: JMM, MS, EHO, SRG, ESA, BS, IG, HS, EG, GA, WD, WSB
Samples collected by: SOS, HAA, KM, DFRT, JH
Samples analysed by: MS, SOS, HAA, KM, DFRT, JH, KD
Interpretation of data: JMM, MS, SOS, EHO, SRG
Drafting of manuscript: JMM, EHO, SRG

CARBON SEQUESTRATION

Rapid carbon mineralization for permanent disposal of anthropogenic carbon dioxide emissions

Juerg M. Matter,[1,2]* Martin Stute,[2] Sandra Ó. Snæbjörnsdottir,[3] Eric H. Oelkers,[3,4,5] Sigurdur R. Gislason,[3] Edda S. Aradottir,[6] Bergur Sigfusson,[6,7] Ingvi Gunnarsson,[6] Holmfridur Sigurdardottir,[6] Einar Gunnlaugsson,[6] Gudni Axelsson,[8] Helgi A. Alfredsson,[3] Domenik Wolff-Boenisch,[3,9] Kiflom Mesfin,[3] Diana Fernandez de la Reguera Taya,[2] Jennifer Hall,[2] Knud Dideriksen,[10] Wallace S. Broecker[2]

Carbon capture and storage (CCS) provides a solution toward decarbonization of the global economy. The success of this solution depends on the ability to safely and permanently store CO_2. This study demonstrates for the first time the permanent disposal of CO_2 as environmentally benign carbonate minerals in basaltic rocks. We find that over 95% of the CO_2 injected into the CarbFix site in Iceland was mineralized to carbonate minerals in less than 2 years. This result contrasts with the common view that the immobilization of CO_2 as carbonate minerals within geologic reservoirs takes several hundreds to thousands of years. Our results, therefore, demonstrate that the safe long-term storage of anthropogenic CO_2 emissions through mineralization can be far faster than previously postulated.

The success of geologic CO_2 storage depends on its long-term security and public acceptance, in addition to regulatory, policy, and economical factors (*1*). CO_2 and brine leakage through a confining system above the storage reservoir or through abandoned wells is considered one of the major challenges associated with geologic CO_2 storage (*2*–*4*). Leakage rates into the atmosphere of ≤0.1% are required to ensure effective climate change mitigation (*5*, *6*). To avoid CO_2 leakage, caprock integrity needs to be evaluated and monitored (*7*). Leakage risk is further enhanced by induced seismicity, which may open fluid flow pathways in the caprock (*8*). Mineral carbonatization (i.e., the conversion of CO_2 to carbonate minerals) via CO_2-fluid-rock reactions in the reservoir minimizes the risk of leakage and thus facilitates long-term and safe carbon storage and public acceptance (*9*). The potential for carbonatization is, however, limited in conventional CO_2 storage reservoirs such as deep saline aquifers and depleted oil and gas reservoirs in sedimentary basins due to the lack of calcium-, magnesium-, and iron-rich silicate minerals required to form carbonate minerals (*10*, *11*). An alternative is to inject CO_2 into basaltic rocks, which contain up to 25% by weight of calcium, magnesium, and iron. Basaltic rocks are highly reactive and are one of the most common rock types on Earth, covering ~10% of continental surface area and most of the ocean floor (*12*, *13*).

The CarbFix pilot project in Iceland was designed to promote and verify in situ CO_2 mineralization in basaltic rocks for the permanent disposal of anthropogenic CO_2 emissions (*14*). Two injection tests were performed at the CarbFix injection site near the Hellisheidi geothermal power plant. Phase I: 175 tons of pure CO_2 from January to March 2012, and phase II: 73 tons of a CO_2-H_2S gas mixture in June to August 2012, of which 55 tons were CO_2. H_2S is not only a major constituent of geothermal gases but also of CO_2-rich sour gas. Because the cost of carbon capture and storage (CCS) is dominated by the cost of capture and gas separation, the overall cost could be lowered substantially by injecting gas mixtures rather than pure CO_2 (*9*). Hence, the purpose of the mixed CO_2/H_2S injection was to assess the feasibility of injecting impurities in the CO_2 stream.

The CarbFix injection site is situated about 25 km east of Reykjavik and is equipped with a 2000-m-deep injection well (HN02) and eight monitoring wells ranging in depth from 150 to 1300 m (Fig. 1). The target CO_2 storage formation is at between 400 and 800 m depth and consists of basaltic lavas and hyaloclastites with lateral and vertical intrinsic permeabilities of 300 and 1700 × 10^{-15} m^2, respectively (*15*, *16*). It is overlain by low-permeability hyaloclastites. The formation water temperature and pH in the injection interval range from 20° to 33°C and from 8.4 to 9.4, and it is oxygen-depleted (*15*). Due to the shallow depth of the target storage reservoir and the risk of CO_2 gas leakage through fractures, a novel CO_2 injection system was designed and used, which dissolves the gases into down-flowing water in the well during its injection (*17*). To avoid potential degassing, the CO_2 concentration in the injected fluids was kept below its solubility at reservoir conditions (*17*). Once dissolved in water, CO_2 is no longer buoyant (*17*), and it immediately starts to react with the Ca-Mg-Fe–rich reservoir rocks.

Because dissolved or mineralized CO_2 cannot be detected by conventional monitoring methods such as seismic imaging, the fate of the injected CO_2 was monitored with a suite of chemical and isotopic tracers. The injected CO_2 was spiked with carbon-14 (^{14}C) to monitor its transport and reactivity (*18*). For the pure CO_2 and the CO_2/H_2S injections, the ^{14}C concentrations of the injected fluids were 40.0 Bq/liter ($^{14}C/^{12}C$: 2.16 × 10^{-11}) and 6 Bq/liter ($^{14}C/^{12}C$: 6.5 × 10^{-12}), respectively. By comparison, the ^{14}C concentration in the reservoir before the injections was 0.0006 Bq/liter ($^{14}C/^{12}C$: 1.68 × 10^{-13}). This novel carbon tracking method was previously proposed for geologic CO_2 storage monitoring, but its feasibility has not been tested previously (*19*, *20*). Because $^{14}CO_2$ chemically and physically behaves identically to $^{12}CO_2$ and is only minimally affected by isotope fraction during phase transitions (*21*), it provides the means to accurately inventory the fate of the injected carbon.

In addition to ^{14}C, we continuously co-injected nonreactive but volatile sulfur hexafluoride (SF_6) and trifluoromethyl sulfur pentafluoride (SF_5CF_3) tracers to assess plume migration in the reservoir. The SF_6 was used during phase I and SF_5CF_3 during phase II. The SF_6 and SF_5CF_3 concentrations in the injected fluids were 2.33 × 10^{-8} cc at standard temperature and pressure (ccSTP)/cc and 2.24 × 10^{-8} ccSTP/cc, respectively.

The CO_2 and CO_2/H_2S mixtures, together with the tracers, were injected into the target storage formation fully dissolved in water pumped from a nearby well. Typical injection rates during phase I injection were 70 g/s for CO_2 and 1800 g/s for H_2O, respectively (*17*). Injection rates during phase II varied between 10 and 50 g/s for CO_2 and 417 and 2082 g/s for H_2O. The dissolved inorganic carbon (DIC) concentration and pH of the injectates were 0.82 mol/liter and 3.85 (at 20°C) for phase I and 0.43 mol/liter and 4.03 for phase II. Fluid samples for SF_6, SF_5CF_3, ^{14}C, DIC, and pH analyses were collected without degassing using a specially designed downhole sampler from the injection well HN02 (*22*) or with a submersible pump from the first monitoring well, HN04, located about 70 m downstream from HN02 at 400 m depth below the surface before, during, and after injection (tables S1 to S3).

The arrival of the injectate from phase I at monitoring well HN04 was confirmed by an increase in SF_6 concentration, and a sharp decrease in pH and DIC concentration (Fig. 2, A and B, and table S3). Based on the SF_6 data, the initial breakthrough in HN04 occurred 56 days after injection. Subsequently, the SF_6 concentration slightly decreased before a further increase in concentration occurred, with peak concentration 406 days after initiation of the injection. SF_5CF_3 behaves similarly (Fig. 2A); its initial arrival was detected 58 days after initiation of the phase II injection,

[1]Department of Ocean and Earth Science, University of Southampton, Southampton, UK. [2]Lamont-Doherty Earth Observatory, Columbia University, Palisades, NY, USA. [3]Institute of Earth Sciences, University of Iceland, Iceland. [4]CNRS/UMR 5563, Université Paul Sabatier, Toulouse, France. [5]Department of Earth Science, University College London, UK. [6]Reykjavik Energy, Reykjavik, Iceland. [7]European Commission, Joint Research Center, Institute for Energy and Transport, Petten, Netherlands. [8]Iceland GeoSurvey, Reykjavik, Iceland. [9]Department of Applied Geology, Curtin University, Perth, Western Australia. [10]Nano-Science Center, Department of Chemistry, University of Copenhagen, Copenhagen, Denmark.
*Corresponding author. Email: j.matter@southampton.ac.uk

followed by decreasing concentrations until 350 days after the injection started. Subsequently, the SF_5CF_3 concentration increased, consistent with the SF_6 tracer breakthrough curve. The double peaks in these tracer breakthrough curves are also in agreement with results from previous tracer tests showing that the storage formation consists of relatively homogenous porous media intersected by a low-volume and fast flow path that channels about 3% of the tracer flow between HN02 and HN04 (*23*).

The time series of DIC, pH, and ^{14}C in HN04 are initially coincident with the SF_6 record, showing peak concentrations in ^{14}C and DIC and a decrease in pH around 56 days after injection (Figs. 2B and 3). The small drop in pH and increase in DIC around 200 days after injection is caused by the phase II injection, as confirmed by the SF_5CF_3 time series (Fig. 2A). The similar initial pattern in the tracer breakthrough curves and the DIC concentration suggests identical transport behavior of carbon and tracers in the reservoir. However, ^{14}C and DIC concentrations subsequently decreased and stayed more or less constant for the remaining monitoring period, with the exception of a small increase in concentration induced by the phase II injection (Figs. 2B and 3, A and B).

The fate of the injected CO_2 was quantified using mass balance calculations (*18*). The resulting calculated DIC and ^{14}C concentrations are much higher than those measured in the collected water samples, suggesting a loss of DIC and ^{14}C along the subsurface flow path toward the monitoring well (Fig. 3, A and B). The most plausible mechanism for this difference is carbonate precipitation. The differences between calculated and measured DIC and ^{14}C indicate that >95% of the injected CO_2 was mineralized through water-CO_2-basalt reactions between the injection (HN02) and monitoring (HN04) wells within 2 years (Fig. 3, A and B). The initial peak concentrations in DIC and ^{14}C detected around 56 days after injection suggest that travel time along the low-volume fast-flowing flow path was too short for significant CO_2 mineralization to occur. Most of the injected CO_2 was probably mineralized within the porous matrix of the basalt that allows for longer fluid residence times and thus extended reaction time. This conclusion is confirmed by (i) calculated fluid saturation states showing that the collected monitoring fluids are at saturation or supersaturation with respect to calcite at all times except during the initial low-volume flow path contribution; (ii) x-ray diffraction and scanning electron microscopy with energy-dispersive x-ray spectroscopy analysis of secondary mineral precipitates collected from the submersible pump in monitoring well HN04 after it was hauled to the surface, showing these precipitates to be calcite (*18*) (figs. S1 to S3); and (iii) the similarity in the ^{14}C concentration of the injected CO_2 and the precipitated collected calcite (7.48 ± 0.8 and 7.82 ± 0.05 fraction modern).

Although monitoring continues, the time scale of the tracer and DIC data discussed is limited to 550 days, because most of the injected CO_2 was mineralized by this time (Figs. 2 and 3). This 550-day

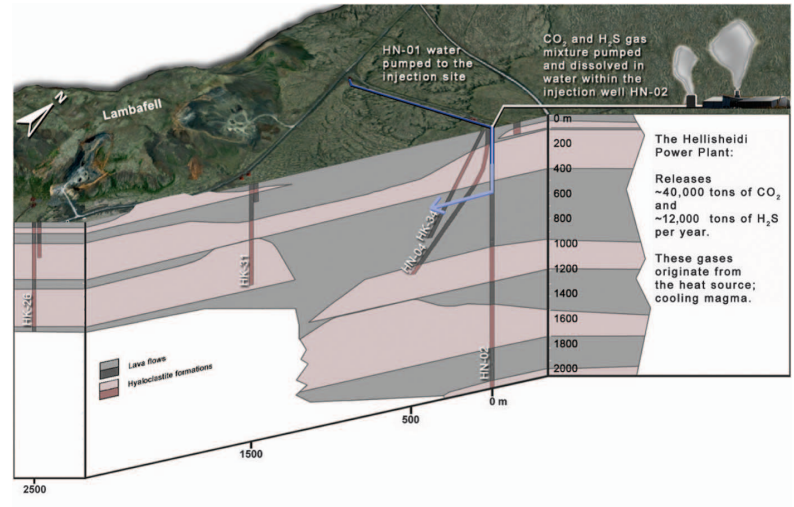

Fig. 1. Geological cross-section of the CarbFix injection site. CO_2 and H_2S are injected fully dissolved in water in injection well HN02 at a depth between 400 and 540 m. For this study, fluid samples were collected in the injection well HN02 and the monitoring well HN04 [modified from (*15*)].

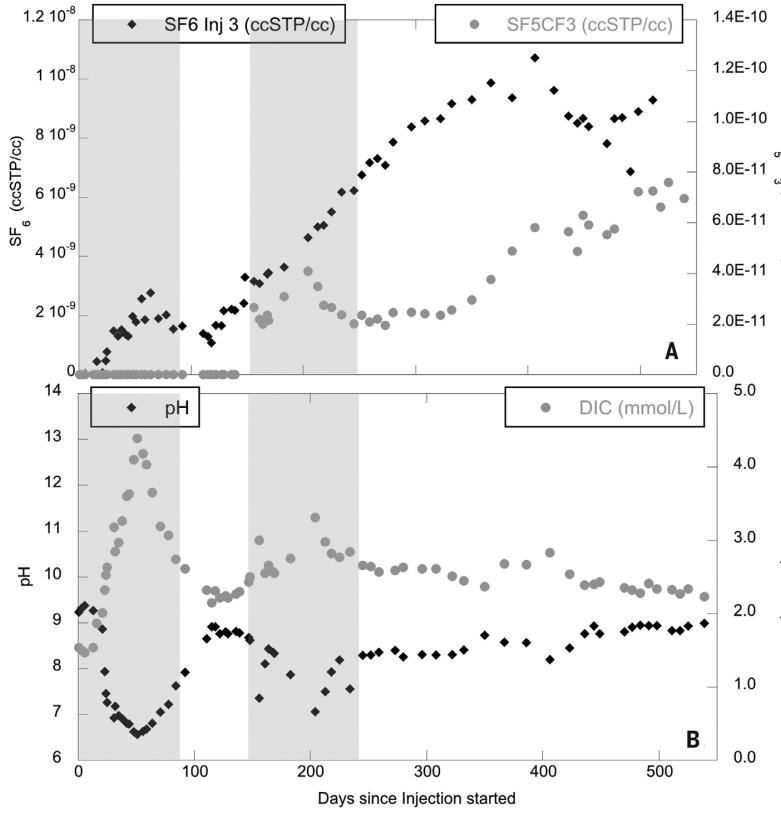

Fig. 2. Change of tracer concentrations, DIC, and pH in the target CO_2 storage formation fluid. Time series of (**A**) SF_6 and SF_5CF_3 tracer concentrations (ccSTP/cc) and (**B**) pH and DIC in monitoring well HN04 for the pure CO_2 and the CO_2 and H_2S injections. The shaded area indicates the phase I and II injection period.

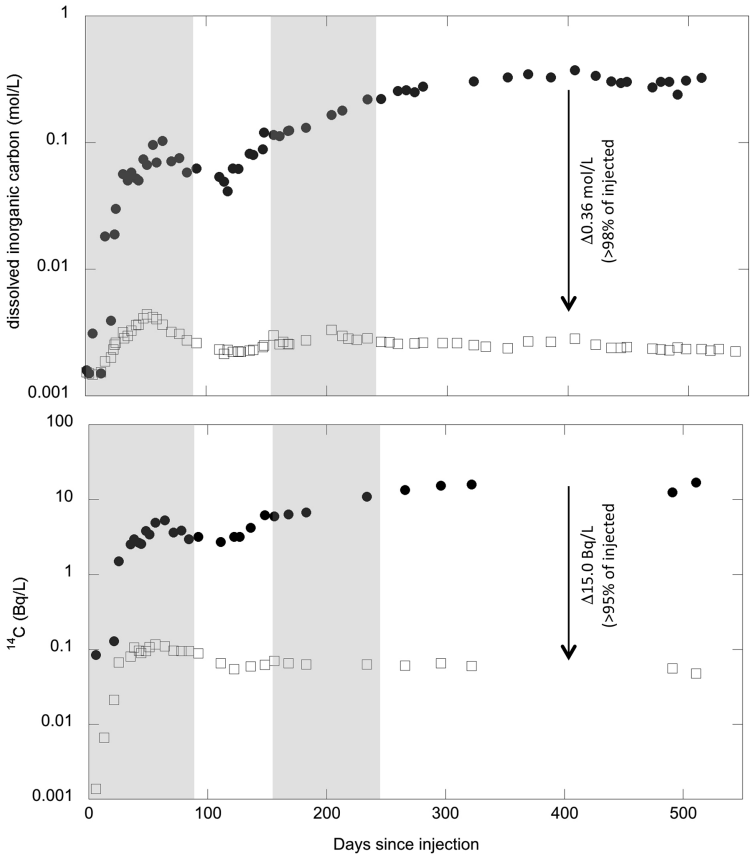

Fig. 3. Comparison of calculated and measured DIC and ^{14}C concentrations in the target CO_2 storage formation fluid. (**A**) Time series of expected (solid circles) versus measured (open squares) DIC (mol/liter) in monitoring well HN04, indicating >98% conversion of injected CO_2 to carbonate minerals, and (**B**) time series of expected (solid circles) versus measured (open squares) $^{14}C_{DIC}$ (Bq/liter) in monitoring well HN04, showing >95% of injected CO_2 to be converted to carbonate minerals. The shaded area indicates the phase I and II injection periods.

limit also coincides with the breakdown of the submersible pump in HN04 monitoring well, which resulted in a 3-month gap in the subsequent monitoring data. The pump was clogged and coated with calcite (*18*).

The fast conversion rate of dissolved CO_2 to calcite minerals in the CarbFix storage reservoir is most likely the result of several key processes: (i) the novel CO_2 injection system that injected water-dissolved CO_2 into the subsurface; (ii) the relatively rapid dissolution rate of basalt, releasing Ca, Mg, and Fe ions required for the CO_2 mineralization; (iii) the mixing of injected water with alkaline formation waters; and (iv) The dissolution of preexisting secondary carbonates at the onset of the CO_2 injection, which may have contributed to the neutralization of the injected CO_2-rich water via the reaction $CaCO_3 + CO_2 + H_2O = Ca^{2+} + 2\ HCO_3^-$.

The dissolution of preexisting calcite is supported by the $^{14}C/^{12}C$ ratio of the collected fluid samples, which suggest a 50% dilution of the carbon in the fluid, most likely via calcite dissolution just after it arrives in the basaltic reservoir. Nevertheless, the mass balance calculations clearly demonstrate that these preexisting carbonates re-precipitated during the mineralization of the injected CO_2.

The results of this study demonstrate that nearly complete in situ CO_2 mineralization in basaltic rocks can occur in less than 2 years. Once stored within carbonate minerals, the leakage risk is eliminated and any monitoring program of the storage site can be significantly reduced, thus enhancing storage security and potentially public acceptance. Natural aqueous fluids in basalts and those at the CarbFix site tend to be at or close to equilibrium with respect to calcite, limiting its redissolution (*16*). The scaling up of this basaltic carbon storage method requires substantial quantities of water and porous basaltic rocks (*9*). Both are widely available on the continental margins, such as off the coast of the Pacific Northwest of the United States (*12*).

REFERENCES AND NOTES

1. B. Metz, O. Davidson, H. de Coninck, M. Loos, L. A. Meyer, Eds., *IPCC Special Report on Carbon Dioxide Capture and Storage* (Cambridge Univ. Press, New York, 2005).
2. A. Esposito, S. Benson, in Proceedings of the Society of Petroleum Engineers 2010 Western North American Regional Meeting, Anaheim, CA, 27 to 29 May 2010 (Society of Petroleum Engineers, 2010), SPE-133604.
3. B. Ellis *et al.*, *Sci. Technol.* **1**, 248–260 (2011).
4. J. M. Bielicki, M. F. Pollak, J. P. Fitts, C. A. Peters, E. J. Wilson, *Int. J. Greenhouse Gas Control* **20**, 272–284 (2014).
5. P. M. Haugan, F. Joos, *Geophys. Res. Lett.* **31**, L18202 (2004).
6. B. van der Zwaan, L. Smekens, *Environ. Model. Assess.* **14**, 135–148 (2009).
7. H. S. Eggleston *et al.*, Eds., *IPCC Guidelines for National Greenhouse Gas Inventories – A Primer* (National Greenhouse Gas Inventories Programme, Institute for Global Environmental Strategies, Japan, 2008).
8. M. D. Zoback, S. M. Gorelick, *Proc. Natl. Acad. Sci. U.S.A.* **109**, 10164–10168 (2012).
9. S. R. Gislason, E. H. Oelkers, *Science* **344**, 373–374 (2014).
10. J. M. Matter, P. B. Kelemen, *Nat. Geosci.* **2**, 837–841 (2009).
11. S. M. V. Gilfillan *et al.*, *Nature* **458**, 614–618 (2009).
12. D. S. Goldberg, T. Takahashi, A. L. Slagle, *Proc. Natl. Acad. Sci. U.S.A.* **105**, 9920–9925 (2008).
13. B. P. McGrail *et al.*, *J. Geophys. Res.* **111**, B12201 (2006).
14. S. R. Gislason *et al.*, *Int. J. Greenhouse Gas Control* **4**, 537–545 (2010).
15. H. A. Alfredsson *et al.*, *Int. J. Greenhouse Gas Control* **12**, 399–418 (2013).
16. E. S. Aradóttir, E. L. Sonnenthal, G. Björnsson, H. Jónsson, *Int. J. Greenhouse Gas Control* **9**, 24–40 (2012).
17. B. Sigfusson *et al.*, *Int. J. Greenhouse Gas Control* **37**, 213–219 (2015).
18. Materials and methods are available as supplementary materials on *Science* Online.
19. P. P. Bachelor *et al.*, *J. Radioanal. Nucl. Chem.* **277**, 85–89 (2008).
20. K. S. Lackner, S. Brennan, *Clim. Change* **96**, 357–378 (2009).
21. I. D. Clark, P. Fritz, *Environmental Isotopes in Hydrogeology* (Lewis Publishers, Boca Raton, FL, 1997).
22. H. A. Alfredsson, K. Mesfin, D. Wolff-Boenisch, *Greenhouse Gas Sci. Technol.* **6**, 167–177 (2016).
23. M. Rezvani Khalilabad, G. Axelsson, S. Gislason, *Mineral. Mag.* **72**, 121–125 (2008).

ACKNOWLEDGMENTS

We acknowledge funding from Reykjavik Energy; the U.S. Department of Energy under award number DE-FE0004847 to J.M.M and M.S.; the European Commission through the projects CarbFix (EC coordinated action 283148), Min-GRO (MC-RTN-35488), Delta-Min (PITN-GA-2008-215360), and CO_2-REACT (EC Project 317235) to S.R.G., E.H.O., and Reykjavik Energy; Nordic fund 11029-NORDICCS; and the Icelandic GEORG Geothermal Research fund (09-02-001) to S.R.G. and Reykjavik Energy. We thank T. Kristinsson and E. Ó. Þrastarsonfor for helping with sample collection in the field. All data used in this study are included in the supplementary materials.

SUPPLEMENTARY MATERIALS

www.sciencemag.org/content/352/6291/1312/suppl/DC1
Materials and Methods
Supplementary Text
Figs. S1 to S3
Tables S1 and S2
References (*24*–*34*)

10.1126/science.aad8132

Rapid carbon mineralization for permanent disposal of anthropogenic carbon dioxide emissions
Juerg M. Matter, Martin Stute, Sandra Ó. Snæbjörnsdottir, Eric H. Oelkers, Sigurdur R. Gislason, Edda S. Aradottir, Bergur Sigfusson, Ingvi Gunnarsson, Holmfridur Sigurdardottir, Einar Gunnlaugsson, Gudni Axelsson, Helgi A. Alfredsson, Domenik Wolff-Boenisch, Kiflom Mesfin, Diana Fernandez de la Reguera Taya, Jennifer Hall, Knud Dideriksen and Wallace S. Broecker (June 9, 2016)
Science **352** (6291), 1312-1314. [doi: 10.1126/science.aad8132]

Editor's Summary

Inject, baby, inject!

Atmospheric CO^2 can be sequestered by injecting it into basaltic rocks, providing a potentially valuable way to undo some of the damage done by fossil fuel burning. Matter *et al.* injected CO^2 into wells in Iceland that pass through basaltic lavas and hyaloclastites at depths between 400 and 800 m. Most of the injected CO^2 was mineralized in less than 2 years. Carbonate minerals are stable, so this approach should avoid the risk of carbon leakage.

Science, this issue p. 1312

Science (print ISSN 0036-8075; online ISSN 1095-9203) is published weekly, except the last week in December, by the American Association for the Advancement of Science, 1200 New York Avenue NW, Washington, DC 20005.

Paper IV

The chemistry and saturation states of subsurface fluids during the in situ mineralisation of CO_2 and H_2S at the CarbFix site in SW-Iceland

Snæbjörnsdóttir, S.Ó., Oelkers, E.H., Mesfin, K., Aradóttir, E.S., Dideriksen, K., Gunnarsson, I., Gunnlaugsson, E., Matter, J.M., Stute, M., Gislason, S.R., 2017. International Journal of Greenhouse Gas Control 58, 87–102.
DOI:10.1016/j.ijggc.2017.01.007

International Journal of Greenhouse Gas Control 58 (2017) 87–102

Contents lists available at ScienceDirect

International Journal of Greenhouse Gas Control

journal homepage: www.elsevier.com/locate/ijggc

The chemistry and saturation states of subsurface fluids during the *in situ* mineralisation of CO_2 and H_2S at the CarbFix site in SW-Iceland

Sandra Ó. Snæbjörnsdóttir[a,*], Eric H. Oelkers[a,b,c], Kiflom Mesfin[a], Edda Sif Aradóttir[d], Knud Dideriksen[e], Ingvi Gunnarsson[d], Einar Gunnlaugsson[d], Juerg M. Matter[f,g], Martin Stute[g], Sigurdur R. Gislason[a]

[a] *Institute of Earth Science, University of Iceland, Iceland*
[b] *CNRS/UMR 5563, Université Paul Sabatier, France*
[c] *Earth Science, University College London, UK*
[d] *Reykjavik Energy, Iceland*
[e] *Nano-Science Center, Department of Chemistry, University of Copenhagen, Denmark*
[f] *Ocean and Earth Science, University of Southampton, UK*
[g] *Lamont-Doherty Earth Observatory, Columbia University, USA*

ARTICLE INFO

Article history:
Received 31 May 2016
Received in revised form 24 October 2016
Accepted 9 January 2017

Keywords:
SulFix
Basaltic rocks
CCS
Mineral storage
Mineral trapping
Solubility trapping
Carbonation
Gas mixtures

ABSTRACT

In situ carbonation of basaltic rocks could provide a long-term carbon storage solution, which is essential for the success and public acceptance of carbon storage. To demonstrate the viability of this carbon storage solution, 175 tonnes (t) of pure CO_2 and 73 tonnes (t) of a 75% CO_2-24% H_2S-1% H_2-gas mixture were sequentially injected into basaltic rocks at the CarbFix site at Hellisheidi, SW-Iceland from January to August 2012. This paper reports the chemistry and saturation states with respect to potential secondary minerals of sub-surface fluids sampled prior to, during, and after the injections. All gases were dissolved in water during their injection into permeable basalts located at 500–800 m depth with temperatures ranging from 20 to 50 °C. A pH decrease and dissolved inorganic carbon (DIC) increase was observed in the first monitoring well, HN-04, about two weeks after each injection began. At storage reservoir target depth, this diverted monitoring well is located ~125 m downstream from the injection well. A significant increase in H_2S concentration, however, was not observed after the second injection. Sampled fluids from the HN-04 well show a rapid increase in Ca, Mg, and Fe concentration during the injections with a gradual decline in the following months. Calculations indicate that the sampled fluids are saturated with respect to siderite about four weeks after the injections began, and these fluids attained calcite saturation about three months after each injection. Pyrite is supersaturated prior to and during the mixed gas injection and in the following months. In July 2013, the HN-04 fluid sampling pump broke down due to calcite precipitation, verifying the carbonation of the injected CO_2. Mass balance calculations, based on the recovery of non-reactive tracers co-injected into the subsurface together with the acid-gases, confirm that more than 95% of the CO_2 injected into the subsurface was mineralised within a year, and essentially all of the injected H_2S was mineralised within four months of its injection. These results demonstrate the viability of the *in situ* mineralisation of these gases in basaltic rocks as a long-term and safe storage solution for CO_2 and H_2S.

1. Introduction

Attenuating the current increasing atmospheric CO_2 concentration is one of the greatest challenges of this century (e.g. Broecker, 2007; Broecker and Kunzig, 2008; Global CCS Institute, 2015; Hoffert et al., 2002; International Energy Agency, 2015; IPCC, 2005, 2014; Lackner, 2003; Oelkers and Schott, 2005; Oelkers and Cole, 2008; Pacala and Socolow, 2004). One potential solution to this challenge is carbon capture and storage (CCS). A critical step in CCS is identifying locations and methods for secure subsurface CO_2 storage.

This paper follows two previous reports on the CarbFix injection, 1) a detailed description of the injection method and data from the

* Corresponding author at: Institute of Earth Sciences, University of Iceland, Askja, Sturlugata 7, 101 Reykjavík, Iceland.
E-mail address: sos22@hi.is (S.Ó. Snæbjörnsdóttir).

http://dx.doi.org/10.1016/j.ijggc.2017.01.007
1750-5836/

injection well was presented by Sigfusson et al. (2015) and 2) the monitoring of tracers, carbon and pH in the first monitoring well downstream from the injection well was reported by Matter et al. (2016). The CarbFix project is focussed on CO_2 and H_2S injected into basaltic rocks. Carbon storage in basaltic rocks offers several advantages, due to their ability to promote permanent CO_2 storage by mineralisation and due to their large potential storage volume (Gislason and Oelkers, 2014; Goldberg and Slagle, 2009; Goldberg et al., 2010; McGrail et al., 2006; Snæbjörnsdóttir et al., 2014). As such, a large number of past studies have focussed on developing the technology to safely store CO_2 in basaltic rocks (Assayag et al., 2009; Bacon et al., 2014; Flaathen et al., 2009; Galeczka et al., 2014; Goldberg et al., 2013, 2008; Gudbrandsson et al., 2011; Gysi and Stefánsson, 2012a; Matter et al., 2007; McGrail et al., 2012, 2006, 2011; Rogers et al., 2006; Rosenbauer et al., 2012; Sigfusson et al., 2015; Stockmann et al., 2011; Van Pham et al., 2012). Basaltic rocks are rich in divalent cations such as Ca^{2+}, Mg^{2+}, and Fe^{2+}. Acidic gas-charged water accelerates the release of these metals, promoting the formation of carbonate minerals such as calcite, magnesite, and siderite (Gislason et al., 2014; Gislason and Oelkers, 2014; Olsson et al., 2014; Gislason et al., 2010; Gunnarsson et al., 2011; Oelkers et al., 2008; Stefánsson et al., 2011). About 5% of the continents and most of the oceanic floor are comprised of basaltic rocks, including the mid-oceanic ridges. The largest basaltic storage potential lies offshore; theoretically all CO_2 from the burning of fossil fuel carbon (~5000 GtC; Archer, 2005) could be stored by mineral carbonation along the mid-ocean ridges (Snæbjörnsdóttir et al., 2014). The flanks of the ridges contain highly fractured and permeable basaltic layers (Fisher, 1998) with a pervasive circulation of about 1000 Gt seawater/yr (Harris and Chapman, 2004). The potential for using these systems for carbon storage is confirmed by the results of Wolff-Boenisch et al. (2011), who demonstrated the rapid dissolution basaltic rocks in CO_2 charged seawater.

About 90% of Icelandic bedrock is basaltic (Hjartarson and Sæmundsson, 2014). In total, Iceland produced 1.6 $MtCO_2$ by industrial processes in 2012 and about 0.2 $MtCO_2$ by geothermal energy production (Wöll et al., 2014). Iceland is the largest (103,000 km^2) part of the mid-ocean ridge systems exposed above sea level. Iceland, therefore, provides an excellent opportunity to explore the feasibility of mineral storage of CO_2 and gas mixtures in basaltic rocks at the oceanic ridges since drilling and detailed monitoring of injected gas and water by reactive and non-reactive tracers is much less costly onshore than offshore.

The potential advantages in storing carbon by the *in situ* carbonation of Icelandic basalts motivated creation of the CarbFix project, which was designed to inject CO_2 into subsurface adjacent to the Hellisheidi geothermal power plant. Extensive research was carried out prior to the injection of acid gases at the CarbFix site. Gislason et al. (2010) described the thermodynamics and kinetic basis for carbon storage at this site. Alfredsson et al. (2013) characterised the geology, and rock and water chemistry of the CarbFix site. Wiese et al. (2008) determined the amount and spatial distribution of naturally mineralised CO_2 within the Icelandic geothermal systems. The dissolution and precipitation rates of the subsurface rocks at the site were investigated in mixed flow reactors (e.g. Gudbrandsson et al., 2011; Gysi and Stefánsson, 2012a; Stockmann et al., 2013), in pressurised plug flow experiments (e.g. Galeczka et al., 2014), by hydrological modelling (Khalilabad et al., 2008), and using reactive transport modelling (Aradóttir et al., 2012).

The CarbFix project is unique in that it injects CO_2 into basalts as a dissolved aqueous phase. In contrast, most subsurface carbon storage projects have injected CO_2 as a separate phase into large sedimentary basins; this method requires high integrity cap-rocks to keep the injected buoyant gas in the subsurface (Gislason and Oelkers, 2014; Rutqvist et al., 2007). However, there are numerous advantages of injecting CO_2 into the subsurface within an aqueous phase. First, many of the risks associated with buoyancy can be mitigated by dissolving the gases into water during their injection (Gislason et al., 2010; Sigfusson et al., 2015). Once dissolved, the injected gases are no longer buoyant, making it possible to inject CO_2 into fractured rocks, such as basalts along the ocean ridges and on the continents. Furthermore, this injection method may also make it possible to simultaneously store a number of acid gases including SO_2 and H_2S as sulphide minerals such as pyrite and pyrrhotite, lowering substantially gas capture/storage costs (Gislason et al., 2014; Gislason and Oelkers, 2014; WorleyParsons and Schlumberger, 2011).

Large SO_2 emissions are associated with fossil fuel power production and heavy industry such as metal smelters (Smith et al., 2011). These emissions peaked in 1970–1980 at about 80 Mt per year in the USA and Europe leading to acid rain and Al mobilisation, degrading aquatic and terrestrial ecosystems (Gensemer and Playle, 1999; Gislason and Torssander, 2006). Due to intervening regulations, these emissions have been in decline, and were less than 11 Mt in 2011 (European Environment Agency, 2014; United States Environmental Protection Agency, 2015) due, in large part due to SO_2 capture. This SO_2 capture could potentially be combined with CO_2 capture in water, and this water-soluble gas mixture injected into reactive rocks for mineral storage.

Emissions of H_2S are an inevitable consequence of geothermal energy exploitation, pulp and paper production and the use of fossil fuels (e.g.World Health Organization, 2000). Regulations for H_2S emissions have obliged Icelandic geothermal energy producers to reduce their emissions of this gas (Aradóttir et al., 2015; Gunnarsson et al., 2011). One mitigation option is to capture H_2S and inject it into the subsurface. This approach has been adopted by an ongoing carbon storage project at Weyburn Canada in connection with enhanced oil recovery, which has been co-injecting supercritical CO_2 and H_2S into subsurface sedimentary rocks (Bachu and Gunter, 2005). The behaviour of co-injecting H_2S has not been studied to the same extent as injection of pure CO_2. Some work has, however, been done in terms of geochemical modelling and laboratory experiments (e.g. Bacon et al., 2014; Gudbrandsson and Stefánsson, 2014; Gunnarsson et al., 2011; Stefánsson et al., 2011; Knauss et al., 2005). One goal of the CarbFix project is to assess the feasibility of co-injecting dissolved H_2S and CO_2 into basalts which can provide a cost effective storage solution for both of these gases.

This paper reports on our further efforts to develop the technology to store CO_2 through the *in situ* carbonation of basaltic rocks at the CarbFix storage site in southwest Iceland. Two field injections were carried out at this storage site. In January to March 2012, 175 t of pure CO_2 were injected into the CarbFix site. In June to August 2012, 73 t of a gas mixture from the Hellisheidi geothermal power plant were injected, consisting of 75 mol% CO_2, 24 mol% H_2S and 1 mol% H_2. In each case, the gases were dissolved into formation water during their injection, releasing a single aqueous fluid into the storage formation. Here we report the compositions and saturation states of fluid samples collected from a diverted monitoring well located 125 m in the down-flow direction of the injection well at target storage reservoir depth, before, during, and after the CO_2 and CO_2-H_2S injections, and use these results to better understand the fate of these injected gases in the subsurface.

2. Methods

2.1. Description of the CarbFix site

The CarbFix injection site is located in SW-Iceland, about 30 km east of Reykjavík. The site is ~260 m above sea level and located 3 km SW of the Hellisheidi geothermal power plant (Fig. 1), which is

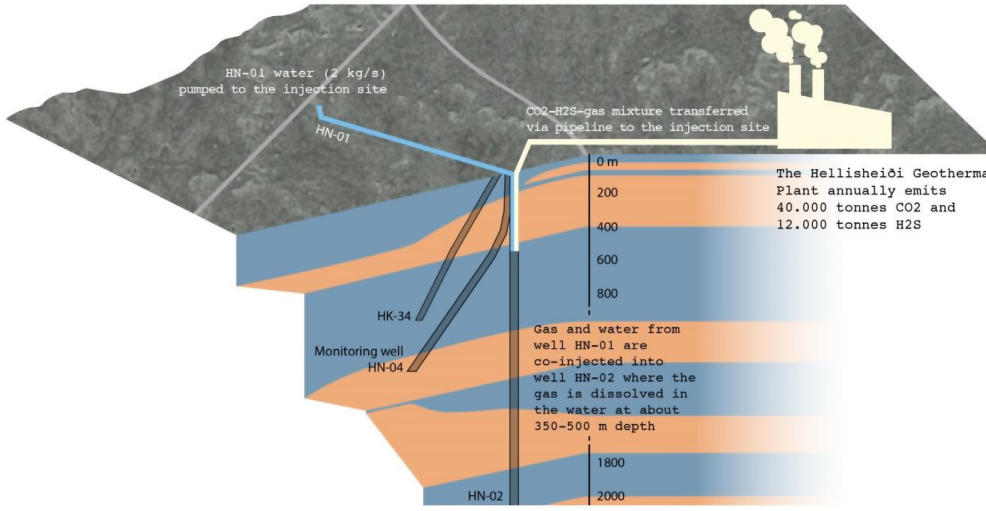

Fig. 1. Geological cross section of the CarbFix injection site, modified from Alfredsson et al. (2013). Blue indicates lava flows and brown indicates hyaloclastic (glassy) formations. The CO_2-H_2S-H_2 gas mixture used in the second injection was separated from other geothermal gases at the power plant and transported via gas pipe to the injection site where it was dissolved in water from well HN-01 within the injection well HN-02. The gas charged water enters the basalts as a single phase. Water was pumped from well HN-01 to the injection well HN-02 at the rate of 7.2 m^3/h. Water was pumped from the monitoring well at the rate of 3.5 m^3/h, throughout this study. Graphic work by Sölvi Snæbjörnsson.

owned and operated by Reykjavik Energy. During 2015, the power plant generated 303 MW of electricity and 133 MW of thermal energy using hot water and steam from a high temperature reservoir located at 800–3000 m depth E and NE of the power plant. The power plant annually produces 40,000 t CO_2 and 12,000 t H_2S. These gases are of magmatic origin produced as a by-product of the geothermal energy production.

Acidic gases injected at the CarbFix site were dissolved into water collected from HN-01, a well located about 1 km west of the 2001 m deep HN-02 injection well (Fig. 1). Well HN-01 is 1306 m deep; water collected from this well was transported via pipeline to HN-02 where the HN-01 water was injected through a pipe as described in detail by Sigfusson et al. (2015). The injected gas was released into the down flowing water via a sparger at a depth of 340 m. The gas dissolved in the water as it was carried down a mixing pipe to a depth of 540 m, where the hydrostatic pressure is above 40 bar, ensuring complete dissolution of the CO_2 before it was released into the subsurface rocks (Aradóttir et al., 2012; Gislason et al., 2010; Sigfusson et al., 2015).

The geology of the CarbFix site was described in detail by Alfredsson et al. (2013). The subsurface rocks at the injection site are primarily olivine tholeiite basalts, consisting of post-glacial lava flows and glassy hyaloclastite formations, formed beneath the ice-sheet during glaciations (Fig. 1). The bedrock down to about 200–300 m depth consists of relatively unaltered olivine tholeiite lava flows that host an oxygen-rich groundwater system with a static water table at about 100 m depth. Below the lava flows lies a 200 m thick, slightly altered hyaloclastite that separates the near surface water system from a deeper system, which is oxygen depleted. The site follows an approximately linear temperature gradient of 80 °C/km. The target injection formation consists of a series of altered lava flows from about 400 m to 800 m depth overlain by the low permeability hyaloclastites (Alfredsson et al., 2013; Helgadóttir, 2011). The lateral and vertical intrinsic permeabilities of the storage formation were estimated to be 300 and 1700×10^{-15} m^2, respectively, having an effective matrix porosity of 8.5% and a 25 m/year estimated regional groundwater flow velocity (Aradóttir et al., 2012). The most abundant alteration minerals from 200 m to 1000 m depth are smectites, calcite, and Ca- and Na-rich zeolites (Alfredsson et al., 2013; Helgadóttir, 2011).

The injection site is equipped with eight monitoring wells ranging from 50 to 1300 m depth. Six of the eight wells are located downstream from the HN-02 injection well. Four of the wells penetrate the groundwater system in the topmost 200–300 m and four are drilled down through the target storage formation. These deeper wells are cased down to 400 m depth and serve as monitoring wells of the deeper system. All monitoring wells were sampled during the experiment, but evidence of tracers from the injections has only been found, to date, in samples collected from well HN-04, which is the closest to the injection well as shown in Fig. 1. Well HN-04 is located about 10 m west of HN-02 at the surface, but it is diverted in the subsurface such that the distance between the wells is 125 m at 520 m depth, where the target carbon storage aquifer is located (Alfredsson et al., 2013; Aradóttir et al., 2012). Field injections at the CarbFix site were performed from 2008 to 2012. Tracer tests were conducted both under natural and forced flow conditions from 2008 to 2011 to define the system hydrology and for scaling reactive transport models (Aradóttir et al., 2012; Gislason et al., 2010; Khalilabad et al., 2008; Matter et al., 2011).

2.2. Acid gas injections at the CarbFix site

The injection of acid gases at the CarbFix site was performed in two phases during 2012 (Table 1):

Phase I began in late January 2012 with the injection of 175 t of pure CO_2. The CO_2 was stored in a 30 m^3 reservoir tank pressurised at 26–28 bars and co-injected with water collected from well HN-01 into well HN-02, as described by Sigfusson et al. (2015). The predicted *in situ* pH and DIC concentrations of the injected fluid during Phase I were 3.85 and 0.823 mol kg^{-1} respectively, based on the mass flow rates of water and gas into the injection well, chemical speciation calculations (Parkhurst and Appelo, 2013), and direct measurement (Sigfusson et al., 2015). The chemical tracers listed in Table 1 were co-dissolved into the injected water as described by Sigfusson et al. (2015) to aid in determining the fate of the dissolved

Table 1
Characteristics of the two gas injections into the CarbFix storage site considered in this study.

	Phase I: Injection of 100% CO_2	Phase II: Injection of 75% CO_2, 24% H_2S, 1% H_2
Period:	24th of January–9th March 2012	15th of June–1st of August 2012
Injection period (days)	45	48
	Active:	Active:
	40	29
Mass of injected gas (tonnes)	175	73
Tracers:		
Reactive	^{14}C	^{14}C
Concentration:	40.0 Bq/L[a]	6 Bq/L[a]
^{14}C:^{12}C ratio	2.16×10^{-11}[a]	6.5×10^{-12}[a]
Non-reactive	SF_6	SF_5CF_3
Concentration:	2.33×10^{-8} ccSTP/cc[a]	2.24×10^{-8} ccSTP/cc[a]

[a] From Matter et al. (2016).

CO_2 as described by Matter et al. (2016). The Phase I injection ran continuously until it was terminated on the 9th of March 2012.

Phase II began in mid-June 2012 with the injection of 73 t of a gas mixture containing 75 mol% CO_2, 24 mol% H_2S, and 1 mol% H_2 originating from the Hellisheidi power plant. The gas mixture was obtained by diverting power plant emissions to a gas abatement plant, where it was separated into water soluble gases (CO_2, H_2S), and less soluble gases (N_2, CH_4, H_2, Ar). The power plant emission gas contained about 20% H_2; a small fraction of this dissolves in the water along with the CO_2 and H_2S according to the solubility and partial pressure of the gases. Subsequently the soluble gas mixture was co-injected into the surface with HN-01 water. The predicted *in situ* pH, DIC, H_2S, and H_2 concentrations of the injected water during the Phase II, based on the mass flow rates of water and gas into the injection well and chemical speciation calculations performed using PHREEQC (Parkhurst and Appelo, 2013) were 4.03, 0.43 mol kg^{-1}, 0.14 mol kg^{-1} and less than 0.01 mol kg^{-1}, respectively. The chemical tracers listed in Table 1 were co-dissolved into the injected water as for the pure CO_2 injection to monitor subsurface reactivity. The gas mixture injection rate was less stable than that of the pure CO_2 injection and was stopped several times due to injection problems. The injection was terminated on the 1st of August 2012.

2.3. Analytical methods

Sampling of the fluids from the HN-04 first monitoring well began in 2008. Water samples for chemical analysis were collected several times prior to the Phase I injection in January 2012 (Alfredsson et al., 2013). During the injections and until mid-September 2012 this well was sampled twice weekly. Weekly sampling continued until mid-July 2013 with few exceptions.

Water was pumped from the monitoring well at the rate of 3.5 m^3/h throughout this study, to maintain a constant head from the injection to the monitoring well. The pump used was a 163 cm long, submersible Grundfos model SP3A-60 made of stainless steel, located at 303 m depth and ~200 m below the water table. This pump was connected to a 53 mm diameter steel pipe to the surface where the effluent was deposed via a service pipe extending east of the injection site and eventually re-injected into a deep geothermal system.

Fluid samples were collected via a 10 m long, 10 mm diameter stainless steel pipe connected to the 53 mm diameter monitoring well lining pipe extending down to the pump. The 10 mm sample pipe was connected directly to a sampling valve inside an on-site field laboratory. After flushing the sampling pipe, the sampled waters were immediately filtered through 0.2 μm Millipore cellulose acetate membranes using silicon tubing and a 140 mm Sartorius® polypropylene filter holder. All air in the filtration system was expelled through a valve prior to sampling and at least 3 L of water was pumped through the system before the samples were collected in distinct bottles depending on the subsequent chemical analysis. Amber glass bottles were used to collect samples for pH and alkalinity. Acid washed high density polyethylene bottles were used to collect samples for cations and trace metals. These samples were acidified using Suprapur® HNO_3, 1% (v/v). Acid washed low density polypropylene bottles were used to collect samples for Fe-species measurement. These samples were acidified with Suprapur® HCl, 1% (v/v) immediately after collection. Low density polypropylene bottles were used for collecting samples for anion concentration measurements. Acid washed polycarbonate bottles were used to collect samples for dissolved organic carbon (DOC). These samples were acidified with 1.2 M concentrated HCl 2% (v/v). All sample bottles were rinsed three times by half filling them with the filtrated water and then emptying them prior to sample collection.

Temperature and conductivity were measured at the sampling site using a Eutech Instruments Oakalon 2-cell Conductivity meter. The *in situ* temperature of the sampled fluid was determined using down-hole temperature logging at the depth of the main feedpoint of well HN-04, at about 420 m depth (Alfredsson et al., 2013; Thorarinsson et al., 2006). The pH was determined on site with a Eutech InstrumentsTM CyberScan pH 110 electrode and again in the laboratory a few hours after sampling with a Cole Parmer combined glass electrode together with an Orion pH meter. The uncertainty of the analyses is estimated to be ±0.02. The pH was then re-calculated at *in situ* conditions using PHREEQC (Parkhurst and Appelo, 2013). Alkalinity was measured in the laboratory by alkalinity titration using the Gran function to determine the end point of the titration (Stumm and Morgan, 1996). Total dissolved inorganic carbon (DIC) was calculated with PHREEQC (Parkhurst and Appelo, 2013) using measured pH, alkalinity, temperature and total dissolved elements concentrations. The uncertainties of the DIC calculations are estimated to be within 10%.

Dissolved oxygen was fixed on site and later determined by Winkler titration. This method has a precision of 1 μmol/L O_2 (0.03 ppm) for the 50 ml sample bottles, but there is a risk of atmospheric contamination for samples containing no or little oxygen. Such is the case for the samples collected from HN-04, which are oxygen depleted. The O_2 concentrations of the sampled fluids ranged from 2 to 24 μmol/L. The difference between the O_2 concentration in the samples and the reagents was determined using the method described by Arnórsson et al. (2000). The results show that the oxygen measured in the samples is mostly derived from the reagents. Some oxygen contamination during sampling was also inevitable.

Dissolved hydrogen sulphide was measured by titration on site using mercury and dithizone as an indicator (Arnórsson et al., 2000). The sensitivity of this method is about 0.29 μmol/L H_2S (about 0.01 ppm) when using a 50 ml sample aliquot.

The major elements Si, Ca, K, Mg, Na, and S and the trace metals Fe and Al were analysed using a Spectro Ciros Vision Inductively Coupled Plasma Optical Emission Spectrometer (ICP-OES) using an in-house multi-elements standard checked against the SPEX Certified Reference standard at the University of Iceland. The samples were analysed again using a Agilent 725 ICP-OES for major elements and an ELEMENT XR Inductively Coupled Plasma Sector Field Mass Spectrometer (ICP-SFMS) from ThermoScientific for the trace elements Fe and Al at ALS Scandinavia, Luleå, Sweden. Analytical measurements for the major elements had an inter-laboratory reproducibility within 12%. The average difference between corresponding concentration measurements is 3.7% with a standard deviation of 2.3%. Analytical measurements for the trace elements Fe and Al had an inter-laboratory reproducibility within 19%. The average difference in corresponding Fe and Al concentration measurements was 4.9%. Dissolved F^-, Cl^-, and $SO_4{}^{-2}$ concentrations were quantified using a DIONEX, ICS-2000 Ion Chromatograph. The addition of zinc-acetate to the SO_4 sample was not needed for its analysis since the H_2S concentrations were small compared to the SO_4 concentrations as shown below. Concentrations of Fe^{2+} and Fe^{3+} were measured using a DIONEX IC-3000 Ion Chromatograph. Due to ambiguities in the Fe^{3+} measurements, the Fe^{2+} measurements were used along with the Fe_{total} concentrations measured by ICP-SFMS at ALS Scandinavia to calculate Fe^{3+} concentrations. Analysis of dissolved organic carbon (DOC) was carried out at Umeå Marine Science Center in Umeå, Sweden using a Shimadzu TOC-VcPH total organic carbon analyser.

The precipitates collected from the pump recovered from the HN-04 monitoring well were analysed by X-ray Powder Diffraction (XRD) at ISOR, Iceland for phase identification. The samples were measured using a Bruker AXS D8 Focus X-ray diffractometer with Cu kα radiation at 1.54 Å wavelength, set at 40 kV and 40 mA using 1° divergence and receiving slits. The chemical composition of the precipitates was also analysed by ALS, Scandinavia. The precipitates were digested in HNO_3 and HCl with a trace of HF in a microwave oven. The resulting fluids were then analysed using both ICP-OES and High Resolution Inductively Coupled Plasma Mass Spectrometry (HR-ICP-MS). Detection limits were in the range of 0.01 ppm for trace elements to single ppm for major elements, and uncertainties for concentrations 10 times these detection limits are within 10% of the reported value.

Precipitates from samples collected from an air-lift of the HN-02 injection well in June 2013, were analysed for phase identification by XRD at the University of Copenhagen, Denmark with a Bruker D8 Discover equipped with a Co tube. One L slurries collected from the air-lift were sealed immediately after sampling, transported to Denmark, where they were kept in an anaerobic chamber prior to analysis to minimise oxidation. Within the chamber, the samples were centrifuged, dried, crushed and mounted on low-background sample holders that were then covered with X-ray transparent cups to minimise oxidation during measurements.

2.4. Mass balance calculations

The fate of injected gases in this study are evaluated with the aid of mass balance calculations based on the injected non-reactive tracers SF_6 and SF_5CF_3 (Assayag et al., 2009; Matter et al., 2007, 2016). All collected water samples consist of a mixture from three sources; the original groundwater, that injected during Phase 1 and that injected during Phase 2. In the absence of reactions that remove or add material to the mixed fluid, mass balance requires that the concentration of chemical component i in the monitoring well samples (c_i) to be

$$c_i = c_{i,GW}X_{GW} + c_{i,1}X_{i,1} + c_{i,2}X_2 \quad (1)$$

where $c_{i,GW}$, $c_{i,1}$, and $c_{i,2}$ refers to the concentration of the ith chemical component in the original groundwater, the Phase 1 injection and the Phase 2 injection, respectively, whereas and X_{GW}, X_1, and X_2 designate the fraction of the these three fluid sources in each monitoring sample.

The fraction of each water source in each monitoring sample was determined from the measured concentrations of the two non-reactive tracers, SF_6 and SF_5CF_3 together with the requirement that

$$X_{GW} + X_1 + X_2 = 1 \quad (2)$$

Comparison of values based on the assumption of non-reactive mixing, obtained from Eqs. (1) and (2), with those measured in the monitoring wells provides an estimate of the percentage of injected gases fixed by chemical reactions, and the mass of elements added or removed from the fluid by mineral dissolution and precipitation reactions due to the injections. The background concentration of SF_6 in Eq. (1) ($c_{i,GW}$) was not constant with time since SF_6 had been used in previous hydrological tests. This background concentration was corrected by taking account of the sample sodium fluorescein tracer concentrations; this tracer was co-injected with the SF_6 in the previous tests as described by Matter et al. (2016).

Sample 12KGM06 (Table 2) of the injected water from well HN-01 was used to constrain the elemental concentrations of the injected fluid, apart from the elements C and S, which were determined by accounting for the concentration of CO_2 and H_2S added to these injected fluids. Sample 12KGM01 (Table A1 in the electronic Supplements) collected from well HN-04 before injection was used for representing the ambient groundwater concentrations. Mass balance calculations were performed for the major elements Ca, Mg, Si, Na, K, and Cl, and the trace elements Fe and Al.

2.5. Geochemical modelling

Modelling of the water chemistry, including the calculation of percent error in charge balance, the *in situ* saturation state of the water with respect to mineral and gas phases, and the effect of CO_2 and CO_2-H_2S-H_2 gas injection on the aqueous chemistry of the subsurface fluids was performed using PHREEQC (Parkhurst and Appelo, 2013). In no case did the charge imbalance exceed 6.1%. The standard PHREEQC database was used in all calculations after including revised thermodynamic data on secondary minerals taken from Gysi and Stefánsson (2011), and pyrrotite and greigite taken from the MINTEQ and the llnl databases, respectively, as described in Alfredsson et al. (2013). Dissolved inorganic carbon (DIC) was calculated for each water sample using measured alkalinity, pH and temperature defined at 35 °C at the *in situ* conditions. All saturation indices were calculated assuming the oxygen fugacity was controlled by equilibrium with the $H_2S/SO_4{}^{2-}$ as a redox couple. For samples having no measured excess H_2S, the H_2S concentration was assumed to be equal to the detection limit of the H_2S titration, as geothermal waters always contain a small fraction of H_2S although below the detection limit.

3. Results

The compositions of all sampled fluids are shown in Figs. 2, 3 and 8, Table 2 and Table A1 in the electronic Supplements. An increase in the non-reactive sulphur hexafluoride (SF_6) tracer, indicating the initial arrival of the migrating dissolved CO_2 plume in the HN-04 monitoring well, occurred about two weeks after the start of the Phase I injection (Fig. 2a). The concentration of this tracer increased until a maximum 56 days after the Phase 1 injection started (Matter et al., 2016). The SF_6 tracer concentration again increased about 100 days after the injection started, reaching an overall maximum about 13 months after Phase I was started (see Fig. 2a; Matter et al., 2016). This is the same pattern observed

Table 2
The measured chemical composition of water collected from well HN-01, and co-injected with pure CO_2 gas or CO_2/H_2S gas mixtures into the CarbFix storage site.

Date	Sample ID	pH	Conductivity µs/cm	H_2S µmol/L	O_2 mmol/L	Alk. meq./L	DIC mmol/L	$S_{(total)}$ mmol/L
3.2.2012	12KGM06	9.29	292	0.45	0.051	2.109	1.460	0.118
4.7.2012	12SOS03	9.21	300	0.32[a]	0.082	2.046	1.550	0.085

Date	Sample ID	Ca mmol/L	Mg mmol/L	Fe µmol/L	Si mmol/L	Na mmol/L	K mmol/L	Al µmol/L	Cl mmol/L
3.2.2012	12KGM06	0.13	0.16	0.021	0.59	2.04	0.024	1.19	0.31
4.7.2012	12SOS03	0.15	0.20	0.068	0.39	1.83	0.024	0.65	0.25

[a] Measured on 12th of July.

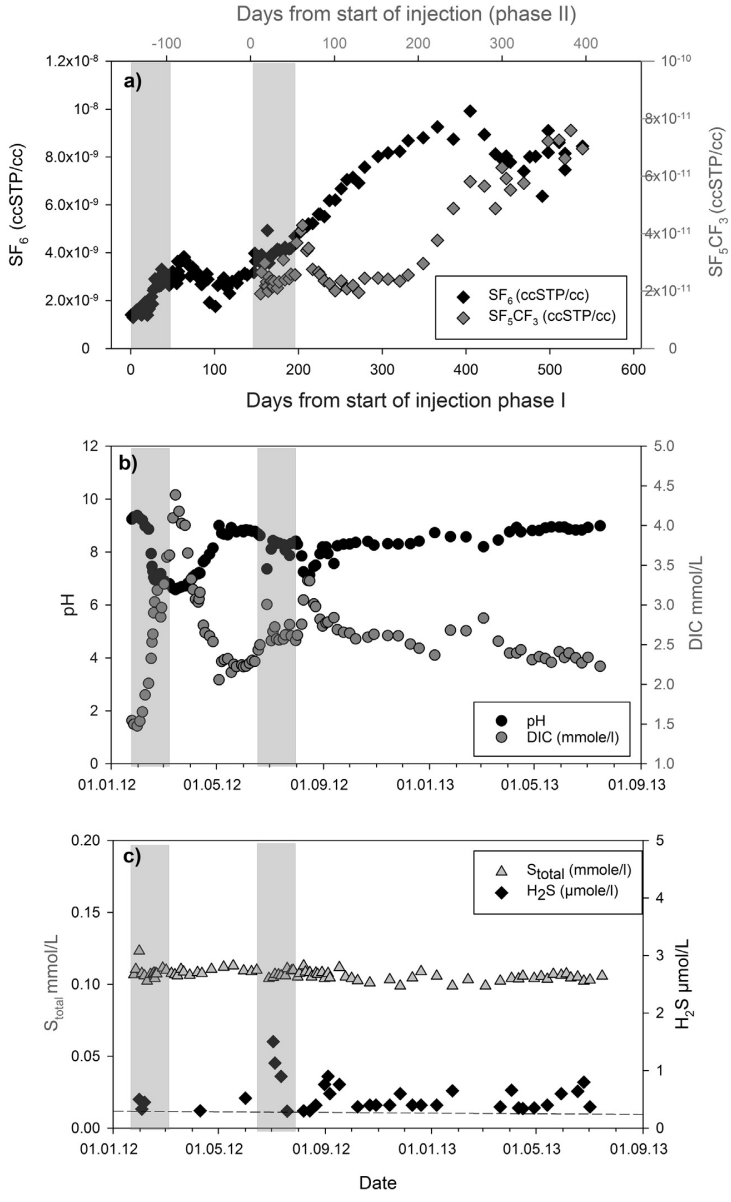

Fig. 2. Concentrations of a) SF_6 and SF_5CF_3 non-reactive tracers; b) dissolved inorganic carbon (DIC) along with fluid pH calculated at in situ temperature (35 °C), c) total dissolved sulphur and $H_2S_{(aq)}$ in samples from monitoring well HN-04 prior to, during, and after the injection of pure CO_2 and mixed CO_2/H_2S gas into the CarbFix Storage site. The timing of both gas injections is indicated by grey bars. The detection limit of the H_2S concentration measurements is 0.3 µmol/L and is indicated as a dotted line.

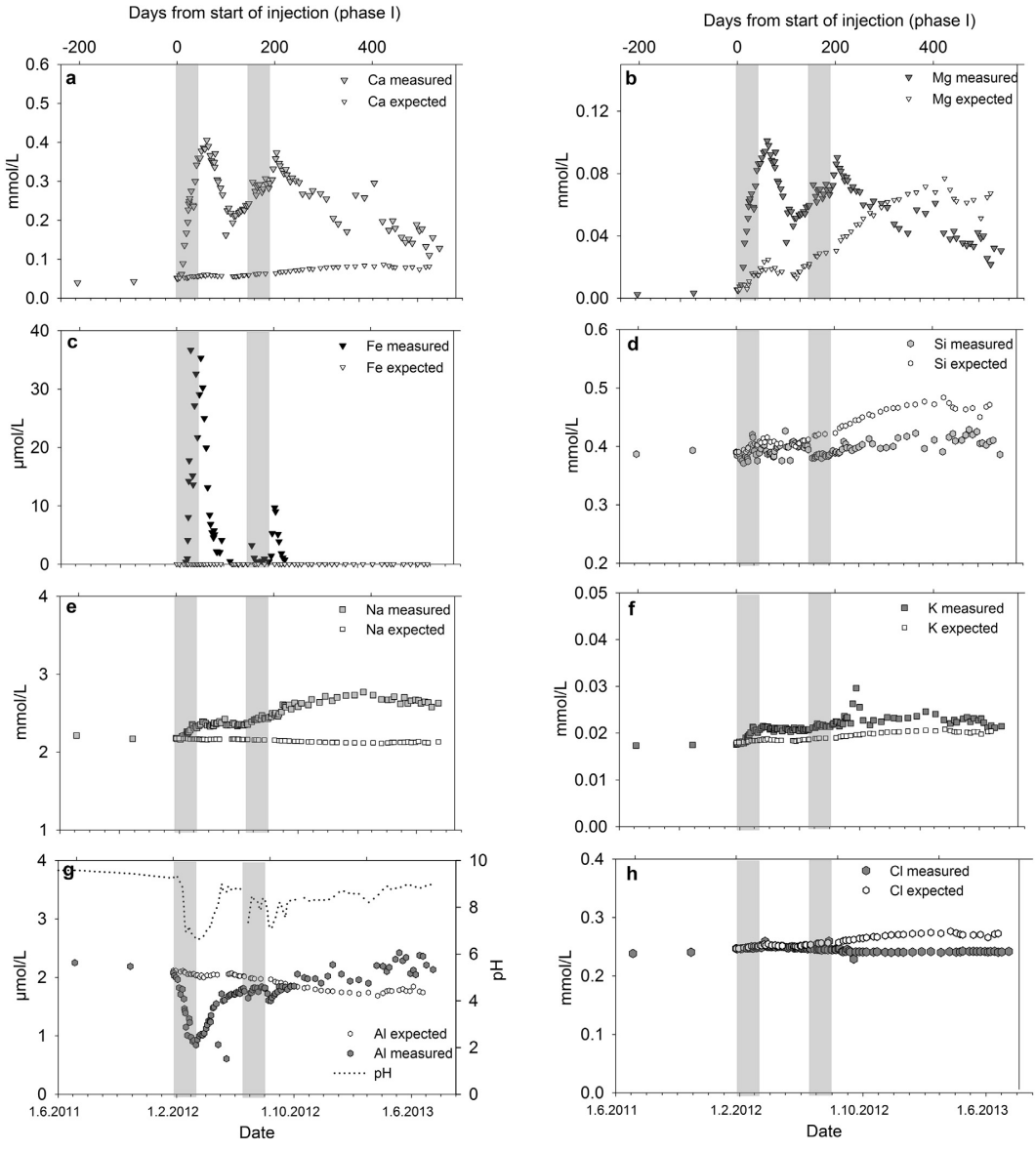

Fig. 3. Concentrations of Ca, Mg, Fe, Si, Na, K, Al, Cl and F collected from monitoring well HN-04 prior to, during, and after the injection of CO_2 and CO_2/H_2S into the CarbFix Storage site. The timing of both gas injections is indicated by grey bars. Note the pH of the fluid samples is plotted together with the Al concentrations. The results of mass balance calculations depicting expected values for these concentrations, assuming pure mechanical mixing of the injected solution is also shown in these plots.

during the previous tracer test (Khalilabad et al., 2008), indicating that the storage formation consists of relatively homogenous porous media intersected by a low volume and fast flow path that channels about 3% of the tracer flow between wells HN-02 and HN-04. The same pattern was observed for Phase II, with the first arrival of the non-reactive trifluoromethyl sulphur pentafluoride (SF_5CF_3) tracer observed about two weeks after the start of the mixed-gas injection (Fig. 2a), with an initial smaller maximum about 60 days after the injection began (Matter et al., 2016). A further increase in SF_5CF_3 was noted about 150 days after Phase II injection began (Fig. 2a), consistent with the behaviour of SF_6 (Matter et al., 2016). The second SF_5CF_3 concentration maximum was not observed due to a breakdown of the submersible pump in the monitoring well HN-04, resulting in a three month gap in the monitoring data as described below.

3.1. Fluid pH, carbon, and sulphur

Prior to the injections, the pH of the HN-04 monitoring well samples was 9.5–9.6, the DIC was 1.3–1.4 mmol/L, and the total S concentration was 0.09–0.11 mmol/L (see Fig. 2b–c, Table A1 in the electronic supplements, and Alfredsson et al. (2013)). The measured pH and DIC before, during and after the two injection phases are shown in Fig. 2b. The pH of the sampled fluids is extremely

sensitive to the injection of dissolved gases. The pH *in situ* (35 °C) decreases from 9.6 prior to each injection to approximately 7 near the end the injection then subsequently recovers to a value higher than 9. The decrease starts about two weeks after the start of Phase I, contemporary with the first arrival of the non-reactive tracer. The lowest pH following Phase I was 6.6 and occurred at the same time as the highest DIC value of 4.4 mmol/L, about 50 days after the Phase I injection was started, but ten days before the first reactive tracer maximum. Subsequently, both DIC and pH trended back towards their initial values (Fig. 2b). A similar pattern was observed during Phase II; the pH began to drop about two weeks after the injection was started, with the lowest pH of 7.1 measured at the same time as the highest DIC value of 3.3 mmol/L, about 60 days after the Phase II injection was started and concurrent the first SF_5CF_3 tracer maximum (see Fig. 2).

No corresponding increase in DIC was observed during the second and larger SF_6 tracer maximum. This suggests significant mineral storage of the injected carbon; the difference between measured and calculated DIC indicate that >95% of the injected CO_2 was mineralised in less than two years, as previously reported by Matter et al. (2016). The second and larger SF_5CF_3 tracer maximum was not observed due to a pump failure in the HN-04 monitoring well, but an increase was noted in this concentration approximately one year after the start of the Phase II injection, consistent with the increase during the second breakthrough of SF_6. No corresponding increase in DIC was observed. Analysis of dissolved organic carbon (DOC) show continuous decrease in DOC concentrations from the start of Phase I, and throughout the monitoring period, except for a small increase shortly after the termination of the Phase II, from August to September 2012 (Table A1 in the electronic Supplements). The measured DIC concentration is more than two orders of magnitude greater than the measured DOC concentration throughout most of the monitoring period after the Phase I injection (Fig. 2b and Table A1 in the electronic Supplements).

The measured sulphur concentrations (SO_4^{-2}, H_2S, and S total) from before, during and after the Phase II injection are shown in Fig. 2c and Table A1 in the electronic Supplements. The concentrations are close to constant throughout this two year study. The average SO_4^{-2} concentration measured by IC-2000 during the period was 0.10 ± 0.01 mmol/L, with a standard deviation of 0.005. The average total S concentration measured by ICP-OES was 0.10 ± 0.02 mmol/L, with standard deviation of 0.003. The H_2S concentrations were, in most cases, close to the 0.3 μmol/L detection limit. The highest H_2S concentration, 1.5 μmol/L, was measured during the Phase II injection. The H_2S sulphur species always comprised less than 1.5% of the total dissolved S measured by the ICP-OES. This suggests an even more rapid mineralisation of the injected H_2S than the injected CO_2; no significant increase in sulphur concentrations was noted during this field injection experiment, indicating that all of the injected sulphur was mineralised before the first reactive tracer maximum of the SF_5CF_3 was observed in the monitoring well HN-04, or within 60 days of the start of the injection.

3.2. Major and trace elements

The release of the divalent cations Ca^{2+}, Mg^{2+}, and Fe^{2+} from the host basalt is essential for the mineralisation of the injected gases. The chemical compositions of the HN-04 monitoring samples demonstrate the rapid increase in Ca, Mg, and Fe concentration during the two injection phases with a gradual decline in the following weeks and months (see Fig. 3a–c). The increases in these concentrations were first observed concurrently with the first appearance of the non-reactive tracers. The Fe^{2+} was not detected in any sample after early April 2013, or about 6 weeks after the major part of the injected Phase 1 fluid arrived in well HN-04 and the Fe^{2+} concentrations were close to the detection limit for the two months following the start of the gas mixture injection.

Fig. 4. Photograph illustrating the presence of precipitates on the water sampling pump recovered from monitoring well HN-04 on the 13th of August 2013. The diameter of the pump is 101 mm. (For interpretation of the references to colour in this figure legend, the reader is referred to the web version of this article).

In contrast, dissolved Si concentrations were close to constant throughout the monitoring period (Fig. 3d). An increase in Na concentration was most prominent at the beginning of the Phase I injection when its concentration increased from 2.1 to 2.2 mmol/L to about 2.3–2.4 mmol/L (Fig. 3e). Another increase was observed during the Phase II injection to about 2.5 mmol/L. The Na-concentration at the end of the monitoring period was about 2.6–2.7 mmol/L. A similar trend is evident for K, but the increase in its concentration was somewhat lower than that of Na (Fig. 3f). The only major difference between the responses of these concentrations to the dissolved gas injections was the presence of a small concentration peak in K during October 2012. The origin of this peak in unclear. The Al concentrations were strongly pH dependent, consistent with its solubility dependence on pH from neutral to basic conditions (e.g. Drever, 1982). As such, a strong correlation was observed between Al concentrations and pH before, during, and after the injections (Fig. 3g). The Cl concentrations were generally constant throughout the monitoring period with a concentration of 2.4 mmol/L (Fig. h).

3.3. Calcite precipitates

In July 2013, about one and a half years after the start of the Phase I injection, the submersible pump in well HN-04 broke down. When the pump was brought to the surface, it was found to be clogged and coated with a green precipitate as shown in Fig. 4. No precipitation was observed on the pump prior to the injections. The bulk chemical compositions of the precipitate samples are shown in Table 3. The cation concentration of the precipitates consisted mostly of calcium (>94%) with some iron (<3%), silica (<2%) and magnesium (<1%). The XRD-analysis (Fig. A2 in the electronic Supplements) confirmed that calcite was the dominant mineral phase of this precipitate and no other crystalline phases were identified. A ^{14}C analysis of the carbon in the precipitates confirms that they originated from the injected ^{14}C labelled CO_2 (Matter et al., 2016).

3.4. Mineral saturation states of C- and S-bearing minerals

The saturation indices (SI) of calcite ($CaCO_3$), magnesite ($MgCO_3$) and siderite ($FeCO_3$), as calculated using PHREEQC, are shown in Fig. 5a. Calculations show that calcite was saturated both before and after the Phase I and Phase II injections. This mineral was, however, strongly undersaturated just after these injections concurrent with the drop in monitoring fluid pH below 8, even

Table 3
The measured chemical composition of the major elements of two solid samples collected from the water pump recovered from well HN-04 on the 13th of August 2013.

Si mmol/L	Na mmol/L	K mmol/L	Ca mmol/L	Mg mmol/L	S mmol/L	Al mmol/L	Fe mmol/L
185	14.8	1.00	9,480	136	10.0	0.027	287
171	11.3	0.49	10,200	123	5.30	0.019	197

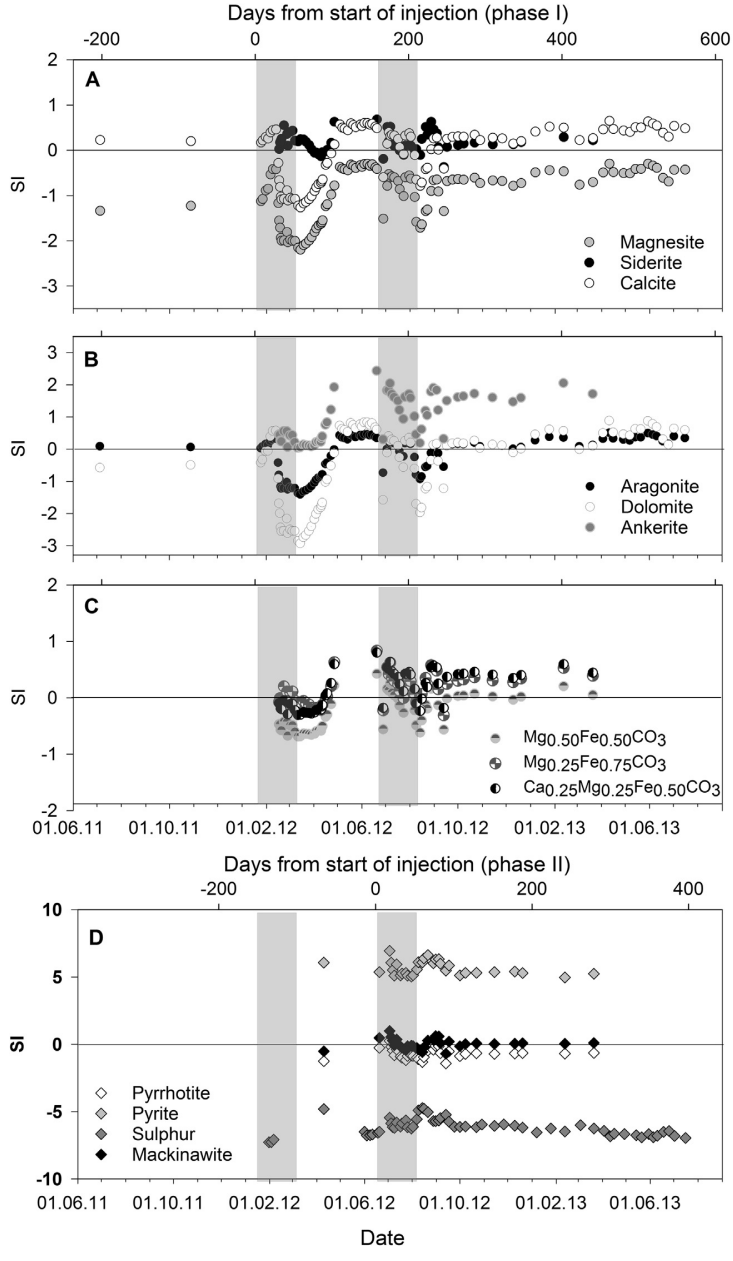

Fig. 5. Saturation indices (SI) of collected HN-04 well water samples with respect to A) magnesite siderite and calcite; B) dolomite, aragonite and ankerite, C) Mg-Fe and Ca-Mg-Fe solid solutions, and D) pyrrhotite, pyrite, sulphur and mackinawite prior to, during, and after the injection of pure CO_2 and a CO_2/H_2S gas mixture into the CarbFix Storage site. All saturation indices were calculated assuming the oxygen fugacity was controlled by equilibrium of the H_2S/SO_4^{2-} as a redox couple. Note that positive, negative, and zero SI values correspond to aqueous fluids that are supersaturated, undersaturated, and at equilibrium with the indicated mineral. The timing of both gas injections is indicated by grey bars.

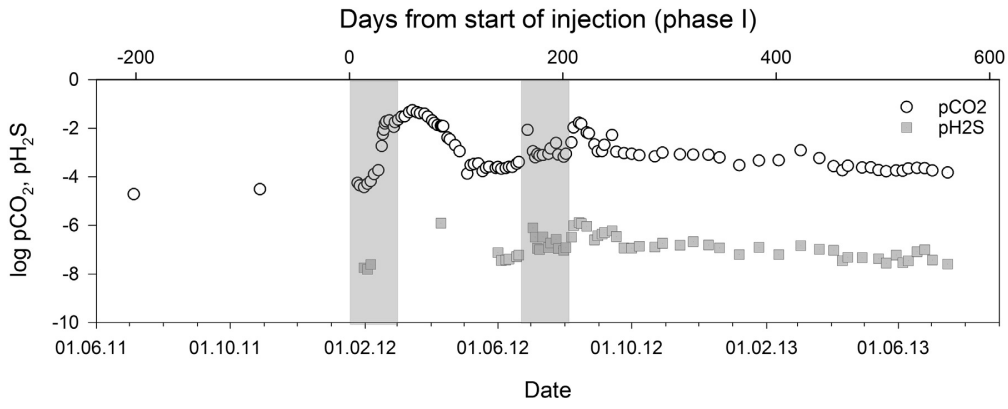

Fig. 6. Partial pressures of CO_2 and H_2S prior to, during and after both injection experiments.

though the DIC and Ca concentrations were relatively high (Figs. 2 a and 3 a). Note that calcite was identified by XRD-analysis in drill-cuttings from the area prior to the injections (Alfredsson et al., 2013) and within and on the pump in the monitoring well at the end of the monitoring period (Figs. 4 and A2 in the electronic supplements). The monitoring fluid samples attained calcite saturation at the end of April 2012, about seven weeks after the Phase I injection was terminated, and at end of August, about four weeks after the Phase II injection was terminated, when the fluid pH had increased to >8. In contrast, the monitoring fluid samples were calculated to be supersaturated with respect to siderite shortly after both injections, whereas magnesite was strongly undersaturated during this time (Fig. 5a). Magnesite and siderite were not identified at the Hellisheidi site prior to the injections, but both minerals have been identified by XRD-analysis of drill-cuttings from the Svartsengi geothermal field in SW-Iceland (Franzson, 1983; Richter et al., 1999), which has a significantly higher salinity and higher temperature gradient than the CarbFix site. Magnesite-siderite solid solutions were identified in low temperature CO_2 metasomatised basalts in Nuussuaq, West Greenland (Rogers et al., 2006). There calcite appears at a relatively low CO_2 partial pressure, and magnesite-siderite at higher partial pressures (Fig. 6), as predicted by the PHREEQC modelling (Fig. 5a).

The calculated saturation indices of a number of other carbonate minerals are shown in Fig. 5b. Ankerite ($CaFe(CO_3)_2$) is the only carbonate-phase that was supersaturated during the whole monitoring period, that is while Fe^{2+} concentrations are above the detection limit of the spectroscopic method. Ankerite has not been identified in the area. It was however identified during basaltic glass-CO_2 charged water interaction experiments performed at 75 °C by Gysi and Stefánsson (2012b), and during basalt, water, supercritical CO_2 interaction experiments reported by McGrail et al. (2006). Similar to calcite, the sampled fluids were calculated to be supersaturated with respect to aragonite ($CaCO_3$) throughout the monitoring period, with the exception of several weeks near the end of, and shortly after both injections (see Fig. 5b). Aragonite was identified by XRD-analysis of drill-cuttings from the area prior to the injections (Alfredsson et al., 2013). Although the fluids were calculated to be supersaturated with respect to dolomite ($CaMg(CO_3)_2$) following both injections, this mineral has not been observed at the CarbFix site. It has been observed however by XRD-analysis as a secondary mineral in drill-cuttings from the saline Svartsengi high-temperature geothermal field in SW-Iceland, as is the case for magnesite and siderite (Franzson, 1983). The calculated saturation indices of three different Ca-Mg-Fe-solid solutions are shown in Fig. 5c. All three show similar trends as calcite and aragonite. The $Mg_{0.50}$-$Fe_{0.50}$-CO_3 is the least saturated of the three, but attained saturation after both injections.

The calculated saturation indices for some sulphur-bearing minerals are shown in Fig. 5d. The monitoring well fluids were calculated to be undersaturated with respect to native sulphur during the whole monitoring period. In contrast, pyrite (FeS_2), which is one of the most abundant secondary minerals at Hellisheidi at elevated temperature, and was identified at 780 m depth within the HN-02 injection well (Helgadóttir, 2011), was calculated to be supersaturated in all the monitoring fluid samples, showing a slight decrease in its saturation index at the beginning of the Phase II injection and a peak mid-August 2012 concurrent with the first maximum in SF_5CF_3 concentration, indicating the initial breakthrough of the injected Phase II fluids (Fig. 5d). As previously mentioned, calcite was the only crystalline phase identified in the precipitates forming on the pump from well HN-04. Pyrite was, however, identified by XRD-analysis on samples collected from an airlift of the injection well HN-02, confirming formation of pyrite during or after the Phase II injection (Fig. A3 in the electronic Supplement). Greigite (Fe_3S_4) showed a similar behaviour as pyrite, as this mineral was supersaturated in all monitoring well fluid samples. This mineral was not identified in the area previously, and was not identified by XRD analysis on the airlift samples collected from the injection well HN-02. It is, however, a metastable phase that may be a precursor of pyrite (Deer et al., 1992). Pyrrhotite (Fe_7S_8- FeS) was slightly supersaturated in the fluids sampled during the first weeks of the Phase II injection but undersaturated in all other samples (Fig. 5d). Pyrrhotite was previously identified within the high-temperature system in the Hellisheidi area (e.g. Gunnarsdóttir, 2012), but was not found at the CarbFix site nor identified in XRD analysis on the airlift samples from the injection well HN-02 (Fig. A3 in the electronic Supplements). Gunnlaugsson and Arnórsson (1982) reported that below 180 °C, geothermal waters in Iceland equilibrate with marcasite (FeS_2) instead of pyrite; marcasite is a pyrite dimorph generally found at lower temperatures (Deer et al., 1992). There was no evidence of marcasite in samples from the CarbFix site, either prior to the injections or in the XRD-analysis from the airlift pumping of well HN-02 (Fig. A3 in the electronic Supplement). Mackinawite ($(Fe,Ni)_9S_8$) became supersaturated in the fluids sampled at the beginning of the Phase II injection, during the initial breakthrough of the injected Phase II fluid, and it is near to saturation in some monitoring samples collected from October to April 2013 (Fig. 5d). Mackinawite was not been identified in the area, and was not detected by XRD-analysis on the airlift samples from HN-02 (Fig. A3 in the electronic Supplement). However, mackinawite

typically forms as a nanocrystalline material, whose broad peaks in XRD would be complicated to identify.

3.5. Saturation indices for other minerals

Saturation indices for other selected minerals are shown in Fig. 7. Chalcedony (SiO_2) was slightly undersaturated in the monitoring fluid samples prior to the injections, but becomes saturated during Phase I; it then remains saturated for the rest of the monitoring period (Fig. 7a). Chalcedony is a common secondary mineral in the area (e.g. Alfredsson et al., 2013).

The mineral saturation states for those zeolites that are common in the area are shown in Fig. 7b. Analcime, a common Na-zeolite found as an alteration phase at the CarbFix site, was undersaturated in the sampled fluids until about two months after the beginning of the Phase II injection, and then it is subsequently saturated (Fig. 7b). The samples were supersaturated with respect to other zeolites previously found in the area; and the general trend was a decrease in the monitoring fluid saturation index during the Phase I injection with an increase 6–8 weeks after Phase I was started. A slight dip was observed during the Phase II injection and an increase was observed during the second breakthrough of the injected fluid from Phase I (Fig. 7b).

The mineral saturation states for common clay minerals are shown in Fig. 7c. Kaolinite ($Al_2Si_2O_5OH_4$) remained strongly supersaturated in the fluids sampled during the entire monitoring period (Fig. 7c), but increasingly so when the samples had a pH <8, during the injections and in the first weeks thereafter. Kaolinite was

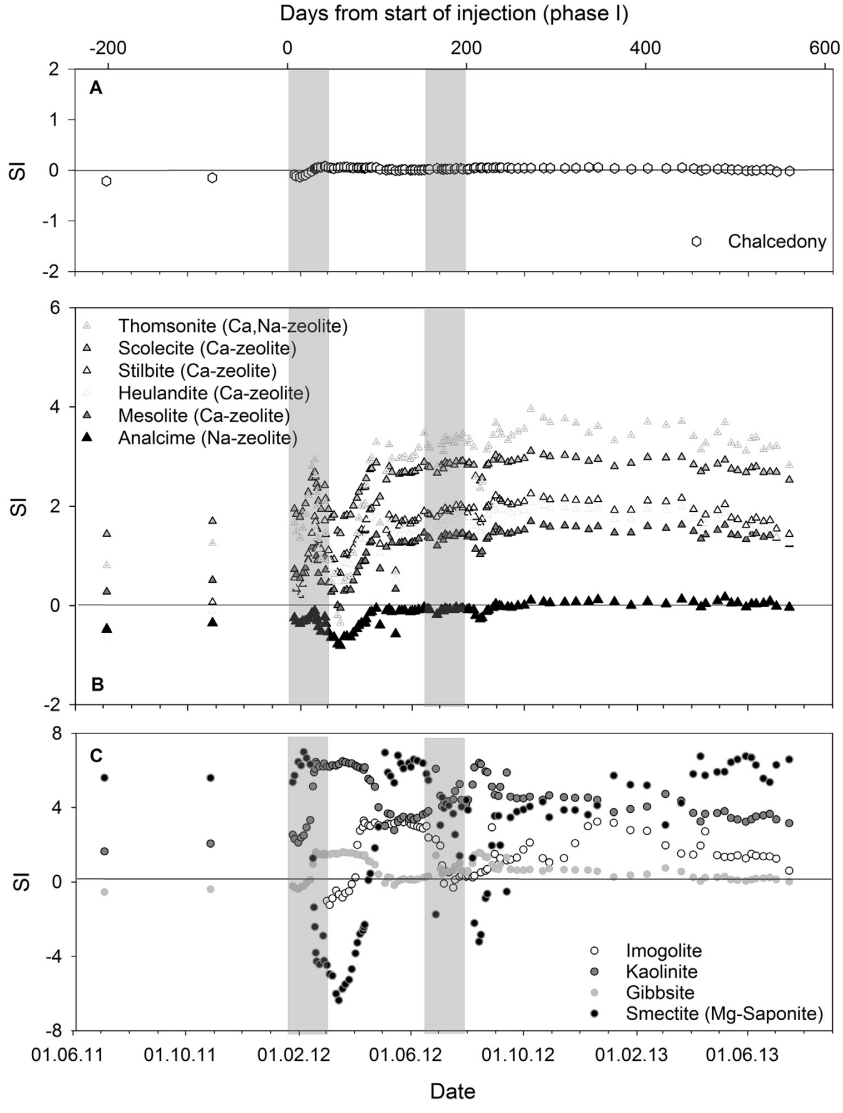

Fig. 7. Saturation indices (SI) of collected HN-04 well water samples with respect to A) chalcedony, B) the zeolites previously identified in the area, and C) selected clay-minerals prior to, during, and after the injection of pure CO_2 and a CO_2/H_2S gas mixture into the CarbFix Storage site. Note that positive, negative, and zero SI values correspond to aqueous fluids that are supersaturated, undersaturated, and at equilibrium with the indicated mineral. The timing of both gas injections is indicated by grey bars.

identified as a surface alteration product in geothermal areas (e.g. Markússon and Stefánsson, 2011) but has not been identified in subsurface samples collected from wells at Hellisheidi. The saturation state of gibbsite ($Al(OH)_3$) is depicted with the clay minerals; its behaviour was similar to kaolinite, except that it was undersaturated prior to the injections and became saturated when pH dropped below 8 during Phase I. It remained slightly supersaturated during the rest of the monitoring period (Fig. 7c). The saturation states of two other members of the kaolinite group; imogolite ($Al_2SiO_3OH_4$) and allophane ($Al_2O_3SiO_2{\cdot}H_2O$), were also calculated. Imogolite was undersaturated prior to the injections but became strongly supersaturated during Phase I when the pH drops below 8, and remained supersaturated for the rest of the monitoring period, but decreasingly so as the pH increased (Fig. 7c). Allophane was undersaturated during the whole monitoring period. Smectite was supersaturated in all samples except for the samples taken during, and shortly after the two injections while the pH was <8 (Fig. 7c). Smectite is one of the most abundant secondary minerals in basaltic rocks and has been identified in all wells drilled at Hellisheidi (e.g. Schiffman and Fridleifsson, 1991).

4. Discussion

Concentrations for the major elements Ca, Mg, Si, Na, K and Cl and the trace elements Fe and Al calculated using Eqs. (1) and (2), based on the assumption of non-reactive conservative fluid mixing, are shown in Fig. 3 together with their corresponding measured concentrations. Corresponding plots for the injected constituents are shown in Fig. 2. Measured concentrations, greater than those calculated based on conservative fluid mixing, suggest net dissolution, lower concentrations suggest net precipitation (i.e. "fixation"). Measured Ca, Mg, and Fe concentrations were much higher during the injections and the subsequent days and weeks than that calculated assuming non-reactive conservative mixing. This indicates a net-input of these elements to the fluid consistent with the dissolution of the basalt originally present in the reservoir. The measured concentrations of these elements eventually became lower, and in the case of Mg, measured concentrations became lower than that calculated from non-reactive mechanical mixing (Fig. 3b) about 300 days after the start of the Phase 1 injection, suggesting net-precipitation into secondary minerals after these times.

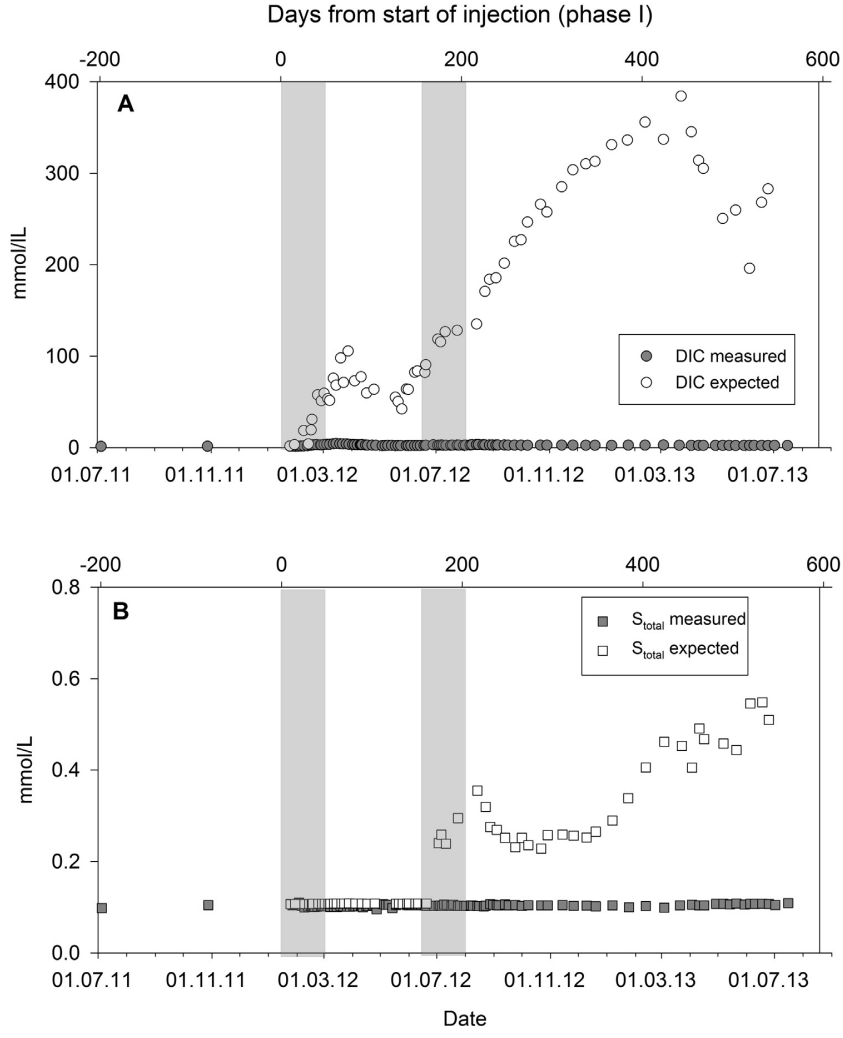

Fig. 8. Comparison of measured and calculated non-reactive mixing concentrations of DIC and sulphur – see text. The timing of both gas injections is indicated by grey bars.

Measured and calculated non-reactive conservative mixing concentrations of Si were approximately identical during the first breakthrough of Phase I, but the measured concentrations were lower during the second breakthrough (Fig. 3d). Measured Na and K concentrations were higher than the calculated from non-reactive conservative mixing, with a continuous increase up until the second breakthrough of Phase I, indicating net-release of these elements from the rock to the fluid (Fig. 3e–f). Na and K are the most mobile major elements during the weathering and low temperature alteration of basaltic rocks (Alfredsson et al., 2013; Eiriksdottir et al., 2015; Gislason et al., 1996). Measured Al concentrations were much lower during Phase I than corresponding calculated non-reactive conservative mixing concentrations indicating net Al precipitation during the injection and during the following weeks, while the pH of the samples from well HN-04 was below 8 (Fig. 3g). Subsequently, the measured Al concentration rises slowly, with a small drop during the Phase II injection. From about 300 days after the start of the Phase I injection, and throughout the sampling period, the measured Al concentration in the samples exceeded the corresponding calculated concentrations, indicating a net release of this element from the rocks. Chlorine is a trace element in basaltic rocks (Sigvaldason and Oskarsson, 1976), but is sparingly taken up by secondary minerals, providing an example of a mobile element that behaves conservatively during mechanical mixing and moderate water rock interactions (Arnórsson and Andrésdóttir, 1995; Gislason and Eugster, 1987; Olsson et al., 2014). Measured and calculated conservative mixing concentrations of Cl were approximately identical, except during the second breakthrough of Phase I, when the measured concentrations were slightly lower than the calculated values (Fig. 3h) suggesting its possible uptake into carbonates (Olsson et al., 2014).

4.1. The fate of the injected carbon

The results and calculations presented above provide insight into the fate of the injected dissolved CO_2 gas. As previously reported by Matter et al. (2016), the difference between the measured and calculated non-reactive mixing DIC concentration (Fig. 8a), indicates its loss along the flow-path towards the monitoring well. Matter et al. (2016) also suggest that the dissolution of pre-existing carbonates at the onset of the CO_2 injection may have contributed to the neutralisation of the injected CO_2-rich water, along with dissolution of other phases such as basaltic glass, primary minerals of the host rock and other secondary minerals. This liberation of cations and neutralization of the originally acidic gas-rich injected aqueous fluid lead to the precipitation of carbonate minerals; Matter et al. (2016) concluded that over 95% of the carbon injected during Phase I was fixed as carbonate minerals in less than two years.

These previous conclusions are supported by the observations reported in this study. Shortly after the injections, the measured concentrations of dissolved Mg, Fe, and Ca increased substantially (Fig. 3a–c), and were greatly above that computed for non-reactive mixing, consistent with the rapid dissolution of the original reservoir rock. The dissolved concentration of Ca in these fluids was far greater than that of Mg and Fe, suggesting the preferential dissolution of calcium bearing minerals, such as calcite, during and shortly after both injection phases. Indeed, the saturation state of calcite, the major carbonate phase present in the basaltic reservoir became undersaturated during and just after the Phase I injection (Fig. 5a), consistent with the initial dissolution of the calcite originally present in the host rock. Approximately 100 days after the start of the Phase I injection the monitoring fluid samples became supersaturated with respect to calcite with a saturation index of 0.6; this degree of supersaturation would be sufficient to grow calcite on the surfaces of the silicate minerals present in the reservoir (Stockmann et al., 2014). A similar variation of the calcite saturation state was evident following the Phase II injection. Moreover, calcite was observed to have precipitated within the monitoring well following the injection.

The saturation state of the monitoring fluid samples with respect to the carbonate phases magnesite and dolomite followed a similar pattern as calcite (Fig. 5b), but these were not identified in the study area. Such minerals have been reported to be kinetically inhibited from forming abiotically at temperatures less than 80 °C (Higgins and Hu, 2005; Kessels et al., 2000; Lippmann, 1973; Saldi et al., 2009, 2012). Similarly, siderite was calculated to be supersaturated in the sampled fluid but has not been found at the study site to date.

4.2. The fate of the injected sulphur

A noteworthy observation in this study is that the dissolved sulphur concentrations in the monitoring well samples remained close to constant during and after the injection of the H_2S-rich phase II injection. In contrast, non-reactive mixing calculations suggest these concentrations should have been as high as 0.6 mmol/L in the absence of sulphur precipitation (Fig. 8b). This indicates that vast majority of the sulphur injected into the subsurface was fixed within several weeks, before the Phase II fluids arrived at the first monitoring well. Indeed, numerous sulphur-bearing minerals, including pyrite, pyrrhotite, mackinawite, and greigite were supersaturated during the first weeks of Phase II injection (Fig. 5d).

Pyrite was strongly supersaturated favouring its nucleation and subsequent precipitation. The pyrite formation was confirmed by XRD-analysis on solids collected from the water samples taken during airlift from the injection well HN-02 in the spring of 2013. The analysis showed peaks from pyrite, amounting to 5-10 wt% of the solid material present in the air-lift samples, based on Rietveld analysis using the software Topas (Fig. A3 in the electronic Supplement). No other well-crystalline sulphides were identified in these airlift samples. Moreover, sulphide minerals were not identified in the precipitates recovered from the HN-04 monitoring well pump, which supports the conclusion that the H_2S mineralises prior to the arrival of the injection fluid at the first monitoring well. This rapid mineralisation of the injected H_2S is also in agreement with experimental studies on H_2S sequestration in basaltic rocks (Gudbrandsson and Stefánsson, 2014).

4.3. The timescale of carbon and sulphur mineralisation: carbon storage in sedimentary basins versus basaltic rocks

Carbon storage in sedimentary basins typically proceeds via the injection of pure CO_2 into porous sedimentary rocks (Fig. 9a). For common geothermal gradients, CO_2 is a supercritical fluid below 800 m in sedimentary basins. As supercritical CO_2 is less dense than the formation waters near this depth, it is buoyant and tends to rise to the surface. Ideally this CO_2 is trapped below an impermeable cap rock via structural or stratigraphic trapping. Eventually some of this CO_2 becomes stuck in small pores, limiting its mobility (residual trapping). Over time, CO_2 dissolves in the formation water (solubility trapping). As CO_2 charged water is denser than the original formation water, this CO_2-charged water will tend to sink. Some of this dissolved CO_2 may react to form stable carbonate minerals (mineral trapping). As one progresses from structural to mineral trapping, the CO_2 becomes more immobile and thus the storage more secure, though this process can take thousands of years or more as summarized in Fig. 9a (Benson and Cole, 2008; Benson et al., 2005). Mineral trapping in sedimentary basins is slow and sometimes limited because of a lack of the calcium, magnesium, and iron bearing minerals required to mineralise the injected CO_2 (Gilfillan et al., 2009; Gislason and Oelkers, 2014).

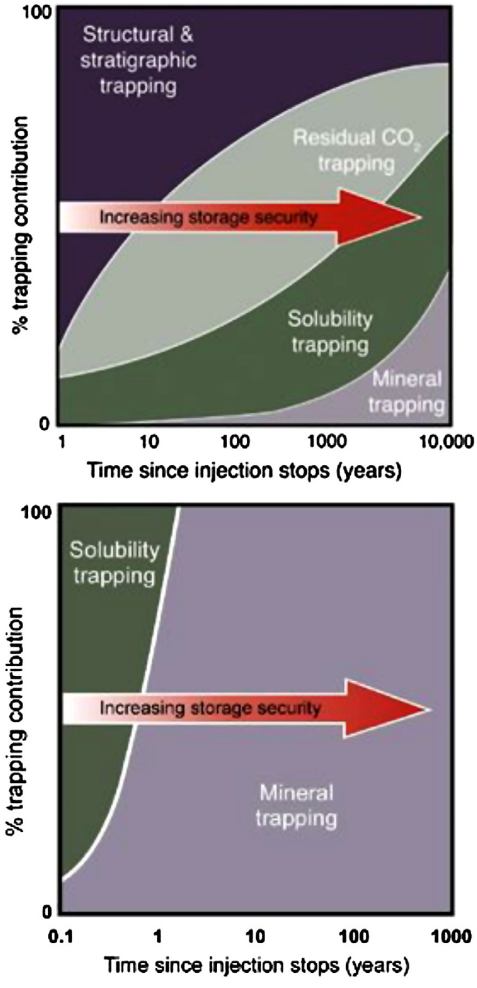

Fig. 9. Schematic illustration of the contribution of various trapping mechanisms to the geologic storage as a function of time, a) injection of buoyant supercritical CO_2 into sedimentary rocks, modified from Benson et al. (2005), b) injection of CO_2 dissolved in water into basaltic rocks via the CarbFix method.

In contrast during the CarbFix method, CO_2 is dissolved into water during its injection into porous basaltic rocks. No cap rock is required because the dissolved CO_2 is not buoyant and will not tend to migrate back to the surface. Solubility trapping occurs within 5 minutes during the CO_2 injection process (Sigfusson et al., 2015), and due to the reactivity of the basaltic rocks the bulk of the carbon is trapped in minerals within two years as shown in Fig. 9b (this study; Matter et al., 2016). This rapid carbonation of injected CO_2 provides a permanent and safe carbon storage option; once fixed into a carbonate mineral, the risk of leakage is minimal and little if any further monitoring of the site will be necessary.

The results of this study suggest that the co-injection of H_2S with CO_2 into the subsurface both rapidly fixes this gas through pyrite precipitation and does not detrimentally effect the carbonation of the injected CO_2. Indeed, the results from this study indicate that this pyrite mineralization is even faster than the carbonate mineralization; the bulk of the sulphur is trapped in minerals within four months from injection. The co-injection of these two acid gases may provide a number of advantages, most notably, it may lower substantially the energy and cost required to capture and separate the CO_2 from industrial exhaust. This possibility is now being explored in the SulFix-CarbFix project, where a CO_2-H_2S gas mixture is being captured and separated from the gas stream of the Hellisheidi power plant by its dissolution in water at the surface at about 5 bars pressure and 20 °C. The resulting gas charged water is directly injected to 700 m depth and 200–270°, aiming to store 8000–10,000 t of the gas mixture annually.

The degree to which the CarbFix method can be applied at other sites will depend on the availability of suitable host-rocks, sufficient water to dissolve the CO_2 during its injection, and economic considerations. This on-shore CarbFix project, demonstrates the feasibility of carbon storage in basaltic rocks. Nevertheless, the largest geological storage potential for CO_2 lies offshore (Goldberg and Slagle, 2009; Goldberg et al., 2010, 2008; Snæbjörnsdóttir et al., 2014), where the mid-oceanic ridges contain permeable basaltic layers and the oceans provide an unlimited reservoir for the required water (Snæbjörnsdóttir and Gislason, 2016).

5. Conclusions

This paper reported the chemical composition and mineral saturation states of fluids collected prior to, during and after the injection of 175 t of pure CO_2 and 73 t of a gas-mixture consisting of 75 mol% CO_2, 24 mol% H_2S and 1 mol% H_2, into basaltic rocks at the CarbFix site in SW-Iceland. All results indicate that the vast majority of injected CO_2 and H_2S were rapidly fixed within minerals in subsurface basalts. The results presented above confirm that this fixation occurred by the initial dissolution of the host basalts due to the injection of acidic gas-charged water; mass balance indicates the net input from host rock dissolution of Mg, Fe, and Ca following each injection. The dissolution of host basalts and fluid mixing neutralized the pH of the injected fluid such that calcite became supersaturated approximately 100 days after the start of each injection favouring the fixation of the injected CO_2 within this mineral. This results, which supports those of Matter et al. (2016) who concluded that CO_2 mineralization fixed over 95% of the injected carbon within 2 years, was further validated by observations of calcite precipitation within the monitoring well itself. Although other metal carbonate minerals, notably, ankerite, siderite and mixed Ca, Mg, Fe-carbonates, were also supersatutated in the monitoring fluids these were not observed to form during this study.

Similar results support the even more rapid mineralization of injected H_2S as pyrite, as this mineral is supersaturated before, during and after the injection of a mixed CO_2-H_2S charged water into the basalts. The rapid fixation of H_2S into this mineral is further evidenced by the observation of pyrite precipitation in the injection well but not in the first monitoring well. Such observations suggest that H_2S fixation by pyrite precipitation was essentially complete before the injected mixed-gas plume arrived at the monitoring well. Notably there appears to have been little difference in the chemical response in the subsurface of the mixed H_2S-CO_2 gas mixture injection compared to that of the pure CO_2 injection. Their similar success towards the CO_2 mineralization suggests that the injection of mixed gases might prove to be a simpler and more cost-effective approach to subsurface carbon storage than the injection of pure CO_2.

Acknowledgements

We acknowledge funding from the Reykjavik Energy; Environmental Fund of Reykjavik Energy; the European Commission through the projects CarbFix (EC coordinated action 283148), Min-GRO (MC-RTN-35488), Delta-Min (PITN-GA-2008-215360), and CO_2-REACT (EC Project 317235); the U.S. Department of

Energy under award number DE-FE0004847; Nordic fund11029-NORDICCS; and the Icelandic GEORG Geothermal Research fund (09-02-001). We are indebted to Hólmfríður Sigurðardóttir and Bergur Sigfússon at Reykjavík Energy, Magnús Þór Arnarson at Mannvit Engineering, Domenik Wolff-Boenisch at Curtin University in Australia, Helgi A. Alfreðsson at the University of Iceland and Wallace S. Broecker at Columbia University for their contributions to the CarbFix project. We thank Einar Örn Þrastarson, Trausti Kristinsson, Vordís Eiríksdóttir, Halldór Bergmann, and Þorsteinn A. Þorgeirsson at Reykjavík Energy; Vigdís Harðardóttir, Finnbogi Óskarsson, Kristján Hrafn Sigurðsson and Steinþór Níelsson at ISOR; Jennifer Hall at Columbia University, and Þorsteinn Jónsson, Sveinbjörn Steinþórsson, Iwona Galezcka, Eydís S. Eiríksdóttir, Deirdre Clark, Chris Grimm and Flora Brocza at the University of Iceland for helping during the injection and sampling campaign. We also are grateful for the assistance of Rósa Ólafsdóttir at the University of Iceland. Finally, the first author would like to thank Becca Neely for all her help and assistance in the field, in the lab and in our office.

Appendix A. Supplementary data

Supplementary data associated with this article can be found, in the online version, at http://dx.doi.org/10.1016/j.ijggc.2017.01.007.

References

Alfredsson, H.A., Oelkers, E.H., Hardarsson, B.S., Franzson, H., Gunnlaugsson, E., Gislason, S.R., 2013. The geology and water chemistry of the Hellisheidi, SW-Iceland carbon storage site. Int. J. Greenh. Gas Control 12, 399–418.

Aradóttir, E.S.P., Sonnenthal, E.L., Björnsson, G., Jónsson, H., 2012. Multidimensional reactive transport modeling of CO_2 mineral sequestration in basalts at the Hellisheidi geothermal field, Iceland. Int. J. Greenh. Gas Control 9, 24–40.

Aradóttir, E.S.P., Gunnarsson, I., Sigfússon, B., Gislason, S.R., Oelkers, E.H., Stute, M., Matter, J.M., Snæbjörnsdóttir, S.Ó., Mesfin, K.G., Alfredsson, H.A., Hall, J., Arnarsson, M.T., Dideriksen, K., Júlíusson, B.M., Broecker, W.S., Gunnlaugsson, E., 2015. Towards cleaner geothermal energy: subsurface sequestration of sour gas emissions from geothermal power plants. In: Proceedings World Geothermal Congress 2015, Melbourne, Australia, 19–25 April.

Archer, D., 2005. Fate of fossil fuel CO_2 in geologic time. J. Geophys. Res. 110, C09S05.

Arnórsson, S., Andrésdóttir, A., 1995. Processes controlling the distribution of boron and chlorine in natural waters in Iceland. Geochim. Cosmochim. Acta 59 (20), 4125–4146.

Arnórsson, S., D'Amore, F., Gerardo-Abaya, J., 2000. Isotopic and geochemical techniques in geothermal exploration, development and use. In: Arnórsson, S. (Ed.), Sampling Methods, Data Handling, Interpretation. International Atomic Energy Agency Publication, Vienna.

Assayag, N., Matter, J., Ader, M., Goldberg, D., Agrinier, P., 2009. Water–rock interactions during a CO_2 injection field-test: implications on host rock dissolution and alteration effects. Chem. Geol. 265 (1–2), 227–235.

Bachu, S., Gunter, W.D., 2005. Overview of acid-gas injection operations in Western Canada. In: Wilson, E.S., Rubin, D.W., Keith, C.F., Gilboy, M., Thambimuthu, T., Morris, J., Gale, K. (Eds.), Greenhouse Gas Control Technologies 7. Elsevier Science Ltd., Oxford, pp. 443–448.

Bacon, D.H., Ramanathan, R., Schaef, H.T., McGrail, B.P., 2014. Simulating geologic co-sequestration of carbon dioxide and hydrogen sulfide in a basalt formation. Int. J. Greenh. Gas Control 21, 165–176.

Benson, S.M., Cole, D.R., 2008. CO_2 sequestration in deep sedimentary formations. Elements 4, 325–331.

Benson, S.M., Cook, P., Coordinating Lead Authors. Anderson, J., Bachu, S., Nimir, H.B., Basu, B., Bradshaw, J., Deguchi, G., Gale, J., von Goerne, G., Heidug, W., Holloway, S., Kamal, R., Keith, D., Lloyd, P., Rocha, P., Senior, B., Thomson, J., Torp, T., Wildenborg, T., Wilson, M., Zarlenga, F., Zhou, D, Lead Authors. Celia, S.M., Gunter, B., Ennis King, J., Lindegerg, E., Lombardi, S., Oldenburg, C., Pruess, K., Rigg, A., Stevens, S., Wilson, E., Whittaker, S., 2005. Underground Geological Storage, IPCC Special Report on Carbon Dioxide Capture and Storage, Chapter 5. Intergovernmental Panel on Climate Change, Cambridge University Press Cambridge, U.K.

Broecker, W.S., Kunzig, R., 2008. Fixing climate. The story of climate science—and how to stop global warming. Green Profile.

Broecker, W., 2007. Climate change: CO_2 arithmetic. Science 315, 1371.

Deer, W.A., Howie, R.A., Zussman, J., 1992. An Introduction to the Rock Forming Minerals, 2nd edition. Pearson, Prestice Hall, Harlow, England, 696 p.

Drever, J.I., 1982. The Geochemistry of Natural Waters. Prentice-Hall, Englewood Cliffs, N.J.

Eiriksdottir, E.S., Gislason, S.R., Oelkers, E.H., 2015. Direct evidence of the feedback between climate and nutrient, major, and trace element transport to the oceans. Geochim. Cosmochim. Acta 166, 249–266.

European Environment Agency, 2014. Sulphur Dioxide (SO_2) Emissions (APE 001)—Assessment Published in Jan 2014, vol. 2015. European Environment Agency.

Fisher, A.T., 1998. Permeability within basaltic oceanic crust. Rev. Geophys. 36 (2), 143–182.

Flaathen, T.K., Gislason, S.R., Oelkers, E.H., Sveinbjörnsdóttir, Á.E., 2009. Chemical evolution of the Mt. Hekla, Iceland, groundwaters: a natural analogue for CO_2 sequestration in basaltic rocks. Appl. Geochem. 24 (3), 463–474.

Franzson, H., 1983. Svartsengi, Well SG-12: Drilling, Stratigraphy and Aquifers (in Icelandic). National Energy Authority of Iceland, OS/83003/ JHD-02.

Galeczka, I., Wolff-Boenisch, D., Oelkers, E.H., Gislason, S.R., 2014. An experimental study of basaltic glass–H_2O–CO_2 interaction at 22 and 50 °C: implications for subsurface storage of CO_2. Geochim. Cosmochim. Acta 126, 123–145.

Gensemer, R.W., Playle, C., 1999. The bioavailability and toxicity of aluminum in aquatic environments. Crit. Rev. Environ. Sci. Technol. 29 (4), 315–450.

Gilfillan, S.M.V., Lollar, B.S., Holland, G., Blagburn, D., Stevens, S., Schoell, M., Cassidy, M., Ding, Z., Zhou, Z., Lacrampe-Couloume, G., Ballentine, C.J., 2009. Solubility trapping in formation water as dominant CO_2 sink in natural gas fields. Nature 458 (7238), 614–618.

Gislason, S.R., Eugster, H.P., 1987. Meteoric water-basalt interactions I: a laboratory study. Geochim. Cosmochim. Acta 51 (10), 2827–2840.

Gislason, S.R., Oelkers, E.H., 2014. Carbon storage in basalt. Science 344, 373–374.

Gislason, S.R., Torssander, P., 2006. Response of sulfate concentration and isotope composition in icelandic rivers to the decline in global atmospheric SO_2 emissions into the North Atlantic Region. Environ. Sci. Technol. 40, 680–686.

Gislason, S.R., Arnórsson, S., Ármannsson, H., 1996. Chemical weathering of basalt in SW Iceland: effects of runoff, age of rocks and vegetative/glacial cover. Am. J. Sci. 296, 837–907.

Gislason, S.R., Wolff-Boenisch, D., Stefansson, A., Oelkers, E.H., Gunnlaugsson, E., Sigurdardottir, H., Sigfusson, B., Broecker, W.S., Matter, J., Stute, M., Axelsson, G., Fridriksson, T., 2010. Mineral sequestration of carbon dioxide in basalt: a preinjection overview of the CarbFix project. Int. J. Greenh. Gas Control 4, 537–545.

Gislason, S.R., Broecker, W.S., Gunnlaugsson, E., Snæbjörnsdóttir, S.Ó., Mesfin, K.G., Alfredsson, H.A., Aradottir, E.S., Sigfusson, B., Gunnarsson, I., Stute, M., Matter, J.M., Arnarson, M.T., Galeczka, I.M., GuÞbrandsson, S., Stockman, G., Wolff-Boenisch, D., Stefansson, A., Ragnheidardottir, E., Faathen, T., Gysi, A.P., Olssen, J., Didriksen, K., Stippe, S., Menez, B., Oelkers, E.H., 2014. Rapid solubility and mineral storage of CO_2 in basalt. Energy Procedia 63, 4561–4574.

Global CCS Institute, 2015. The global Status of CCS 2015–summary report. Melbourne, Australia.

Goldberg, D., Slagle, A.L., 2009. A global assessment of deep-sea basalt sites for carbon sequestration. Energy Procedia 1, 3675–3682.

Goldberg, D.S., Takahashi, T., Slagle, A.L., 2008. Carbon dioxdie sequestration in deep-sea basalt. PNAS 105 (29), 9920–9925.

Goldberg, D.S., Kent, D.V., Olsen, P.E., 2010. Potential on-shore and off-shore reservoirs for CO_2 sequestration in Central Atlantic magmatic province basalts. Proc. Natl. Acad. Sci. U. S. A. 107, 1327–1332.

Goldberg, D., Lackner, K., Han, P., Wang, T., 2013. Co-location of air capture subseafloor CO_2 sequestration, and energy production on the Kerguelen plateau. Environ. Sci. Technol. 47 (13).

Gudbrandsson, S., Stefánsson, A., 2014. Experimental study of H_2S sequestration in geothermal systems, RH-14-2014.

Gudbrandsson, S., Wolff-Boenisch, D., Gislason, S.R., Oelkers, E.H., 2011. An experimental study of crystalline basalt dissolution from 2 < pH < 11 and temperatures from 5 to 75 °C. Geochim. Cosmochim. Acta 75 (19), 5496–5509.

Gunnarsdóttir, S.H., 2012. The Geology and Hydrothermal Alteration near the Mt. Reykjafell Area in the Hellisheidi Geothermal Field. University of Iceland (MSc thesis).

Gunnarsson, I., Sigfusson, B., Stefansson, A., Arnorsson, S., Scott, S., Gunnlaugsson, E., 2011. Injection of H_2S from Hellisheidi Power Plant, Iceland. In: Workshop on Geothermal Reservoir Engineering, Stanford California.

Gunnlaugsson, E., Arnórsson, S., 1982. The chemistry of iron in geothermal systems in iceland. J. Volcanol. Geotherm. Res. 14 (3–4), 281–299.

Gysi, A.P., Stefánsson, A., 2011. CO_2–water–basalt interaction. Numerical simulation of low temperature CO_2 sequestration into basalts. Geochim. Cosmochim. Acta 75 (17), 4728–4751.

Gysi, A.P., Stefánsson, A., 2011. CO_2–water–basalt interaction. Low temperature experiments and implications for CO_2 sequestration into basalts. Geochim. Cosmochim. Acta 81, 129–152.

Gysi, A.P., Stefánsson, A., 2011. Mineralogical aspects of CO_2 sequestration during hydrothermal basalt alteration – an experimental study at 75–250 °C and elevated pCO_2. Chem. Geol. 306–307, 146–159.

Harris, R.N., Chapman, D.S., 2004. Deep-seated oceanic heat flux, heat deficits and hydrothermal circulation. In: Hydrogeology of the Oceanic Lithosphere. Cambridge University Press, Cambridge.

Helgadóttir, H.M., 2011. Stratigraphy and Hydrothermal Alteration of the Gráuhnúkar Geothermal System in the Southern Part of the Hengill Area. University of Iceland (MSc Thesis) 123 p.

Higgins, S.R., Hu, X., 2005. Self-limiting growth on dolomite: experimental observations with *in situ* atomic force microscopy. Geochim. Cosmochim. Acta 69, 2085–2094.

Hjartarson, Á., Sæmundsson, K., 2014. Geological Map of Iceland. Bedrock. 1:600 000: Iceland GeoSurvey.
Hoffert, M., Caldeira, K., Benford, G., Criswell, D., Green, C., Herzog, H., Jain, A., Kheshgi, H., Lackner, K., Lewis, J., Lightfood, H., Manheimer, W., Mankins, J., Mauel, M., Perkins, L., Schlesinger, M., Volk, T., Wigley, T., 2002. Advanced technology paths to global climate stability: energy for a greenhouse planet. Science 298, 981–987.
IPCC, 2005. In: Metz, B., Davidson, O., de Coninck, H.C., Loos, M., Meyer, L.A. (Eds.), IPCC Special Report on Carbon Dioxide Capture and Storage. Prepared By. Working Group III of the Intergovernmental Panel on Climate Change. Cambridge University Press, Cambridge, United Kingdom and New York, NY USA, 442 pp.
International Energy Agency, 2015. Mobilising Innovation to Accelerate Climate Action, Executive Summary.
IPCC, 2014. Contribution of Working Groups I, II and III to the Fifth Assessment Report of the Intergovernmental Panel on Climate Change.
Kessels, L.A., Sibley, D.F., Nordeng, S.H., 2000. Nanotopography of synthetic and natural dolomite crystals. Sedimentology 47, 173–186.
Khalilabad, M.R., Axelsson, G., Gislason, S.R., 2008. Aquifer characterization with tracer test technique; permanent CO_2 sequestration into basalt, SW Iceland. Mineral. Mag. 72, 121–125.
Knauss, K.G., Johnson, J.W., Steefel, C.I., 2005. Evaluation of the impact of CO_2, co-contaminant gas, aqueous fluid and reservoir rock interactions on the geologic sequestration of CO_2. Chem. Geol. 217 (3–4), 339–350.
Lackner, K., 2003. A guide to CO_2 sequestration. Science 300, 1677–1678.
Lippmann, F., 1973. Sedimentary Carbonate Minerals. Springer-Verlag, New York.
Markússon, S.H., Stefánsson, A., 2011. Geothermal surface alteration of basalts, Krýsuvík Iceland—alteration mineralogy, water chemistry and the effects of acid supply on the alteration process. J. Volcanol. Geotherm. Res. 206 (1–2), 46–59.
Matter, J., Takahashi, T., Goldberg, D., 2007. Experimental evaluation of *in situ* CO_2-water-rock reactions during CO_2 injection in basaltic rocks: implications for geological CO_2 sequestration. Geochem. Geophys. Geosyt. 8 (2), 19.
Matter, J.M., Broecker, W., Gislason, S.R., Gunnlaugsson, E., Oelkers, E., Stute, M., Sigurdardóttir, H., Stefansson, A., Wolff-Boenisch, D., Axelsson, G., Sigfússon, B., 2011. The CarbFix pilot project – storing carbon dioxide in basalt. Energy Procedia 4, 5579–5585.
Matter, J.M., Stute, M., Snæbjörnsdóttir, S.Ó., Oelkers, E.H., Gislason, S.R., Aradottir, E.S., Sigfusson, B., Gunnarsson, I., Sigurdardottir, H., Gunnlaugsson, E., Axelsson, G., Alfredsson, H.A., Wolff-Boenisch, D., Mesfin, K., Fernandez de la Reguera Taya, D., Hall, J., Dideriksen, K., Broecker, W.S., 2016. Rapid carbon mineralisation for permanent and safe disposal of anthropogenic carbon dioxide emissions. Science 352 (6291), 1312–1314.
McGrail, B.P., Freeman, C.J., Brown, C.F., Sullivan, E.C., White, S.K., Reddy, S., Garber, R.D., Tobin, D., Gilmartin, J.J., Steffensen, E.J., 2012. Overcoming business model uncertainty in a carbon dioxide capture and sequestration project: case study at the Boise White Paper Mill. Int. J. Greenh. Gas Control 9, 91–102.
McGrail, B.P., Schaef, H.T., Ho, A.M., Chien, Y.-J., Dooley, J.J., Davidson, C.L., 2006. Potential for carbon dioxide sequestration in flood basalts. J. Geophys. Res.: Solid Earth 111, B12201.
McGrail, B.P., Spane, F.A., Sullivan, E.C., Bacon, D.H., Hund, G., 2011. The Wallula basalt sequestration pilot project. Energy Procedia 4, 5653–5660.
Oelkers, E., Schott, J., 2005. Geochemical aspects of CO_2 sequestration. Chem. Geol. 217, 183–186.
Oelkers, E.H., Cole, D.R., 2008. Carbon dioxide sequestration: a solution to a global problem. Elements 4, 305–310.
Oelkers, E.H., Gislason, S.R., Matter, J., 2008. Mineral carbonation of CO_2. Elements 4, 331–335.
Olsson, J., Stipp, S.L.S., Makovicky, E., Gislason, S.R., 2014. Metal scavenging by calcium carbonate at the Eyjafjallajökull volcano: a carbon capture and storage analogue. Chem. Geol. 384, 135–148.
Pacala, S., Socolow, R., 2004. Stabilization wedges: solving the climate problem for the next 50 years with current technologies. Science 305, 968–972.
Parkhurst, D.L., Appelo, C.A.J., 2013. Description of input and examples for PHREEQC version 3—A computer program for speciation, batch-reaction, one-dimensional transport, and inverse geochemical calculations, U.S. Geological Survey Techniques and Methods, v. chap. A43, 497 p.
Richter, B., Guðlaugsson, S.Þ., Steingrímsson, B., Björnsson, G., Bjarnason, J.Ö., Þórhallsson, S., 1999. Svartsengi well SJ-18: Drilling, research and production (in Icelandic), OS-99117.
Rogers, K.L., Neuhoff, P.S., Pedersen, A.K., Bird, D.K., 2006. CO_2 metasomatism in a basalt-hosted petroleum reservoir, Nuussuaq, West Greenland. Lithos 92 (1–2), 55–82.
Rosenbauer, R.J., Thomas, B., Bischoff, J.L., Palandri, J., 2012. Carbon sequestration via reaction with basaltic rocks: geochemical modelling and experimental results. Geochim. Cosmochim. Acta 89, 116–133.
Rutqvist, J., Birkholzer, J., Cappa, F., Tsang, C.-F., 2007. Estimating maximum sustainable injection pressure during geological sequestration of CO_2 using coupled fluid flow and geomechanical fault-slip analysis. Energy Convers. Manage. 48, 1798–1807.
Saldi, D., Jordan, G., Schott, J., Oelkers, E.H., 2009. Magnesite growth rates as a function of temperature and saturation state. Geochim. Cosmochim. Acta 73, 5646–5657.
Saldi, G.D., Schott, J., Pokrovsky, O.S., Gautier, Q., Oelkers, E.H., 2012. An experimental study of magnesite precipitation rates at neutral to alkaline conditions and 100–200C as a function of pH, aqueous solution composition and chemical affinity. Geochim. Cosmochim. Acta 83, 93–109.
Schiffman, P., Fridleifsson, G.O., 1991. The smectite-chlorite transition in drillhole NJ-15, Nesjavellir Geothermal Field, Iceland: XRD BSE and electron microprobe investigations. J. Metamorph. Geol. 9 (6), 679–696.
Sigfusson, B., Gislason, S.R., Matter, J.M., Stute, M., Gunnlaugsson, E., Gunnarsson, I., Aradottir, E.S., Sigurdardottir, H., Mesfin, K.G., Alfredsson, H.A., Wolff-Boenisch, D., Arnarson, M.T., Oelkers, E.H., 2015. Solving the carbon-dioxide buoyancy challenge: the design and field testing of a dissolved CO_2 injection system. Int J. Greenh. Gas Control 37, 213–219.
Sigvaldason, G.E., Oskarsson, N., 1976. Chlorine in basalts from Iceland. Geochim. Cosmochim. Acta 40, 777–789.
Smith, S.J., Van Aardenne, J., Klimont, Z., Anders, R.J., Volke, A., Delgato Arias, S., 2011. Anthropogenic sulfur dioxide emissions 1850–2005. Atmos. Chem. Phys. 11, 1101–1116.
Snæbjörnsdóttir, S.Ó., Gislason, S.R., 2016. CO_2 storage potential of basaltic rocks offshore Iceland. Energy Procedia 86, 371–380.
Snæbjörnsdóttir, S.Ó., Wiese, F., Fridriksson, T., Ármannsson, H., Einarsson, G.M., Gislason, S.R., 2014. CO_2 storage potential of basaltic rocks in Iceland and the oceanic ridges. Energy Procedia 63, 4585–4600.
Stefánsson, A., Arnórsson, S., Gunnarsson, I., Kaasalainen, H., Gunnlaugsson, E., 2011. The geochemistry and sequestration of H_2S into the geothermal system at Hellisheidi, Iceland. J. Volcanol. Geotherm. Res. 3 (3–4), 179–188.
Stockmann, G.J., Wolff-Boenisch, D., Bovet, N., Gislason, S.R., Oelkers, E.H., 2014. The role of silicate surfaces on calcite precipitation kinetics. Geochim. Cosmochim. Acta 135, 231–250.
Stockmann, G.J., Wolff-Boenisch, D., Gislason, S.R., Oelkers, E.H., 2011. Do carbonate precipitates affect dissolution kinetics? 1: Basaltic glass. Chem. Geol. 284 (3–4), 306–316.
Stockmann, G.J., Wolff-Boenisch, D., Gislason, S.R., Oelkers, E.H., 2013. Do carbonate precipitates affect dissolution kinetics? 2: Diopside. Chem. Geol. 337–338, 56–66.
Stumm, W., Morgan, J.J., 1996. Aquatic Chemistry: Chemical Equilibria and Rates in Natural Waters, third ed. John Wiley & Sons, New York, 1022 p.
Thorarinsson, S.B., Helgadóttir, H.M., Franzson, H., Harðarson, B.S., Hjartarson, A., Ásmundsson, R., Sigurdsson, G., 2006. Hellisheidi – well HN-04. 1st to 3rd stages: Drilling of 18 5/8 security casing in 105 m, production casing in 400 m and 12 1/4 production part in 1204 m: ISOR, Iceland GeoSurvey, ISOR-2006/055.
United States Environmental Protection Agency, 2015. The National Emissions Inventory. National Summary of Sulfur Dioxide Emissions, NEI 2011 v2 GPR.
Van Pham, H., Aagaard, P., Hellevang, H., 2012. On the potential for CO_2 mineral storage in continental flood basalts – PHREEQC batch and 1D diffusion – reaction simulations. Geochem. Trans. 13 (5), p12.
Wiese, F., Fridriksson, T., Armannsson, H., 2008. CO_2 Fixation by Calcite in High-temperature Geothermal Systems in Iceland: ISOR, Iceland Geosurvey, ISOR-2008/003.
Wolff-Boenisch, D., Wenau, S., Gislason, S.R., Oelkers, E.H., 2011. Dissolution of basalts and peridotite in seawater, in the presence of ligands, and CO_2: implications for mineral sequestration of carbon dioxide. Geochim. Cosmochim. Acta 75 (19), 5510–5525.
World Health Organization, 2000. WHO Air Quality Guidelines for Europe, 2nd edition. WHO regional office for Europe.
WorleyParsons, Schlumberger, 2011. Assessment of Carbon Capture and Storage Technologies: 2011 Update. Global CCS Institute.
Wöll, C., Hallsdóttir, B.S., Guðmundsson, J., Snorrason, A., Þórsson, J., Jónsson, P.V.K., Andrésson, K., Einarsson, S., 2014. Emissions of Greenhouse Gases in Iceland from 1990 to 2012: National Inventory Report 2014. Environment Agency of Iceland, UST-2014-2.

Paper V

Reaction path modelling of *in situ* mineralisation of CO_2 at the CarbFix site in SW-Iceland

Snæbjörnsdóttir S. Ó., Gislason S.R., Galeczka M.I., Oelkers E.H., 2017. Geochimica et Cosmochimica Acta. *Manuscript prepared for submission*.

Reaction path modelling of *in-situ* mineralisation of CO_2 at the CarbFix site in SW-Iceland

Sandra Ó. Snæbjörnsdóttir[1], Sigurdur R. Gislason[1], Iwona M. Galeczka[1, 2], Eric H. Oelkers[3, 4]

[1]*Institute of Earth Science, University of Iceland, Iceland*

[2] *ISOR, Iceland GeoSurvey, Iceland*

[3]*Earth Science, University College London, UK*

[4]*CNRS/UMR 5563, Université Paul Sabatier, France*

Abstract

Results from injection of 175 tonnes of CO_2 into the basaltic subsurface rocks at the CarbFix site in SW-Iceland in 2012 show almost complete mineralisation of the injected carbon in less than two years (Matter et al., 2016; Snæbjörnsdóttir et al., 2017). Reaction path modelling was carried out to illuminate the rate and extent of CO_2-water-rock reactions during and after the injection. The modelling calculations were constrained by the fluid composition sampled prior to, during, and after the injection, from the injection well and the first monitoring well at the injection site. The mineralisation of the main breakthrough of the injected fluid, occurring about 400 days after the onset of the injection, appears to be dominated by basaltic glass dissolution. Basaltic glass glazes the tops and bases of the lava flows that host the main flow paths of fresh to moderately altered lava piles. However, considerable mineralisation appears to be driven by crystalline basalt dissolution during the first 60 days of the injection via fast fracture flow. The crystalline basalts of the interiors of the lava pile are transected by the fracture that hosts the flow path. The initial pH of the injected fluid, prior to injection and CO_2 dissolution was measured to be ~9.5, and the pH of the background waters in the monitoring well was measured to be ~9.4 prior to the injections The pH of the sampled fluids used in the modelling ranged from 3.7 at the injection well to as high as 8.2 in the monitoring well. At low pH, Mg, and Fe are preferentially released from crystalline basalts due to the higher dissolution rates of olivine, and to lesser extent pyroxene, compared to plagioclase and glass (Gudbrandsson et

al., 2011). This favours the formation of siderite and Fe-Mg carbonates over calcite during this early mineralisation. The model suggests the formation of carbonate mineral sequences; siderite at pH below 5, Mg-Fe-carbonates at pH ~5, and Ca-Mg-Fe-carbonates and calcite at higher pH. Other minerals forming along with the carbonates are Al- and Fe-hydroxides, chalcedony, zeolites, and clays. Dissolution of pre-existing calcite at the onset of the injection does not have a net effect on the carbonation, but does contribute to more rapid pH rise early on during the injection, and influences which carbonates form.

1 Introduction

The reduction of CO_2 emissions to the atmosphere is the one of the biggest scientific challenges of this century (Broecker, 2007; Hoffert et al., 2002; IEA, 2015; IPCC, 2014; Lackner, 2003; Oelkers and Schott, 2005; Pacala and Socolow, 2004). The Paris Agreement (UN, 2015b) aims to keep the global temperature rise "well below 2°C" from pre-industrial levels, and to pursue efforts to limit the temperature increase to 1.5 °C above pre-industrial levels. Achieving the goals of the Paris Agreement requires a substantial and sustained reduction in the net flow of CO_2 into the atmosphere. This necessitates the rapid and extensive employment of low-emission technologies and mitigation options (Erbach, 2016; IEA, 2016; OECD/IEA, 2016; UN, 2015a; Yann et al., 2017).

Carbon Capture and Storage (CCS) technologies are expected to play an important role in meeting the Paris Agreement targets. Currently it is the only available technology that can significantly reduce emissions from fossil fuel-based power generation, as well as other industrial processes, such as steel and cement production, for the foreseeable future (Global CCS Institute, 2016; IEA, 2016a). However, the pace of CCS deployment is still far from meeting these challenges (IEA, 2016a; IPCC, 2014). A critical step in CCS is identifying locations and methods for secure subsurface storage of carbon.

The CarbFix project aims at mineralising CO_2 injected into basaltic rocks for safe and long-term storage. This paper follows three previous reports:

1) a detailed description of the injection method and data from the injection well was (Sigfusson (2015); 2) monitoring of tracers, dissolved inorganic carbon, and pH in the first monitoring well downstream from the injection well (Matter et al. 2016); and 3) dissolved major elements during and after injection in the first monitoring well, along with the saturation indices of potential secondary minerals (Snæbjörnsdóttir et al. 2017).

The injection of CO_2 into basaltic rocks offers several advantages over more conventional storage, due to their ability to promote rapid mineralisation and large potential storage volume (Gislason and Oelkers, 2014; Goldberg and Slagle, 2009; McGrail et al., 2006; Snæbjörnsdóttir et al., 2014). Basaltic rocks are rich in divalent cations such as Ca^{2+}, Mg^{2+}, and Fe^{2+}. Acidic gas-charged water accelerates the release of these metals, promoting the formation of carbonate minerals such as calcite, magnesite, siderite, and solid-solutions thereof (Gislason et al., 2014; Gislason and Oelkers, 2014), providing safe and long-term carbon storage.

Here we use data collected prior to, during, and after the injection of 175 tonnes of pure CO_2 into the subsurface basaltic rocks at the CarbFix site in SW-Iceland, in attempt to model the CO_2-water-rock interaction during and after the injection. Such efforts will be used to illuminate the fate of the CO_2 following its injection.

2 Methods

2.1 Site description

The CarbFix injection site has been described in detail in several papers (Alfredsson et al., 2013; Aradóttir et al., 2012; Snæbjörnsdóttir et al., 2017). The site is located in SW-Iceland, about 30 km east of Reykjavík, and about 3 km SW of the Hellisheidi geothermal power plant, which is owned and operated by Reykjavik Energy. The power plant annually produces about 40,000 tonnes CO_2 and 12,000 tonnes of H_2S as a by-product of geothermal energy production. The gases are of magmatic origin.

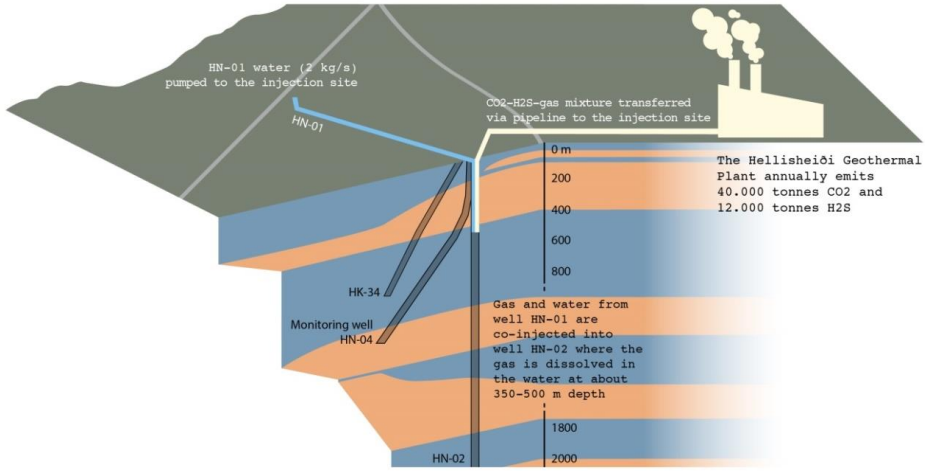

Fig. 1. Overview of the injection site at Hellisheidi. Modified from Snæbjörnsdóttir et al. 2017, and Alfredsson et al. 2013. The HN-01 water was injected into well HN-02 at a rate of 2 kg/s, and co-injected with the CO_2, which dissolves into the HN-02 water during injection. One kg/s of water was produced out of the first monitoring well HN-04 during, and after the injections.

In January to March 2012, 175 tonnes of pure CO_2 were dissolved into co-injected water as it descended into well HN-02, a 2001 m deep injection well located at the site (Fig.1), as described in detail by Sigfusson et al. (2015), Matter et al. (2016), and Snæbjörnsdóttir et al. (2017). Both reactive and non-reactive tracers were used for the injection. The injected CO_2 was spiked with carbon-14 (^{14}C), and sulphur hexafluoride, a non-reactive tracer, was co-injected with the injection fluids. The injection site is equipped with monitoring wells that penetrate the groundwater system affected by the injection. The pH of the background waters in the monitoring wells penetrating the target groundwater system was 8.9-9.9 prior to the injections (Alfredsson et al., 2013). Extensive monitoring was carried out prior to, during, and after the injection via sampling of the first monitoring well, HN-04. At the surface the distance between HN-04 and the injection well, HN-02, is some 10 m but due to the subsurface diversion of HN-04, the distance between the wells is ~125 m at 520 m

depth, where the target carbon storage aquifer is located (Alfredsson et al., 2013; Aradóttir et al., 2012; Fig. 1).

Table 1. *Secondary phases identified in drill cuttings in the top 1000 m of the injection well, HN-02 (Alfredsson et al., 2013; Helgadóttir, 2011). The total depth of the well is 2001 m. The depth of the targeted storage formation is ~400-800 m (e.g. Alfredsson et al., 2013; Aradóttir et al., 2012).*

	Chemical composition	**Depth of appearance**
Zeolites		
Thomsonite	$NaCa_2Al_5Si_5O_{10}\cdot 6H_2O$	250-650
Chabazite	$NaCa_2Al_5Si_{13}O_{36}\cdot 14H_2O$	250-760
Analcime	$NaAlSi_2O_6\cdot H_2O$	250-*1000*
Mesolite	$Na_2Ca_2Al_6Si_9O_{30}\cdot 8H_2O$	600-*1000*
Scolecite	$CaAl_2Si_3O_{10}\cdot 3H_2O$	220-*1000*
Heulandite	$NaCa_4(Al_9Si_{27}O_{72})\cdot 28H_2O$	480-*1000*
Stilbite	$(Ca,Na)_{2-3}Al_3(Al,Si)2Si_{13}O_{36}\cdot 12H_2O$	820-*1000*
Carbonates		
Aragonite	Ca_8CO_3	150-500
Calcite	Ca_8CO_3	500-*1000*
Dogtooth calcite	Ca_8CO_3	180-*1000*
Chalcedony	SiO_4	500-*1000*
Smectite (saponite)	$Ca_{0.1}Na_{0.1}Mg_{2.25}Fe^{2+}_{0.75}Si_3AlO_{10}(OH)_2\cdot 4(H_2O)$	200-*1000*

The storage formation consists of basaltic lavas of olivine tholeiitic composition, as described in detail by Alfredsson et al. (2013) and Helgadóttir (2011). The lava flows are characterized by crystalline interiors, and glassy scoria-rich tops and bases formed due to more rapid cooling. The initial porosity ranges from 5 to 40% (Franzson et al., 2008) and is mostly present at the glassy boundaries of these flows, but also via cooling cracks and columnar jointing, and younger cracks, fractures, and tectonic faults (e.g. Alfredsson et al. 2013). The major alteration phases at the depth of the CO_2 injection, at about 500 m and 30-50°C, are pore filling Ca–Mg–Fe–smectite, Ca-rich zeolites, chalcedony, and calcite, forming in vesicles and fractures of the primary rocks (Alfredsson et al., 2013; Helgadóttir, 2011; Table 1). These phases are characteristic for low temperature alteration of basaltic rocks (Kristmannsdóttir and Tómasson, 1978), and reflect the low partial pressure of CO_2

and high pH of the groundwater of the storage formation. Smectite-zeolite alteration leads to up to 40% decrease of the initial porosity (Neuhoff et al., 2008).

Tracer tests were conducted during the period of 2008-2011, both under natural and forced flow conditions to define the system hydrology. Hydrological modelling (Khalilabad et al., 2008), and later reactive transport models (Aradóttir et al., 2012) were used to define the hydrology of the system. Most of the storage formation consists of relatively homogenous porous media with effective matrix porosity of 8.5%, but a fast breakthrough path, most likely caused by a fracture, was found to channel about 3% of the flow between wells HN-02 and HN-04 (Aradóttir et al., 2012; Khalilabad et al., 2008). The lateral and vertical intrinsic permeabilities were estimated to be 300 and 1700 $\times 10^{-15}$ m^2, respectively, and the regional undisturbed groundwater flow velocity was estimated to be about 25 m/year (Aradóttir et al., 2012).

The groundwater flow between the wells was accelerated during the injection period, and in the following monitoring period, by pumping water into the injection well HN-02 at 2 kg/s and by producing 1 kg/s out of the first monitoring well HN-04. The fast breakthrough, channelling about 3% of the injected solution, occurred some 60 days after the onset of the injection based on the non-reactive SF_6 tracer data. The second and main breakthrough, with peak concentration of the injected solution, occurred about 400 days after the imitation of the injection (Matter et al., 2016; Fig.2).

2.2 Geochemical modelling

Reaction path modelling was performed in an attempt to illuminate the identity and extent of fluid-mineral reactions during and after the CarbFix injection at Hellisheidi from January to March 2012. An effort was made to model the reaction path of the first breakthrough of the injected CO_2-rich fluid, channelling about 3% of the injected fluid and arriving at the first monitoring well HN-04 about 60 days after the onset of the injection, and the second, main breakthrough of the bulk of the injected fluid, arriving about 400 days after the onset (Fig. 2).

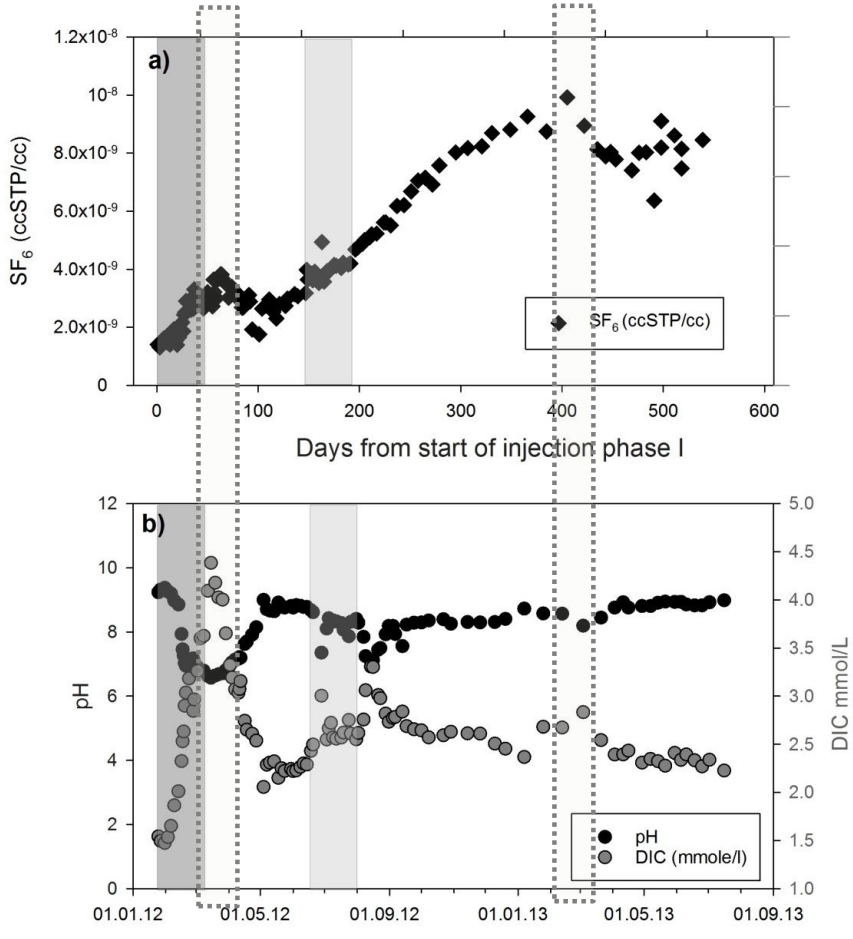

Fig. 2. Time evolution of the SF_6 tracer (a) and the pH and DIC (b) concentrations in the first monitoring well HN-04 during and after injections. The period of the pure CO_2 injection is shaded (dark grey). A second injection of 73 tonnes of 75%CO_2-25%H_2S gas mixture is also shaded (light grey). The two superimposed columns frame represents the first and second breakthrough of the pure CO_2 injected solution.

The geochemical reactions were studied as a function of reaction progress as the basalts reacted with the CO_2-charged injection fluid: both in terms of secondary mineral formation and water chemistry. Aqueous speciation, mineral saturation states, and reaction path modelling was performed using PHREEQC (Parkhurst and Appelo, 2013). The standard PHREEQC database was used in all calculations after including revised thermodynamic data on secondary minerals taken from Gysi and Stefánsson (2011, Table 2). The calculations were carried out assuming that the oxygen fugacity was controlled by equilibrium with the H_2S/SO_4^{2-} redox couple.

The pH measured in the sampled monitoring well fluids, representing the two breakthroughs, was used as a guideline in the modelling. The aim was to produce fluids with similar chemical composition to those sampled. The mass and volume of dissolved and precipitated phases and the chemical compositions of the precipitating phases were then evaluated.

Three processes have been identified to account for the pH rise and the chemical evolution of the injected fluids (Matter et al., 2016; Snæbjörnsdóttir et al., 2017) sampled in the monitoring well HN-04:

1) The mixing of the acidic injection fluids with the alkaline formation waters.
2) The dissolution of the pre-existing glasses and minerals of the storage host rock formation during and after the injection.
3) The dissolution of calcite at the onset of the injection, accounting for about 50% of the carbon dilution in the fluid as suggested by the $^{12}C/^{14}C$ ratio of fluid samples collected during the first breakthrough.

The role of these processes is evaluated via modelling of the system. The mixing of the injection fluid with the background waters is most certainly a gradual process, which starts taking place as soon as the injected fluid enters the storage formation and continues until this fluid enters the first monitoring well. This process has been simplified in the model. Preliminary mixing calculations show best fit with the sampled monitoring fluids if the solid phases are dissolved into the injection fluids prior to mixing with the background

fluids; rather than after the mixing takes place. This approach is therefore taken in the modelling calculations.

2.2.1 The fluid phases

A representative composition of the formation waters, un-affected by the CO_2 injection, was sampled from the first monitoring well HN-04 on the 25th of January 2012, prior to the arrival of the injected fluids. The chemical composition of this sample, 12KGM01, was previously reported by Snæbjörnsdóttir et al. (2017) and is provided in Table 3.

Similarly, the composition of the injection fluid prior to its injection was evaluated via a sample, 12KGM06, collected from well HN-01 on the 3rd of February 2012. This chemical composition was previously reported by Snæbjörnsdóttir et al. (2017) and is shown in Table 3. The injected fluid was pumped from well HN-01, as shown in Fig. 1. The CO_2 gas was then dissolved into this water during its injection into the subsurface as described by Sigfusson et al. (2014). The CO_2-rich fluid was then released into the basaltic storage formation at a depth of ~520 m and a temperature of about 35°C (Fig. 1). The dissolved inorganic carbon (DIC) concentration of the fluid as it enters the storage formation was 0.82 mol/L on average. After its injection into the subsurface, the fluid is affected by both fluid-mineral interaction with the subsurface rocks, and dilution via mixing with the pre-existing formation waters.

The fluids continuously produced out of the first monitoring well, HN-04, were regularly sampled during the injection and over the following months. The samples consist of a mixture of the two fluids; the injected fluid and the formation fluids. The mixing fraction of the injected fluid versus the formation fluids was calculated using the non-reactive SF_6 tracer concentration and mass balance calculations by Matter et al. (2016).

Two samples representative of those collected during the arrival of the major parts of the CO_2-rich water plume to the first monitoring well are sample 12KGM33, collected about 60 days after the onset of the injection, and sample 13SOS06, collected about 400 days after

the onset of the injection. These samples are representative of the chemical compositions of the subsurface fluids during the original and main plume breakthroughs (Fig.2). The chemical compositions of these samples are provided in 3, and were previously reported by Snæbjörnsdóttir et al. (2017).

Table 3. The measured and calculated chemical compositions of water samples collected from wells HN-01 and HN-04, used in the reaction path calculations.

Well	**HN-04**	**HN-01**	**HN-04**	**HN-04**
Sample representation (in model)	Background waters	Injected fluid after CO_2 dissolution	First breakthrough	Second breakthrough
Date	25.1.2012	3.2.2012	26.3.2012	3.4.2013
Sample ID	12KGM01	12KGM06	12KGM33	13SOS06
pH	9.2	3.7*	6.7	8.2
T (°C)	35	35	35	35
Alk. (meq/kg)	1.87	2.0	2.93	2.87
DIC (mmol/kg)	1.55	820*	4.00	2.83
Si (mmol/kg)	0.39	0.59	0.392	0.41
Ca (mmol/kg)	0.052	0.13	0.41	0.24
3Mg (mmol/kg)	0.005	0.16	0.100	0.200
Na (mmol/kg)	2.18	2.04	2.37	2.73
K (mmol/kg)	0.018	0.024	0.021	0.024
Fe (µmol/kg)	0.061	0.021	20.0	0.184
Al (µmol/kg)	2.08	1.19	1.01	1.90

** Calculated value based on dissolution of 0.82 moles CO_2 per L of the injected solution*

2.2.2 The solid dissolving phases

The subsurface storage formation at the CarbFix site consists mainly of a combination of glassy and crystalline basalts along with some secondary phases as previously described in section 2.1. The interaction between the basaltic rock and the CO_2-charged acidic injection fluid can be viewed as a titration process, where the basaltic rocks act like a base which titrates into the carbonic acid, by consuming protons and releasing cations upon dissolution (Table 2). This raises the pH to a range favouring carbonate precipitation and many of the released cations combine with the injected CO_2 to form stable carbonate minerals.

The composition of the glassy basalts is close to that of the Stapafell Mountain located in SW–Iceland, near the CarbFix injection site. Its chemical composition, normalised to one Si atom, is consistent with $SiTi_{0.024}Al_{0.358}Fe_{0.188}Ca_{0.264}Na_{0.079}K_{0.008}O_{3.370}$ (e.g. Gysi and Stefánsson, 2011; Oelkers and Gislason, 2001), and its molar weight based on its Si normalized composition is 123 g/mol. The reactivity of the Stapafell basaltic glass has been extensively studied (Galeczka et al., 2014; Gislason and Oelkers, 2003; Oelkers and Gislason, 2001; Stockmann et al., 2011; Wolff-Boenisch et al., 2004) The dissolution rate of basaltic glass is considered to include two basic steps: Non-stoichiometric dissolution due to a formation of a leached layer where alkali and alkaline-earth metals are preferentially removed, followed by a second step of steady-state, stoiciometric dissolution of the leached layer enriched in Al and Si (Oelkers and Gislason, 2001). The dissolution of this Al- and Si-rich surface layer is the rate limiting step of the dissolution (e.g. Gislason and Oelkers, 2003; Guy and Schott, 1989). The chemical composition of Stapafell basaltic glass and its reactivity is used in the model calculations as described below.

The crystalline basalts consist of olivine, pyroxene, plagioclase, and to a lesser extent iron oxides and glass. More than 90% of the crystalline fraction of the CarbFix subsurface storage consists of plagioclas (plag), pyroxene (pyr) and olivine (ol). Glass and iron oxides were therefore excluded in the modelling. The relative volume proportion of these three major phases, plag: pyr: ol is 44: 39: 17, based on analysis from Gudbrandsson et al. (2011)

on crystalline Stapafell rocks. This corresponds to 30 mol% plag, 42 mol% pyr, 28 mol% ol (Table 2). The relative reactivities of these minerals in Icelandic basalts have been reported by Gudbrandsson et al. (2011). These relative reactivities were used together with the thermodynamic properties of these phases reported by Gysi and Stefánsson (2011) – see Table 2.

In addition to dissolution of the primary rocks in the storage formation, some dissolution of pre-existing secondary phases likely occurred. This applies particularly to calcite, due to its rapid dissolution kinetics. Matter et al. (2016) measured the $^{14}C/^{12}C$ ratio of samples collected from the first monitoring well, suggesting a 50% dilution of the injected ^{14}C in the fluid during the first breakthrough, most likely via calcite dissolution shortly after the injection into the basaltic storage formation. The effect of the carbonate dissolution is demonstrated in following section 4.3.

2.2.2.1 The fast-flow path of the first breakthrough

This first breakthrough path is characterized by a relatively fast fracture flow between the injection well HN-02 and the first monitoring well HN-04, channelling a small fraction (~3%) of the injected fluid (Khalilabad et al., 2008). The pH range is from 3.7 in the injected fluids up to 6.7 in the sampled monitoring fluids. The primary phases, clinopyroxene, olivine ($Fo_{43}Fa_{57}$), and plagioclase (An_{70}) were selected to represent the primary rock of the first breakthrough for two reasons:

1) Preliminary modelling calculations of the first breakthrough using basaltic glass as the dissolving phase result in fluids that correlate poorly with the sampled fluids of the first breakthrough, with too high concentration of both Na and DIC. This could, in contrast, be explained by the different release rates of divalent cations between crystalline basalts and corresponding basaltic glass. At acid to neutral conditions, Mg and Fe are preferentially released from crystalline basalts due to the higher dissolution rates of olivine, and to lesser extent pyroxene, compared to plagioclase

and glass dissolution. This favours the formation of siderite, magnesite, and Fe-Mg carbonates rather than calcite (Gudbrandsson et al., 2011).

2) This is further supported by the aquifer characterisation that was carried out at the site (Khalilabad et al., 2008), indicating the first breakthrough to be associated with a fast fracture flow between the two wells at shallow depth. The depth of the aquifer in the injection well HN-02 is at about ~550 m, but the depth of the aquifer channelling the first breakthrough to well HN-04 is at about ~420 m. This indicates fracturing through the interiors of the lava-pile, likely transecting the crystalline surfaces of the bedrock.

Taking these observations into account, the primary crystalline rock was dissolved into the CO_2-charged injection fluid, along with calcite, and later mixed with the background waters, as described in Fig. 3 in the model calculations.

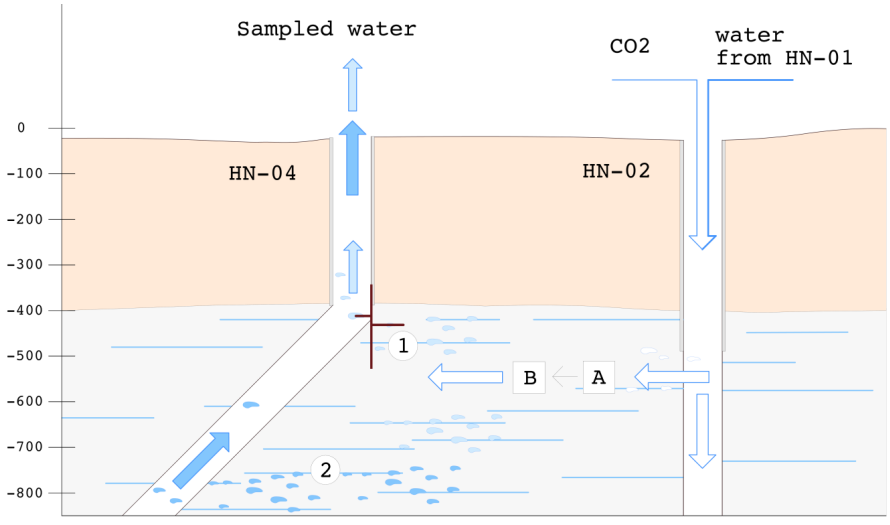

Fig. 3. Schematic figure illustrating the modelling of the two breakthroughs. The modelling is done in two steps. A) The solid phases (crystalline basalt and calcite for the first breakthrough, basaltic glass for the second breakthrough) are dissolved into the injected fluid. B) The resulting fluid is mixed into the background waters in the ratio determined by the SF_6 non-reactive tracer concentration of the sampled fluid. This is applied for both of the two breakthroughs, the first breakthrough characterized by a fast fracture flow (1) and the second and main breakthrough characterized by porous flow (2).

2.2.2.2 The second breakthrough flow-path of the bulk of the injected fluid

This second breakthrough path is characterised by a flow-path hosted within a large volume of homogenous media with excessive, inter-connected porosity, channelling the bulk of the injected fluid (Khalilabad et al., 2008). Such a slow flow is likely dominated by basaltic glass dissolution; basaltic glass tends to glaze the tops and bases of individual lava flows of the olivine-tholeiit lava pile in the storage formation (e.g. Alfredsson et al., 2013) and hosts the main flow paths of fresh to moderately altered lava pile (e.g. Franzson, 2000; Neuhoff et al., 2008). The pH ranges between 3.7 in the injected fluid to 8.2 in the sampled fluids.

Within the model calculations the basaltic glass was dissolved into the CO_2-charged injection fluid and later mixed with the background waters, as described in Fig. 3. Preliminary modelling calculations of the second breakthrough show a relatively good fit with the sampled fluids when using basaltic glass.

2.2.3 The precipitating phases

The secondary phases allowed to precipitate in the reaction path modelling are consistent with those found during the low temperature (<100°C), alteration of Icelandic basaltic rocks as well as those carbonate minerals that potentially form at low temperatures and elevated CO_2-pressures from the release of Ca, Mg, and Fe (Table 2). The choice of these mineral assemblages is further justified by field observations of both natural processes (e.g. Alfredsson et al., 2013; Kristmannsdóttir and Tómasson, 1978; Neuhoff et al., 1999; Rogers et al., 2006), laboratory experimental low temperature CO_2-water-basalt interaction (Gysi and Stefánsson, 2012), and from previous CO_2 field injection experiments (Matter et al., 2016; Snæbjörnsdóttir et al., 2017).

The saturation states of Al-hydroxides, zeolites, and clays depend strongly on the database used, both in terms of mineral composition and thermodynamical data. The zeolites taken into account in this study are those observed in drill cuttings from the injection well (Alfredsson et al., 2013) and stable at temperatures below 75°C (Helgadóttir, 2011;

Kristmannsdóttir and Tómasson, 1978). The clay minerals considered are smectites, with chemical composition similar to reported composition of samples from the area (Schiffman and Fridleifsson, 1991; Snæbjörnsdóttir, 2011).

The chemical composition of the secondary phases that were allowed to precipitate if saturated in the aqueous phases is provided in Table 2. Due to the low pH, and the short residence time for CO_2-water-rock interaction to take place, clay minerals and zeolites were excluded in the modelling of the first fast flow breakthrough path due and their sluggish precipitaiton rates at low temperatures (e.g. Kloprogge et al., 1999; Neuhoff et al., 2000).

3 Results

3.1 The injected fluid

The initial pH of the injected fluid, prior to injection and CO_2 dissolution, was measured to be ~9.5. The CO_2 was then dissolved into the fluid, to a concentration of 0.82 moles per kg of water. Fluid speciation calculations indicate that the pH of the resulting fluid was 3.7 at 35°C. The chemical composition of this CO_2-rich injection fluid, as represented by sample 12KGM06, is shown in Table 3. The only saturated phase in this CO_2-charged fluid at this point was chalcedony. All carbonates were highly undersaturated.

The pH of the monitoring well HN-04 was measured to be 9.2 at the onset of the injection, as represented by sampled 12KGM01 (Table 3). The saturated phases in the fluid were smectites, zeolites, calcite, and aragonite.

The pH of the sampled fluids of the first and second breakthrough was measured to be 6.7 and 8.2 respectively, as represented by samples 12KGM33, and 13SOS06 respectively (Table 3). This indicates significant water-CO_2-rock interaction of the injected fluid with the subsurface bedrock of the storage formation, and mixing with the alkaline background waters along the flow-paths between the injection well and the first monitoring well.

The fraction of the acidic injected fluid versus the alkaline background waters in the samples was calculated using the SF_6 non-reactive tracer, as described by Matter et al. (2016). Non-reactive, conservative fluid mixing calculations were carried out to evaluate the effect of the mixing of these two fluids. The results are shown in Fig. 4. The pH rise resulting from mixing of the two fluids accounts for a pH rise from 3.7 to 4.6 during the first breakthrough with a 90% mixing fraction of the alkaline background waters (Fig. 2-3), and from 3.7 to 4.1 during the second breakthrough of the injected solution breakthrough with a 60% mixing fraction of the alkaline background waters. Chalcedony is the only saturated phase in both fluid mixtures, as in the injection fluid. All carbonates are highly undersaturated.

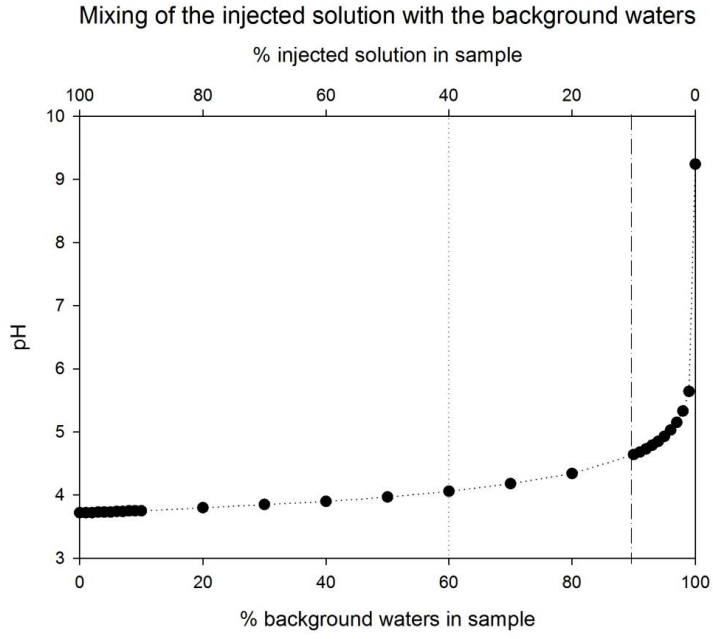

Fig. 4. The effect of mixing the injected solution with the background waters on the pH of the sampled fluids. The mixing fraction of the sample representing the first breakthrough (pH 4.6, 90% background water) is shown with a dashed-dotted line, and the mixing fraction of the sample representing the second breakthrough (pH 4.1, 60% background water) is presented as a dotted line.

3.2 The first breakthrough

The fast breakthrough resulting from the arrival of ~3% of the injected CO_2-charged water occurred in well HN-04 about 60 days after the onset of the injection, as indicated by the SF_6 non-reactive tracer (Matter et al. 2016, Fig. 2) resulting in a pH drop in this monitoring well. The pH of the fluids of this first breakthrough was about 6.7 and the DIC concentration was 4.0 mmol/L (Table 3). The ratio of the injected CO_2-charged water versus the background water was 1:9 based on conservative tracer concentration and mass balance calculations. Pure mechanical mixing of the injected CO_2-charged water with the background waters, in this 1:9 ratio in the sample, would result in pH 4.6 and DIC concentration of 88 mmol/L (Fig.6), indicating the significance of mineral fluid reaction.

The best match between the modelled results and field observations was obtained when 0.42 moles/L of the crystalline rock (~64 g) were assumed to have dissolved into the each litre of the injected CO_2-charged water; in total 0.36 moles/kg olivine, 0.05 moles/kg clinopyroxene, and 0.01 moles/kg plagioclase, were calculated to have dissolved using relative dissolution rates from Gudbrandsson et al. (2011). The primary rock was dissolved into the CO_2-charged injection fluid along with 0.82 moles/kg of calcite. The calcite dissolution is supported by the $^{14}C/^{12}C$ ratio that suggests ~50% dilution of the carbon in the fluid due to dissolution of pre-existing calcite (see section 2.2.2 and Matter et al. (2016)). The resulting fluids were then mixed with the background waters, based on the mixing fraction calculated by the SF_6 tracer (Fig. 3).

The results of the reaction path simulations are shown in Fig.5, including the pH change, pCO_2, and secondary phase mineralogy, with increased dissolution of the basalts. A comparison between the fluids sampled from the HN-04 monitoring well (Table 3) after the first breakthrough, and the resulting fluid of mixing calculations and the reaction path modelling is shown in Fig.6.

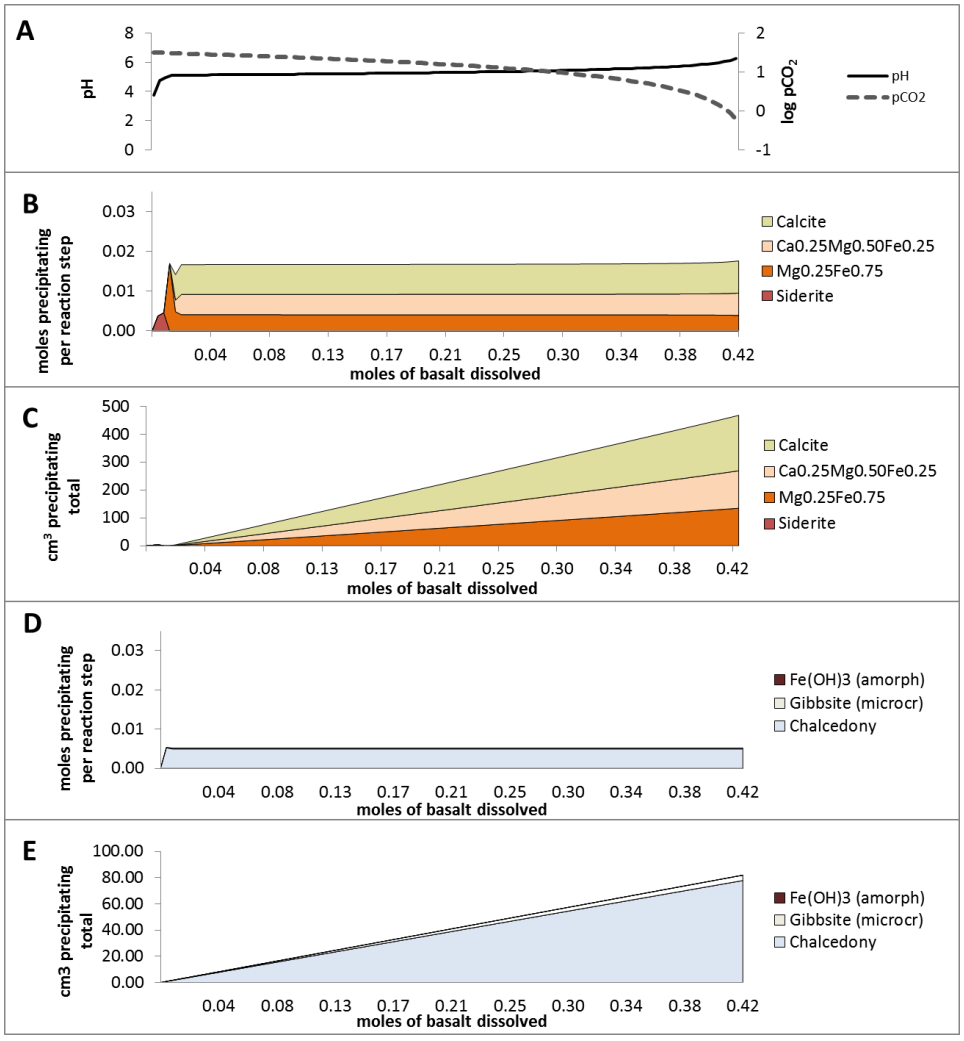

Fig.5. Results for reaction path calculations at 35°C simulating the first breakthrough of the injected solution from the CO_2 injection at Hellisheidi in 2012. Progressive dissolution of crystalline basalt is represented by 28 mol% olivine ($Fo_{43}Fa_{57}$), 42 mol% clinopyroxene, and 28 mol% plagioclase ($an_{70}ab_{30}$) into one L of the solution, using relative dissolution rates from Gudbrandsson et al. (2011) and 0.82 moles of calcite. a) The evolution of pH and pCO_2 during the reaction progress. b) Carbonates along the reaction path forming in one L of the solution in the following sequence; siderite, $Mg_{0.25}Fe_{0.75}$-solid solution, $Ca_{0.25}Mg_{0.50}Fe_{0.25}$-solid solution, and calcite, c) the volume of carbonates precipitating, c) other secondary minerals forming, and d) the volume of those secondary phases precipitating.

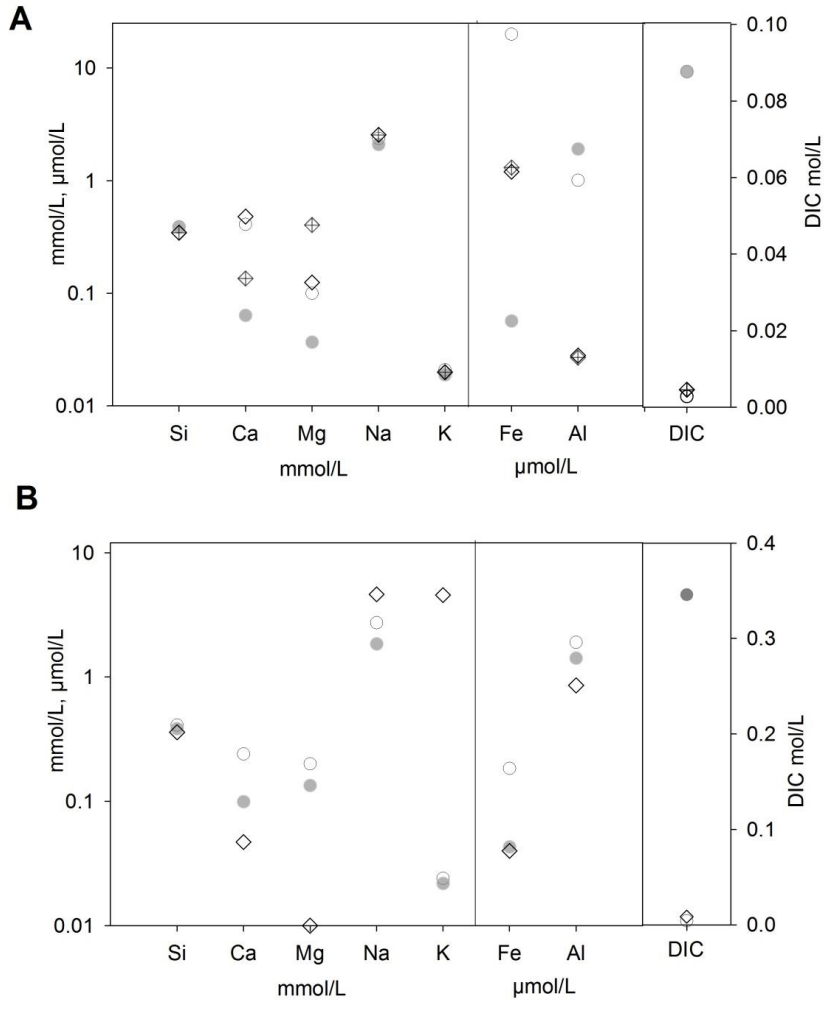

Fig.6. Chemical composition of the sampled fluids, modelled fluids, and fluids after non-reactive mixing of the injected solution with the background waters. A) The first breakthrough. Sample 12KGM33 is represented by empty circles, mechanical mixing (0.1:0.9) is represented by grey dots, modelled fluid composition using crystalline basalts and calcite is represented by crossed diamonds, and modelled fluid using crystalline basalts and excluding calcite dissolution is represented by empty diamonds. B) The second breakthrough. Sample 13SOS06 is represented by empty circles, mechanical mixing (0.4:0.6) is represented by grey dots, and modelled fluid composition using basaltic glass is represented by empty diamonds.

Chalcedony is calculated to be the first alteration phase to form, along with minor amounts of Fe and Al-hydroxides (microcrystalline gibbsite) (Fig 5.d-e). The first carbonate-phase calculated to form is siderite ($FeCO_3$) at pH ~5 (Fig.5a-c). Gradually, the carbonates become more Mg-, and Ca-rich, with the formation of $Mg_{.25}Fe_{0.75}$-solid solution, and finally $Ca_{0.25}Mg_{0.50}Fe_{0.25}$-solid solution, and calcite (Fig.5b-c).

3.3 The second breakthrough

The peak concentration of the SF_6-non reactive tracer in samples from the monitoring well HN-04, indicating the arrival of the bulk of the injected solution, occurred about 400 days after the onset of the injection (Matter et al., Fig.2). A slight drop in pH along with a slight increase in DIC was noted in the fluid samples from the monitoring well HN-04. The pH of this second breakthrough was measured to be about 8.2 and the DIC concentration about 3 mmol/L. The ratio of the injected CO_2-charged water versus the background water was 2:3 based on conservative tracer concentration and mass balance calculations. Pure mechanical mixing of the two fluids would result in pH of 4.1 and DIC concentration of about 350 mmol/L (Fig. 6). This indicates that the bulk of the injected carbon was mineralised along the flow-path towards the monitoring well within the 400 days after the onset of the injection, as previously stated by Matter et al. (2016) and Snæbjörnsdóttir et al. (2017). This is also supported by ^{14}C-data as described by Matter et al. (2016), and net-input of Ca, Mg, and Fe via dissolution of the host rock as described by Snæbjörnsdóttir et al. (2017).

The results of the reaction path simulations are shown in Fig.6b, in terms of fluid composition, and Fig.7 in terms of pH, and pCO_2, and secondary phase mineralogy, as a function of mass of basaltic rock dissolved. The best match between the modelling results and the measured monitoring well compositions, for the pH of the sampled fluid, requires 0.86 moles of basaltic glass (~106 g) to dissolve into each litre of the injected CO_2-charged water. The basaltic glass was dissolved into the injection fluid, and then mixed with the

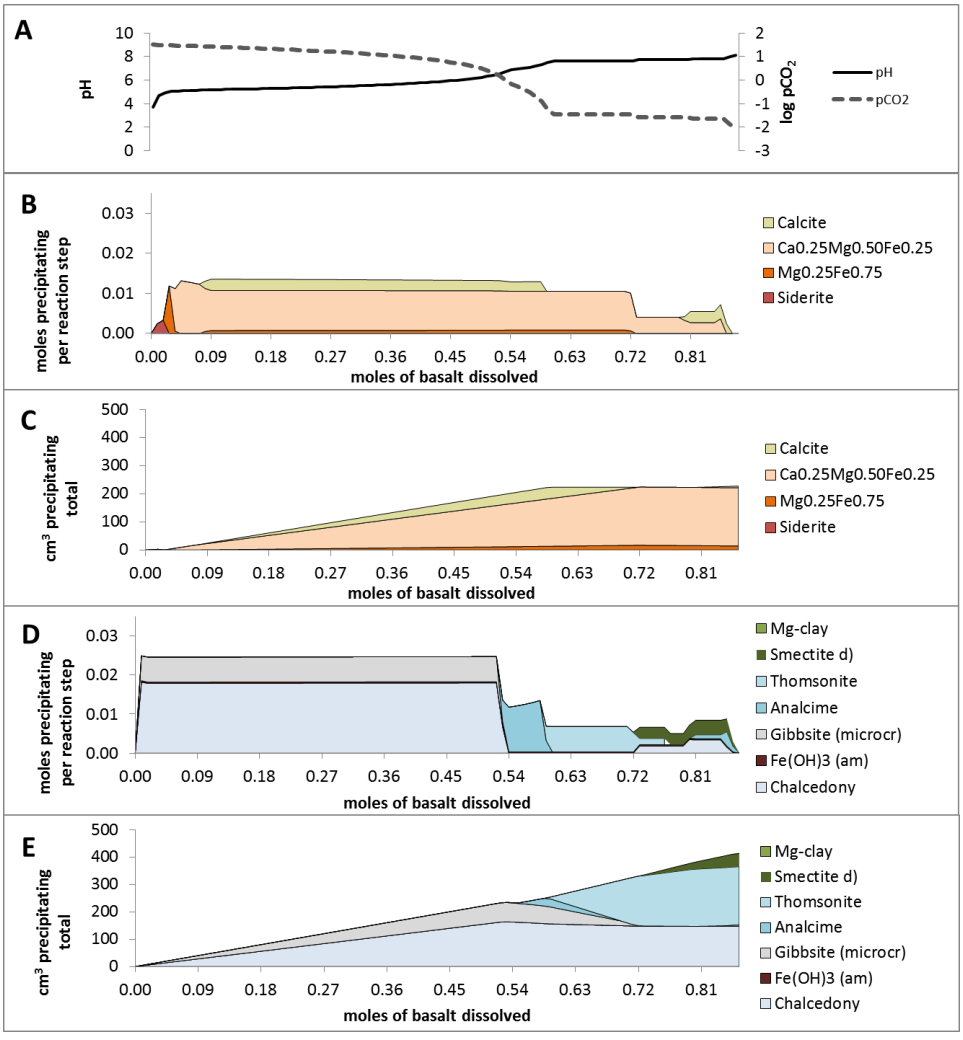

Fig. 7. Results for reaction path calculations at 35°C simulating the second breakthrough of the injected solution at Hellisheidi in 2012. Progressive dissolution of 0.86 moles basaltic glass into one L of the solution is represented, using dissolution rates from Gislason and Oelkers (2003); Oelkers and Gislason (2001). a) the evolution of pH and pCO_2 during the reaction progress. b) Carbonates forming in one L of the solution in the following sequence; siderite, $Mg_{0.25}Fe_{0.75}$-solid solution, $Ca_{0.25}Mg_{0.50}Fe_{0.25}$-solid solution, and calcite, c) the volume of carbonates precipitating, c) other secondary minerals forming, and d) the volume of those secondary phases precipitating.

background waters, based on the mixing fraction calculated by the SF_6 tracer. The resulting fluids of the modelling are in close agreement with the sampled fluid during the second breakthrough of the injected fluid in the monitoring well HN-04, as shown in Fig. 6b.

The model calculations suggest that the first minerals to precipitate from the injected CO_2-charged fluid, at high pCO_2 and pH < 6.5, are aluminium hydroxides (microcrystalline gibbsite) and chalcedony, with some minor amount of iron-hydroxides (Fig.7d-e). There is a sequence of carbonates forming at around pH 5. The first carbonate-phase predicted to form is siderite at pH <5. As the fluid evolves, at above pH 5, the carbonates become more Mg-rich, and eventually Ca-rich, with the formation of $Mg_{0.25}Fe_{0.75}$-solid solution, $Ca_{0.25}Mg_{0.50}Fe_{0.25}$-solid solution, and lastly calcite (Fig.7b-c). Calcite is the dominant carbonate forming when the pH reaches ~8.

At at pH ~6.5 the zeolite analcime is calculated to start forming, and thomsonite at pH ~7.5. Finally, smectite[d)] (Table 2) is calculated to become supersaturated at pH ~7.7, and Mg-clays at pH ~8.1 (Fig.7c-d).

4 Discussion

4.1 Mineral sequences – comparison to experiments and natural analogues of basalt-CO_2 interactions

The results of the reaction path modelling described above indicate the formation of mineral sequences in agreement with observations of secondary mineralogy formed by the alteration of basaltic rocks in natural systems with high pCO_2 and temperatures below 100°C (Rogers et al., 2006), and during CO_2-water-basalt experimental work (Gysi and Stefánsson, 2012). The results of the reaction path modelling are also in good agreement with the modelling of saturation states of the sampled fluids during and after the injection (Snæbjörnsdóttir et al., 2017).

Speciation calculations indicate that all carbonates are undersaturated in the acidic injection fluid, and in the acidic mixtures representing the first (pH 4.6) and second (pH

4.1) breakthrough solutions, prior to water-CO_2-rock interaction. As the pH reaches ~5, iron rich carbonates, such as siderite and $Mg_{0.25}Fe_{0.75}$-solid solutions are calculated to form. The formation of such iron-rich carbonates is highly dependent on the oxidation state, and the availability of Fe^{2+} dissolved from the primary rock. The formation of Fe-rich carbonates is also favored by higher dissolution rates of Fe-containing olivines and pyroxene (augite) in crystalline basalts. Siderite and $Mg_{0.25}Fe_{0.75}$-carbonate are the only carbonates calculated to be supersaturated in the sampled fluids during the first breakthrough (Snæbjörnsdóttir et al., 2017). These carbonates are the first carbonates to form in the reaction path modelling for both breakthroughs.

Siderite has not been identified in the area, but was identified as a result of basalt-CO_2-water interaction in Greenland, along with the $Mg_{0.25}Fe_{0.75}$-solid solution (Rogers et al., 2006), and in drill-cuttings from the Svartsengi geothermal field in SW-Iceland (Richter et al., 1999), which has a significantly higher salinity and higher temperature gradient than the CarbFix site.

With progressive basaltic rock-dissolution during the reaction path modelling, and subsequent rise of pH along with decrease in dissolved CO_2 concentration, more Ca-rich carbonates, such as calcite, and Ca-Mg-Fe-solid solutions, become supersaturated. At that point carbonates become more abundant, forming along with chalcedony, and later both zeolites, and smectites (Fig.7b-e). Speciation calculations of the sampled fluids during the second breakthrough show that these fluids are saturated with respect to siderite, Ca-Mg-Fe-solid solutions, and calcite, along with both smectites and zeolites (Snæbjörnsdóttir et al., 2017).

As previously mentioned, calcite and aragonite are the only carbonate phases identified prior to the injections (Alfredsson et al., 2013). Furthermore, calcite was the only carbonate phase identified on the precipitates forming on the submersible pump in the monitoring well HN-04 in the months after the second breakthrough, along with some trace amounts of clays (Snæbjörnsdóttir et al., 2017). This is in agreement with the reaction path calculations at pH >8, where the only carbonate phase precipitating is calcite, along with smectites and zeolites (Fig.7b-c).

However, this does not exclude the formation of other carbonate minerals during, and after the injections. As demonstrated here, the reaction path calculations, and the saturation states of the sampled fluids during the first breakthrough, point towards precipitation of some Fe-rich phases. These phases could either have formed closer to the injection well, and/or were dissolved when pH increased, and re-precipitated as more stable carbonates such as Ca. Note also that the specation calculations are both sensitive towards the oxidation state of the fluids, and the limitations of the excisting databases, as previously declared.

4.2 The efficiency of carbon mineralisation in basaltic rocks

Two key factors are essential for successful mineral storage of CO_2 in basaltic rocks:

1) Permeability and/or active porosity, providing flow paths for efficient injection of the CO_2-rich fluid, and mineral surfaces essential for geochemical reactions to take place
2) Conditions favourable for efficient formation of carbonates

The CO_2-water-rock interaction between the injected fluid and the basaltic rocks results in formation of secondary phases with significant volume and porosity change (Fig.5c and e, Fig.7c and e). The efficiency of the carbon mineralisation in the system can be evaluated by the mineral sequences forming as described in section 4.1, and in Fig.5 and Fig 7.

In the near vicinity of the injection well, where the pH is low and the pCO_2 is high, the only phase calculated to be supersaturated is chalcedony. At these low pH and high pCO_2-conditions, dissolution of the pre-existing phases occurs, rather than the precipitation of new phases. This leads to increased permeability near the injection well, providing flow paths for the injected solution.

Further on, as the pH increases, formation of some secondary minerals starts to take place. The efficiency of the carbonation depends on the availability of the cations, mostly Ca, Mg,

and Fe, provided by the dissolution of the primary rock, and the potential formation of other minerals such as zeolites and smectites competing over cations and pore-space, as demonstrate in section 4.1., and Fig. 7. As previously described, the first secondary phase to form is chalcedony, Al- and Fe-hydroxides, along with carbonates (Fig.5 and 7). At this stage no other secondary minerals compete for the available Ca-, Fe-, and Mg-cations liberated by the basalt dissolution, nor for the available pore space. These conditions, which are present at a pH range from ~5.2-6.5 in the calculations for the second breakthrough, provide conditions for the most efficient mineralisation of the injected carbon.

At lower CO_2 partial pressures, and higher pH, the formation of carbonate minerals is limited somewhat by the formation of zeolites and smectites, and other clay minerals. This can affect the efficiency of the carbon mineralisation dramatically, since these minerals consume both cations and pore space. Additionally, both zeolites and smectites are among the most hydrated minerals and can contain large amounts of water making them extra voluminous. This large volume is demonstrated in Fig. 7e.

This indicates that the most effective mineralisation of the injected CO_2 takes place when the pH is high enough for substantial formation of carbonates but not high enough for considerable formation of zeolites and clay minerals along with the carbonates formation., at pH ~5.2-6.5.

Provided that the storage formation consists of relatively fresh, porous, and permeable basalts that respond to the injection by gradually increasing the pH to conditions suitable for carbonate formation, the efficiency of the system is provided by injecting at a rate fast enough to keep the pH low in the vicinity of the injection well. That would prevent clogging by ensuring only minimum secondary precipitation, and keep the pCO_2 high enough so that the formation of zeolites and clays only occurs in some distance from the injection well. This also emphasises the importance of continuous injection, to avoid pH fluctuations favouring the precipitation of these voluminous minerals in the vicinity of the injection

well, clogging up pore space and diminishing the permeability – and thereby the efficiency of the injection (Fig.7c and e).

However, as clearly seen e.g. in the high-temperature geothermal fields, there are other ways for preserving or retrieving permeability. Basaltic formations are mostly located in tectonically active areas, where faults and fractures are common and have large effect on the permeability (e.g. Fisher, 1998; Flóvenz and Saemundsson, 1993), as demonstrated by the fracture flow of the first breakthrough of the injected solution. The injection of the CO_2-rich fluid can also cause hydrological fracturing due to overpressure of the rock, and thermal cracking in areas with high geothermal gradient where the temperature change due to the injection of colder fluid causes thermal cracking of the host rock (e.g. Axelsson et al., 2006). Lastly, the volume change due to the precipitation of voluminous secondary minerals can also cause micro-fracturing of the host-rock. The permeability of basaltic rocks is naturally diminished with increased age, due to progressive alteration, and gradual burial of the strata (e.g. Sigurdsson and Stefánsson, 1994)

The reaction path calculations demonstrate the amount of basaltic rocks required for mineralisation of the injected CO_2. For the second and main breakthrough, 106 g of basaltic glass are required for each litre of the injected fluid, to mineralise about 95% of the injected carbon. This equals to about 600 tonnes of basaltic glass dissolved, in response to the 175 tonnes of CO_2 that were injected at the CarbFix-site in January 2012. This would result in the formation of about 400 tonnes of carbonates, 460 tonnes of zeolites, and about 125 tonnes of smectites.

4.3 The effect of the presence of calcite in the original reservoir rock

The rapid dissolution rates of calcite in acidic fluids, if present, could play a significant role at the onset of the injection by raising the pH of the fluids via the reaction:

$$CaCO_3 + CO_2 + H_2O = Ca^{2+} + 2CO_3^{2-} + 2H^+ \leftrightarrow Ca^{2+} + 2HCO_3^-$$

The $^{14}C/^{12}C$ ratio of samples collected during the first breakthrough from the first monitoring well HN-04 suggests a 50% dilution of the carbon in the fluid, most likely via calcite dissolution at the onset of the injection (Matter et. al. 2016). This points towards significant calcite dissolution, where one carbon is released via calcite dissolution, for every injected carbon. However, this does not have a net effect on the carbon mineralisation, since one Ca is released for every C.

The effect of the added calcite was evaluated by removing calcite from the previous calculations for the first breakthrough. The results, in terms of carbonates supersaturated in the calculations, are shown in Fig.8d-e.

The addition of the calcite to the system affects the chemical composition of the carbonates forming during the first breakthrough. Instead of the more Ca-rich carbonates formed in the modelling, such as calcite and Ca-Mg-Fe-solid solution, more Fe-Mg rich carbonates are calculated to form when the calcite dissolution is excluded due to the decreased availability of Ca in the system (Fig.8b-e).

The calcite dissolution contributes slightly to the pH rise early on during the injection (Fig8.a). In these calculations the pH rise contributes somewhat – but not significantly to an earlier onset of the carbonate precipitation. However, this could be underestimated due to the limitations of the modelling, such as lack of kinetic data. This addition of carbon to the system does not affect the resulting fluids dramatically (Fig.6a). The resulting fluids are in good agreement with the sampled fluids during the first breakthrough of the injected solution (Table 3, Fig. 6a).

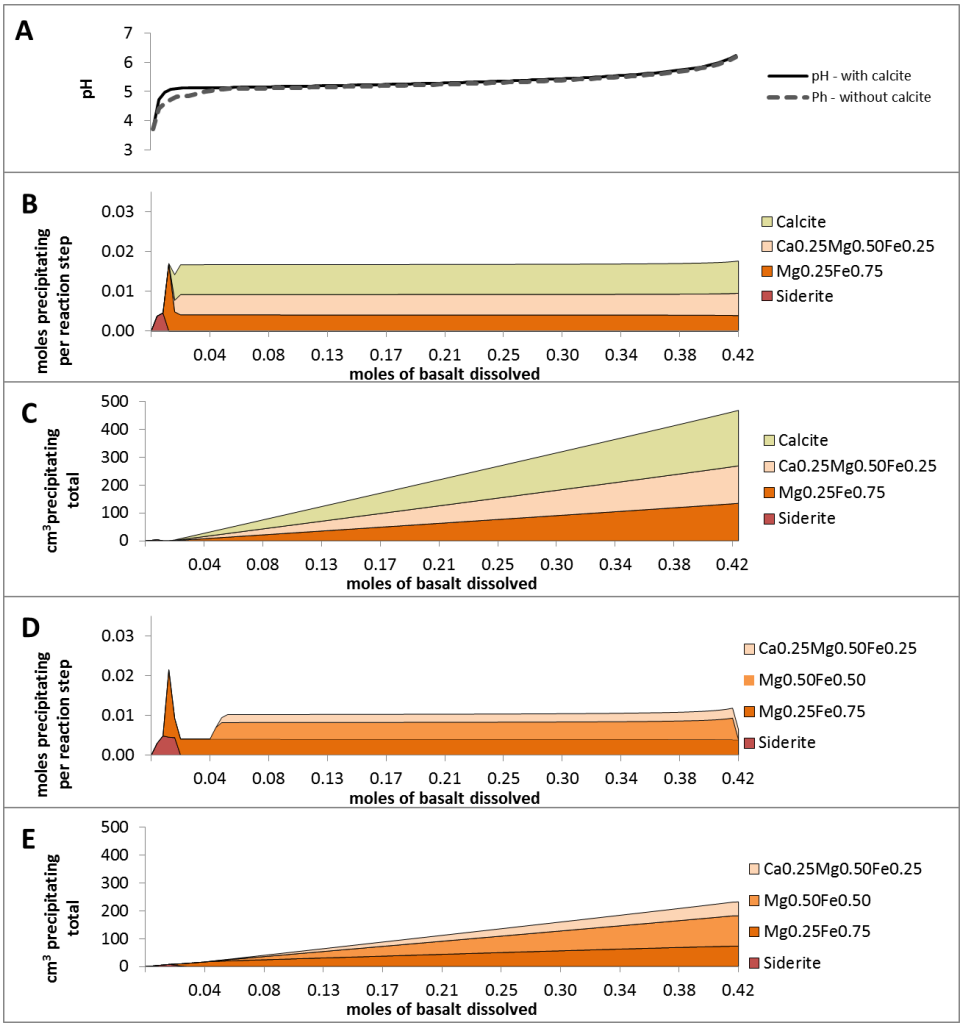

Fig.8. Results for reaction path calculations simulating the effect of calcite dissolution on A) carbonates forming during the first breakthrough of the injected solution - calculations excluding the calcite dissolution are displayed above the initial calculations including the calcite dissolution. B) The evolution of pH for the calculations with calcite (solid line), and when calcite is excluded in the calculations (broken line).

5 Conclusions

Several major conclusions result from this study.

1. The mineralisation of the bulk of the CO_2 injected during the CarbFix project appears to be mainly driven by basaltic glass dissolution, during the first ~400 days from the onset of the injection. However, considerable mineralisation appears to be driven by crystalline basalt dissolution during the first 60 days of the injection via fast fracture flow. The crystalline basalts of the interiors of the lava pile are transected by the fracture that hosts the flow path.
2. Even though the dissolution of the primary rocks is the main contributor to the pH rise of the fluids, the mixing of the injected fluids with the background waters also contributes considerably to the pH rise. The pH of the injected fluids increases from 3.7 to 4.6 during the first breakthrough and from 3.7 to 4.1 during the second breakthrough, due to mixing of the fluids with the more alkaline background waters.
3. The efficiency of the carbon injection is limited by the permeability and/or porosity in the area, and the availability of cations, both of which are limited by the formation of zeolites and smectites at higher pH and lower pCO_2, as indicated by the model. It is therefore essential to keep the pCO_2 high enough to prevent the formation of zeolites and clays in the vicinity of the injection well, but still pH high enough to be favourable for formation of carbonate. The most efficient carbonate formation takes place at pH ~5.2-6.5 in the modelling calculations.
4. The mineralization of ~95% of the 175 tonnes of CO_2 that were injected at the CarbFix-site in January 2012 would, according to the modelling calculations, require dissolution of about 600 tonnes of basaltic glass. This would result in the formation of about 400 tonnes of carbonates, 460 tonnes of zeolites, and about 125 tonnes of smectites.
5. Calcite dissolution taking place at the onset of the injection does not affect the net effect of the injection (one Ca for one C), but does contribute to more rapid pH rise early on during the injection. It influences which carbonates form – but has only a minor effect on when the formation of carbonates starts taking place. This might be due to limitations of the modelling.

References

Alfredsson, H.A., Oelkers, E.H., Hardarsson, B.S., Franzson, H., Gunnlaugsson, E. and Gislason, S.R. (2013) The geology and water chemistry of the Hellisheidi, SW-Iceland carbon storage site. International Journal of Greenhouse Gas Control 12, 399-418.

Appelo, C.A.J., Parkhurst, D.L. and Post, V.E.A. (2014) Equations for calculating hydrogeochemical reactions of minerals and gases such as CO2 at high pressures and temperatures. Geochimica et Cosmochimica Acta 125, 49-67.

Aradóttir, E.S.P., Sonnenthal, E.L., Björnsson, G. and Jónsson, H. (2012) Multidimensional reactive transport modeling of CO_2 mineral sequestration in basalts at the Hellisheidi geothermal field, Iceland. International Journal of Greenhouse Gas Control 9, 24-40.

Axelsson, G., Þórhallson, S., Björnsson, G. and 1 (2006) Stimulation of geothermal wells in basaltic rock in Iceland, ENGINE – ENhanced Geothermal Innovative Network for Europe, Workshop 3, "Stimulation of reservoir and microseismicity", Zürich, Switzerland.

Broecker, W. (2007) Climate change: CO_2 arithmetic. Science 315, 1371.

Erbach, G. (2016) The Paris Agreement - A new framework for global climate action. European Parliamentary Research Service. European Parliament.

Fisher, A.T. (1998) Permeability within basaltic oceanic crust. Reviews of Geophysics 36, 143-182.

Flóvenz, Ó.G. and Saemundsson, K. (1993) Heat flow and geothermal processes in Iceland. Tectonophysics 225, 123-138.

Franzson, H. (2000) Hydrothermal evolution of the Nesjavellir high-temperature system, Iceland, World Geothermal Congress, Kyushu - Tohoku, Japan.

Franzson, H., Zierenberg, R. and Schiffman, P. (2008) Chemical transport in geothermal systems in Iceland: Evidence from hydrothermal alteration. Journal of Volcanology and Geothermal Research 173, 217-229.

Galeczka, I., Wolff-Boenisch, D., Oelkers, E.H. and Gislason, S.R. (2014) An experimental study of basaltic glass–H_2O–CO_2 interaction at 22 and 50°C: Implications for subsurface storage of CO_2. Geochimica et Cosmochimica Acta 126, 123-145.

Gislason, S.R., Broecker, W.S., Gunnlaugsson, E., Snæbjörnsdóttir, S.Ó., Mesfin, K.G., Alfredsson, H.A., Aradottir, E.S., Sigfusson, B., Gunnarsson, I., Stute, M., Matter, J.M., Arnarson, M.T., Galeczka, I.M., Guðbrandsson, S., Stockman, G., Wolff-Boenisch, D.,

Stefansson, A., Ragnheidardottir, E., Faathen, T., Gysi, A.P., Olssen, J., Didriksen, K., Stippe, S., Menez, B. and Oelkers, E.H. (2014) Rapid solubility and mineral storage of CO_2 in basalt. . Energy Procedia 63, 4561-4574.

Gislason, S.R. and Oelkers, E.H. (2003) Mechanism, rates, and consequences of basaltic glass dissolution: II. An experimental study of the dissolution rates of basaltic glass as a function of pH and temperature. Geochimica et Cosmochimica Acta 67, 3817-3832.

Gislason, S.R. and Oelkers, E.H. (2014) Carbon Storage in Basalt. Science 344, 373-374.

Goldberg, D. and Slagle, A.L. (2009) A global assessment of deep-sea basalt sites for carbon sequestration. Energy Procedia 1, 3675-3682.

Gudbrandsson, S., Wolff-Boenisch, D., Gislason, S.R. and Oelkers, E.H. (2011) An experimental study of crystalline basalt dissolution from $2 < pH < 11$ and temperatures from 5 to 75 °C. Geochimica et Cosmochimica Acta 75, 5496-5509.

Guy, C. and Schott, J. (1989) Multisite surface reaction versus transport control during the hydrolysis of a complex oxide. Chemical Geology 78, 181–204.

Gysi, A.P. and Stefánsson, A. (2011) CO_2–water–basalt interaction. Numerical simulation of low temperature CO_2 sequestration into basalts. Geochimica et Cosmochimica Acta 75, 4728-4751.

Gysi, A.P. and Stefánsson, A. (2012) CO_2-water–basalt interaction. Low temperature experiments and implications for CO_2 sequestration into basalts. Geochimica et Cosmochimica Acta 81, 129-152.

Helgadóttir, H.M. (2011) Stratigraphy and hydrothermal alteration of the Gráuhnúkar geothermal system in the southern part of the Hengill area, p. 123.

Hoffert, M., Caldeira, K., Benford, G., Criswell, D., Green, C., Herzog, H., Jain, A., Kheshgi, H., Lackner, K., Lewis, J., Lightfood, H., Manheimer, W., Mankins, J., Mauel, M., Perkins, L., Schlesinger, M., Volk, T. and Wigley, T. (2002) Advanced technology paths to global climate stability: energy for a greenhouse planet. Science 298.

IEA (2015) Energy Technology Perspectives 2015 - Mobilising Innovation To Accelerate Climate Action. International Energy Agency, Paris, France.

IEA (2016b) World Energy Outlook 2016 - Executive summary. International Energy Agency, Paris, France.

IPCC (2014) Climate Change 2014: Mitigation of Climate Change. Contribution of Working Group III to the Fifth Assessment, in: Edenhofer, O., R. , Pichs-Madruga, r., Sokona, Y.,

Farahani, E., Kadner, S., Seyboth, K., Adler, A., Baum, I., Brunner, S., Eickemeier, P., Kriemann, B., Savolainen, J., Schlömer, S., von Stechow, C., Zwickel T., Minx, J.C. (Eds.). International Panel on Climate Change

Khalilabad, M.R., Axelsson, G. and Gislason, S.R. (2008) Aquifer characterization with tracer test technique; permanent CO_2 sequestration into basalt, SW Iceland. Mineralogical Magazine 72, 121-125.

Kloprogge, T., Komarneni, S. and Amonette, J.E. (1999) Synthesis of smectite clay minerals: A critical review. Clays and Clay minerals 47, 529-554.

Kristmannsdóttir, H. and Tómasson, J. (1978) Zeolite zones in geothermal areas in Iceland. Pergamon Press, Elmsford, New York.

Lackner, K. (2003) A guide to CO_2 sequestration. Science 300, 1677–1678.

Matter, J.M., Stute, M., Snæbjörnsdóttir, S.Ó., Oelkers, E.H., Gislason, S.R., Aradottir, E.S., Sigfusson, B., Gunnarsson, I., Sigurdardottir, H., Gunnlaugsson, E., Axelsson, G., Alfredsson, H.A., Wolff-Boenisch, D., Mesfin, K., Fernandez de la Reguera Taya, D., Hall, J., Dideriksen, K. and Broecker, W.S. (2016) Rapid carbon mineralization for permanent and safe disposal of anthropogenic carbon dioxide emissions. Science 352, 1312-1314.

McGrail, B.P., Schaef, H.T., Ho, A.M., Chien, Y.-J., Dooley, J.J. and Davidson, C.L. (2006) Potential for carbon dioxide sequestration in flood basalts. Journal of Geophysical Research Solid Earth (111).

Neuhoff, P.S., Fridriksson, T. and Armannsson, H. (2008) Porosity evolution and mineral paragenesis during low-grade metamorphism of basaltic lavas at Teigarhorn, Eastern Iceland. American Journal of Science 299, 467-501.

Neuhoff, P.S., Fridriksson, T. and Bird, D.K. (2000) Zeolite Parageneses in the North Atlantic Igneous Province: Implications for Geotectonics and Groundwater Quality of Basaltic Crust

Philip S. Neuhoff , Thráinn Fridriksson & Dennis K. Bird. INternational Geology Review 42, 15-44.

Neuhoff, P.S., Th., F., Arnorsson, S. and Bird, D.K. (1999) Porosity evolution and mineral paragenesis during lowögrade metamorphism of basaltic lavas at Teigarhorn, Eastern Iceland. American Journal of Science 299, 467-501.

OECD/IEA (2016) Enhancing transparency of climate change mitigation under the Paris agreement: Lessons from experience, in: Briner, G., Moarif, S. (Eds.). OECD/IEA, Paris, France.

Oelkers, E. and Schott, J. (2005) Geochemical aspects of CO_2 sequestration. . Chemical Geology 217, 183–186.

Oelkers, E.H. and Gislason, S.R. (2001) The mechanism, rates and consequences of basaltic glass dissolution: I. An experimental study of the dissolution rates of basaltic glass as a function of aqueous Al, Si and oxalic acid concentration at 25°C and pH = 3 and 11. Geochimica et Cosmochimica Acta 65, 3671-3681.

Pacala, S. and Socolow, R. (2004) Stabilization wedges: solving the climate problem for the next 50 years with current technologies. Science 305.

Parkhurst, D.L. and Appelo, C.A.J. (2013) Description of input and examples for PHREEQC version 3—A computer program for speciation, batch-reaction, one-dimensional transport, and inverse geochemical calculations.

Richter, B., Guðlaugsson, S.Þ., Steingrímsson, B., Björnsson, G., Bjarnason, J.Ö. and Þórhallson, S. (1999) Svartsengi well SJ-18: Drilling, research and production (in Icelandic).

Rogers, K.L., Neuhoff, P.S., Pedersen, A.K. and Bird, D.K. (2006) CO_2 metasomatism in a basalt-hosted petroleum reservoir, Nuussuaq, West Greenland. Lithos 92, 55-82.

Schiffman, P. and Fridleifsson, G.O. (1991) The smectite-chlorite transition in drillhole NJ-15, Nesjavellir Geothermal Field, Iceland: XRD, BSE and electron microprobe investigations. . Journal of Metamorphic Geology 9, 679-696.

Sigfusson, B., Gislason, S.R., Matter, J.M., Stute, M., Gunnlaugsson, E., Gunnarsson, I., Aradottir, E.S., Sigurdardottir, H., Mesfin, K.G., Alfredsson, H.A., Wolff-Boenisch, D., Arnarson, M.T. and Oelkers, E.H. (2015) Solving the carbon-dioxide buoyancy challenge: The design and field testing of a dissolved CO_2 injection system. Int. J. Greenhouse Gas Control 37, 213-219.

Sigurdsson, Ó. and Stefánsson, V. (1994) Reservoir parameters—measurements from rock core (in Icelandic).

Snæbjörnsdóttir, S.Ó. (2011) The Geology and Hydrothermal Alteration at the Western Margin of the Hengill Volcanic System *(Master thesis, in Icelandic)*, Institute of Earth Sciences. University of Iceland, Reykjavik, p. 263.

Snæbjörnsdóttir, S.Ó., Oelkers, E.H., Mesfin, K., Aradóttir, E.S., Dideriksen, K., Gunnarsson, I., Gunnlaugsson, E., Matter, J.M., Stute, M. and Gislason, S.R. (2017) The chemistry and saturation states of subsurface fluids during the in situ mineralisation of CO_2 and H_2S at the CarbFix site in SW-Iceland. International Journal of Greenhouse Gas Control 58, 87-102.

Snæbjörnsdóttir, S.Ó., Wiese, F., Fridriksson, T., Ármannsson, H., Einarsson, G.M. and Gislason, S.R. (2014) CO_2 storage potential of basaltic rocks in Iceland and the oceanic ridges. Energy Procedia 63, 4585-4600.

Stockmann, G.J., Wolff-Boenisch, D., Gislason, S.R. and Oelkers, E.H. (2011) Do carbonate precipitates affect dissolution kinetics? 1: Basaltic glass. Chemical Geology 284, 306-316.

UN (2015a) United Nations/ Framework Convention on Climate Change. Adoption of the Paris Agreement, 21st Conference of the Parties, Paris.

UN (2015b) The Paris Agreement. Report of the Conference of the Parties on its twenty-first session, held in Paris from 30 November to 13 December 2015.

Wolff-Boenisch, D., Gislason, S.R., Oelkers, E.H. and Putnis, C.V. (2004) The dissolution rates of natural glasses as a function of their composition at pH 4 and 10.6, and temperatures from 25 to 74°C. Geochimica et Cosmochimica Acta 68, 4843-4858.

Yann, R.d.P., Jeffery, M.L., Gutschow, J., Rogelj, J., Christoff, P. and Meinshausen, M. (2017) Equitable mitigation to achieve the Paris Agreement goals. Nature Clim. Change 7, 38-43.

Table 2. The dissolution reactions for primary and secondary minerals included in the reaction path calculations (Appelo et al., 2014; Gysi and Stefánsson, 2011).

Mineral	Reaction	Solubility constants (Log K at 35°C)
Primary minerals/glasses		
Stapafell basaltic glass	$SiTi_{0.024}Al_{0.358}Fe_{0.188}Mg_{0.281}Ca_{0.264}Na_{0.079}K_{0.008}O_{3.370} + 2.644H^+ + 0.726H_2O$ $= 0.358Al^{+3} + 0.264Ca^{+2} + 0.171Fe^{+2} + 0.017Fe^{+3} + H_4SiO_4 + 0.008K^+ + 0.281Mg^{+2} + 0.079Na^+ + 0.024Ti(OH)_4$	-0.07
Crystalline basalt[a]:		
Plagioclase (An_{70}) *44vol%; 30mol%*	$Ca_{0.7}Na_{0.3}Al_{1.7}Si_{2.3}O_8 + 8H_2O = 1.7Al(OH)_4^- + 0.7Ca^{+2} + 2.3H_4SiO_4 + 0.3Na^+$	-18.56
Olivine ($Fo_{43}Fa_{57}$) *17 vol%; 28mol%*	$(Mg_{0.43}Fe_{0.57})2SiO_4 + 4H+ = 1.14Fe^{+2} + H_4SiO_4 + 0.86Mg^{+2}$	22.29
Clinopyroxene *39 vol%; 42 mol%*	$Ca_{0.7}Mg_{0.84}Fe_{0.46}(SiO_3)_2 + 4H^+ + 2H_2O = 0.7Ca^{+2} + 0.46Fe^{+2} + 2H_4SiO_4 + 0.84Mg^{+2}$	8.91
Secondary minerals		
Carbonates		
Calcite	$CaCO_3 + H^+ = Ca^{2+} + HCO_3^-$	-8.54
Aragonite	$CaCO_3 + H^+ = Ca^{2+} + HCO_3^-$	-8.41
Siderite	$FeCO_3 + H^+ = Fe^{2+} + HCO_3^-$	-0.94
$Ca_{0.25}Mg_{0.50}Fe_{0.25}$ carbonate	$Ca_{0.25}Mg_{0.50}Fe_{0.25}CO_3 + H^+ = 0.25Ca^{+2} + 0.5Mg^{+2} + 0.25Fe^{+2} + HCO_3^-$	0.77
$Mg_{0.25}Fe_{0.75}$ carbonate	$Mg_{0.25}Fe_{0.75}CO_3 + H^+ = 0.75Fe^{+2} + 0.25Mg^{+2} + HCO_3^-$	-0.44
$Mg_{0.50}Fe_{0.50}$ carbonate	$Mg_{0.50}Fe_{0.50}CO_3 + H^+ = 0.50Fe^{+2} + 0.50Mg^{+2} + HCO_3^-$	0.25
$Mg_{0.75}Fe_{0.25}$ carbonate	$Mg_{0.75}Fe_{0.25}CO_3 + H^+ = 0.25Fe^{+2} + 0.75Mg^{+2} + HCO_3^-$	1.05
Zeolites		
Analcime	$Na_{0.96}Al_{0.96}Si_{2.04}O_6H_2O + 5H_2O = 0.96Al(OH)4^- + 2.04H_4SiO_4 + 0.96Na^+$	-15.10
Chabazite	$CaAl_2Si_4O_{12}:6H_2O + 6H_2O = 2Al(OH)_4^- + Ca^{+2} + 4H_4SiO_4$	-30.11

Thomsonite	$Ca_2NaAl_5Si_5O_{20}{:}6H_2O + 14H_2O = 5Al(OH)_4^- + 2Ca^{+2} + 5H_4SiO_4 + Na^+$	-59.54
Silica polymorphs		
Chalcedony	$SiO_2 + 2H_2O = H_4SiO_4$	-3.46
Clay minerals		
Smectite[b)]	$K_{0.03}Na_{0.05}Ca_{0.13}Mg_{0.81}Fe_{0.71}Al_{0.98}Si_{3.92}O_{10}(OH)_2 + 2.4H^+ + 7.6H_2O$ $= 0.98Al(OH)_4^- + 0.13Ca^{+2} + 0.71Fe^{+2} + 3.92H_4SiO_4 + 0.03K^+ + 0.81Mg^{+2} + 0.05Na^+$	-10.44
Smectite[c)]	$K_{0.01}Na_{0.02}Ca_{0.25}Mg_{2.16}Fe_{0.78}Al_{0.77}Si_{3.32}O_{10}(OH)_2 + 5.64H^+ + 4.36H_2O$ $= 0.77Al(OH)_4^- + 0.25Ca^{+2} + 0.78Fe^{+2} + 3.32H_4SiO_4 + 0.01K^+ + 2.16Mg^{+2} + 0.02Na^+$	12.21
Smectite[d)]	$K_{0.02}Na_{0.10}Ca_{0.26}Mg_{1.27}Fe_{1.91}Al_{01.08}Si_{2.94}O_{10}(OH)_2 + 5.92H^+ + 4.08H_2O$ $= 1.08Al(OH)_4^- + 0.26Ca^{+2} + 1.91Fe^{+2} + 2.94H_4SiO_4 + 0.02K^+ + 1.27Mg^{+2} + 0.01Na^+$	8.47
Smectite[e)]	$K_{0.05}Na_{0.03}Ca_{0.18}Mg_{1.41}Fe_{1.78}Al_{1.02}Si_{3.03}O_{10}(OH)_2 + 5.8H^+ + 4.2H_2O$ $= 1.02Al(OH)_4^- + 0.18Ca^{+2} + 1.78Fe^{+2} + 3.03H_4SiO_4 + 0.05K^+ + 1.41Mg^{+2} + 0.03Na^+$	7.89
Ca-Saponite	$Ca_{0.165}Mg_3Al_{0.33}Si_{3.67}O_{10}(OH)_2 + 6H^+ + 4H_2O = 0.33Al(OH)_4^- + 0.165Ca^{+2} + 3.67H_4SiO_4 + 3Mg^{+2}$	20.42
Mg-clay [e)]	$Ca_{0.04}Mg_{3.01}Al_{0.1}Si_{3.9}O_{10}(OH)_2 + 6H^+ + 4H_2O = 0.1Al(OH)_4^- + 0.04Ca^{+2} + 3.9H_4SiO_4 + 3.01Mg^{+2}$	19.31
Al- and Fe-hydroxides		
$Al(OH)_3$ amorph	$Al(OH)_3 + 3H^+ = Al^{3+} + 3H_2O$	1.10
Gibbsite (mircrocrystalline)	$Al(OH)_3 + H_2O = AlOH_4^- + H^+$	8.40
$Fe(OH)_3$ amorph	$Fe(OH)_3 + 3H^+ = Fe^{3+} + 3H_2O$	4.89

a) Modal abundances from Gudbrandsson et al. (2011)
b) Natural di-/tri-octahedral smectite from Rogers et al. (2006)
c) Natural di-/tri-octahedral smectite from Rogers et al. (2006)
d) Natural di-/tri-octahedral smectite from Neuhoff et al. (2006)
e) Natural clay mixtures from Crovisier et al. (1992)

Appendix A

Rapid carbon mineralization for permanent disposal of anthropogenic carbon dioxide emissions

Matter J.M, Stute M., **Snæbjörnsdóttir S.Ó**., Oelkers E.H., Gislason S.R., Aradottir E.A., Sigfusson B., Gunnarsson I., Sigurdardottir H., Gunnlaugsson E., Axelsson G., Alfredsson H.A., Wolff-Boenisch D., Mesfin K., Fernandez de la Reguera Taya D., Hall J., Dideriksen K., Broecker W.S., 2016. Science 352, 1312-1314. *DOI:10.1126/science.aad8132*

Electronic supplement

www.sciencemag.org/content/352/6291/1312/suppl/DC1

Supplementary Materials for

Rapid carbon mineralization for permanent disposal of anthropogenic carbon dioxide emissions

Juerg M. Matter,*, Martin Stute, Sandra Ó. Snæbjörnsdottir, Eric H. Oelkers, Sigurdur R. Gislason, Edda S. Aradottir, Bergur Sigfusson, Ingvi Gunnarsson, Holmfridur Sigurdardottir, Einar Gunnlaugsson, Gudni Axelsson, Helgi A. Alfredsson, Domenik Wolff-Boenisch, Kiflom Mesfin, Diana Fernandez de la Reguera Taya, Jennifer Hall, Knud Dideriksen, Wallace S. Broecker

*Corresponding author. Email: j.matter@southampton.ac.uk

Published 10 June 2016, *Science* **352**, 1312 (2016)
DOI: 10.1126/science.aad8132

This PDF file includes:

Materials and Methods

1) The SF_6 and SF_5CF_3 tracers

SF_6 and SF_5CF_3, originally stored in gas cylinders, were mixed into the CO_2 and CO_2+H_2S flue gas stream using mass flow controllers. Carbon-14 was added to the water injection stream as an aqueous $H^{14}CO_3^-$ solution using a Milton Roy micro-dosing pump (Model AA973-352S3). The $H^{14}CO_3^-$ solution was created by adding 10 mCi of a ^{14}C-rich sodium bicarbonate aqueous solution obtained from Perkin Elmer to 100 liter of groundwater collected from the target storage reservoir prior to CO_2 injection.

Fluid samples for SF_6 and SF_5CF_3 analyses were collected in evacuated 100 ml glass serum bottles from the monitoring well HN04. Concentrations in the headspace were measured with a precision of ±2% using gas chromatography (SRI 8610C) and ultrapure nitrogen as the carrier gas. The headspace samples were injected into a 6ft long, 1/8" wide pre-column with a 5 ångström molecular sieve (MS-5A) and a 6ft chromatographic column at 60°C. SF_6 and SF_5CF_3 concentrations were measured using a SRI 8610C gas chromatograph with an electron capture detector and a Alltech Carbograph column. Results were recorded using the PeakSimple 3.07.2 software, and concentrations in the water samples were calculated based on the volume of headspace and the solubility.

The SF_6 concentration data from the Phase I injection had to be corrected for the SF_6 that originated from a previous hydrological tracer test. In 2008, we injected SF_6 and sodium fluorescein (Na-Flu) into the target storage reservoir during a short duration tracer test to characterize the hydrology of the injection site. During the Phase I CO_2 injection only SF_6 was injected. Thus, the difference between the observed Na-Flu and the SF_6/Na-Flu ratio can be used to calculate how much SF_6 in the collected water samples is from the Phase I injection (Table S2). Without the addition from the Phase I injection, the SF_6/Na-Flu ratio would follow the trajectory of the Na-Flu concentration. Thus, multiplying the expected ratio by the observed Na-Flu

concentration provides a measure of the expected SF_6 concentration. The difference between the observed and expected SF_6 concentration is the actual SF_6 from the Phase I injection (Table S2).

2) Carbon-14

Fluid samples for ^{14}C analysis were collected in 125 ml glass serum bottles. For ^{14}C analysis, water samples were acidified to release the dissolved inorganic carbon as CO_2. The ^{14}C concentration was measured with ^{14}C-AMS first in the W.M. Keck Carbon Cycle Accelerator Mass Spectrometry Laboratory at the University of California, Irvine, and later in the BioAMS laboratory at Lawrence Livermore National Laboratory, USA. Results are reported as fractions of the Modern Standard, $\Delta^{14}C$, following the conventions of Stuiver and Polach (*24*). All results are corrected for isotopic fractionation with $\delta^{13}C$ values measured on prepared samples using AMS spectrometer. Data and uncertainties are reported in Table S2.

3) Dissolved inorganic carbon (DIC)

Dissolved inorganic carbon (DIC) was calculated using PHREEQC (*25*) from measured pH, alkalinity, *in-situ* temperature and total dissolved element concentration measurements. The pH was determined in the field with a Eutech InstrumentsTM CyberScan pH 110 electrode calibrated using NBS standards, and verified in the laboratory a few hours after sampling with a Cole Parmer glass pH electrode. Alkalinity titration was performed using the Gran function to determine the end point of the titration (*26*). The concentration of major elements including Si, Ca, K, Mg, Na, and S and the trace metals Fe and Al were determined by Inductively Coupled Plasma Optical Emission Spectrometry (ICP-OES) using an in-house multi-elements standard checked against the SPEX Certified Reference standard at the University of Iceland. The uncertainties on calculated DIC measurements are estimated to be ±5%

4) Mass balance calculations

Mass balance calculations for dissolved inorganic carbon and ^{14}C were performed to assess the reactivity of the injected CO_2 (27). The mixing fraction between the injected solution (IS) and ambient groundwater (BW) was calculated for each extracted water sample (i) using

$$[SF_6]_i = X[SF_6]_{IS} + (1-X)[SF_6]_{BW} \quad (1)$$

with *X* being the fraction of injected solution in the extracted water sample. The expected DIC and ^{14}C values due to pure mixing was then determined from

$$DIC_{mix} = X \cdot DIC_{IS} + (1-X) \cdot DIC_{BW} \quad (2)$$

and

$$^{14}C_{mix} = X \cdot {}^{14}C_{IS} + (1-X) \cdot {}^{14}C_{BW} \quad (3)$$

Differences in DIC and ^{14}C concentrations between the values measured in the retrieved fluid samples and the expected values assuming only mixing between injectate and ambient groundwater yield the loss of DIC and ^{14}C due to carbonate precipitation.

5) Analysis of solid phases

Mineral precipitate samples collected from the submersible pump in monitoring borehole HN04 were analyzed by X-Ray diffraction (XRD), scanning electron microscopy (SEM), and energy dispersive X-ray spectroscopy (EDXS) mapping. Prior to analysis, the samples were stored and treated in an anaerobic chamber to minimize oxidation.

Samples for XRD were mounted on low background Si sample holders and covered with an X-ray transparent cup (Bruker) to decrease oxidation of the fine-grained material during measurement. Measurements were conducted on a Bruker D8 DISCOVER equipped with a LynxEye detector and a Co-source. Scan range was 5-80° using a 0.05° step size and a count time of 10 s per step. Two types of samples were prepared for SEM-EDXS. One set was mounted directly on the Al-sample stubs to avoid a carbon signal from carbon tape. The material

was resuspended in anoxic ethanol and a drop of it transferred to the sample holder and left to dry. These samples were imaged by SEM using low vacuum (60 Pa) to minimize sample charging. For another set of samples, the Al-sample holders were covered with carbon tape and grains were picked from the samples and mounted upright to enable imaging of these grains perpendicular to the growth direction. These samples were sputter coated with Au and imaged under high vacuum (4×10^{-4} Pa) to resolved detailed morphological features. SEM/EDXS measurements were conducted on a FEI Quanta 3D FEG SEM equipped with an Oxford instrument X-max 20 mm^2 EDXS detector having a nominal energy resolution of 0.125 keV for MnKα (FWMH). During imaging, accelerating voltage was 20 KeV and currents were 3.8 pA for SEM imaging and 8 nA for EDXS mapping. In the EDXS maps, color intensity for an element is linearly correlated with the integrated intensity measured in a narrow range round it characteristic X-ray (CaKα: 3.63-3.75 KeV; FeKα: 6.32-6.48 KeV; SiKα: 1.69-1.79 KeV; OKα: 0.49-0.56 KeV; CKα: 0.24-0.29 KeV; peak from CKα has a slight contribution of <5% from Au_N lines).

XRD of all materials from the monitoring borehole (Fig. S1) shows only the Bragg peaks expected for calcite [e.g. (*28, 29*)]. Please note that the broad peaks between 10 and 30° are from the cap protecting the sample from oxidation. SEM imaging and EDXS mapping clearly show 10 um to 1 mm slightly elongated grains rich in Ca, C, and O, as expected for calcite, with trace concentrations of Mg, Mn, and Fe (Fig. S2). Imaging of samples EDXS mapping of the grains collected from inside the pump shows a banded structure where they were fractured, with a first generation of calcite containing rich in Fe- and Si and a second generation largely without such material (Fig. S3).

Laboratory studies of basalt carbonation.

A large number of laboratory experiments have been performed to assess the feasibility of basalt carbonation as a carbon storage strategy (e.g. 15, 16, 30, 31, 32, 33). Such experiments demonstrate the efficient carbonation of basalts and its constituent minerals. During basalt-water-CO_2 interaction, calcium liberated by

basalt dissolution tends to provoke calcite precipitation, whereas the liberated magnesium, aluminum and silicon tend to provoke the formation of zeolite and clay minerals (15, 16, 32).

Several experimental studies have been aimed at assessing if precipitated carbonate minerals would eventually slow the overall carbonation rates of basalts and its constituent minerals (9,10). Such studies suggest that the carbonate minerals that precipitate on the surfaces of these rocks and minerals have little effect on the dissolution rates of the original solid and on their carbonation rates. These results were attributed to the poor structural match between the dissolving silicate and precipitating carbonate, which leaves sufficient pathways for chemical mass transfer to and from the adjoining fluid phase (e.g. 34). Such results suggest that the in-situ carbonation of basalts will be little effected by the precipitation of carbonate phases on their surfaces.

In situ fluid chemistry and transport

Representative pre-injection fluid chemistries at the injection site are summarized in Table S2. The temperature gradient at the injection site is 80 °C/km. Groundwater flow in the top tens of meters is to southwest (16); water flow in the lower part of the system is focused in lava flows located at the CO_2 injection depth of 400–800 m depth. The flow rate in this lower system is on the order of 25 m per year and the hydraulic head decreases toward southwest (15, 16). Hydrological models, pump tests and tracer tests, suggest that the effective matrix porosity of this lava formation is 8.5% (16).

The injection of CO_2-charged waters lead to a pH drop in the formation waters provoking the dissolution of basalt and the eventual precipitation of carbonate minerals. In addition to the natural ambient water flow in the target basaltic reservoir, advective transport in the system was enhanced by the continuous pumping of water into the HN-02 injection well and pumping of water from the HN-04 monitoring well at a rate of 1 l/s throughout the study period. The dominance of advection as the chemical transport mechanism in the

system is evident in the concentration of chemical tracer in the monitoring fluid shown in Fig. 2; aqueous diffusion is far too slow to transport substantial material from the injection to the monitoring well over the 2-year study period.

Supporting Tables

Table S1. Injection test parameters, including results from the tracer and chemical analysis of injectate.

Injection Phase	CO_2 (tons)	H_2O (liters)	SF_6 (ccSTP/cc)	SF_5CF_3 (ccSTP/cc)	^{14}C (fraction modern)	DIC (mol/L)	pH
I	175	4.8×10^{6}	2.33×10^{-8}	none	16.17	0.82	3.85 (@20°C)
II	54.75	2.25×10^{6}	none	2.24×10^{-8}	4.65	0.43	4.03 (@20°C)

Table S2. Representative water chemistries at the CarbFix injection site prior to the gas injections (after 15).

	Well		
Parameter or aqueous concentration	HN-1 (source of injection water)	HN-2	HN-4
Sample	08HAA02	09HAA16	08HAA01
Sampling date	1 July 2008	19 May 2009	1 July 2008
Temperature °C	19.0	15.5	32.3
pH at 20 ±2 °C	8.87	8.79	9.43
O_2 (mmol/L)	0.057	0.011	0.037
Alkalinity (meq/kg)	1.91	1.45	1.91
F (mmol/L)	0.014	0.013	0.026
Cl (mm/L)	0.247	0.222	0.228
SO_4 (mmol/L)	0.075	0.077	0.089
Na (mmol/L)	1.301	1.338	2.114
K (mmol/L)	0.027	0.012	0.019
Ca (mmol/L)	0.164	0.124	0.041
Mg (mmol/L)	0.313	0.149	0.005
Fe (µmol/)	0.016	0.399	0.064
Al (µmol/)	0.419	0.097	1.905
Si (mmol/L)	0.363	0.337	0.897

Table S3: Result from the tracer and chemical fluid analyses.

Sample ID	Days since injection started	Na-Flu (g/L)	SF_6 (ccSTP/cc)	SF_6 Phase I (ccSTP/cc)*	SF_5CF_3 Phase II (ccSTP/cc)	pH	DIC (mmol/L)	^{14}C (frac. modern)	±	^{14}C (Bq/L)
619	1	4.94E-05	1.51E-09	2.44E-12		9.24	1.54			
621	2		1.54E-09							
623	3	4.98E-05	1.45E-09			9.32	1.5			
629	6	5.05E-05	1.62E-09	4.34E-11		9.38	1.47	0.3119	0.0008	0.001377
643	13	5.15E-05	1.56E-09			9.27	1.54	1.328	0.002	0.006584
651	16	5.15E-05	2.09E-09	4.52E-10		8.98	1.87			
655	18		1.90E-09							
661	21	5.14E-05	1.70E-09	6.58E-11		8.86	2.01	3.5054	0.0049	0.02117
665	23		2.02E-09			7.94	2.32			
667	24	5.14E-05	2.10E-09	4.70E-10		7.46	2.53			
669	25	5.14E-05	2.41E-09	7.75E-10		7.27	2.63	8.4908	0.0119	0.06685
679	31	5.23E-05	3.18E-09	1.48E-09		6.93	3.18			
681	32		3.25E-09			7.18	2.85			
687	35	5.36E-05	3.09E-09	1.31E-09		6.98	2.97	9.0563	0.0217	0.08001
693	38	5.43E-05	3.35E-09	1.52E-09		6.91	3.26	10.8941	0.0516	0.10575
699	42	5.54E-05	3.26E-09	1.36E-09		6.81	3.6	9.8633	0.0338	0.09663
703	44	5.46E-05	3.16E-09	1.31E-09		6.79	3.63	9.2766	0.0647	0.08921
705	48	5.00E-05	3.52E-09	1.97E-09		6.63	4.1	9.1683	0.0641	0.09506
709	49		3.70E-09							
715	51	4.92E-05	3.27E-09	1.78E-09		6.57	4.39	9.908	0.0758	0.10749
721	56	4.90E-05	4.05E-09	2.57E-09		6.64	4.18	10.9666	0.0696	0.11732
723	59	4.90E-05	3.34E-09	1.86E-09		6.68	4.03			
733	64	4.88E-05	4.24E-09	2.78E-09		6.81	3.65	11.1269	0.0637	0.10968
741	71	4.86E-05	3.36E-09	1.91E-09		7.06	3.19	10.3135	0.0805	0.09608
747	78	4.85E-05	3.47E-09	2.03E-09		7.22	3.07	10.963	0.089	0.09488
753	84	4.83E-05	2.99E-09	1.55E-09		7.63	2.74	10.963	0.089	0.09488
763	92	5.03E-05	3.21E-09	1.65E-09		7.92	2.61	11.2236	0.1119	0.08778
775	111	5.51E-05	3.28E-09	1.40E-09		8.65	2.32	9.0533	0.052	0.06502
777	115	4.96E-05	2.81E-09	1.30E-09		8.92	2.15			
781	118	4.90E-05	2.56E-09	1.08E-09		8.92	2.31			
783	122	4.85E-05	3.12E-09	1.67E-09		8.76	2.22	8.0588	0.0616	0.05473
785	127	4.74E-05	3.04E-09	1.66E-09		8.81	2.24			
787	129	4.70E-05	3.52E-09	2.16E-09		8.76	2.22			
789	136	4.57E-05	3.49E-09	2.21E-09		8.82	2.27	8.6288	0.0795	0.05938
793	139	4.50E-05	3.41E-09	2.17E-09		8.78	2.3			
797	147	4.29E-05	3.53E-09	2.41E-09		8.68	2.43			
801	148	4.29E-05	4.42E-09	3.30E-09		8.62	2.5	8.4219	0.0742	0.06251
803	149		4.04E-09							
813	156	4.16E-05	4.22E-09	3.17E-09	2.66E-11	7.36	3	8.0027	0.0593	0.06998

819	161	4.18E-05	4.15E-09	3.09E-09	2.18E-11	8.11	2.55			
825	164		4.19E-09		1.99E-11	8.43	2.66			
831	168	4.00E-05	4.37E-09	3.40E-09	2.35E-11	8.36	2.57	8.4363	0.0521	0.06516
833	169	3.90E-05	4.37E-09	3.45E-09	2.14E-11	8.33	2.55			
841	183	3.78E-05	4.50E-09	3.64E-09	3.09E-11	7.87	2.75	7.769	0.0512	0.0628
847	204	3.64E-05	5.43E-09	4.64E-09	4.09E-11	7.07	3.31			
849	213	3.60E-05	5.78E-09	5.01E-09	3.49E-11	7.50	2.98			
850	218	3.56E-05	5.81E-09	5.06E-09	2.75E-11	7.93	2.82			
851	225	3.51E-05	6.23E-09	5.50E-09	2.65E-11	8.19	2.77			
853	234	3.42E-05	6.87E-09	6.17E-09	2.36E-11	7.56	2.84	7.9298	0.0512	0.06267
855	245	3.37E-05	6.90E-09	6.22E-09	2.01E-11	8.29	2.66			
857	252	3.34E-05	7.42E-09	6.76E-09	2.35E-11	8.30	2.64			
858	259	3.34E-05	7.84E-09	7.18E-09	2.08E-11	8.36	2.57			
859	266	3.26E-05	7.94E-09	7.32E-09	2.20E-11			7.4848	0.0776	0.06051
860	273	3.21E-05	7.69E-09	7.08E-09	1.95E-11	8.40	2.59			
861	280	3.09E-05	8.42E-09	7.86E-09	2.45E-11	8.26	2.63			
863	296	3.00E-05	8.92E-09	8.39E-09	2.46E-11	8.31	2.61	8.4791	0.0742	0.06498
865	308	2.94E-05	9.09E-09	8.58E-09	2.42E-11	8.30	2.61			
869	322	2.92E-05	9.15E-09	8.66E-09	2.35E-11	8.31	2.51	8.3668	0.0657	0.06009
873	332	2.88E-05	9.65E-09	9.17E-09	2.56E-11	8.41	2.45			
875	350	2.88E-05	9.79E-09	9.31E-09	2.96E-11	8.73	2.37			
877	367	2.69E-05	1.03E-08	9.88E-09	3.77E-11	8.58	2.68			
879	386	2.47E-05	9.72E-09	9.37E-09	4.88E-11	8.57	2.67			
881	406	2.31E-05	1.10E-08	1.07E-08	5.81E-11	8.20	2.83			
883	423	2.33E-05	9.94E-09	9.63E-09	5.65E-11	8.45	2.54			
881	436	2.26E-05	9.03E-09	8.75E-09	4.87E-11	8.76	2.39			
889	444	2.15E-05	8.77E-09	8.52E-09	6.30E-11	8.93	2.4			
893	449	2.17E-05	8.93E-09	8.67E-09	5.92E-11	8.76	2.43			
895	454	2.15E-05	8.65E-09	8.40E-09	5.52E-11					
897	470	2.13E-05	8.07E-09	7.82E-09	5.76E-11	8.81	2.35			
901	477	2.09E-05	8.90E-09	8.66E-09		8.91	2.32			
905	484	2.05E-05	8.93E-09	8.70E-09		8.95	2.28			
907	491	1.92E-05	7.07E-09	6.87E-09		8.94	2.41	7.5505	0.0467	0.05559
909	498	1.92E-05	9.10E-09	8.91E-09		8.94	2.34			
913	511	2.20E-05	9.57E-09	9.30E-09	7.26E-11	8.83	2.33	6.5517	0.0472	0.04745
915	518		8.28E-09		6.61E-11	8.83	2.27	6.2029		0.04231
917	525		9.80E-09		7.59E-11	8.93	2.34	7.2165		0.05075
918	539		9.39E-09		6.96E-11	8.99	2.23	6.6135		0.04571

Supporting Figures

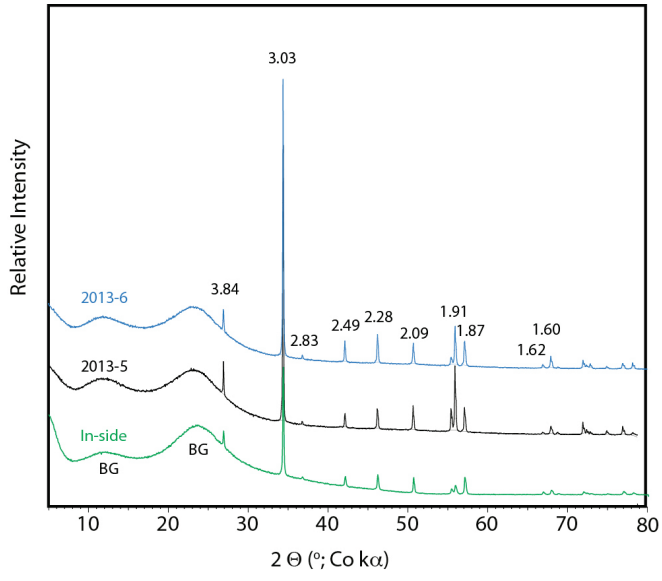

Figure S1. X-ray tracers of sample 2013-5 and 2013-6 taken from the submersible pump. The two broad peaks are from the cap protecting the sample from further oxidation is marked BG.

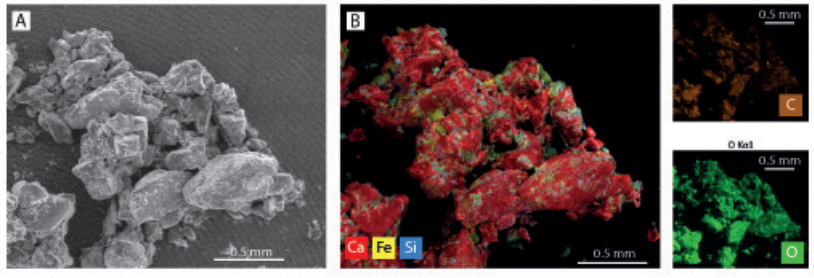

Figure S2. Overview SEM images and EDX maps of material from sample 2013-6. (**A**) SEM image. (**B**) EDX map of are shown in SEM image A. The maps for Ca, Fe and Si has been overlain the SEM image, whereas the maps for C and O are presented individually.

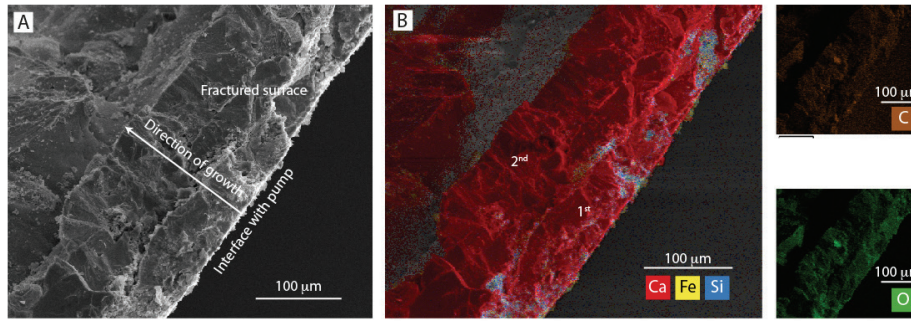

Figure S3. SEM images and EDX maps of fractured flake from a sample collected inside the submersible pump. (**A**) SEM image of the fractured flake mounted upright so that the internal regions of the material could be imaged. Fractured region, where the material interfaced with the pump surface and the direction of mineral growth is indicated. (**B**) EDX maps of area shown in SEM image A. The maps for Ca, Fe and Si has been overlain the SEM image, whereas the maps for C and O are presented individually. The location of two generations of calcite have been indicated based on the frequency of Fe- and Si-rich material.

REFERENCES AND NOTES

1. B. Metz, O. Davidson, H. de Coninck, M. Loos, L. A. Meyer, Eds., *IPCC Special Report on Carbon Dioxide Capture and Storage* (Cambridge Univ. Press, New York, 2005).

2. A. Esposito, S. Benson, in Proceedings of the Society of Petroleum Engineers 2010 Western North American Regional Meeting, Anaheim, CA, 27 to 29 May 2010 (Society of Petroleum Engineers, 2010), SPE-133604 (2010).

3. B. Ellis, C. Peters, J. Fitts, G. Bromhal, J. McIntyre, R. Worzinski, E. Rosenbaum, *Greenhouse Gases Sci. Technol.* **1**, 248–260 (2011).

4. J. M. Bielicki, M. F. Pollak, J. P. Fitts, C. A. Peters, E. J. Wilson, Causes and financial consequences of geologic CO_2 storage reservoir leakage and interference with other subsurface resources. *Int. J. Greenhouse Gas Control* **20**, 272–284 (2014). doi:10.1016/j.ijggc.2013.10.024

5. P. M. Haugan, F. Joos, Metrics to assess the mitigation of global warming by carbon capture and storage in the ocean and in geological reservoirs. *Geophys. Res. Lett.* **31**, L18202 (2004). doi:10.1029/2004GL020295

6. B. van der Zwaan, L. Smekens, CO_2 capture and storage with leakage in an energy-climate model. *Environ. Model. Assess.* **14**, 135–148 (2009). doi:10.1007/s10666-007-9125-3

7. H. S. Eggleston *et al*., Eds., *IPCC Guidelines for National Greenhouse Gas Inventories – A Primer* (National Greenhouse Gas Inventories Programme, Institute for Global Environmental Strategies, Japan, 2008).

8. M. D. Zoback, S. M. Gorelick, Earthquake triggering and large-scale geologic storage of carbon dioxide. *Proc. Natl. Acad. Sci. U.S.A.* **109**, 10164–10168 (2012). Medline doi:10.1073/pnas.1202473109

9. S. R. Gislason, E. H. Oelkers, Carbon storage in basalt. *Science* **344**, 373–374 (2014). Medline doi:10.1126/science.1250828

10. J. M. Matter, P. B. Kelemen, Permanent storage of carbon dioxide in geological reservoirs by mineral carbonation. *Nat. Geosci.* **2**, 837–841 (2009). doi:10.1038/ngeo683

11. S. M. V. Gilfillan, B. S. Lollar, G. Holland, D. Blagburn, S. Stevens, M. Schoell, M. Cassidy, Z. Ding, Z. Zhou, G. Lacrampe-Couloume, C. J. Ballentine, Solubility trapping in formation water as dominant CO_2 sink in natural gas fields. *Nature* **458**, 614–618 (2009). Medline doi:10.1038/nature07852

12. D. S. Goldberg, T. Takahashi, A. L. Slagle, Carbon dioxide sequestration in deep-sea basalt. *Proc. Natl. Acad. Sci. U.S.A.* **105**, 9920–9925 (2008). Medline doi:10.1073/pnas.0804397105

13. B. P. McGrail, H. T. Schaef, A. M. Ho, Y.-J. Chien, J. J. Dooley, C. L. Davidson, *J. Geophys. Res*. **111**, B12201 (2006).

14. S. R. Gislason, D. Wolff-Boenisch, A. Stefansson, E. H. Oelkers, E. Gunnlaugsson, H. Sigurdardottir, B. Sigfusson, W. S. Broecker, J. M. Matter, M. Stute, Mineral sequestration of carbon dioxide in basalt: A pre-injection overview of the CarbFix project. *Int. J. Greenhouse Gas Control* **4**, 537–545 (2010). doi:10.1016/j.ijggc.2009.11.013

15. H. A. Alfredsson, E. H. Oelkers, B. S. Hardarsson, H. Franzson, E. Gunnlaugsson, S. R. Gislason, The geology and water chemistry of the Hellisheidi, SW-Iceland carbon storage site. *Int. J. Greenhouse Gas Control* **12**, 399–418 (2013). doi:10.1016/j.ijggc.2012.11.019

16. E. S. Aradóttir, E. L. Sonnenthal, G. Björnsson, H. Jónsson, Multidimensional reactive transport modeling of CO_2 mineral sequestration in basalts at the Hellisheidi geothermal field, Iceland. *Int. J. Greenhouse Gas Control* **9**, 24–40 (2012). doi:10.1016/j.ijggc.2012.02.006

17. B. Sigfusson, S. R. Gislason, J. M. Matter, M. Stute, E. Gunnlaugsson, I. Gunnarsson, E. S. Aradottir, H. Sigurdardottir, K. Mesfin, H. A. Alfredsson, D. Wolff-Boenisch, M. T. Arnarsson, E. H. Oelkers, Solving the carbon-dioxide buoyancy challenge: The design and field testing of a dissolved CO_2 injection system. *Int. J. Greenhouse Gas Control* **37**, 213–219 (2015). doi:10.1016/j.ijggc.2015.02.022

18. Materials and methods are available as supplementary materials on *Science* Online.

19. P. P. Bachelor, J. I. McIntyre, J. E. Amonette, J. C. Hayes, B. D. Milbrath, P. Saripalli, Potential method for measurement of $_{CO2}$ leakage from underground sequestration fields using radioactive tracers. *J. Radioanal. Nucl. Chem.* **277**, 85–89 (2008). doi:10.1007/s10967-008-0713-8

20. K. S. Lackner, S. Brennan, Envisioning carbon capture and storage: Expanded possibilities due to air capture, leakage insurance, and C-14 monitoring. *Clim. Change* **96**, 357–378 (2009). doi:10.1007/s10584-009-9632-0

21. I. D. Clark, P. Fritz, *Environmental Isotopes in Hydrogeology* (Lewis Publishers, Boca Raton, FL, 1997).

22. H. A. Alfredsson, K. Mesfin, D. Wolff-Boenisch, *Greenhouse Gases Sci. Technol.* **6**, 167–177 (2016).

23. M. Rezvani Khalilabad, G. Axelsson, S. Gislason, Aquifer characterization with tracer test technique; permanent CO_2 sequestration into basalt, SW Iceland. *Mineral. Mag.* **72**, 121–125 (2008). doi:10.1180/minmag.2008.072.1.121

24. M. Stuiver, H. A. Polach, *Radiocarbon* **19**, 355–363 (1977).

25. D. L. Parkhurst, C. A. J. Appelo, *Description of Input and Examples for PHREEQC Version 3*, U.S. Geological Survey Techniques and Methods, Book 6 (U.S. Geological Survey, Denver, CO, 2013).

26. W. Stumm, J. J. Morgan, *Aquatic Chemistry: Chemical Equilibria and Rates in Natural Waters* (Wiley, New York, ed. 3, 1996).

27. N. Assayag, J. Matter, M. Ader, D. Goldberg, P. Agrinier, Water–rock interactions during a CO_2 injection field-test: Implications on host rock dissolution and

alteration effects. *Chem. Geol.* **265**, 227–235 (2009). doi:10.1016/j.chemgeo.2009.02.007

28. D. L. Graf, *Am. Mineral.* **46**, 1283 (1961).

29. S. A. Markgraf, R. J. Reeder, *Am. Mineral.* **70**, 590 (1985).

30. H. T. Schaef, B. P. McGrail, Dissolution of Columbia River Basalt under mildly acidic conditions as a function of temperature: Experimental results relevant to the geological sequestration of carbon dioxide. *Appl. Geochem.* **24**, 980–987 (2009). doi:10.1016/j.apgeochem.2009.02.025

31. D. Wolff-Boenisch, S. Wenau, S. R. Gislason, E. H. Oelkers, Dissolution of basalts and peridotite in seawater, in the presence of ligands, and CO_2: Implications for mineral sequestration of carbon dioxide. *Geochim. Cosmochim. Acta* **75**, 5510–5525 (2011). doi:10.1016/j.gca.2011.07.004

32. A. P. Gysi, A. Stefansson, CO_2-water–basalt interaction. Low temperature experiments and implications for CO_2 sequestration into basalts. *Geochim. Cosmochim. Acta* **81**, 129–152 (2012). doi:10.1016/j.gca.2011.12.012

33. I. Galeczka, D. Wolff-Boenisch, E. H. Oelkers, S. R. Gislason, An experimental study of basaltic glass–H_2O–CO_2 interaction at 22 and 50°C: Implications for subsurface storage of CO_2. *Geochim. Cosmochim. Acta* **126**, 123–145 (2014). doi:10.1016/j.gca.2013.10.044

34. P. Cubillas, S. Köhler, M. Prieto, C. Causserand, E. H. Oelkers, How do mineral coatings affect dissolution rates? An experimental study of coupled $CaCO_3$ dissolution—$CdCO_3$ precipitation. *Geochim. Cosmochim. Acta* **69**, 5459–5476 (2005). doi:10.1016/j.gca.2005.07.016

Appendix B

The chemistry and saturation states of subsurface fluids during the in situ mineralisation of CO_2 and H_2S at the CarbFix site in SW-Iceland

Snæbjörnsdóttir, S.Ó., Oelkers, E.H., Mesfin, K., Aradóttir, E.S., Dideriksen, K., Gunnarsson, I., Gunnlaugsson, E., Matter, J.M., Stute, M., Gislason, S.R., 2017. International Journal of Greenhouse Gas Control 58, 87–102.
DOI:10.1016/j.ijggc.2017.01.007

Electronic supplement

Electronic supplements - figures

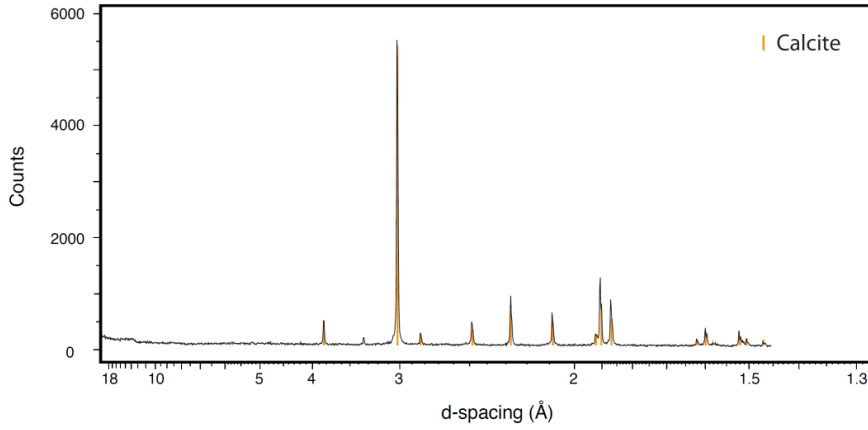

Figure A2. X-ray diffractrogram of two samples of solids (red and green curves) collected from the submersible pump on the 13th of August 2013. Red dots show locations and height of representative calcite-peaks. Analyses performed by ISOR IcelandGeoSurvey.

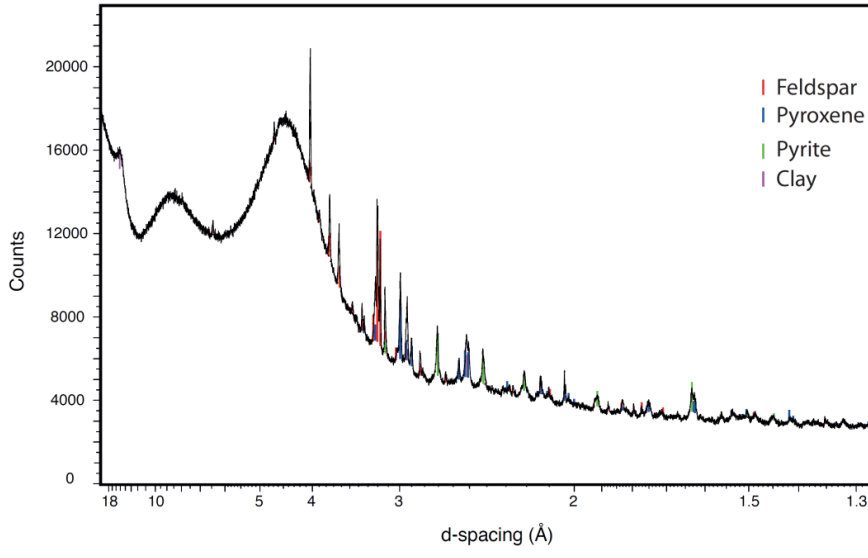

Figure A3. X-ray diffractrogram of samples collected on the 10th of June 2013, during airlift from the injection well HN-02. Red lines show locations and height of representative feldspar-peaks, blue lines show locations and height of representative pyrite peaks, green lines show locations and height of representative pyroxene peaks and purple lines show locations and height of representative clay peaks. The two broad peaks at 12° and 24° are from the cup protecting the sample from oxidation.

Table 1. *The pH, H_2S-concentration, alkalinity, dissolved inorganic carbon (DIC) concentration, dissolved organic carbon (DOC) concentration, and the concentrations of F, Cl, SO_4, S, Si, Na, K, Ca, Mg, Fe, and Al in samples collected prior to, during, and after the CO_2 and CO_2-H_2S-gas mixture injections in Hellisheidi in 2012. The samples were analysed at the University of Iceland, and ALS, Sweden. The methods are described in Snæbjörnsdóttir et al. (2017). The mixing fraction of the SF_6 and SF_5CF_3 non-reactive tracers in the samples, as described by Matter et al. (2016), is also included in the tables.*

Sample code	Date	pH	H_2S	Alk.	DIC	DOC	F	Cl	SO_4	$S_{(total)}$	$S_{(total)}$	% diff	Si	Si	% diff	Na	Na	% diff
concentration			µmol/L	meq./L	mmol/L	mmol/L	mmol/L	mmol/L	mmol/L	mmol/L	mmol/L		mmol/L	mmol/L		mmol/L	mmol/L	
DL/RL			0.29 µmol/L							0.30 µmol/L	01 µmol/L		0.78 µmol/L	07 µmol/L)		0.43 µmol/L	35 µmol/L	1.
method			*(titr.)*	*(titr.)*	*(PhreeqC)*	*(TOC analyser)*	*(IC)*	*(IC)*	*(IC)*	*(ICP-OES)*	*(ICP-SFMS)*		*(ICP-OES)*	*(ICP-OES)*		*(ICP-OES)*	*(ICP-OES)*	
11KGM03	21.1.2011	9.56		1.91	1.36	0.020	0.024	0.237	0.094	0.095	0.096	1.5	0.409	0.446	9.0	2.28	2.16	5.4
11KGM08	5.7.2011	9.58		1.87	1.32	0.049	0.022	0.238	0.093	0.098	0.095	3.3	0.387	0.406	4.8	2.21	2.07	6.5
11KGM14	28.10.2011	9.44	*BDL*	1.88	1.43	0.039	0.022	0.241	0.096	0.105	0.107	2.0	0.393	0.419	6.5	2.17	2.04	5.9
12KGM01	25.1.2012	9.24	*BDL*	1.87	1.54	0.052	0.022	0.247	0.100	0.107	0.107	0.4	0.390	0.406	4.0	2.18	2.04	6.5
12KGM02	27.1.2012	9.32	*BDL*	1.87	1.50	0.036	0.021	0.246	0.100	0.104	0.110	5.8	0.385	0.411	6.8	2.17	2.01	7.5
12KGM04	31.1.2012	9.38	0.499	1.89	1.47	0.052	0.021	0.258	0.100		0.123		0.387	0.409	5.6	2.18	1.99	8.5
12KGM05	3.2.2012	9.27	0.329	1.88	1.54	0.050	0.020	0.247	0.100	0.110	0.108	1.9	0.379	0.407	7.6	2.16	1.98	8.3
12KGM07	6.2.2012	9.2	0.449	1.97	1.65	0.031	0.020	0.247	0.104	0.103	0.106	2.6	0.375	0.402	7.2	2.20	2.04	7.5
12KGM08	9.2.2012	8.98		2.09	1.87	0.042	0.013	0.267	0.087	0.100	0.102	2.7	0.371	0.397	7.0	2.21	2.01	9.1
12KGM10	13.2.2012	8.86		2.20	2.01	0.032	0.020	0.248	0.102	0.102	0.107	5.1	0.383	0.389	1.6	2.22		
12KGM11	16.2.2012	7.94		2.31	2.32	0.030	0.020	0.248	0.102	0.102	0.107	4.8	0.381	0.394	3.5	2.26	2.18	3.5
12KGM13	17.2.2012	7.46		2.39	2.53	0.027	0.019	0.248	0.101	0.101	0.108	6.7	0.378	0.392	3.8	2.23	2.20	1.5
12KGM14	18.2.2012	7.27		2.40	2.63	0.024	0.019	0.248	0.101	0.100	0.104	3.7	0.374	0.391	4.4	2.25	2.14	5.2
12KGM15	19.2.2012	7.04		2.48	2.90	0.027	0.020	0.248	0.101	0.100	0.108	7.3	0.391	0.402	2.9	2.25	2.17	3.7
12KGM16	20.2.2012	6.95		2.51	3.04	0.023	0.020	0.248	0.101	0.101	0.107	6.6	0.398	0.411	3.1	2.26	2.21	2.2
12KGM17	23.2.2012	6.93		2.61	3.18	0.024	0.021	0.248	0.100	0.101			0.396			2.28		
12KGM19	27.2.2012	7.18		2.54	2.85	0.027	0.023	0.247	0.103	0.103	0.111	7.8	0.420	0.441	4.9	2.36	2.26	4.1
12KGM20	28.2.2012	6.98		2.48	2.97	0.026	0.022	0.247	0.102	0.104			0.415			2.35		
12KGM22	2.3.2012	6.91		2.65	3.26	0.027	0.020	0.249	0.100	0.102	0.110	7.5	0.392	0.412	5.1	2.31	2.26	2.0
12KGM23	5.3.2012	6.81		2.79	3.60	0.032	0.020	0.248	0.099	0.102			0.386			2.33		
12KGM25	8.3.2012	6.79		2.78	3.63	0.021	0.019	0.249	0.099	0.100	0.108	7.3	0.376	0.402	7.1	2.31	2.28	1.4
12KGM27	12.3.2012	6.63		2.84	4.10	0.025	0.020	0.249	0.099	0.101	0.107	6.1	0.389	0.406	4.3	2.34	2.27	2.9
12KGM28	15.3.2012	6.57		2.91	4.39	0.025	0.020	0.249	0.099	0.101	0.106	5.3	0.396	0.414	4.5	2.35	2.29	2.6
12KGM30	19.3.2012	6.64		2.92	4.18	0.025	0.020	0.397	0.100	0.102	0.110	7.8	0.403	0.419	4.0	2.39	2.32	2.9
12KGM31	22.3.2012	6.68		2.89	4.03	0.022	0.020	0.259	0.099	0.102	0.109	6.3	0.402	0.426	5.8	2.39	2.31	3.5
12KGM33	26.3.2012	6.71		2.93	4.00	0.020	0.019	0.250	0.099	0.101			0.392			2.37		
12KGM34	29.3.2012	6.81		2.83	3.65	0.025	0.019	0.250	0.100	0.101	0.106	5.1	0.387	0.402	4.0	2.34	2.27	3.1
12KGM36	2.4.2012	6.96		2.76	3.32	0.025	0.019	0.250	0.101	0.102			0.388			2.34		
12KGM37	4.4.2012	7.06		2.75	3.19	0.025	0.019	0.250	0.101	0.102			0.390			2.33		
12KGM39	7.4.2012	7.14		2.71	3.07	0.021	0.019	0.251	0.101	0.103	0.108	5.4	0.387	0.406	4.7	2.35	2.29	2.7
12KGM40	10.4.2012	7.17	0.300	2.70	3.03	0.022	0.018	0.250	0.101	0.102			0.382			2.35		
12KGM41	11.4.2012	7.22		2.77	3.07	0.035	0.019	0.250	0.101	0.102			0.383			2.34		
12KGM42	12.4.2012	7.2		2.83	3.15	0.019	0.019	0.249	0.100	0.100	0.108	7.4	0.392	0.417	6.5	2.38	2.31	2.6
12KGM43	16.4.2012	7.63		2.65	2.74	0.017	0.020	0.250	0.102	0.103			0.398			2.36		
12KGM44	18.4.2012	7.7		2.58	2.65	0.019	0.020	0.250	0.102	0.103			0.400			2.37		
12KGM46	23.4.2012	7.92		2.59	2.61	0.018	0.020	0.251	0.103	0.104	0.110	6.2	0.401	0.419	4.4	2.39	2.36	1.6
12KGM47	27.4.2012	8.15		2.56	2.54	0.023	0.020	0.250		0.095			0.376			2.37		
12KGM49	4.5.2012	9		2.32	2.06	0.019	0.023	0.248	0.104	0.106			0.427			2.43		
12KGM51	7.5.2012	8.71		2.44	2.29	0.028	0.021	0.248	0.107	0.105	0.112	6.4	0.399	0.422	5.8	2.35	2.33	0.8
12KGM52	10.5.2012	8.67		2.45	2.31	0.020	0.021	0.249	0.107	0.105			0.399			2.35		
12KGM54	14.5.2012	8.65		2.45	2.32	0.019	0.022	0.250	0.101	0.098			0.376			2.35		
12KGM55	18.5.2012	8.92		2.38	2.15	0.014	0.022	0.248	0.107	0.105	0.113	7.4	0.407	0.429	5.3	2.35	2.32	1.2
12KGM57	21.5.2012	8.81		2.44	2.25	0.011	0.022	0.248	0.106	0.106			0.408			2.38		
12KGM58	24.5.2012	8.76		2.39	2.22	0.017	0.021	0.248	0.106	0.106			0.405			2.36		
12KGM60	30.5.2012	8.81		2.43	2.24	0.010	0.021	0.249	0.106	0.105	0.109	4.4	0.399	0.426	6.7	2.34	2.34	0.0
12KGM61	1.6.2012	8.76	0.519	2.39	2.22	0.012	0.021	0.247	0.106	0.105			0.400			2.35		
12KGM63	4.6.2012	8.84	*BDL*	2.43	2.23	0.015	0.021	0.247	0.106	0.106			0.407			2.36		
12KGM64	8.6.2012	8.82	*BDL*	2.46	2.27	0.012	0.021	0.247	0.106	0.105	0.109	3.6	0.402	0.419	4.3	2.36	2.28	3.2
12KGM66	11.6.2012	8.78	*BDL*	2.48	2.30	0.015	0.021	0.248	0.105	0.105			0.398			2.34		
12KGM67	14.6.2012	8.78		2.47	2.29	0.013	0.021	0.246	0.106	0.104	0.110	5.1	0.402	0.426	5.8	2.35	2.30	2.2
12KGM68	18.6.2012	8.68	*BDL*	2.58	2.43	0.010	0.020	0.247	0.104	0.104			0.401			2.37		
12KGM69	20.6.2012	8.62	*BDL*	2.63	2.50	0.009	0.020	0.247	0.110	0.103			0.395			2.35		

Table 2. *Continuation.*

Sample code	Date	pH	H_2S	Alk.	DIC	DOC	F	Cl	SO_4	$S_{(total)}$	$S_{(total)}$	% diff	Si	Si	% diff	Na	Na	% diff
concentration			µmol/L	meq./L	mmol/L	mmol/L	mmol/L	mmol/L	mmol/L	mmol/L	mmol/L		mmol/L	mmol/L		mmol/L	mmol/L	
DL/RL		0.29	µmol/L						0.30	µmol/L	01 µmol/L		0.78 µmol/L	37 µmol/L)		0.43 µmol/L	35 µmol/L	1.
method			*(titr.)*	*(titr.)*	*(PhreeqC)*	*(TOC analyser)*	*(IC)*	*(IC)*	*(IC)*	*(ICP-OES)*	*(ICP-SFMS)*		*(ICP-OES)*	*(ICP-OES)*		*(ICP-OES)*	*(ICP-OES)*	
12SOS01	28. 6. 2012	7.36		2.79	3.00	0.017	0.020	0.246	0.104	0.103	0.104	0.8	0.380	0.386	1.5	2.39	2.31	3.2
12SOS02	3. 7. 2012	8.11	1.502	2.57	2.55	0.010	0.021	0.245	0.106	0.103	0.105	1.8	0.380	0.387	1.8	2.42	2.34	3.1
12SOS04	5. 7. 2012	8.43	1.129	2.75	2.66	0.014	0.016	0.248	0.105	0.104	0.107	2.7	0.383	0.392	2.5	2.42	2.39	1.2
12SOS05	7. 7. 2012	8.3	*BDL*	2.78	2.72	0.014	0.021	0.245	0.105	0.103			0.386			2.42		
12SOS06	9. 7. 2012	8.36	*BDL*	2.64	2.57	0.012	0.021	0.245	0.106	0.106	0.107	0.9	0.383	0.396	3.2	2.42	2.37	2.1
12SOS07	12. 7. 2012	8.33	0.898	2.62	2.56	0.011	0.021	0.244	0.105	0.105	0.106	0.6	0.387	0.396	2.4	2.44	2.37	2.8
12SOS09	17. 7. 2012	8.28	*BDL*	2.62	2.57	0.008	0.021	0.245	0.105	0.103	0.106	3.0	0.380	0.391	2.9	2.42	2.39	1.3
12SOS10	19. 7. 2012	8.07	0.293	2.63	2.62	0.011	0.024	0.245	0.105	0.106	0.111	5.1	0.388	0.411	6.0	2.47	2.41	2.3
12SOS12	24. 7. 2012	7.87	*BDL*	2.72	2.75	0.012	0.021	0.245	0.106	0.103	0.109	6.7	0.385	0.406	5.3	2.44	2.44	0.1
12SOS13	26. 7. 2012	8.32	*BDL*	2.67	2.61	0.009	0.021	0.259	0.106	0.103	0.110	6.3	0.383	0.402	5.0	2.43	2.37	2.5
12SOS15	31. 7. 2012	8.41	*BDL*	2.63	2.55	0.010	0.021	0.245	0.106	0.103	0.105	2.4	0.383	0.394	2.8	2.43	2.33	4.0
12SOS16	2. 8. 2012	8.29	*BDL*	2.67	2.62	0.011	0.021	0.245	0.106	0.103	0.108	4.4	0.386	0.406	5.2	2.45	2.34	4.4
12SOS18	7. 8. 2012	7.85	0.299	2.72	2.76	0.011	0.021	0.245	0.106	0.104	0.113	8.3	0.389	0.421	8.1	2.46	2.50	1.7
12SOS19	9. 8. 2012	7.25	*BDL*	2.78	3.06	0.009	0.025	0.245	0.105	0.103	0.109	4.9	0.393	0.412	5.0	2.50	2.45	1.9
12SOS21	14. 8. 2012	7.07	0.299	2.86	3.31	0.010	0.021	0.246	0.103	0.102	0.108	5.7	0.389	0.416	6.9	2.48	2.49	0.3
12SOS23	16. 8. 2012	7.13	*BDL*	2.91	3.30	0.008	0.021	0.247	0.102	0.103	0.105	2.1	0.391	0.396	1.3	2.50	2.39	4.5
12SOS25	21. 8. 2012	7.45	0.399	2.84	3.01	0.014	0.022	0.242	0.108	0.102	0.108	5.9	0.389	0.409	5.2	2.46	2.49	1.3
12SOS26	23. 8. 2012	7.5		2.83	2.98	0.013	0.020	0.241	0.104	0.103	0.107	3.4	0.390	0.401	2.7	2.49	2.40	3.7
12SOS28	28. 8. 2012	7.93	*BDL*	2.80	2.82	0.019	0.020	0.242	0.105	0.107	0.108	1.2	0.395	0.409	3.5	2.52	2.43	3.4
12SOS29	31. 8. 2012	8.19	0.758	2.77	2.73	0.012	0.020	0.246	0.105	0.105	0.104	1.2	0.408	0.399	2.3	2.61	2.34	10.6
12SOS31	4. 9. 2012	8.19	0.898	2.81	2.77	0.017	0.020	0.243	0.104	0.105	0.108	2.7	0.404	0.401	0.9	2.60	2.42	6.7
12SOS32	6. 9. 2012	7.94	0.599	2.76	2.78	0.012	0.020	0.241	0.104	0.104	0.104	0.5	0.398	0.396	0.5	2.58	2.40	7.0
12SOS33	13. 9. 2012	7.56	*BDL*	2.72	2.84	0.021	0.020	0.229	0.104	0.106			0.397			2.61		
12SOS33B	17. 9. 2012	8.23	0.758	2.73	2.69	0.018	0.020	0.241	0.104	0.104	0.112	7.2	0.393	0.417	6.2	2.55	2.53	0.8
12SOS34	24. 9. 2012	8.29	*BDL*	2.71	2.66	0.018	0.020	0.241	0.103	0.105	0.105	0.3	0.397	0.394	0.6	2.63	2.43	7.6
12SOS35	1. 10. 2012	8.3	*BDL*	2.70	2.64	0.016	0.020	0.241	0.105	0.103	0.104	1.2	0.399	0.394	1.3	2.58	2.44	5.5
12SOS36	8. 10. 2012	8.36	0.369	2.64	2.57	0.011	0.021	0.241	0.104	0.104	0.103	1.8	0.403	0.396	1.9	2.63	2.50	5.0
12SOS38	22. 10. 2012	8.4	0.399	2.67	2.59	0.014	0.021	0.241	0.104	0.104	0.101	3.0	0.413	0.394	4.6	2.61	2.55	2.0
12SOS39	29. 10. 2012	8.26	0.399	2.68	2.63		0.020	0.241	0.103	0.104			0.405			2.68		
12SOS40	14. 11. 2012	8.31	0.399	2.67	2.61	0.014	0.020	0.241	0.102	0.105	0.103	1.5	0.397	0.384	3.2	2.64	2.57	2.6
12SOS41	26. 11. 2012	8.3	0.599	2.67	2.61	0.012	0.020	0.240	0.102	0.103	0.099	4.2	0.398	0.384	3.5	2.72	2.53	6.8
12SOS42	10. 12. 2012	8.31	0.399	2.56	2.51	0.012	0.021	0.241	0.102	0.104	0.104	0.9	0.400	0.411	2.6	2.66	2.51	5.8
12SOS43	20. 12. 2012	8.41	0.399	2.53	2.45	0.011	0.021	0.241	0.103	0.102	0.109	6.7	0.415	0.436	5.0	2.70	2.64	2.2
13SOS01	7. 1. 2013	8.73	0.399	2.53	2.37	0.013	0.022	0.241	0.101	0.104	0.106	1.9	0.417	0.424	1.6	2.73	2.57	5.9
13SOS02	25. 1. 2013	8.58	0.648	2.81	2.68	0.011	0.019	0.242	0.101	0.100	0.099	1.1	0.423	0.391	7.6	2.73	2.54	6.9
13SOS04	12. 2. 2013	8.57	*BDL*	2.80	2.67	0.012	0.020	0.242	0.104	0.103	0.103	0.6	0.396	0.416	4.9	2.77	2.63	5.2
13SOS06	4. 3. 2013	8.2	*BDL*	2.87	2.83	0.010	0.018	0.240	0.103	0.099	0.099	0.2	0.411	0.379	7.8	2.73	2.54	7.1
13SOS07	21. 3. 2013	8.45	0.369	2.63	2.54	0.010	0.021	0.242	0.104	0.104	0.102	1.8	0.391	0.409	4.6	2.68	2.58	3.8
13SOS08	3. 4. 2013	8.76	0.658	2.57	2.39	0.009	0.022	0.241	0.105	0.106	0.104	1.3	0.416	0.416	0.0	2.67	2.55	4.6
13SOS09	11. 4. 2013	8.93	0.349	2.65	2.40	0.038	0.020	0.241	0.104	0.104	0.104	0.4	0.422	0.401	5.0	2.68	2.57	3.9
13SOS10	16. 4. 2013	8.76	0.339	2.61	2.43	0.008	0.021	0.243	0.104	0.104	0.106	1.7	0.409	0.417	2.0	2.71	2.67	1.7
13SOS11	29. 4. 2013	8.81	0.349	2.50	2.31	0.008	0.022	0.242	0.113	0.107	0.104	3.0	0.411	0.416	1.2	2.62	2.73	4.2
13SOS12	7. 5. 2013	8.81		2.54	2.35	0.007	0.022	0.242	0.108	0.108	0.105	2.0	0.419	0.424	1.1	2.70	2.71	0.4
13SOS13	14. 5. 2013	8.91	0.399	2.56	2.32	0.013	0.021	0.242	0.109	0.106	0.104	2.6	0.429	0.411	4.2	2.63	2.64	0.6
13SOS14	21. 5. 2013	8.95	*BDL*	2.53	2.28	0.008	0.020	0.242	0.107	0.108	0.107	0.8	0.420	0.419	0.3	2.66	2.71	2.0
13SOS15	30. 5. 2013	8.94	0.599	2.67	2.41	0.007	0.020	0.242	0.106	0.106	0.106	0.4	0.425	0.401	5.8	2.67	2.79	4.4
13SOS16	5. 6. 2013	8.94	*BDL*	2.59	2.34	0.007	0.020	0.241	0.106	0.108	0.107	0.2	0.405	0.406	0.2	2.67	2.78	4.4
13SOS17	10. 6. 2013	8.86	*BDL*	2.61	2.39	0.009	0.021	0.242	0.107	0.108	0.104	2.8	0.406	0.397	2.1	2.63	2.79	6.3
13SOS18	18. 6. 2013	8.83	0.640	2.53	2.33	0.016	0.019	0.242	0.105	0.108	0.105	2.3	0.402	0.402	0.0	2.65	2.77	4.5
13SOS19	25. 6. 2013	8.83	0.798	2.46	2.27	0.008	0.021	0.241	0.105	0.107	0.102	4.6	0.408	0.402	1.4	2.64	2.72	3.1
13SOS20	2. 7. 2013	8.93	0.369	2.58	2.34	0.007	0.032	0.241	0.104	0.105	0.103	1.9	0.411	0.379	7.7	2.58	2.70	4.5
13SOS21	16. 7. 2013	8.99	*BDL*	2.49	2.23	0.008	0.032	0.242	0.108	0.109	0.106	3.1	0.386	0.397	2.9	2.63	2.69	2.4

Table 3. *Continuation*

Sample code	Date	K	K	% diff	Ca	Ca	% diff	Mg	Mg	% diff	Fe^{2+}	Fe ICP	Fe ICP	% diff	Al	Al	% diff	mixing fraction	mixing fraction
concentration		mmol/L	mmol/L		mmol/L	mmol/L		mmol/L	mmol/L		µmol/L	µmol/L	µmol/L		µmol/L	µmol/L		SF_6	SF_5CF_3
DL/RL		1.14 µmol/L	0.2 µmol/L		0.03 µmol/L	70 µmol/L		0.21 µmol/L	70 µmol/L			0.36 µmol/L	107 µmol/L		0.37 µmol/L	107 µmol/L			
method		*(ICP-OES)*	*(ICP-OES)*		*(ICP-OES)*	*(ICP-OES)*		*(ICP-OES)*	*(ICP-OES)*		*IC*	*(ICP-OES)*	*(ICP-OES)*		*(ICP-OES)*	*(ICP-SFMS)*			
11KGM03	21.1.2011	0.018	0.018	1.0	0.036	0.036	1.6	0.002	*BRL*		n.a.	*BDL*	0.041		2.43	2.59	6.4		
11KGM08	5.7.2011	0.017	0.017	0.1	0.040	0.039	1.7	0.002	*BRL*		n.a.	*BDL*	0.036		2.25	2.19	2.9		
11KGM14	28.10.2011	0.017	0.019	8.0	0.043	0.044	1.2	0.003	*BRL*		n.a.	*BDL*	0.048		2.19	2.22	1.6		
12KGM01	25.1.2012	0.018	0.018	1.5	0.052	0.052	0.4	0.005	0.005		n.a.	*BDL*	0.061		2.08	2.12	1.9	0.0001	
12KGM02	27.1.2012	0.018	0.018	1.1	0.052	0.052	0.1	0.005	0.005	4.7	n.a.	*BDL*	0.032		2.03	2.09	3.0		
12KGM04	31.1.2012	0.018	0.018	1.8	0.057	0.058	0.7	0.007	0.007	4.6	n.a.	*BDL*	0.030		2.00	2.00	0.1	0.0020	
12KGM05	3.2.2012	0.018	0.017	2.0	0.062	0.061	0.6	0.009	0.008	6.5	n.a.	*BDL*	0.032		1.96	1.99	1.6		
12KGM07	6.2.2012	0.018	0.017	7.5	0.089	0.089	0.7	0.020	0.019	3.6	n.a.	*BDL*	0.048		1.82	1.88	2.9		
12KGM08	9.2.2012	0.018	0.018	2.0	0.136	0.135	0.8	0.036	0.035	2.2	n.a.	*BDL*	0.134		1.71	1.69	1.2	0.0209	
12KGM10	13.2.2012	0.019	0.017	10.5	0.168	0.161	3.8	0.043	0.040	6.2	n.a.	0.380	0.376	1.0	1.80	1.89	5.4	0.0030	
12KGM11	16.2.2012	0.019	0.018	2.3	0.195	0.202	3.3	0.051	0.050	3.2	n.a.	0.976	1.017	4.2	1.63	1.74	6.4		
12KGM13	17.2.2012	0.019	0.021	7.7	0.227	0.236	4.0	0.059	0.058	2.4	4.001	4.132	4.226	2.3	1.46	1.65		0.0217	
12KGM14	18.2.2012	0.019	0.019	1.3	0.242	0.248	2.1	0.062	0.060	4.0	7.621	8.063	8.130	0.8	1.43	1.53	7.6	0.0358	
12KGM15	19.2.2012	0.020	0.019	1.2	0.249	0.255	2.3	0.062	0.060	3.0	13.326	14.25	14.16	0.6	1.39	1.56			
12KGM16	20.2.2012	0.020	0.021	7.0	0.257	0.264	3.1	0.064	0.063	1.6	17.153	17.79	18.44	3.7	1.15	1.21	5.5		
12KGM17	23.2.2012	0.020			0.275			0.067			34.831	36.70			1.01			0.0686	
12KGM19	27.2.2012	0.021	0.022	2.5	0.239	0.245	2.5	0.058	0.057	2.1	13.184	15.17	15.42	1.6	1.29	1.34	3.4		
12KGM20	28.2.2012	0.021			0.235			0.057			11.836	13.64			1.23			0.0607	
12KGM22	2.3.2012	0.020	0.021	3.4	0.300	0.307	2.3	0.072	0.071	1.3	25.899	27.15	27.58	1.6	0.97	1.00	3.0	0.0707	
12KGM23	5.3.2012	0.021			0.342			0.082			33.141	32.60			0.90			0.0634	
12KGM25	8.3.2012	0.020	0.021	2.0	0.360	0.369	2.6	0.086	0.086	0.9	21.230	21.74	20.59	5.3	0.92	1.00	8.5	0.0611	
12KGM27	12.3.2012	0.021	0.020	3.3	0.360	0.369	2.6	0.086	0.084	2.9	28.424	29.07	28.65	1.4	0.84	0.86	1.4	0.0908	
12KGM28	15.3.2012	0.021	0.022	4.0	0.378	0.389	2.9	0.090	0.090	0.5	36.813	35.33	35.99	1.9	0.94	0.90	3.4	0.0815	
12KGM30	19.3.2012	0.021	0.022	2.9	0.387	0.402	3.9	0.094	0.095	1.2	30.187	30.23	32.77	8.4	1.00	1.09	9.3	0.1178	
12KGM31	22.3.2012	0.021	0.022	1.8	0.383	0.397	3.5	0.094	0.094	0.6	24.909	25.00	26.68	6.7	1.02	1.05	2.1	0.0851	
12KGM33	26.3.2012	0.021			0.406			0.101			19.694	19.97			1.01				
12KGM34	29.3.2012	0.021	0.022	3.0	0.391	0.402	2.8	0.098	0.097	1.4	13.165	13.15	13.57	3.2	1.04	1.11	6.5	0.1271	
12KGM36	2.4.2012	0.021			0.367			0.092			8.252	8.449			1.13				
12KGM37	4.4.2012	0.021			0.354			0.088			6.787	6.877			1.19			0.0872	
12KGM39	7.4.2012	0.021	0.021	1.3	0.350	0.357	1.9	0.087	0.086	1.3	5.381	5.444	5.551	2.0	1.25				
12KGM40	10.4.2012	0.020			0.349			0.088			4.682	4.568			1.25				
12KGM41	11.4.2012	0.021			0.337			0.084			5.006	5.786			1.24			0.0927	
12KGM42	12.4.2012	0.021	0.021	1.6	0.372	0.379	2.0	0.094	0.094	0.0	5.165	5.084	5.265	3.6	1.35	1.40	3.8		
12KGM43	16.4.2012	0.021			0.304			0.075			2.563	2.199			1.48			0.0710	
12KGM44	18.4.2012	0.021			0.299			0.074			2.510	2.155			1.49				
12KGM46	23.4.2012	0.021	0.022	2.2	0.283	0.292	3.1	0.070	0.070	1.1	2.313	2.048	2.095	2.3	1.55	1.67	8.0	0.0759	
12KGM47	27.4.2012	0.020			0.266			0.066			3.871	4.147			0.85				
12KGM49	4.5.2012	0.021			0.162			0.036			n.a.	*BDL*			1.72				
12KGM51	7.5.2012	0.021	0.020	2.2	0.225	0.233	3.5	0.055	0.054	1.7	n.a.	*BDL*	0.238		1.60	1.88			
12KGM52	10.5.2012	0.021			0.232			0.057			n.a.	*BDL*			1.61				
12KGM54	14.5.2012	0.020			0.219			0.056			n.a.	0.504			0.61				
12KGM55	18.5.2012	0.021	0.021	2.2	0.194	0.205	5.4	0.046	0.046	1.8	n.a.	*BDL*	0.111		1.68	1.84	9.5	0.0654	
12KGM57	21.5.2012	0.021			0.212			0.052			n.a.	*BDL*			1.70			0.0596	
12KGM58	24.5.2012	0.021			0.213			0.052			n.a.	*BDL*			1.71			0.0496	
12KGM60	30.5.2012	0.021	0.021	4.0	0.219	0.233	6.7	0.054	0.052	3.3	n.a.	*BDL*	0.057		1.71			0.0763	
12KGM61	1.6.2012	0.021			0.221			0.054			n.a.	*BDL*			1.71			0.0759	
12KGM63	4.6.2012	0.021			0.225			0.054			n.a.	*BDL*			1.74				
12KGM64	8.6.2012	0.021	0.020	4.5	0.229	0.231	0.8	0.056	0.053	4.0	n.a.	*BDL*	0.048		1.74	1.86	6.8	0.0986	
12KGM66	11.6.2012	0.021			0.226			0.054			n.a.	*BDL*			1.72			0.1004	
12KGM67	14.6.2012	0.021	0.021	0.0	0.239	0.246	3.0	0.059	0.057	2.5	n.a.	*BDL*	0.063		1.80				
12KGM68	18.6.2012	0.021			0.238			0.059			n.a.	*BDL*			1.81			0.0985	
12KGM69	20.6.2012	0.021			0.244			0.060			1.832	*BDL*			1.76			0.1087	

Table 4. *Continuation*

Sample code	Date	K	K	% diff	Ca	Ca	% diff	Mg	Mg	% diff	Fe^{2+}	Fe ICP	Fe ICP	% diff	Al	Al	% diff	mixing fraction	mixing fraction
concentration		mmol/L	mmol/L		mmol/L	mmol/L		mmol/L	mmol/L		µmol/L	µmol/L	µmol/L		µmol/L	µmol/L		SF_6	SF_5CF_3
DL/RL		1.14 µmol/L	0.2 µmol/L		0.03 µmol/L	70 µmol/L		0.21 µmol/L	70 µmol/L			0.36 µmol/L	07 µmol/L		0.37 µmol/L	07 µmol/L			
method		*(ICP-OES)*	*(ICP-OES)*		*(ICP-OES)*	*(ICP-OES)*		*(ICP-OES)*	*(ICP-OES)*		*IC*	*(ICP-OES)*	*(ICP-OES)*		*(ICP-OES)*	*(ICP-SFMS)*			
12SOS01	28.6.2012	0.021	0.020	3.6	0.298	0.289	2.9	0.073	0.070	3.4	2.964	3.267	3.331	2.0	1.65	1.675	1.8	0.1489	
12SOS02	3.7.2012	0.021	0.020	3.9	0.275	0.267	2.8	0.065	0.060	8.1	3.133	1.111	1.142	2.8	1.74	1.716	1.3		0.00119
12SOS04	5.7.2012	0.021	0.020	5.8	0.265	0.262	1.1	0.062	0.060	2.2	1.422	*BDL*	0.399		1.74	1.646	5.4	0.1425	0.00098
12SOS05	7.7.2012	0.022			0.285			0.069			2.578	0.472			1.79				0.00096
12SOS06	9.7.2012	0.022	0.021	4.7	0.291	0.287	1.3	0.070	0.068	2.2	1.470	*BDL*	0.369		1.82	1.731	5.0	0.1387	0.00111
12SOS07	12.7.2012	0.022	0.021	5.1	0.292	0.287	1.8	0.070	0.067	3.7	1.373	0.393	0.381	2.9	1.82	1.720	5.7		0.00104
12SOS09	17.7.2012	0.021	0.023	5.3	0.273	0.267	2.2	0.064	0.060	5.8	1.373	*BDL*	0.374		1.82	1.749	3.7	0.1524	0.00097
12SOS10	19.7.2012	0.022	0.021	1.3	0.282	0.287	1.8	0.067	0.067	0.8	1.518	0.586			1.75	1.786	1.8		0.00094
12SOS12	24.7.2012	0.022	0.022	0.1	0.307	0.314	2.2	0.073	0.075	2.8	1.639	0.927			1.83	1.772	3.2		0.00103
12SOS13	26.7.2012	0.021	0.021	0.5	0.294	0.292	0.5	0.070	0.067	4.3	1.386	*BDL*	0.396		1.84	1.838	0.1	0.1541	0.00138
12SOS15	31.7.2012	0.021	0.021	2.0	0.283	0.277	2.0	0.066	0.064	3.4	1.337	*BDL*	0.260		1.82	1.720	5.3		0.00107
12SOS16	2.8.2012	0.021	0.021	2.2	0.296	0.297	0.5	0.070	0.070	0.4	1.422	0.447			1.82	1.735	4.7		0.00109
12SOS18	7.8.2012	0.022	0.022	1.3	0.305	0.317	4.0	0.073	0.074	2.6	1.964	1.449			1.72	1.620	6.0		0.00115
12SOS19	9.8.2012	0.022	0.022	0.5	0.332	0.334	0.6	0.079	0.079	0.2	4.349	5.316	5.551	4.4	1.61	1.505	6.3		0.00115
12SOS21	14.8.2012	0.022	0.023	0.4	0.358	0.369	3.1	0.086	0.088	2.1	7.916	9.706	10.332	6.4	1.60	1.531	4.4		0.00165
12SOS23	16.8.2012	0.022	0.022	3.2	0.374	0.364	2.5	0.090	0.088	3.0	7.181	9.034	9.132	1.1	1.65	1.516	8.3	0.1623	0.00183
12SOS25	21.8.2012	0.021	0.023	5.5	0.347	0.354	2.2	0.083	0.084	1.1	4.747	5.145	5.461	6.2	1.70	1.701	0.3		0.00192
12SOS26	23.8.2012	0.022	0.022	1.4	0.340	0.337	1.0	0.082	0.080	1.6	4.000	3.918	4.029	2.8	1.72	1.742	1.0		0.00152
12SOS28	28.8.2012	0.022	0.022	0.3	0.329	0.327	0.5	0.079	0.077	1.7	2.181	1.851	1.952	5.5	1.75	1.697	3.2	0.2060	0.00156
12SOS29	31.8.2012	0.024	0.021	10.1	0.321	0.304	5.0	0.076	0.071	5.8	1.916	1.147	1.096	4.4	1.84	1.823	1.1	0.2224	0.00123
12SOS31	4.9.2012	0.023	0.023	2.6	0.331	0.322	2.7	0.078	0.075	3.2	1.651	0.795	0.783	1.6	1.78	1.712	4.0		0.00121
12SOS32	6.9.2012	0.023	0.022	6.3	0.317	0.307	3.3	0.076	0.072	5.2	1.494	*BDL*	0.634		1.85	1.709	7.4	0.2243	0.00118
12SOS33	13.9.2012	0.022			0.300			0.070			1.349	*BDL*			1.83				0.00115
12SOS33B	17.9.2012	0.026	0.026	1.7	0.309	0.317	2.4	0.072	0.073	1.7	n.a.	*BDL*	0.144		1.79	1.712	4.5	0.2438	0.00105
12SOS34	24.9.2012	0.030	0.027	8.5	0.302	0.289	4.3	0.069	0.066	4.0	1.337	*BDL*	0.089		1.84	1.757	4.6		0.00101
12SOS35	1.10.2012	0.026	0.024	7.1	0.297	0.284	4.3	0.068	0.065	4.8	1.349	*BDL*	0.073		1.85	1.820	1.7	0.2730	0.00090
12SOS36	8.10.2012	0.023	0.021	6.8	0.268	0.252	6.0	0.060	0.056	7.6	n.a.	*BDL*	0.066		2.06	2.250	9.4	0.2751	0.00105
12SOS38	22.10.2012	0.022	0.021	5.2	0.264	0.246	6.8	0.059	0.056	5.9	1.337	*BDL*	0.082		2.00	2.087	4.5	0.2987	0.00093
12SOS39	29.10.2012	0.023			0.276			0.062			n.a.	*BDL*			1.98			0.3170	
12SOS40	14.11.2012	0.022	0.022	2.5	0.269	0.252	6.4	0.061	0.056	7.5	1.349	*BDL*	0.172		1.98	2.072	4.8	0.3226	0.00087
12SOS41	26.11.2012	0.023	0.021	9.4	0.255	0.237	7.0	0.058	0.053	8.2	n.a.	*BDL*	0.052		1.90	2.024	6.5	0.3120	0.00109
12SOS42	10.12.2012	0.023	0.022	5.1	0.206	0.201	2.5	0.048	0.046	4.2	1.361	*BDL*	0.045		2.02	1.931	4.5	0.3458	0.00110
12SOS43	20.12.2012	0.023	0.023	1.8	0.191	0.197	2.8	0.045	0.046	2.8	1.349	*BDL*	0.050		2.22	2.109	4.8	0.3684	0.00108
13SOS01	7.1.2013	0.023	0.022	3.4	0.171	0.169	1.1	0.042	0.042	0.7	n.a.	*BDL*	0.049		2.06	2.009	2.3	0.3765	0.00105
13SOS02	25.1.2013	0.024	0.022	5.1	0.265	0.255	4.1	0.057	0.055	3.0	n.a.	*BDL*	0.106		1.94	1.846	4.7	0.3797	0.00114
13SOS04	12.2.2013	0.025	0.024	1.3	0.258	0.255	1.4	0.055	0.053	2.7	1.361	*BDL*	0.215		1.96	2.031	3.7	0.4019	0.00132
13SOS06	4.3.2013	0.024	0.022	7.4	0.296	0.277	6.4	0.061	0.058	5.7	n.a.	*BDL*	0.184		1.90	1.909	0.4	0.4079	0.00168
13SOS07	21.3.2013	0.023	0.022	3.3	0.197	0.189	4.1	0.042	0.039	7.1	1.361	*BDL*	0.072		2.20	2.205	0.1	0.4316	0.00218
13SOS08	3.4.2013	0.022	0.023	2.4	0.175	0.168	4.0	0.038	0.036	5.7	n.a.	*BDL*	0.047		2.19	2.120	3.3	0.4084	0.00259
13SOS09	11.4.2013	0.023	0.022	3.7	0.199	0.191	3.9	0.043	0.040	6.4	n.a.	*BDL*	0.057		2.10	1.953	7.1	0.4663	0.00252
13SOS10	16.4.2013	0.022	0.023	1.4	0.180	0.178	1.1	0.039	0.038	2.6	n.a.	*BDL*	0.042		2.17	2.012	7.3	0.4188	0.00218
13SOS11	29.4.2013	0.023	0.022	5.4	0.157	0.148	5.7	0.035	0.034	5.2	n.a.	*BDL*	0.046		2.31	2.339	1.2	0.3801	0.00281
13SOS12	7.5.2013	0.023	0.022	7.0	0.144	0.136	5.3	0.034	0.031	7.9	n.a.	*BDL*	0.054		2.42	2.576	6.4	0.3695	0.00264
13SOS13	14.5.2013	0.022	0.021	4.4	0.152	0.140	7.6	0.035	0.033	7.8	n.a.	*BDL*	0.054		2.29	2.227	2.5	0.3764	
13SOS14	21.5.2013	0.023	0.022	3.8	0.142	0.132	6.6	0.033	0.031	7.5	n.a.	*BDL*	0.038		2.34	2.250	3.9	0.3643	0.00257
13SOS15	30.5.2013	0.023	0.022	4.1	0.189	0.181	4.6	0.042	0.039	6.7	n.a.	*BDL*	0.051		2.07	1.998	3.3	0.3391	
13SOS16	5.6.2013	0.023	0.022	3.4	0.174	0.164	5.6	0.039	0.036	7.0	n.a.	*BDL*	0.049		2.12	2.309	8.8	0.3757	0.00247
13SOS17	10.6.2013	0.022	0.022	1.9	0.178	0.167	6.2	0.040	0.037	6.9	n.a.	*BDL*	0.090		2.05	2.265	10.7	0.3770	
13SOS18	18.6.2013	0.021	0.021	1.5	0.133	0.124	7.0	0.026	0.024	7.1	n.a.	*BDL*	0.038		2.38	2.198	7.5	0.2975	0.00322
13SOS19	25.6.2013	0.022	0.020	5.7	0.111	0.102	7.5	0.022	0.020	9.8	n.a.	*BDL*	0.033		2.36	2.402	1.7		
13SOS20	2.7.2013	0.021	0.022	4.1	0.156	0.146	6.0	0.032	0.030	7.0	n.a.	*BDL*	0.044		2.21	2.365	6.9	0.3855	0.00324
13SOS21	16.7.2013	0.021	0.021	2.3	0.128	0.120	6.3	0.030	0.027	9.8	n.a.	*BDL*	0.023		2.13	2.068	3.0	0.4038	0.00295

Appendix C

Concentrations of trace metals prior to, during, and after the CO_2 and CO_2-H_2S-injections at Hellisheidi, 2012

Unpublished data to be compiled by SOS

Trace metal concentration prior to, during, and after the injections of CO_2 and CO_2-H_2S gas mixture at Hellisheidi in 2012

The reaction between the CO_2-charged water and the basaltic rocks not only releases divalent cations that end up in carbonates, but also other metals that can be harmful for the biota. At low pH the dissolution rates of basaltic glass and primary basaltic minerals is relatively fast (e.g. Gislason and Oelkers, 2003; Gudbrandsson et al., 2011; Oelkers and Gislason, 2001), and the solubility of many secondary minerals constraining the mobility of toxic metals is higher than at elevated pH.

The metals of main concern are Al and Cr, but some other elements, such as Mn, can be both essential for life and toxic depending on their concentration. The toxic metal release is critical at the early stage of the injection of CO_2, before the pH is raised again by water-rock interaction (Flaathen et al., 2009; Galeczka et al., 2013). This is before significant precipitation of carbonates and other minerals that effectively scavenge the potential toxic metals that are released at early stages (Olsson et al., 2014).

Even though water from the lower groundwater system at the CarbFix site, which is affected by the injections, is not meant for consumption it is important to evaluate the effect of the injections on the groundwater. Samples analysed from the monitoring well HN-04, which is situated closest to the injection well, sampled before, during and after both injection experiments show increase in Ba, Cr, Cu,Fe, Mn and Pb which are all elements that can affect quality of drinking water, but no metals exceeded the health-based

values allowed for drinking water, derived by the World Health Organization (WHO) (World Health Organization, 2011).

Iron (Fe) concentrations in samples taken during both injection experiments exceed values proposed by the European Commission (European Commission, 1998) that may affect acceptability of drinking water. Fe is an essential element in human nutrition. The taste and appearance of drinking water will usually be affected below the level for tolerable intake (World Health Organization, 2003). Consumption of water from well HN-04 should therefore not be harmful for consumption, but high Fe concentrations during injections could affect taste and appearance.

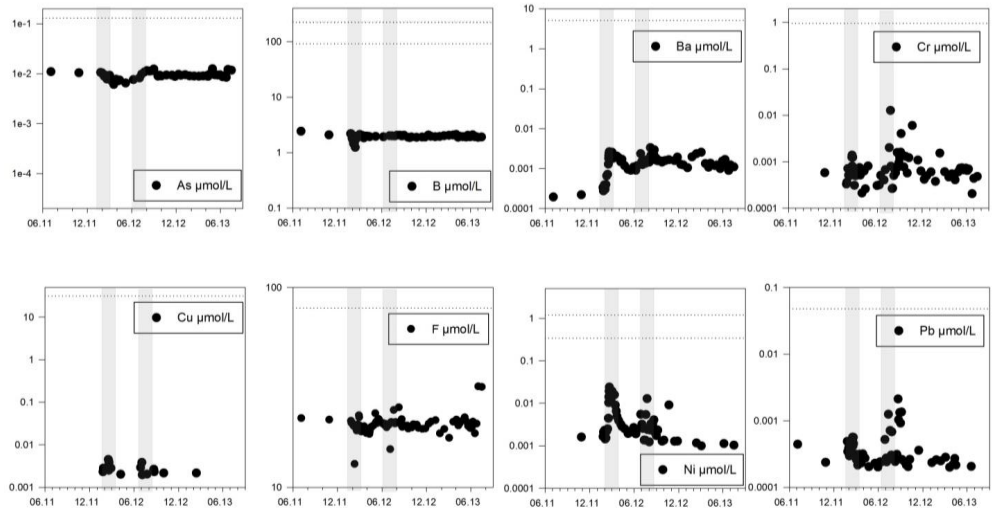

Figure 1. *Concentrations of elements of health concern in drinking water measured in samples from well HN-4 before, during and after the two injections. Allowed drinking water concentrations from WHO and EU are depicted with a dotted line. In case of two lines, the lower line represents EU limitations and the higher one WHO limits. Cd and Hg concentrations are not depicted since these elements were below detection limits of the ICP-MS in almost all samples.*

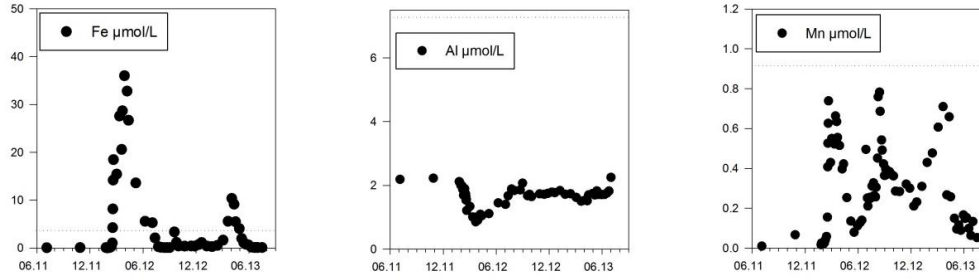

Figure 2. *Concentrations of Fe, Al, and Mn in samples from well HN-04 prior to, during, and after the two injections. Limits proposed by EU are depicted as dotted lines.*

Fe) *No guideline value for iron in drinking-water is proposed by WHO since* ***iron is not of health concern at levels found in drinking water****. The taste and appearance can be affected which may affect the acceptability. EU proposes a limit of 3.6 µmol/L.* ***This is the only limit that the samples taken during the injections exceed.***

Al) *No guideline value for aluminium is proposed by WHO. A health-based value of 33 µmol/L could be derived, but this value exceeds practicable levels based on optimization of the coagulation process in drinking-water plants using aluminium based coagulants: 3.7 µmol/L or less in large water treatment facilities and 7.4 µmol/L or less in small facilities. EU proposes a limit of 7.4 µmol/L.*

Mn) *WHO proposes a limit of 7.3 µmol/L, but state that value of 9.1 µmol/L should be adequate to protect public health. It is also noted that concentrations below 1.8 µmol/L are usually acceptable to consumers, although this may vary with local circumstances. EU proposes a limit of 0.9 µmol/L.*

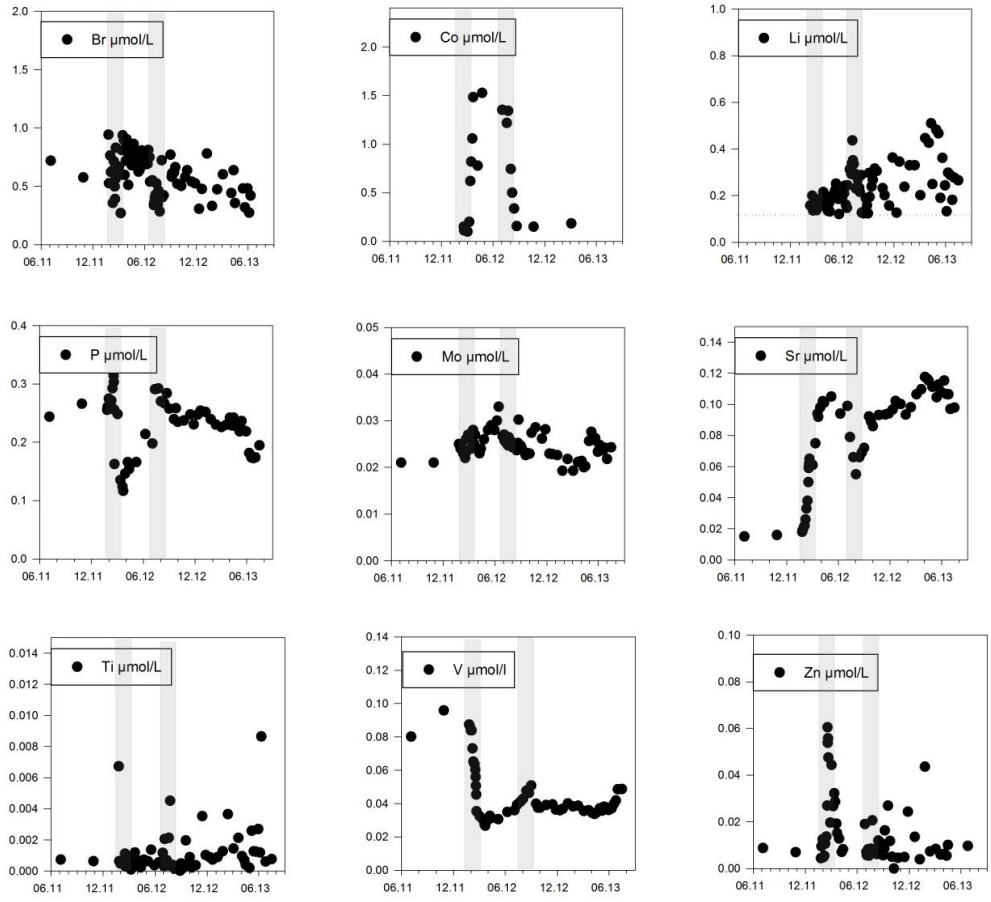

Figure 3. *Trace metal concentrations in samples from well HN-04 prior to, during and after the two injections, Detection limits depicted as a dotted line when applicable.*

Table 1. *Allowed drinking water concentrations from WHO and EU and highest concentrations measured in samples from HN-04 taken before, during and after the pure CO_2-injection in January-March 2012 and the mixed gas injection in June-August 2012.*

Element	World Health Organization	European Union	Phase I	Phase II	Analytical Method
	nmol/l	*nmol/l*	*nmol/l*	*nmol/l*	
Arsenic	130	130	12	13	ICP-MS
Barium	5100	-	3	3	ICP-MS
Cadmium	27	44	0.1	0.1	ICP-MS
Chromium	960	960	10	72	ICP-MS
Copper	31500	31500	4	4	ICP-MS
Lead	48	48	1	2	ICP-MS
Mercury	30	5	0.1	0.5	ICP-MS
Nickel	1190	340	20	10	ICP-MS
	µmol/l	*µmol/l*	*µmol/l*	*µmol/l*	
Fluoride	79.0	79.0	31.0	21.0	IC-2000
Boron (µmol/L)	222	92	2.43	2.18	ICP-MS
Manganese	*	*	*0.78*	*1.06*	ICP-OES
Iron	*	*	*36.70*	*9.71*	ICP-OES
Aluminium	**	*	*3.05*	*3.92*	ICP-OES

*Not of health concern at levels found in drinking-water. May affect acceptability of drinking-water

**A health-based value of 0.9 mg/l could be derived, but this value exceeds practicable levels based on optimization of the coagulation process in drinking-water plants using aluminium based coagulants: 0.1 mg/l or less in large water treatment facilities and 0.2 mg/l or less in small facilities

Table 1. *Trace metal concentrations in samples collected prior to, during, and after the CO_2 and CO_2-H_2S-gas mixture injections in Hellisheidi in 2012. The samples were analysed at the University of Iceland, and ALS, Sweden. The methods are described in Snæbjörnsdóttir et al. (2017).*

Sample code	Date	pH	H_2S	Alk.	DOC	DIC	P	Al	Al	% diff	Fe ICP	Fe ICP	% diff	B	B	% diff	Mn	Mn	% diff
			µmole/l	mmole/l	mmole/l	µmole/l	µmole/l	µmole/l	µmole/l		µmole/l	µmole/l		µmole/l	µmole/l		µmole/l	µmole/l	
			(0.29 µmol/l)				*(0.03 µmole/l)*	*(0.37 µmol/l)*	*(0.007 µmole/l)*		*(0.36 µmol/l)*	*(0.007 µmole/l)*		*(0.92 µmol/l)*	*(0.92 µmol/l)*		*(0.11 µmol/kg)*	*(0.001 µmole/l)*	
			(titr.)	*(titr.)*		*(PhreeqC)*	(ICP-SFMS)	(ICP-OES)	(ICP-SFMS)		(ICP-OES)	(ICP-OES)		(ICP-OES)	(ICP-OES)		(ICP-OES)	(ICP-AES)	
11KGM03	21.1.2011	9.56		1.91	0.020	1.36	0.262	2.432	2.587	6.4		0.041		2.08	2.28	9.9		0.008	
11KGM08	5.7.2011	9.58		1.87	0.049	1.32	0.244	2.251	2.187	2.9		0.036		1.76	2.43	38.1		0.010	
11KGM14	28.10.2011	9.44		1.88	0.039	1.43	0.266	2.189	2.224	1.6		0.048		1.66	2.09	26.0		0.067	
12KGM01	25.1.2012	9.24		1.87	0.052	1.54	0.255	2.077	2.116	1.9		0.061		1.69	2.19	29.5		0.017	
12KGM02	27.1.2012	9.32		1.87	0.036	1.50	0.261	2.028	2.090	3.0		0.032		1.63	2.18	34.1		0.025	
12KGM04	31.1.2012	9.38	0.499	1.89	0.052	1.47	0.275	1.996	1.998	0.1		0.030		1.68	1.80	7.1		0.020	
12KGM05	3.2.2012	9.27	0.329	1.88	0.050	1.54	0.271	1.963	1.994	1.6		0.032		1.55	1.70	9.7		0.021	
12KGM07	6.2.2012	9.2	0.449	1.97	0.031	1.65	0.266	1.822	1.875	2.9		0.048		1.72	1.45	15.5		0.026	
12KGM08	9.2.2012	8.98		2.09	0.042	1.87	0.272	1.710	1.690	1.2		0.134		1.66	1.45	12.3		0.042	
12KGM10	13.2.2012	8.86		2.20	0.032	2.01	0.293	1.797	1.894	5.4	0.380	0.376	1.0	1.79	1.25	30.3		0.058	
12KGM11	16.2.2012	7.94		2.31	0.030	2.32	0.319	1.631	1.735	6.4	0.976	1.017	4.2	1.74	1.99	14.2	0.147	0.155	5.6
12KGM13	17.2.2012	7.46		2.39	0.027	2.53	0.314	1.464	1.646	12.4	4.132	4.226	2.3	1.71	1.90	10.8	0.389	0.408	4.9
12KGM14	18.2.2012	7.27		2.40	0.024	2.63	0.303	1.425	1.534	7.6	8.063	8.130	0.8	1.78	1.79	0.3	0.518	0.526	1.6
12KGM15	19.2.2012	7.04		2.48	0.027	2.90	0.256	1.389	1.557	12.1	14.251	14.164	0.6	1.92	1.91	0.8	0.640	0.626	2.2
12KGM16	20.2.2012	6.95		2.51	0.023	3.04	0.163	1.149	1.212	5.5	17.786	18.444	3.7	2.01	1.97	1.8	0.715	0.739	3.4
12KGM17	23.2.2012	6.93		2.61	0.024	3.18		1.008			36.696			2.26			0.783		
12KGM19	27.2.2012	7.18		2.54	0.027	2.85	0.248	1.293	1.338	3.4	15.168	15.417	1.6	2.16	2.13	1.4	0.419	0.430	2.6
12KGM20	28.2.2012	6.98		2.48	0.026	2.97		1.227			13.640			2.05			0.402		
12KGM22	2.3.2012	6.91		2.65	0.027	3.26	0.135	0.975	1.004	3.0	27.147	27.576	1.6	2.17	2.04	5.6	0.537	0.550	2.4
12KGM23	5.3.2012	6.81		2.79	0.032	3.60		0.905			32.602			2.16			0.598		
12KGM25	8.3.2012	6.79		2.78	0.021	3.63	0.124	0.923	1.001	8.5	21.743	20.592	5.3	1.97	1.85	6.1	0.514	0.528	2.8
12KGM27	12.3.2012	6.63		2.84	0.025	4.10	0.117	0.844	0.856	1.4	29.071	28.650	1.4	2.13	1.91	10.3	0.574	0.522	9.0
12KGM28	15.3.2012	6.57		2.91	0.025	4.39	0.146	0.936	0.904	3.4	35.328	35.992	1.9	2.28	1.99	12.7	0.632	0.663	4.8
12KGM30	19.3.2012	6.64		2.92	0.025	4.18	0.166	0.997	1.090	9.3	30.235	32.769	8.4	2.22	1.97	11.3	0.623	0.635	2.0
12KGM31	22.3.2012	6.68		2.89	0.022	4.03	0.154	1.024	1.045	2.1	24.997	26.681	6.7	2.15	1.93	10.0	0.579	0.555	4.2
12KGM33	26.3.2012	6.71		2.93	0.020	4.00		1.014			19.965			2.15			0.566		
12KGM34	29.3.2012	6.81		2.83	0.025	3.65	0.166	1.044	1.112	6.5	13.154	13.573	3.2	1.94	1.96	1.0	0.500	0.515	3.1
12KGM36	2.4.2012	6.96		2.76	0.025	3.32		1.126			8.449			1.85			0.436		
12KGM37	4.4.2012	7.06		2.75	0.025	3.19		1.188			6.877			1.89			0.413		
12KGM39	7.4.2012	7.14		2.71	0.021	3.07	0.214	1.255	1.449	15.5	5.444	5.551	2.0	1.96	1.92	1.6	0.389	0.397	1.9
12KGM40	10.4.2012	7.17	0.300	2.70	0.022	3.03		1.249			4.568			1.82			0.372		
12KGM41	11.4.2012	7.22		2.77	0.035	3.07		1.236			5.786			1.86			0.386		
12KGM42	12.4.2012	7.2		2.83	0.019	3.15	0.198	1.349	1.401	3.8	5.084	5.265	3.6	1.94	2.02	4.1	0.402	0.422	5.1
12KGM43	16.4.2012	7.63		2.65	0.017	2.74		1.477			2.199			1.83			0.274		
12KGM44	18.4.2012	7.7		2.58	0.019	2.65		1.494			2.155			1.93			0.272		
12KGM46	23.4.2012	7.92		2.59	0.018	2.61	0.291	1.549	1.672	8.0	2.048	2.095	2.3	1.90	2.01	5.9	0.241	0.253	5.1
12KGM47	27.4.2012	8.15		2.56	0.023	2.54		0.850			4.147			1.92			0.359		
12KGM49	4.5.2012	9		2.32	0.019	2.06		1.718						2.01					
12KGM51	7.5.2012	8.71		2.44	0.028	2.29	0.292	1.601	1.883			0.238		1.95	2.00	2.4	0.128	0.135	5.8
12KGM52	10.5.2012	8.67		2.45	0.020	2.31		1.611						1.97			0.138		
12KGM54	14.5.2012	8.65		2.45	0.019	2.32		0.607			0.504			2.07			0.151		
12KGM55	18.5.2012	8.92		2.38	0.014	2.15	0.270	1.678	1.838	9.5		0.111		1.98	2.06	4.0		0.080	
12KGM57	21.5.2012	8.81		2.44	0.011	2.25		1.700						2.00					
12KGM58	24.5.2012	8.76		2.39	0.017	2.22		1.711						2.01					
12KGM60	30.5.2012	8.81		2.43	0.010	2.24	0.267	1.712				0.057		2.00	2.06	3.0		0.112	
12KGM61	1.6.2012	8.76	0.519	2.39	0.012	2.22		1.712						1.93					
12KGM63	4.6.2012	8.84		2.43	0.015	2.23		1.744						1.92					
12KGM64	8.6.2012	8.82		2.46	0.012	2.27	0.284	1.739	1.857	6.8		0.048		1.91	2.00	4.8	0.114	0.128	12.2
12KGM66	11.6.2012	8.78		2.48	0.015	2.30		1.724						1.98			0.112		
12KGM67	14.6.2012	8.78		2.47	0.013	2.29	0.258	1.796	2.068	15.2		0.063		1.94	2.06	6.3	0.123	0.140	13.6
12KGM68	18.6.2012	8.68		2.58	0.010	2.43		1.811						1.94			0.120		
12KGM69	20.6.2012	8.62		2.63	0.009	2.50		1.764						1.87			0.134		
12SOS01	28.6.2012	7.36		2.79	0.017	3.00	0.240	1.645	1.675	1.8	3.267	3.331	2.0	1.95	1.90	2.9	0.503	0.495	1.6
12SOS02	3.7.2012	8.11	1.502	2.57	0.010	2.55	0.258	1.738	1.716	1.3	1.111	1.142	2.8	1.92	1.87	2.8	0.256	0.251	2.0

Table 2. *Continuation*

Sample code	Date	pH	H_2S	Alk.	DOC	DIC	P	Al	Al	% diff	Fe ICP	Fe ICP	% diff	B	B	% diff	Mn	Mn	% diff
			µmole/l	mmole/l	mmole/l	µmole/l	µmole/l	µmole/l	µmole/l		µmole/l	µmole/l		µmole/l	µmole/l		µmole/l	µmole/l	
			(0.29 µmol/l)				*(0.03 µmole/l)*	*(0.37 µmol/l)*	*(0.007 µmole/l)*		*(0.36 µmol/l)*	*(0.007 µmole/l)*		*(0.92 µmol/l)*	*(0.92 µmol/l)*		*(0.11 µmol/kg)*	*(0.001 µmole/l)*	
			(titr.)	*(titr.)*		*(PhreeqC)*	(ICP-SFMS)	(ICP-OES)	(ICP-SFMS)		(ICP-OES)	(ICP-OES)		(ICP-OES)	(ICP-OES)		(ICP-OES)	(ICP-AES)	
12SOS04	5.7.2012	8.43	1.129	2.75	0.014	2.66	0.235	1.739	1.646	5.4		0.399		1.91	1.91	0.4	0.209	0.211	1.1
12SOS05	7.7.2012	8.3		2.78	0.014	2.72		1.786			0.472			1.89			0.244		
12SOS06	9.7.2012	8.36		2.64	0.012	2.57	0.237	1.821	1.731	5.0		0.369		1.96	1.89	4.0	0.242	0.246	1.4
12SOS07	12.7.2012	8.33	0.898	2.62	0.011	2.56	0.248	1.823	1.720	5.7	0.393	0.381	2.9	1.87	1.91	2.1	0.250	0.255	2.0
12SOS09	17.7.2012	8.28		2.62	0.008	2.57	0.231	1.816	1.749	3.7		0.374		1.86	1.91	2.2	0.250	0.253	1.2
12SOS10	19.7.2012	8.07	0.293	2.63	0.011	2.62	0.247	1.755	1.786	1.8	0.586	0.709	21.1	1.88	2.07	10.3	0.297	0.311	5.0
12SOS12	24.7.2012	7.87		2.72	0.012	2.75	0.254	1.830	1.772	3.2	0.927	1.105	19.2	1.90	1.97	3.8	0.318	0.328	3.0
12SOS13	26.7.2012	8.32		2.67	0.009	2.61	0.252	1.841	1.838	0.1		0.396		1.86	1.93	4.2	0.255	0.264	3.4
12SOS15	31.7.2012	8.41		2.63	0.010	2.55	0.240	1.816	1.720	5.3		0.260		1.90	1.95	2.8	0.256	0.257	0.1
12SOS16	2.8.2012	8.29		2.67	0.011	2.62	0.230	1.821	1.735	4.7	0.447	0.528	18.0	1.86	2.02	8.6	0.297	0.306	2.9
12SOS18	7.8.2012	7.85	0.299	2.72	0.011	2.76	0.226	1.722	1.620	6.0	1.449	1.626	12.2	1.81	2.05	13.1	0.425	0.451	6.2
12SOS19	9.8.2012	7.25		2.78	0.009	3.06	0.230	1.606	1.505	6.3	5.316	5.551	4.4	2.00	2.07	3.6	0.741	0.759	2.4
12SOS21	14.8.2012	7.07	0.299	2.86	0.010	3.31	0.242	1.601	1.531	4.4	9.706	10.332	6.4	2.03	2.13	4.6	0.749	0.783	4.5
12SOS23	16.8.2012	7.13		2.91	0.008	3.30	0.229	1.653	1.516	8.3	9.034	9.132	1.1	2.12	1.90	10.4	0.698	0.686	1.7
12SOS25	21.8.2012	7.45	0.399	2.84	0.014	3.01	0.242	1.697	1.701	0.3	5.145	5.461	6.2	1.99	1.98	0.5	0.524	0.542	3.5
12SOS26	23.8.2012	7.5		2.83	0.013	2.98	0.226	1.724	1.742	1.0	3.918	4.029	2.8	1.90	1.94	2.1	0.484	0.491	1.5
12SOS28	28.8.2012	7.93		2.80	0.019	2.82	0.219	1.753	1.697	3.2	1.851	1.952	5.5	1.87	1.93	3.3	0.418	0.422	1.1
12SOS29	31.8.2012	8.19	0.758	2.77	0.012	2.73	0.236	1.844	1.823	1.1	1.147	1.096	4.4	1.83	1.91	3.9	0.377	0.364	3.4
12SOS31	4.9.2012	8.19	0.898	2.81	0.017	2.77	0.220	1.783	1.712	4.0	0.795	0.783	1.6	1.86	2.05	10.3	0.401	0.397	1.1
12SOS32	6.9.2012	7.94	0.599	2.76	0.012	2.78	0.219	1.846	1.709	7.4		0.634		2.01	1.92	4.4	0.381	0.368	3.6
12SOS33	13.9.2012	7.56		2.72	0.021	2.84		1.834						1.77			0.349		
12SOS33B	17.9.2012	8.23	0.758	2.73	0.018	2.69	0.181	1.794	1.712	4.5		0.144		1.79	2.09	16.6	0.380	0.384	1.0
12SOS34	24.9.2012	8.29		2.71	0.018	2.66	0.174	1.842	1.757	4.6		0.089		1.65	1.93	17.4	0.383	0.370	3.6
12SOS35	1.10.2012	8.3		2.70	0.016	2.64	0.173	1.852	1.820	1.7		0.073		1.82	1.93	5.9	0.343	0.362	5.5
12SOS36	8.10.2012	8.36	0.369	2.64	0.011	2.57	0.174	2.056	2.250	9.4		0.066		1.81	1.89	4.0	0.283	0.286	1.0
12SOS38	22.10.2012	8.4	0.399	2.67	0.014	2.59	0.195	1.996	2.087	4.5		0.082		1.94	1.91	1.2	0.288	0.284	1.5
12SOS39	29.10.2012	8.26	0.399	2.68		2.63		1.976						1.63			0.335		
12SOS40	14.11.2012	8.31	0.399	2.67	0.014	2.61	0.152	1.977	2.072	4.8		0.172		1.62	1.89	16.2	0.321	0.321	0.0
12SOS41	26.11.2012	8.3	0.599	2.67	0.012	2.61	0.180	1.901	2.024	6.5		0.052		1.69	1.95	15.3	0.320	0.300	6.0
12SOS42	10.12.2012	8.31	0.399	2.56	0.012	2.51	0.113	2.021	1.931	4.5		0.045		1.72	2.03	17.6	0.204	0.211	3.8
12SOS43	20.12.2012	8.41	0.399	2.53	0.011	2.45	0.123	2.216	2.109	4.8		0.050		1.96	2.18	11.2	0.213	0.231	8.7
13SOS01	7.1.2013	8.73	0.399	2.53	0.013	2.37	0.126	2.055	2.009	2.3		0.049		1.92	2.08	8.3	0.310	0.310	0.0
13SOS02	25.1.2013	8.58	0.648	2.81	0.011	2.68	0.156	1.936	1.846	4.7		0.106		1.78	1.89	6.0	0.436	0.430	1.5
13SOS04	12.2.2013	8.57		2.80	0.012	2.67	0.143	1.959	2.031	3.7		0.215		1.85	1.95	5.4	0.478	0.477	0.2
13SOS06	4.3.2013	8.2		2.87	0.010	2.83	0.166	1.900	1.909	0.4		0.184		1.70	1.78	4.2	0.607	0.607	0.0
13SOS07	21.3.2013	8.45	0.369	2.63	0.010	2.54	0.139	2.202	2.205	0.1		0.072		2.05	2.03	0.6	1.064	0.710	33.3
13SOS08	3.4.2013	8.76	0.658	2.57	0.009	2.39	0.128	2.192	2.120	3.3		0.047		2.02	2.01	0.5	0.267	0.267	0.0
13SOS09	11.4.2013	8.93	0.349	2.65	0.038	2.40	0.128	2.101	1.953	7.1		0.057		1.87	1.87	0.1	0.659	0.659	0.0
13SOS10	16.4.2013	8.76	0.339	2.61	0.008	2.43	0.130	2.171	2.012	7.3		0.042		2.09	1.97	5.9	0.258	0.258	0.0
13SOS11	29.4.2013	8.81	0.349	2.50	0.008	2.31	0.161	2.310	2.339	1.2		0.046		1.88	1.99	5.7	0.157	0.150	4.9
13SOS12	7.5.2013	8.81		2.54	0.007	2.35	0.157	2.421	2.576	6.4		0.054		2.24	2.04	8.7		0.095	
13SOS13	14.5.2013	8.91	0.399	2.56	0.013	2.32	0.149	2.286	2.227	2.5		0.054		2.12	1.99	6.2	0.117	0.116	0.9
13SOS14	21.5.2013	8.95		2.53	0.008	2.28	0.145	2.341	2.250	3.9		0.038		2.30	2.03	11.5		0.089	
13SOS15	30.5.2013	8.94	0.599	2.67	0.007	2.41	0.146	2.066	1.998	3.3		0.051		1.98	1.90	4.3	0.171	0.166	2.8
13SOS16	5.6.2013	8.94		2.59	0.007	2.34	0.163	2.123	2.309	8.8		0.049		2.02	1.95	3.2	0.156	0.149	4.6
13SOS17	10.6.2013	8.86		2.61	0.009	2.39	0.176	2.046	2.265	10.7		0.090		1.70	1.92	13.4	0.169	0.153	9.3
13SOS18	18.6.2013	8.83	0.640	2.53	0.016	2.33	0.159	2.376	2.198	7.5		0.038		1.98	1.94	1.8		0.099	
13SOS19	25.6.2013	8.83	0.798	2.46	0.008	2.27	0.159	2.361	2.402	1.7		0.033		1.93	1.95	1.1	0.066	0.063	4.7
13SOS20	2.7.2013	8.93	0.369	2.58	0.007	2.34	0.173	2.212	2.365	6.9		0.044		1.86	1.84	1.0	0.130	0.133	2.9
13SOS21	16.7.2013	8.99		2.49	0.008	2.23	0.161	2.133	2.068	3.0		0.023		1.96	1.95	0.5		0.052	

Table 3. *Continuation*

Sample code	Date	Sr	Sr	% diff	As	Ba	Cd	Co	Cr	Cu	Ni	Pb	Zn	Hg	Mo	Tl	V
		µmole/l	µmole/l		nmole/l	nmole/l	nmole/l	nmole/l	nmole/l	nmole/l	nmole/l	nmole/l	nmole/l	nmole/l	nmole/l	nmole/l	µmole/l
		(0.02 µmol/kg)	*(0.02 µmol/kg)*		*(0.67 nmole/L)*	*(0.07 nmole/l)*	*(0.02 nmole/l)*	*(0.08 nmole/l)*	*(0.19 nmole/l)*	*(1.57 nmole/l)*	*(0.85 nmole/l)*	*(0.05 nmole/l)*	*(3.1 nmole/l)*	*(0.01 nmole/l)*	*(0.52 nmole/l)*	*(2.59 nmole/*	*(0.10 µmole/*
		(ICP-OES)	(ICP-SFMS)		(ICP-SFMS)	(ICP-SFMS)	(ICP-SFMS)	(ICP-SFMS)	(ICP-SFMS)	(ICP-SFMS)	(ICP-SFMS)	(ICP-SFMS)	(ICP-SFMS)	(AFS)	(ICP-SFMS)	(ICP-SFMS)	(ICP-SFMS)
11KGM03	21.1.2011		0.014		11.48	0.23				0.0025		0.56	23.36	0.053001973	22.0	0.82	0.11
11KGM08	5.7.2011		0.015		10.96	0.20						0.44	8.76		21.0	0.74	0.08
11KGM14	28.10.2011		0.016		10.42	0.22			0.58		1.60	0.24	6.95	0.068706261	21.0	0.63	0.10
12KGM01	25.1.2012		0.018		10.61	0.34			0.33	0.0023	1.64	0.49	4.40		25.0	6.73	0.09
12KGM02	27.1.2012		0.019		10.48	0.28			0.36	0.0028	2.10	0.35	9.44		25.0	0.64	0.09
12KGM04	31.1.2012	0.020	0.021	4.0	10.33	0.39		0.151	0.72		2.30	0.39	12.48		24.0	0.48	0.08
12KGM05	3.2.2012	0.021	0.022	3.1	9.93	0.31		0.112	0.52		1.44	0.30	4.81		25.0	0.51	0.08
12KGM07	6.2.2012	0.028	0.026	6.3	9.70	0.40			0.53		1.52	0.32	5.38		24.0	0.54	0.07
12KGM08	9.2.2012	0.039	0.033	14.5	8.86	0.66			0.51		2.22	0.34	10.60		23.0		0.07
12KGM10	13.2.2012	0.046	0.038	17.4	9.37	0.72		0.100	0.57		2.49	0.53	13.64		23.0	0.75	0.06
12KGM11	16.2.2012	0.053	0.050	6.2	9.08	1.30	0.049	0.200	1.26	0.0045	4.44	0.57	26.89		22.0	1.11	0.06
12KGM13	17.2.2012	0.061	0.059	3.4	8.60	1.82		0.620	1.39	0.0043	10.33	0.54	60.46		23.0	0.78	0.06
12KGM14	18.2.2012	0.064	0.060	6.8	8.42	2.15		0.821	0.81	0.0025	14.09	0.42	53.79	0.045149829	23.0	0.30	0.05
12KGM15	19.2.2012	0.066	0.062	6.0	8.89	2.46	0.063	1.058	0.70	0.0038	19.16	0.56	55.75		26.0	0.96	0.05
12KGM16	20.2.2012	0.068	0.065	4.1	7.82	2.64		1.484	1.25	0.0028	23.95	0.45	47.51		26.0	0.32	0.04
12KGM17	23.2.2012	0.072															
12KGM19	27.2.2012	0.064	0.061	4.9	9.29	1.73		0.779	0.31	0.0028	12.54	0.32	19.61		27.0	0.68	0.03
12KGM20	28.2.2012	0.063															
12KGM22	2.3.2012	0.079	0.075	5.6	7.10	2.58		1.527	0.50		19.14	0.26	44.36		26.0	0.68	0.03
12KGM23	5.3.2012	0.091															
12KGM25	8.3.2012	0.098	0.094	4.0	6.10	1.82		1.353	0.60		16.02	0.22	26.70		24.0	0.10	0.03
12KGM27	12.3.2012	0.097	0.092	5.1	6.93	1.95	0.047	1.219	0.63		15.80	0.28	32.19		26.0	0.35	0.03
12KGM28	15.3.2012	0.102	0.098	3.6	7.73	2.08		1.343	0.67		9.05	0.31	28.66		28.0	0.27	0.03
12KGM30	19.3.2012	0.106	0.102	4.0	7.19	2.09		0.744	0.75		6.54	0.31	19.18		25.0	0.32	0.03
12KGM31	22.3.2012	0.107	0.101	5.8	7.46	2.06		0.501	0.52		4.93	0.23	15.15		27.0	1.19	0.03
12KGM33	26.3.2012	0.114															
12KGM34	29.3.2012	0.110	0.105	4.8	6.51	1.89		0.338	0.21		3.93	0.32	12.80		24.0	0.52	0.03
12KGM36	2.4.2012	0.104															
12KGM37	4.4.2012	0.101															
12KGM39	7.4.2012	0.100	0.094	5.7	7.59	1.49	0.067	0.157	0.63	0.0020	3.18	0.27	7.11		23.0	0.65	0.03
12KGM40	10.4.2012	0.100															
12KGM41	11.4.2012	0.096															
12KGM42	12.4.2012	0.106	0.099	6.3	8.21	1.71		0.151	0.26		2.83		8.21		24.0	0.23	0.04
12KGM43	16.4.2012	0.088															
12KGM44	18.4.2012	0.087															
12KGM46	23.4.2012	0.084	0.079	5.7	9.81	1.19	0.047	0.185	0.81		2.51	0.20			26.0	0.72	0.04
12KGM47	27.4.2012	0.077															
12KGM49	4.5.2012	0.048															
12KGM51	7.5.2012	0.067	0.066	1.8	10.84	0.96					1.94				28.0	0.62	0.04
12KGM52	10.5.2012	0.070															
12KGM54	14.5.2012	0.066															
12KGM55	18.5.2012	0.058	0.055	4.6	11.51	0.91					2.08	0.23			29.0	1.37	0.04
12KGM57	21.5.2012	0.064															
12KGM58	24.5.2012	0.064															
12KGM60	30.5.2012	0.067	0.066	1.5	11.23	1.10			0.31		2.67	0.20			28.0	0.37	0.05
12KGM61	1.6.2012	0.068															
12KGM63	4.6.2012	0.069															
12KGM64	8.6.2012	0.071	0.069	2.8	11.41	0.91			0.32		1.90	0.24			30.0		0.05
12KGM66	11.6.2012	0.071															
12KGM67	14.6.2012	0.074	0.072	2.9	12.36	1.19	0.057		0.51		2.47	0.24			33.0	0.55	0.05
12KGM68	18.6.2012	0.074															
12KGM69	20.6.2012	0.078															
12SOS01	28.6.2012	0.093	0.092	0.7	8.93	2.37	0.112	0.218	0.41	0.0029	5.50	0.52	19.04	0.136234701	26.7	1.17	0.04
12SOS02	3.7.2012	0.087	0.089	2.9	9.30	1.51	0.048	0.206	0.68	0.0038	3.22	0.27	7.09	0.084803157	27.0	0.30	0.04

Table 4. *Contination*

Sample code	Date	Sr	Sr	% diff	As	Ba	Cd	Co	Cr	Cu	Ni	Pb	Zn	Hg	Mo	Ti	V
		µmole/l	µmole/l		nmole/l	nmole/l	nmole/l	nmole/l	nmole/l	nmole/l	nmole/l	nmole/l	nmole/l	nmole/l	nmole/l	nmole/l	µmole/l
		(0.02 µmol/kg)	*(0.02 µmol/kg)*		*(0.67 nmole/L)*	*(0.07 nmole/l)*	*(0.02 nmole/l)*	*(0.08 nmole/l)*	*(0.19 nmole/l)*	*(1.57 nmole/l)*	*(0.85 nmole/l)*	*(0.05 nmole/l)*	*(3.1 nmole/l)*	*(0.01 nmole/l)*	*(0.52 nmole/l)*	*(2.59 nmole/*	*(0.10 µmole/*
		(ICP-OES)	(ICP-SFMS)		(ICP-SFMS)	(ICP-SFMS)	(ICP-SFMS)	(ICP-SFMS)	(ICP-SFMS)	(ICP-SFMS)	(ICP-SFMS)	(ICP-SFMS)	(ICP-SFMS)	(AFS)	(ICP-SFMS)	(ICP-SFMS)	(ICP-SFMS)
12SOS04	5.7.2012	0.085	0.086	0.8	8.98	1.26				0.0020	2.57	0.24	5.65	0.055946527	25.6	2.06	0.04
12SOS05	7.7.2012	0.091															
12SOS06	9.7.2012	0.093	0.093	0.0	9.38	1.32					2.57	0.27	8.23		25.6	0.44	0.04
12SOS07	12.7.2012	0.094	0.093	0.1	9.33	1.38					1.36	1.25	5.50		25.1	0.70	0.04
12SOS09	17.7.2012	0.090	0.094	5.0	8.81	1.35					1.35				24.7	0.44	0.04
12SOS10	19.7.2012	0.093	0.097	3.5	9.68	1.53		0.824	2.02		5.40	0.71	8.46		26.5	2.13	0.04
12SOS12	24.7.2012	0.097	0.102	5.2	9.26	1.67		0.275	12.77	0.0020	12.80	0.30	20.61		25.8	4.51	0.04
12SOS13	26.7.2012	0.094	0.100	6.0	9.52	1.54			0.80		2.39	0.68			25.5	0.35	0.04
12SOS15	31.7.2012	0.093	0.093	0.6	9.04	1.50			0.27					0.045149829	24.8	0.40	0.04
12SOS16	2.8.2012	0.096	0.098	2.1	8.94	1.45		0.100	0.27		1.23			0.085588371	24.3	0.24	0.04
12SOS18	7.8.2012	0.100	0.106	6.5	8.89	3.36	0.047	0.132	0.51		2.34	0.27		0.075969494	24.6	0.28	0.04
12SOS19	9.8.2012	0.107	0.110	2.8	9.01	2.15		0.308	0.71		3.30	0.24	6.16	0.05339458	24.8	0.15	0.04
12SOS21	14.8.2012	0.114	0.118	3.4	9.06	2.31		0.400	0.58		3.18		11.97		24.6	0.19	0.03
12SOS23	16.8.2012	0.118	0.116	1.3	8.86	2.10		0.292	0.73		3.24	0.31	9.62	0.067724743	23.7	0.33	0.03
12SOS25	21.8.2012	0.112	0.115	3.1	9.64	2.20	0.046	0.277	1.59	0.0027	4.06	2.12	11.13	0.070080386	25.2	0.17	0.03
12SOS26	23.8.2012	0.112	0.111	0.2	12.52	2.96	0.069	0.176	0.76	0.0023	2.30	1.03	10.66		30.2		0.04
12SOS28	28.8.2012	0.109	0.112	2.1	9.57	1.91		0.172	0.97		1.94	1.33	6.85		24.7	0.02	0.04
12SOS29	31.8.2012	0.109	0.105	3.8	9.49	1.62			1.22		1.73	0.92	5.59		24.6	0.48	0.04
12SOS31	4.9.2012	0.115	0.113	2.3	9.37	1.71			1.61		2.36	1.35	8.48	0.071650815	24.0	0.38	0.04
12SOS32	6.9.2012	0.108	0.108	0.1	9.46	1.57			4.04		2.32	0.26	16.27	0.057909563	23.7	0.17	0.04
12SOS33	13.9.2012	0.107															
12SOS33B	17.9.2012	0.110	0.115	4.4	8.69	1.56	0.040		0.78			0.24	26.89	0.490759008	22.6	1.96	0.04
12SOS34	24.9.2012	0.109	0.107	2.0	9.05	1.46			1.31		1.28	0.22	11.74	0.369050774	23.0	0.48	0.04
12SOS35	1.10.2012	0.109	0.106	2.3	8.45	1.56			0.57	0.0022	1.35	0.20	5.01	0.280714153	22.9	0.89	0.04
12SOS36	8.10.2012	0.099	0.097	1.8	12.15	1.59	0.086	0.130	1.23			0.26	0.00		27.4	0.22	0.05
12SOS38	22.10.2012	0.100	0.098	2.2	11.72	1.67	0.065	0.279	6.04		9.09		4.55	1.260269132	28.6	0.37	0.05
12SOS39	29.10.2012	0.108															
12SOS40	14.11.2012	0.110	0.108	2.0	11.05	1.59	0.055		1.09		1.27	0.36	4.89	0.233601288	26.2	3.53	0.05
12SOS41	26.11.2012	0.108	0.106	2.0	12.91	1.94	0.074	0.216	0.63		1.28		24.34	0.047309168	28.1	1.03	0.05
12SOS42	10.12.2012	0.094	0.092	2.0	9.48	1.28			0.42					0.051431544	22.9	0.89	0.04
12SOS43	20.12.2012	0.092	0.094	3.2	10.04	1.24			0.50				13.54		22.8	0.74	0.04
13SOS01	7.1.2013	0.085	0.085	0.3	10.09	1.06			0.61			0.24	3.93	0.095207248	22.6	0.90	0.04
13SOS02	25.1.2013	0.125	0.121	3.2	8.40	1.97			0.38			0.26	43.58	0.059479992	19.3	1.27	0.04
13SOS04	12.2.2013	0.120	0.119	1.0	9.90	2.36	0.076	0.165	1.53	0.0022	1.16	0.25	7.30	0.318011837	21.8	3.66	0.04
13SOS06	4.3.2013	0.128	0.123	3.9	8.85	2.57		0.115	0.61		1.00	0.28	8.34		19.3	1.45	0.04
13SOS07	21.3.2013	0.088	0.086	2.1	9.96	1.34			0.47			0.20	5.95		21.2	2.13	0.04
13SOS08	3.4.2013	0.077	0.077	0.3	9.98	1.09			0.55			0.22	6.26	0.070472994	21.4	0.96	0.05
13SOS09	11.4.2013	0.093	0.092	1.2	9.21	1.36			0.53			0.27	5.50	0.039260721	20.0	0.71	0.04
13SOS10	16.4.2013	0.084	0.085	1.2	9.61	1.24			0.41			0.22	10.07	0.039260721	20.2	0.40	0.04
13SOS11	29.4.2013	0.075	0.075	0.3	13.03	1.19	0.053		0.61					0.047309168	25.6	0.20	0.05
13SOS12	7.5.2013	0.068	0.069	0.7	14.55	1.23			0.73						27.6	2.59	0.06
13SOS13	14.5.2013	0.073	0.073	0.3	13.32	1.20	0.048		0.74					0.055946527	25.8	1.27	0.05
13SOS14	21.5.2013	0.070	0.069	0.3	13.75	1.00			0.67					0.0435794	26.3	1.25	0.05
13SOS15	30.5.2013	0.090	0.097	7.1	11.77	1.54			0.73					0.0435794	23.3	2.69	0.05
13SOS16	5.6.2013	0.083	0.088	5.9	12.92	1.46		0.112	0.65		1.12				24.8	1.19	0.05
13SOS17	10.6.2013	0.085	0.089	4.7	12.48	1.70		0.208	0.70						24.1	8.65	0.05
13SOS18	18.6.2013	0.069	0.071	3.6	12.15	1.11						0.21			23.7		0.05
13SOS19	25.6.2013	0.056	0.058	3.9	12.71	0.90			0.21				9.66		24.2	0.61	0.05
13SOS20	2.7.2013	0.078	0.082	5.2	10.89	1.24			0.44						21.8		0.04
13SOS21	16.7.2013	0.067	0.070	4.3	12.29	1.11			0.48		1.03				24.3	0.76	0.05

References

European Commission, E. (1998) Drinking Water Directive. Council Directive 98/83/EC of 3 November 1998 on the quality of water intended for human consumption. European Commisson.

Flaathen, T.K., Gislason, S.R., Oelkers, E.H. and Sveinbjörnsdóttir, Á.E. (2009) Chemical evolution of the Mt. Hekla, Iceland, groundwaters: A natural analogue for CO_2 sequestration in basaltic rocks. Applied Geochemistry 24, 463-474.

Galeczka, I., Wolff-Boenisch, D. and Gislason, S. (2013) Experimental Studies of Basalt-H_2O-CO_2 Interaction with a High Pressure Column Flow Reactor: the Mobility of Metals. Energy Procedia 37, 5823-5833.

Gislason, S.R. and Oelkers, E.H. (2003) Mechanism, rates, and consequences of basaltic glass dissolution: II. An experimental study of the dissolution rates of basaltic glass as a function of pH and temperature. Geochimica et Cosmochimica Acta 67, 3817-3832.

Gudbrandsson, S., Wolff-Boenisch, D., Gislason, S.R. and Oelkers, E.H. (2011) An experimental study of crystalline basalt dissolution from $2 < pH < 11$ and temperatures from 5 to 75 °C. Geochimica et Cosmochimica Acta 75, 5496-5509.

Oelkers, E.H. and Gislason, S.R. (2001) The mechanism, rates and consequences of basaltic glass dissolution: I. An experimental study of the dissolution rates of basaltic glass as a function of aqueous Al, Si and oxalic acid concentration at 25°C and pH = 3 and 11. Geochimica et Cosmochimica Acta 65, 3671-3681.

Olsson, J., Stipp, S.L.S., Makovicky, E. and Gislason, S.R. (2014) Metal scavenging by calcium carbonate at the Eyjafjallajökull volcano: A carbon capture and storage analogue. Chemical Geology 384, 135-148.

Snæbjörnsdóttir, S.Ó., Oelkers, E.H., Mesfin, K., Aradóttir, E.S., Dideriksen, K., Gunnarsson, I., Gunnlaugsson, E., Matter, J.M., Stute, M., Gislason, S.R. (2017). The chemistry and saturation states of subsurface fluids during the in situ mineralisation of CO_2 and H_2S at the CarbFix site in SW-Iceland. International Journal of Greenhouse Gas Control 58, 87–102.

World Health Organization, W. (2003) Iron in Drinking Water. Background document for development of WHO Guidelines for Drinking-water Quality.

World Health Organization, W. (2011) Guidelines for Drinking-water Quality, 4th edition, in: Organization, W.H. (Ed.).

Appendix D

Co-authored papers during the study

1. Anthonsen, K.L., Aagaard, P., Bergmo, P.E.S., Erlström, M., Fareide, J.L., Gislason, S.R., Mortensen, G.M., Snæbjörnsdóttir, S.Ó., 2013. CO_2 storage potential in the Nordic region. *Energy Procedia 37, 5080-5092*

2. Anthonsen, K.L., Aagaard, P., Bergmo, P.E.S., Gislason, S.R., Lothe, A.E., Mothensen, G.M., Snæbjörnsdóttir, S.Ó., 2014. Characterisation and selection of the most prospective CO_2 storage sites in the Nordic region. *Energy Procedia 63, 4884-4896.*

3. Aradóttir, E.S.P., Gunnarsson, I., Sigfússon, B., Gislason, S.R., Oelkers, E.H., Stute, M., Matter, J.M., Snæbjörnsdóttir, S.Ó., Mesfin, K.G., Alfredsson, H.A., Hall, J., Arnarsson, M.Th., Dideriksen, K.,Júliusson, B.M., Broecker, W.S., Gunnlaugsson, E. Towards Cleaner Geothermal Energy: Subsurface Sequestration of Sour Gas Emissions from Geothermal Power Plants. *WGC proceedings, 2015. 12 p.*

4. Gislason S.R, Broecker, W.S., Gunnlaugsson, E., Snæbjörnsdóttir, S., Mesfin, K.G., Alfredsson, H.A., Aradottir,E.S., Sigfusson, B., Gunnarsson, I., Stute,M., Matter, J.M., Arnarson, M.Th., Galeczka, I.M., Gudbrandsson, S., Stockmann,G., Wolff-Boenisch, D., Stefansson, Ragnheidardottir, E., Flaathen, T., Gysi, A.P., Olsen, J., Didriksen, K., Stipp, S., Menez B. and E.H. Oelkers, 2014. Rapid solubility and mineral storage of CO_2 in basalt. *Energy Procedia 63, 4561-4574.*

5. Matter, J.M., Stute, M., Hall, J., Mesfin, K., Snæbjörnsdóttir, S.Ó., Gislason, S.R., Oelkers, E.H., Sigfusson, B., Gunnarsson, I., Aradottir, E.S., Alfredsson, H.A., Gunnlaugsson, E., Broecker, W.S., 2014. Monitoring permanent CO_2 storage by in situ mineral carbonation using a reactive tracer technique. *Energy Procedia 63, 4180-4185*